MIMO Antennas for Mobile Phone Applications

by

Saqer S. Alja'afreh

Submitted in accordance with the requirements for the award of the degree of Doctor of Philosophy of the University of Liverpool

October 2015

Copyright

Table of Contents

Acronyms

AC	Anechoic Chamber
AMPS	American Mobile Phone Services
AUT	Antenna under Test
AWGN	Additive White Gaussian Noise
CCI	Capacitive Coupling Element
CDF	Cumulative Distribution Function
CDMA	Code Division Multiple Access
CPW	Coplanar Waveguide
DCS	Digital Cellular Service
DG	Diversity Gain
DGS	Defect Ground Plane Structures
DMN	Decoupling and Matching Networks
DRA	Dielectric Resonator Antenna
DWM	Dielectric Waveguide Model
EBG	Energy Band gap Structures
ECC	Envelope Correlation Coefficient
EGC	Equal Gain Combining
FCC	Federal Communications Commissions
FDMA	Frequency Division Multiple Access
GSM	Global System of Mobile
GPS	Global Positioning System
IMAT	Isolated Mode Antenna Technology
LTE	Long Term Evolution

MEA	Multiple Element Antennas
MEG	Mean Effective Gain
MIMO	Multiple Input and Multiple Output
MISO	Multiple Input and Single Output
MMS	Multimedia Message Service
MRC	Maximal Ratio Combining
NLOS	Non Line of Sight
OFDM	Orthogonal Frequency Division Multiplexing
PCS	Personal Communication Service
PDE	Parasitic Decoupling Element
PIFA	Planar Inverted F Antenna
PILA	Planar Inverted-L Antenna
RC	Reverberation Chamber
RDRA	Rectangular Dielectric Resonator Antenna
SAR	Specific Absorption Rate
SC	Selection Combining
SIR	Stepped Impedance Resonator
SISO	Single Input Single Output
SM	Spatial Multiplexing
SMS	Short Message Service
SNR	Signal to Noise Ratio
TDMA	Time Division Multiple Access
TE	Transverse Electric
TEM	Transverse Electromagnetic

UMTA	Universal Mobile Telecommunications System
WiFi	Wireless Fidelity
WiMAX	World-wide Interoperability for Microwave Access
WLAN	Wireless Local Area Network

Acknowledgements

First of all, I thank ALLAH ALMIGHTY who has given me the power and confidence to do this work. This thesis would have not seen the light without the support and guidance of many people who are acknowledged here. At the very first, I would like to express all my deepest thankfulness to my research supervisor Professor Yi Huang. I will not forget his valuable ideas, comments and suggestions that guided me in the right direction during my research journey. I have learnt from him about the value of the time, speed and the professionalism. I am very much proud that my name is coupled with his name over this life.

The second special name that should be printed in this work is the name of my beloved wife 'AREEJ'. I would never have succeeded without her love, support, encouragement and patience. Her words and advices were a balsam during this journey. Also, I am extremely grateful for my cute little angel 'ZAINAH' for being a good girl, she is always cheering me up.

Thanks must also be paid to my colleagues in the research group; in particular to Lei Xing and Qain Xu for their help, cooperation and valuable suggestions. Special thanks should go to my friend Dr. Hassan Tariq Chattha from the University of Engineering and Technology/ Pakistan. I have enjoyed getting to know you personally and working with you.

At last but not the least, I am grateful to my parents for their love, prayers and caring for preparing me for the future. Also, I would like to thank all my family members: my sisters and my brothers for their support. Special thanks should go to my second family members: my parents in law, sisters in law and brothers in law for their encouragement.

List of Publications

Journal Publications

[1] **S. S. Alja'afreh**, Y. Huang, L. Xing, Q. Xu and X. Zhu, "A Low Profile and Wideband PILA-based Antenna for Handset Diversity Applications", *IEEE Antennas & Wireless Propagation Letters*, vol. 14, pp. 923-926, 2015.

[2] **S. S. Alja'afreh**, Y. Huang and L. Xing, "A Novel, Low Profile and Wideband PIFA Antenna with Polarization and Pattern Diversities", *IET Microwaves Antennas & Propagation*. Accepted in 5 Sept 2015, to be published.

[3] H. Chattha, M. Nasir, Q. Abbasi, Y. Huang, **S. S. Alja'afreh**, "Compact Low-Profile Dual-Port Single Wideband Planar Inverted-F MIMO Antenna," *IEEE Antennas & Wireless Propagation Letters*, vol.12, pp.1673-1675, 2013.

[4] H. Chattha, M. Nasir, Y. Jamal, Y. Huang, **S. S. Alja'afreh**, "Planar Inverted-E Antenna for Future Generations Applications" *Microwave & Optical Technology Letters*, vol.56, no. 9, pp.2103-2107, 2014.

[5] Q. Xu, Y. Huang**,** X. Zhu**, S. S. Alja'afreh**, L. Xing, "A New Antenna Diversity Gain Measurement Method Using A Reverberation Chamber", *IEEE Antennas & Wireless Propagation Letters*, vol. 14, pp. 935-938, 2015.

[6] Q. Xu, Y. Huang**,** X. Zhu**, S. S. Alja'afreh**, L. Xing, Z. Tian, "Diversity Gain Measurement in A Reverberation Chamber without Extra Antennas", *IEEE Antennas & Wireless Propagation Letters*, vol. 14, 2015.

[7] L. Xing, Y. Huang**,** Y. Shen**, S. S. Alja'afreh**, Q. Xu, R. Alrawashdeh, "Further investigations on Water Antennas", *IET Microwaves Antennas & Propagation*, vol. 9, no. 8, pp. 735-741, 2014..

[8] L. Xing, Y. Huang, Q. Xu and **S. S. Alja'afreh**, "Wideband, Hybrid Rectangular Water Antenna for DVB-H Applications," *Microwave and Optical Technology Letters*, vol. 57, no. 9, pp. 2160-2164, 2015.

[9] L. Xing, Y. Huang, Q. Xu, **S. S. Alja'afreh** and T. Liu "A Broadband Hybrid Water Antenna for Hand-Portable Applications," accepted by *IEEE Antennas and Wireless Propagation Letters*.

[10] L. Xing, Y. Huang, Q. Xu and **S. S. Alja'afreh** "A Wideband Hybrid Water Antenna with an F-Shaped Monopole," *IEEE Access Journal,* vol. 3, pp. 1179-1187, 2015.

[11] L. Xing, Y. Huang, Q. Xu and **S. S. Alja'afreh** "A Compact Water Loaded Reconfigurable Antenna for DVB-H Applications," *Electronic Letters,* to be published

[12] L. Xing, Y. Huang, Q. Xu and **S. S. Alja'afreh** "Complex Permittivity of Water-based Liquids for Liquid Antennas," *IEEE Antennas &Wireless Propagation Letters,* Under revision

[13] **S. S. Alja'afreh**, Y. Huang, Q. Xu and L. Xing, "A Hexa-band Metallic Frame Antenna for Smartphone Applications ", *IEEE Antennas &Wireless Propagation Letters*, under peer review.

[14] **S. S. Alja'afreh**, Y. Huang, Q. Xu and L. Xing, "A Novel Approach for Parasitic Decoupling Element Design for MIMO Applications", *IET Microwaves Antennas & Propagation*, under peer review.

Conference Publications

[1] **S. S. Alja'afreh**, Y. Huang, L. Xing, "A Compact Dual-Feed Water-Based Diversity Antenna", *In Proc. LAPC 2013 Conference*, November 2013, United Kingdom.

[2] H. T. Chattha, **S. S. Alja'afreh**, Y. Huang, I Hameed and M. Nasir, "Single Element Two-Port Planar Inverted-F Diversity Antenna for Wireless Applications", *In Proc. LAPC 2013 Conference*, November, 2013, United Kingdom

[3] **S. S. Alja'afreh**, Y. Huang, L. Xing, "A New Dual-Feed PIFA Diversity Antenna", *In Proc. EuCAP 2014*, April, 2014, Netherlands.

[4] **S. S. Alja'afreh**, Y. Huang, L. Xing, "A Compact Wideband and Low profile Planar Inverted-L Antenna", *In Proc. EuCAP 2014*, April, 2014, Netherlands.

[5] H. T. Chattha, M. Nasir, **S. S. Alja'afreh**, Y. Huang and A. Sharif, "Modified wideband Planar Inverted-F Antenna", *In Proc. EuCAP 2014*, April, 2014, Netherlands.

[6] S. S. Alja'afreh, Y. Huang, L. Xing, "A Small U-Shaped Dielectric Resonator Antenna ", *In Proc. LAPC 2012 Conference*, November 2012, United Kingdom.

[6] L. Xing, Y. Huang, **S. S. Alja'afreh**, S. Boyes, "A Monopole Water Antenna," *In Proc. LAPC 2012 Conference*, November, 2012, United Kingdom.

[7] L. Xing, Y. Huang, Y. Shen, **S. S. Alja'afreh**, Q. Xu, R. Alrawashdeh, "Broadband U-Shaped Water Antenna for DVB-H Applications," *In Proc. of the IEEE International Symposium on Antennas and Propagation and USNC-URSI Radio Science, 2014*, Tennessee, USA.

[8] L. Xing, Y. Huang, **S. S. Alja'afreh**, Q. Xu, M. Kod, C. Song, "Reconfigurable 3D Folded Monopole Antenna Design," *In Proc. LAPC 2014 Conference*, November, 2014, United Kingdom.

[9] L. Xing, Y. Huang, Q. Xu, and **S. S. Alja'afreh**, "Overview of Water Antenna Designs for Wireless Communications," *accepted by The IEEE 4th Asia-Pacific Conference on Antennas and Propagation (APCAP)* 2015.

[10] A. A-B. Sajak, Y. Shen, R. Alrawashdeh, L. Xing and **S. S. Alja'afreh**, "A Comparison of the Effect of Substrate on the Performance of THz Antenna," *In Proc. 4th International Conference on Engineering Technology and Techno preneuship (ICE2T) 2014*, August, 2014, Malaysia.

[11] **S. S. Alja'afreh**, Y. Huang, L. Xing, "A Small Wideband U-Shaped Dielectric Resonator Antenna," *In Proc. LAPC 2012 Conference*, November, 2012, United Kingdom.

[12] M. Stanley, Y. Huang, H. Wang, **S. S. Alja'afreh**, Q. Xu and L. Xing, "LTE MIMO Antenna Using Unbroken Metallic Rim and Non Resonant CCE Element", *Submitted to EuCAP 2016*, April, 2016, Switzerland.

Abstract

Recent evolutions in wireless mobile communications have shown that by employing multiple inputs and multiple outputs (MIMO) technology at both the transmitter and receiver, both the wireless system capacity and reliability can be enhanced without the need for increasing the power transmitted or using more spectrum. Despite a considerable amount of research have been done on the design of MIMO and diversity handset antennas, the design of low profile, small footprint and multi-standard (wideband or multiband) diversity antennas on handset devices remains a challenging issue. Therefore, the purpose of this thesis is to present new antenna structures for handset MIMO and diversity applications. As the MIMO antenna design can be conducted either using multiple element antennas (MEA) or isolated mode antenna technology (IMAT), the work in this thesis is fallen in these two general design themes (areas).

The first area under investigation concerns multiport antennas (IMAT antennas). It has the following two contributions:

- A novel dual-feed water-based antenna is designed from a low cost liquid material with a very high dielectric constant (pure water $\varepsilon_r = 81$). The isolation between feeds is achieved by two back to back L-shaped ground plane strips. A prototype is made and the optimised diversity parameters are obtained, the results show that this design has a good diversity performance over the frequency range of 2.4 – 2.7 GHz.

- A new and low profile (*h = 3 mm*) planar inverted-F antenna (PIFA) with a coplanar-feed is presented. It has a wideband response over the frequency range of 2.35 – 3.25 GHz. The design is based on a comparative study on the mutual coupling between different feed arrangements. As a result, the coplanar feed is employed in the proposed antenna; the polarization diversity is achieved by exciting two orthogonal radiation modes. The isolation between the feeds is achieved by an L-shaped ground plane slot. Both simulated and measured results demonstrate that the design is a very good candidate for mobile diversity and MIMO applications.

The second investigation area concerns multiple element antenna (MEA) systems for wideband and multiband handset applications. It includes the following contributions:

- Three antenna systems of the planar inverted-L (PILA) antenna (*h = 5 mm*) are employed for wideband handset diversity applications over the frequency range of 1.7 – 2.85 GHz: *1)* The first design has a dual-element PILA in which both the pattern and spatial diversities are employed; one antenna element is located on the upper edge of the ground plane while the other is located on the lower edge. *2)* The second design represents a more compact dual-element PILA antenna in which the two elements are placed on the same ground plane edge (collocated on the same edge). The antenna isolation is achieved using a parasitic decoupling element inserted between the two elements. A novel approach for the design of the parasitic decoupling element is proposed. It is based on stepped impedance resonator circuit theory. As a result, more space is saved with this design (*footprint = 385 mm*^{2}) over the first design (*footprint = 702 mm*^{2}). *3)* The third design is a four-element PILA system in which two antenna pairs (one pair at the upper edge which the other pair is located on the lower edge on the system PCB). All the prototypes are made and evaluated; the results show excellent diversity performance over the applications in the frequency range of 1.7-2.7 GHz.

- A dual-element hexa-band antenna is proposed for smartphone MIMO applications. It consists of two elements: a hexa-band metallic frame antenna and a hepta-band PILA antenna coupled with a meandered shorted strip as an internal antenna. The isolation is achieved due to the resulted orthogonal radiation patterns, especially, at 0.85 GHz. The optimized antenna is made and tested and the results show that this design covers a hexa-band and is particularly suitable for GSM850/ DCS1800/ PCS1900/ UMTS2100/ LTE2500/ LTE3600 smartphone applications.

Chapter 1: Introduction

1.1 Evolution of Mobile Communications

Over the last three decades, the cellular and mobile communication system has been evolved according to the mobile user's requirement, market requirement and evolution of the integrated technology. It started with the first generation (1G) which allowed the mobile users to make analogue voice communications. In 1990s, the second generation (2G) mobile services were launched; new mobile services were added in 2G systems such as: digital voice calls for better quality, data transfer in the form of short message service (SMS) and later multimedia message service (MMS). Subsequently, 2G evolved into 2.5G with the introduction of general packet radio systems (GPRS) and higher data rate via higher order modulation schemes in the mid of 1990s. Then, to meet the increasing demand for more digital services, the third generation (3G) was introduced. New digital services were introduced over the existing ones in 2G like a high speed internet access and download speed, high quality video and voice calls. Currently, the 3G system is updated to the fourth generation (4G) system by releasing long-term evolution (LTE). It provides a very fast speed on internet access and a high speed in the downlink channel (up to 100 Mbps) with a high quality service over severe multipath radio environments. Furthermore, the forthcoming fifth generation (5G) system aims to support a complex range of communication services with a tremendous data rate speed up to 10 Gbps. Table 1.1 gives a brief comparative summary about the story of mobile communication system evolutions.

Table 1.1 Brief comparison between the mobile system generations

	Technology	Services	Data rate
1G	AMPS, FDMA	Analogue voice	--------
2G	GSM, CDMA, TDMA	Digital voice and data	14.4 Kbps
3G	UMTS, CDMA2000	Digital voice, data ,video and internet access	(0.1-2 Mbps)
4G	LTE, WiMAX, WiFi, OFDM	High speed internet access, video, voice and data	(0.1-1 Gbps)
5G	Not defined	Very high speed internet access with a wireless world wide web (Wwww)	(1-10 Gbps)

In conjunction with this development, other wireless systems were integrated and merged with the recent handset devices (smartphones) such as: wireless local area network (WLAN), worldwide interoperability for microwave access (WiMAX), global positioning system (GPS) and Bluetooth. Likewise, the recent 4G systems require high speed connectivity over long distances with a high grade of service (more reliability). The conventional solution to increase the system data rate is based on the Shannon-Nyquist theorem over ideal additive white Gaussian noise channel (AWGN) [1], where the maximum achievable data rate of a channel with a capacity *C*, bandwidth *W* and signal to noise ratio SNR is equal to the capacity of the channel as given in (1.1). It shows that the data rate can only be increased either by increasing the channel bandwidth or increasing the SNR (increasing the transmitted power). However, both solutions are unacceptable as the former means to assign more spectrum bandwidth which is limited and expensive, and the latter means increasing the power level (increasing interference).

$$C = W \log_2(1 + SNR) \quad \text{[bps]} \tag{1.1}$$

Therefore, there is a need in finding another domain to improve the wireless system data rate. Years ago, the spatial domain has been used in increasing this limit at the mobile base station end [2, 3]. Increasing demand for higher data rates in the downlink mobile channel has led to the invention of the MIMO system [4, 5]. By introducing multiple transmit and receive antennas at both communication ends, the system capacity can increase with the number of antennas under a certain condition. Recently, MIMO system became one of the key enabling technologies that are deployed to meet the performance requirement of the current mobile system [6]. The use of MIMO systems not only increases the data rate (using spatial multiplexing) but also enhances the system reliability via the spatial diversity (antenna diversity) system. Finally, as the space is limited in mobile handset devices and the installation of multiple antennas requires a certain condition like a low level of mutual coupling, this has attracted more research attention on finding the best antenna configuration with the best condition to get the benefit of using the MIMO technology.

1.2 Evolution of the Mobile Phone Design

The evolution of mobile communications systems has also altered the characteristics and the functionality of mobile handsets. This was driven by the development of the integrated circuit technology, the user demands and the newly added services by the mobile networks. The evolution story can be subdivided into four generations as shown in Fig. 1.1.

Fig. 1.1: Evolution of mobile phone design

During the 1st generation era (1983-1997), all the handset devices had a ‘‘Candy bar’’ form factor and the evolution was mainly on reducing of the mobile phone size. A very few changes had been occurred on the functionality of the mobile phone, it was used only for voice communications till 1990, then by the development of the 2G system the text messaging SMS service was added.

Through the end of 1990s, the Clamshell form factor (feature phone) had been pervaded the mobile market as a new fashion handset. During this era, two interesting changes were done:1) addition of new features and functionalities like: coloured screen, taking photos by the added camera, listening to music, sending multimedia messaging services MMS and introducing to the internet; 2) The miniaturization process reached its limit as most of handset devices had integrated internal antennas inside them.

By 2003, the miniaturization of the mobile phone was no longer the trend of the mobile industry; a huge evolution was done with the invention of the smartphone and this changed the design trend into wide and flat handset devices. Although smartphones have all the same capabilities of feature phones, they have a common operating system, large screen, high speed wireless connection via WiFi, GPS, Bluetooth and TV streaming.

In 2007, the mobile phone industry took a dramatic turn; the touch screen era was started with the announcement of the iPhone. It had a large coloured touch screen display and its user interface was finger-friendly. Consequently, this increases the competitions between the handset designers to find and employ the cutting-end technologies.

1.3 Evolution of Handset Antennas

As discussed in Section 1.1, the last three decades have witnessed a phenomenal growth in the wireless communication technology. This evolution was reflected on the mobile phone design. However, all these evolutions would not have been existed without a development on handset antennas. The evolution of handset antennas was governed by user demands (cosmetic and compactness issues) and by technical requirements like changing the design trend from a single band in the 1G to a dual band in the 2G and then to multiband designs in the 3G and 4G. Moreover, the latest evolution of the wireless technology also led to the emergence of a new antenna design trend which is the multi-element antenna design for MIMO and diversity applications.

In this section, the commonly used antenna structures on mobile phones are discussed in terms of three eras of antenna designs: external antennas, internal antennas and hybrid antennas (combination of external and internal antennas). A detailed review about the development of mobile phone antennas can be found in [7].

1.3.1 External Antennas

Prior to 1997, all mobile phones had an external antenna on the top of the mobile housing [8]. The oldest type was the Whip monopole as shown in Fig. 1.2; it was used widely during the 1G mobile systems as a single band design. Unfortunately, this antenna was quite large as it had to be extended when the phone was in use so this was making it susceptible to breaking and damaging. To overcome this problem, inductive loading had been employed to shorten the length of handset antennas, the solution was named as a helical antenna, which is a simple conductor wire wound into a helix shape and enclosed in a plastic rubber [9]. With the introduction of the 2G mobile technology, a newly added high frequency band was allocated for mobile applications; this led to the need for a dual band antenna solution. One of the solutions was a hybrid combination of a helix antenna and a

whip antenna passing through the helix axis. However, this solution had a difficulty in fixing the whip monopole inside the helix. The most powerful solution that was being used widely is the dual-band helix antenna; it has different pitch for dual band feature as shown in Fig.1. 3 [10]. Although external antennas had excellent bandwidth and efficiency, they had a high specific absorption rate (SAR) that exceeded the FCC limit.

Fig. 1.2: First mobile phone with external Whip antenna

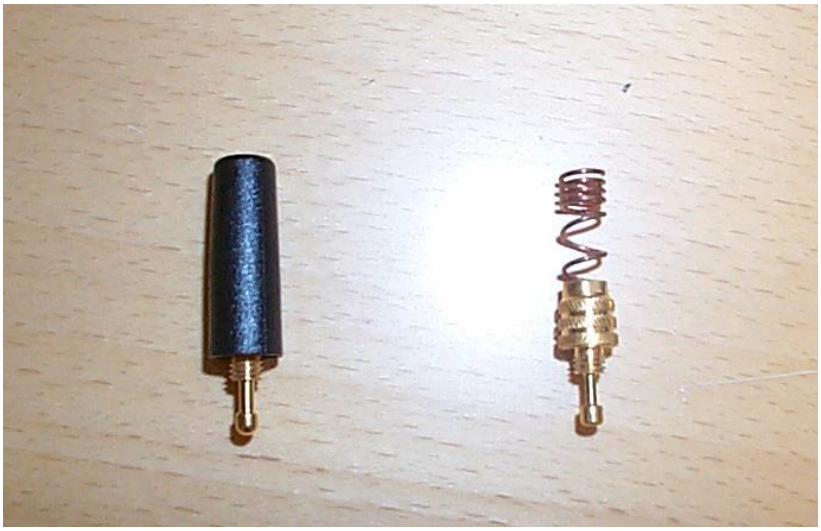

Fig. 1.3: Dual band non-uniform helix antenna invented by Z. Ying [10].

1.3.2 Internal Antennas

By the end of 1990s, Nokia 3210 shown in Fig.1.4 entered the market as the first mobile phone with an internal antenna. After that, internal antennas began to gain more popularity than external antennas. Different antenna structures have been used as internal antennas. Due to its attractive features like: simple design, light weight and low cost planar inverted-F antenna (PIFA) is the most commonly used [11]. Usually, it is defined as a shorted patch or microstrip antenna. As multiband antennas are highly needed in mobile phones, different techniques have been employed to evolve PIFA into a multiband operation. Such techniques like: creating slit cuts in the patch to alter the current paths [12], using grounded parasitic elements in a region of high electric field strength [13], creating ground plane slots underneath PIFA [14], a combination of patch slots and parasitic elements [15, 16], and a combination of ground plane slots and patch slots [17-19].

As the design trend of mobile phones was focused on the miniaturization, the preferable place for internal antennas was the top of the mobile phone. This led to neglect the use of other antenna structures (planar monopoles and slot monopole antennas) that produce a high SAR value due to the cleared ground plane area underneath them. These structures received great research attentions after the releasing of the Motorola Razor in 2004 [20], a folded monopole antenna was used on the bottom of the mobile phone. The success of the Razor started the new trend for the ultra slim phone using printed monopoles [21-26] and slot antennas [27, 28].

Fig. 1.4: Nokia 3210, the first mobile phone with an internal antenna

Recently, the design of handset antennas became challenging due to the added new frequency bands which increased the need for multi-broadband antenna solutions [29]. The conventional antennas like PIFA and planar monopoles are difficult to adjust their impedance bandwidth in a multi-broadband between 700 MHz and 3.8 GHz. Also, these antenna structures usually excite a large surface current on the system ground plane which acts as a part of the radiator and this increases the SAR effect and antenna detuning by biological bodies [30, 31]. As the loop antenna excites a small amount of surface current on the system ground plane and the broadband impedance bandwidth can be achieved by merging different loop modes together [29], loop antennas received a considerable attention from researchers in both the academic field and the mobile industry [29-32]. Another successful story with loop antennas is initiated after releasing iPhone 4 in 2010 [33, 34]. Further details are presented in the next section.

1.3.3 Hybrid Combination of External and Internal Antennas (Metallic Frame Antennas)

In 2010, Apple Inc. released iPhone 4 which was the first smartphone with a metallic frame house. The interesting thing from this product was the hidden function of the metal frame. Apple used both external antennas and internal antennas to find a hybrid type of antenna. This hybrid antenna consists of a metallic frame (as external antenna) casing the mobile chassis around the perimeter and it is coupled with a loop antenna as an internal antenna which is fed directly from the gap as shown in Fig. 1.5 [34]. After this, the idea has been propagated through the whole industry of the mobile market. Moreover, recent years have witnessed a lot of research publications about this new era of the antenna design for mobile phones [35-42]. Table 1.2 summarizes and compares the basic antenna structures that are widely used as mobile phone antennas

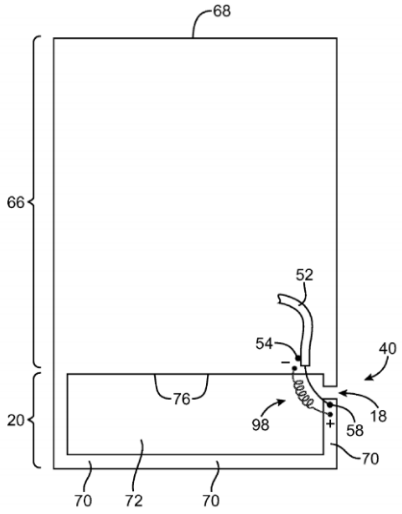

(a)

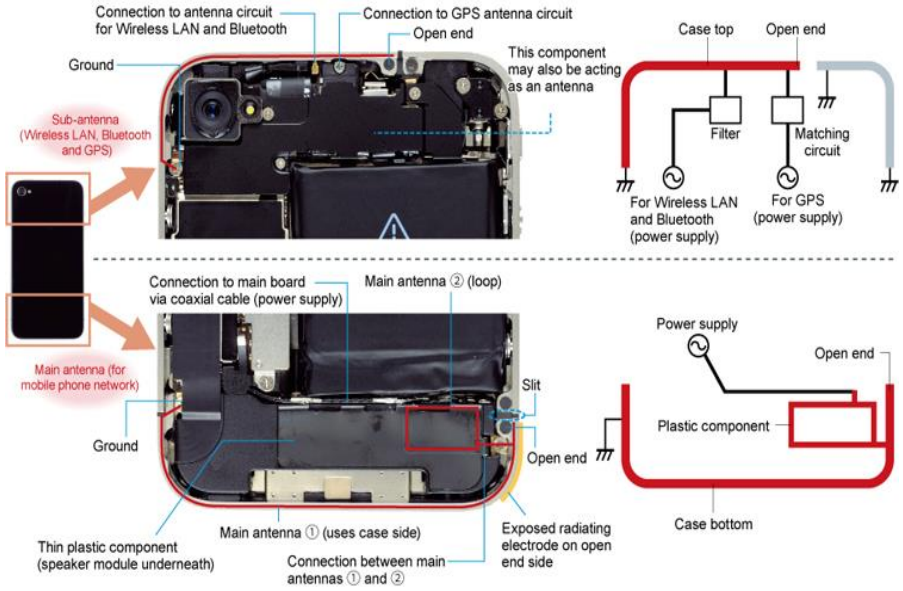

(b)

Fig. 1.5: Hybrid antenna (a) Schematic diagram [34] and (b) iPhone 4, the first mobile phone with a metallic frame antenna

Table 1.2 Comparison of mobile phone antenna types

Type	Theory	Advantages	Disadvantages
External Antennas			
Whip	$\lambda/4$ antenna	Excellent impedance bandwidth, east to manufacture	Poor performance, large especially at the extended mode, susceptible to breaking and damage, to achieve multiband is not easy
Helix	$\lambda/8 \rightarrow \lambda/4$ antenna (with inductive loading)	Short size, good impedance bandwidth and easy to manufacture	High SAR
Internal Antenna [7]			
Slot	$\lambda/4$ or $\lambda/2$ slot	Not sensitive to detuning	SAR is high for slot monopole antennas
Ceramic Antennas	$\lambda/4$ monopole type ceramic antenna, DRA antenna $\varepsilon = 10 \rightarrow 30$	Small and compact	Narrow bandwidth, fragile material
PIFA	$\lambda/4$ shorted microstrip antenna	Low SAR, easy to design, light weight, simple design	Narrow bandwidth, 3D structure (some designs are high profile)
Printed Monopole antennas	$\lambda/4 \rightarrow \lambda/2$ planar antenna without ground underneath	Very low profile (slim antenna), light weight, simple design	High SAR
Hybrid Antenna (Metal Frame Antenna)			
Metal Frame with Gaps	Metallic frame coupled with internal loop or slot antenna	Multiband design, add nice cosmetic appearance	High detuning due to gaps in the frame, high SAR if the feeding point is near the gap
Closed Ring Metal Frame	Loop Antenna formed from both metal frame and the system PCB.	Multiband design, add nice cosmetic appearance	Affects the performance of internal antennas due to the undesired coupling created between them.

1.4 Current Challenges in Handset MIMO Antenna Design

Despite of the aforementioned developments that have occurred on the cellular mobile communication technology, several system's design challenges are appeared. In regard to the handset antenna design, the following challenges are appeared:

1) **Universal and compact mobile antenna:** By the releasing of the new LTE 4G frequency bands, the wireless spectrum of the current 2G, 3G and 4G systems are scattered between 700 MHz to 3800 MHz as shown in Fig. 1.6. Also, other wireless systems likes GPS, WiFi, Bluetooth and WiMAX are now integrated with recent Smartphone devices. All these increase the need for universal (multi-standard) handset antenna (wideband or multiband antennas) without increasing the volume occupied for antenna integration [43].

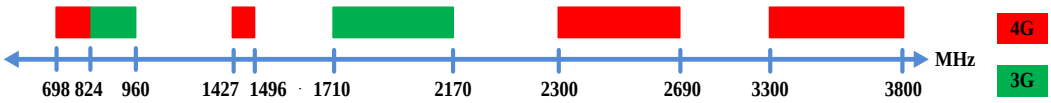

Fig. 1.6: Radio spectrum for 3G and 4G applications

2) **Multiple antenna system (MIMO antenna):** As the MIMO system represents one of the recent important technologies that are deployed to meet the current performance requirements in 3G and 4G systems. The 4G system (advanced LTE) has set the peak data rate up to 1 Gbps for low mobility scenarios and up to 100 Mbps for high mobility cases. Therefore, to deploy this in the current technology, it requires a number of antenna elements to be installed at both wireless communication ends. Subsequently, the biggest challenge lies in the integration of multiple antennas into a small handset device, especially, for applications below 1GHz; antenna elements are closely spaced in terms of the wavelength and the common ground plane will act as a main radiator, thus, the antennas tend to be more correlated (coupled). The high level of correlation affects and destroys all the performance parameters of the MIMO and diversity system, as an example, the antenna efficiency becomes worse and the system capacity will decrease.

3) **Upcoming 5G and massive MIMO:** The next generation (5G) system is expected to be started in 2020; the expected throughput will be between 1-10 Gbps. It tends to provide unlimited, fast and huge access to information at anytime and everywhere in the world, high traffic capacity, short latency time, data integrity [44]. Thus, it will require a massive upgrade on the existing technology tools. As an example, the existing utilized radio spectrum will be extended to higher microwave frequency bands (above 10 GHz) and even to millimeter wave frequencies (above 60 GHz). All of these will add some challenges regarding the design of antenna systems. A massive MIMO antenna system (large number of antenna elements) is to be installed at both the mobile station and the base station. Table 1.2 gives a clear view on the upcoming MW massive MIMO and mm-Wave MIMO. On the other hand, one of the antenna design challenges for 5G will be on the material of the antenna; at the higher microwave frequency bands and the millimeter wave frequencies, both the substrate loss and the metal loss will increase.

Table 1.2 Massive MIMO schemes [44]

	Microwave (1-30 GHz)	**Millimeter Wave (30- 300 GHz)**
Bandwidth	20-50 MHz	>256 MHz
# of antennas @ BS	32-64	64-256
# of antennas @ MS	1-4	4-12
Beamforming	Digital	Analogue
Cell size	Micro/Macro	Pico

1.5 Research Motivation

Although much research has been conducted on the design of mobile phone antennas, there is a continuous demand for finding antenna solutions to meet the current and future wireless technology generations. As an example, the avenue of designing compact multi-element antennas or multi-port antennas for small, slim and multi-standard mobile handsets is an interesting area of research [44-47]. Therefore, this work has two general themes: the first one is to find single element MIMO antennas with a multi-feed for mobile phone applications, while the second one is to find multi-element MIMO antennas for either wideband or multiband mobile handset applications. Keeping in the mind the recent requirement for the design of handset antennas like: low profile, compact and for multi-standard use.

Over the last three decades, dielectric resonator antennas (DRAs) have received a great research attention [48]. However, most of the proposed DRA designs were only used dielectric materials that have moderate dielectric constants [49, 50]. Only very few works utilized very high dielectric constant materials [51, 52]; and this is mainly due to their high cost and the resulting narrow bandwidth. Interestingly, in the area of MIMO and antenna diversity technology, there is no work presented DRA with a very high dielectric constant in small handheld devices, even the existing MIMO DRA designs are only with equally-dimension structures like cylindrical and cube shape [53-55]. As a low cost material with a very high dielectric constant, pure water ($\varepsilon_r = 81$) has received a great research attention in the recent years [56, 57]. In this thesis, the focus is on finding a water based antenna for MIMO and diversity handset applications.

The planar inverted-F antenna (PIFA) is one of the most preferable antenna structures in the design of efficient and low profile handset antennas [8, 11]. However, most of the proposed works on PIFA were mainly single element designs [12-19], even the MIMO designs; some of them use the spatial diversity to achieve the isolation condition [58]. Few works used PIFA with a multi-feed to save a space in small handset terminals [59-61], but all of them suffer from several drawbacks like: high antenna profile, narrowband operation and impractical use for the integration [59-61]. Therefore, the second motivation of this work is focused on finding a very low profile, wideband, dual-feed PIFA antenna for handset diversity applications.

PILA is one of the first low profile antenna structures [8, 11]. However, its mismatch problem makes it undesirable for the design of mobile phone antennas. And this led antenna

designers to solve its mismatching problem; the conventional solution was to evolve PILA into PIFA which was simply by adding another shorted-L plate next to the feeding point [11]. Other solutions like: modifying of the antenna feed using a dielectric resonator antenna (DRA) as a feed [62], modifying the top plate [63], however, there is no work dealt with the interaction between the PILA top plate and the ground plane underneath. Also, the presented work in [64] which deals with the interaction between the handset antenna and the ground plane guided this research to solve PILA problem. Therefore, this work proposes a wideband, low profile PILA for mobile applications in the frequency range from 1.7 to 2.85 GHz. Then, the PILA is adopted as a MIMO and diversity antenna using several designs.

In the recent years, smartphones have entered mobile markets and have enjoyed a rapid growth. As an example, the current trend in designing smartphones is to use a metallic frame in the housing [24]. One of the big advantages of the metallic frame lies in using it as a part of the antenna circuitry [34]. However, some of the proposed antenna solutions using this new trend were focused on the design of metallic frame antenna as a single element design, and they did not pay attention on finding MIMO solutions especially for applications below 1 GHz [65, 66]. Interesting design solutions have been reported in [67, 68], a new characteristic mode (orthogonal to the conventional chassis dipole mode below 1 GHz) has been excited by a metal frame antenna. This facilitated the introduction of a dual-element antenna for MIMO applications. However, these proposed solutions are high profile designs and can only cover single band [67] or dual band [68]. The final motivation for this work leads to develop a new multiband metal frame antenna, which is integrated with an internal multiband antenna to form a dual-element multiband antenna for MIMO and diversity applications in the smartphone with a metal frame case.

1.6 Organization of the Thesis

The rest of the thesis is organized as follows:

Chapter 2 discusses MIMO system and its signalling techniques. Then, it discusses the antenna diversity system in detail such as: the types of the diversity techniques, the diversity combining techniques, the MIMO decoupling techniques and the diversity gain. Furthermore, this chapter presents the measurement techniques that are used to characterize all MIMO designs in the rest of the thesis.

Chapter 3 introduces two water-based antenna designs for Bluetooth, 2.4 GHz WiFi and three LTE bands (bands 7, 38 and 41). The first one represents a single feed antenna, while the second one is a dual-feed design. Both designs are fabricated and tested.

Chapter 4 concerns another dual-feed antenna design. It presents a new design of low profile, wideband PIFA antenna for handset diversity applications over the frequency range of (2.35-3.25 GHz). The antenna utilizes a new feed arrangement that maintains a low mutual coupling level compared to the other feed arrangements. Based on the optimized design parameters, the antenna is made, tested and the results are reported in Chapter 4.

Chapter 5 deals with two designs of a low profile planar inverted-L antenna (PILA) for wideband handset applications in the frequency range of (1.7-2.85 GHz). After finding a single-element PILA, two elements are arranged utilizing both pattern and spatial diversities to provide a reasonable isolation level.

Chapter 6 continues the story of Chapter 5, a more compact dual-element PILA antenna (collocated on the top edge of the PCB) is presented, the compactness is achieved using a parasitic decoupling element that is designed and optimized based on the stepped impedance resonator (SIR) circuit theory. This chapter also includes a four-element PILA design that comprises two elements on the top edge of the ground plane PCB while the other two elements are on the lower edge. For both designs, the evaluation metrics provided in chapter 2 are all presented and discussed.

Chapter 7 describes a new design of a multiband metal frame antenna for smartphones applications. This metal frame antenna is also integrated with an internal antenna (PILA and a meandered strip that is shorted to a ground plane). The resulting dual-element antenna is presented for multiband handset applications, such applications like: GSM850/ DCS1800/ PCS1900/ UMTS2100/ LTE2500/ LTE3600.

Chapter 8 draws the conclusions and some thought of the future work.

References

[1] C. E. Shannon, "A mathematical theory of communication," *Bell Syst Tech.*, vol. 27, pp. 379-423, 623-656, July & Oct. 1948.

[2] J. Winters, "On the capacity of radio communication system with diversity in a Rayleigh fading environment," *IEEE Journal on Selected Areas in Communications*., vol. 5, no. 5, pp. 871-878, June. 1987.

[3] R. G. Vaughan and J. B. Anderson, "Antenna diversity in mobile communications," *IEEE Trans.Veh. Thecnol.*, vol. VT-36, no. 4, pp. 149-172, Nov. 1987.

[4] G. J. Foschini, "Layered space-time architecture for wireless communication in a fading environment when using multi-element antennas," *Bell Lab Tech J.*, vol. 1, no. 2, pp. 41-59, 1996.

[5] G. J. Foschini and M. J. Gans, "On limits of wireless communications in a fading environment when using multiple antennas," *Wireless Personal Communications*., pp. 311-335, Mar. 1998.

[6] *3rd Generation Partnership Project; Technical Specification Group Radio Access Network; Evolved Universal Terrestrial Radio Access (E-UTRA) Radio Resource Control; Protocol Specification*, 3GPP TS36.331, v8.4.0, 2008.

[7] C. Rowell and E. Y. Lam, "Mobile –phone antenna design," *IEEE Antennas and Propagation Magazine.*, vol. 54, no. 4, pp. 14-34, August 2004.

[8] Z. N. Chen, *Antennas for portable devices*, John Wiley & Sons, 2007.

[9] K. Fujimoto and J. R. James, *Mobile antenna system handbook*, Norwood USA, Artech House, 2nd Edition, 2001.

[10] Z. Ying, "Some important antenna innovations in the mobile terminal industry in the last decade," *Nordic Antenna Symposium*., Sweden, June. 2006.

[11] Y. Huang and K. Boyle, *Antennas: from theory to practice*, John Wiley & Sons, 2008.

[12] Z. Li, Y. Rahmat-Samii and T. Kaiponen, "Bandwidth study of a dual band PIFA on a fixed substrate for wireless communication," *Antennas and Propagation Society International Symposium.*, USA, 2003.

[13] P. Song and P. S. Hall and H. G. Shiraz and D. Wake, "Triple-band planar inverted F antenna," *Antennas and Propagation Society International Symposium*., USA, 1999.

[14] R. Hossa, A. Byndas and M. E. Bialkowski, "Improvement of compact terminal antenna performance by incorprating open-end slots in ground plane," *IEEE Microwave and Wireless Component Letters.*, vol. 14, no. 6, June, 2004.

[15] P. Ciais, R. Staraj, G. Kossiavas, and C. Luxey, "Design of an internal quad-band antenna for mobile phones," *IEEE Microwave and Wireless Components Letters.,* vol. 14, no. 4, pp. 148-150, 2004.

[16] P. Ciais, R., C. Luxey, A. Diallo, R. Starag and G. Kossiavas, "Penta band internal antenna for handset communication devices," *Microwave and Optical Technology Letters.*, vol. 48, no. 8, pp. 1509-1512, 2006.

[17] M. F. Abedin, M. Ali, "Modifying the ground plane and its effect on planar inverted-F antennas (PIFAs) for mobile phone handsets," *IEEE Antenna Wireless Propag. Lett.,* vol. 2, pp. 226-229, 2003.

[18] A. Cabedo, J. Anguera *et al*., "Multiband handset antenna combining a PIFA slots, and ground plane modes ," *IEEE Trans. Antennas Propag.,* vol. 57, no. 9, pp. 2526-2533, 2009.

[19] J. Anguera, I. Sanz *et al*., "Multiband handset antenna with a parallel excitation of PIFA and slot radiators ," *IEEE Trans. Antennas Propag*., vol. 58, no. 2, pp. 348-356, 2010.

[20] Z. Zhang, *Antenna design for mobile devices*, John Wiley & Sons, 2011.

[21] T. Zhang, R. Li *et al*., "A novel multiband planar antenna for GSM/ UMTS/ LTE/ Zigbee/ RFID mobile devices ," *IEEE Trans. Antennas Propag.,* vol. 59, no. 11, pp. 4209-4214, Nov. 2011.

[22] Y. L. Ban, G.H. Chen *et al*., "Low-profile printed octa-band LTE/WWAN mobile phone antenna using embedded parallel resonance structure ," *IEEE Trans. Antennas Propag.,* vol. 61, no. 7, pp. 3889-3894, July. 2013.

[23] K.C. Lin, C. H. Lin *et al.,* "Simple printed multiband antenna with novel parasitic-element design for multistandard mobile phone applications ," *IEEE Trans. Antennas Propag*., vol. 61, no. 1, pp. 488-491, Jan. 2013.

[24] Y. L. Ban, G. H. Chen *et al*., "Small-size printed coupled-fed antenna for eight-band LTE/GSM/UMTS wireless wide area network operation in an internal mobile handset," *IET Micro. Antennas Propag.,* vol. 7, no.6, pp. 399-407, March. 2013.

[25] S. Wang, Z. Du, "A compact octaband printed antenna for mobile handsets," *IEEE Antenna Wireless Propag.* Lett., vol. 12, pp. 1347-1350, 2013.

[26] H. Liu, R. Li *et al.*, "A multi-broadband planar antenna for GSM/UMTS/LTE and WLAN/WiMAX handsets," *IEEE Trans. Antennas Propag.*, vol. 62, no. 5, pp. 2856-2860, May. 2014.

[27] C. I. Lin and K. L Wong., "Printed monopole slot antenna for internal multiband mobile phone antenna," *IEEE Trans. Antennas Propag.*, vol. 55, no. 12, pp. 3690-3697, Dec. 2007.

[28] H. W. Hsieh, Y. C. Lee *et al.*, "Design of multiband antenna for mobile handset operations," *IEEE Antenna Wireless Propag. Lett.*, vol. 8, pp. 200-203, 2009.

[29] K. L. Wong, C. H. Huang, "Printed loop antenna with a perpindicular feed for penta-band mobile phone application," *IEEE Trans. Antennas Propag.*, vol. 56, no. 7, pp. 2138-2141, July 2008.

[30] Y. W. Chi, K. L. Wong, "Internal compact dual-band printed loop antenna for mobile phone application," *IEEE Trans. Antennas Propag.*, vol. 55, no. 5, pp. 1457-1462, May 2007.

[31] X. Zhang, W. Wu *et al*., "Seven band surface-mount loop antenna with a capacitively coupled feed for mobile phone application," *Microwave and Optical Technology Letters.*, vol. 51, no. 1, pp. 81-88, January 2009.

[32] C.-W. Chiu, C.-H. Chang, "Multiband folded loop antenna for smartphones," *Progress in Electromagnetic Research.*, vol. 102, pp. 213-226, 2010.

[33] Z. Zhang, R. J. Hill, R. W, Schlub, J. Zavala and R. Caballero,"Hybrid antennas with directly fed antenna slots for handheld electronic devices," *U.S. Patent 7551142*, June. 23, 2009.

[34] M. Pascolini, R. J. Hill, J. Zavala, N. Jin, Q. Li, R. W. Schlub and R. Caballero,"Bezel gap antennas," *U.S. Patent 8270914*, Sept. 18, 2012.

[35] J. Zhong, K.-K. Chen and X. Sun, "A novel multi-band antenna for mobile phone with metal frame," *8th Internaltional Conference on Wireless Communication, Networking and Mobile Computing (WiCOM).*, China, Sept. 2012.

[36] Q. Gua, R. Mittra *et al*., "Interaction between internal antenna and external antenna of mobile phone and hand effect," *IEEE Trans. Antennas Propag.*, vol. 61, no. 2, pp. 862-870, Feb. 2013.

[37] Z. Miers, H. Li *et al*., "Design of bandwidth-enhanced and multiband MIMO antennas using charactrestic modes," *IEEE Antenna Wireless Propag. Lett.*, vol. 12, pp. 1696-1699, 2013.

[38] Y.-L. Ban, Y.-F. Qiang *et al*., "Low-profile narrow-frame antenna for seven-band WWAN/LTE smartphone applications," *IEEE Antenna Wireless Propag. Lett*., vol. 13, pp. 463-466, 2014.

[39] L. W. Zhang and Y. L. Ban, "A novel hepta-band coupled-fed antenna for WWAN/LTE metal-ring-frame smartphone applications," *Progress in Electromagnetic Research Symposium (PIERS).*, China, Aug. 2014.

[40] H. Li, Z. Miers *et al*., "Design of orthogonal MIMO handset antennas based on charactrestic mode manipulation at frequency band below 1 GHz," *IEEE Trans. Antennas Propag.*, vol. 62, no. 5, pp. 2756-2766, May. 2014.

[41] S. Eom, H. Kim et al., "Embedded antenna for metallic handheld communication devices," *Progress in Electromagnetics Research B.*, vol. 57, pp. 127-138, 2014.

[42] Y.- L. Ban, Y.- F. Qiang *et al*., "A dual-loop antenna design for hepta-band WWAN/LTE metal-rimmed smartphone applications," *IEEE Trans. Antennas Propag.*, vol. 63, no. 1, pp. 48-58, Jan. 2015.

[43] B. K. Lau and Z. Ying, "Antenna design challenges and solutions for compact MIMO terminals," *International Workshop on Antennas Technology (iWAT)., Hong Kong*, March. 2011.

[44] http://www.ieee-ctw.org/2014/slides/session3/Heath-CTW_v6.pdf, [10 Aug 2015].

[45] Z. Ying, "Antennas in cellular phones for mobile communications," *Proceeding of The IEEE.*, vol. 100, no. 7, pp. 2286-2296, July. 2012.

[46] H. Wong, K.-M. Luk *et al.*, "Small antennas in wireless communications," *Proceeding of The IEEE.*, vol. 100, no. 7, pp. 2109-2121, July. 2012.

[47] J. Anguera, A. Andujar et al., "Advances in antenna technology for wireless handheld devices," *International Journal on Antennas and Propagation.*, vol. 2013, Articale ID: 838364, 2013.

[48] A. Petosa, and A. Ittipiboon, "Dielectric Resonator Antennas: A Historical Review and the Current State of the Art," *Antennas and Propagation Magazine, IEEE,* vol. 52, no. 5, pp. 91-116, 2010.

[49] L. Huitema, M. Koubeissi, C. Decroze, and T. Monediere, "Ultrawideband dielectric resonator antenna for DVB-H and GSM applications," *IEEE Antennas and Wireless Propagation Letters*, vol. 8, pp. 1021-1024, 2009.

[50] T-H. Chang, Y-C. Huang, W-F. Su and J-F. Kiang, "Wideband dielectric resonator antenna with a tunnel," *IEEE Antennas and Wireless Propagation Letters*, vol. 7, pp. 275-278, 2008.

[51] G. Bit-Babik, C. Di Nallo, and A. Faraone. "Multimode dielectric resonator antenna of very high permittivity," *IEEE Antennas and Propagation Society International Symposium*, 2004.

[52] M. Rotaru and J. K, Sykulski, "Numerical Investigation on Compact Multimode Dielectric Resonator Antennas of very High Permittivity," *Science, Measurement & Technology, IET,* vol. 3, no. 3, pp. 217-228, 2009.

[53] K. Ishimiya, J. Takada, Z. Ying, "A Compact MIMO DRA Antenna.", *International workshop on antenna technology. IWAT 2008*, pp. 286-289.

[54] C. Oikonomopoulos-Zachos, and B. Rembold, "A 4-Port Antenna for MIMO Channels.", *EuCAP 2007,* pp. 1-4.

[55] L. Z. Thamae, and Z. Wu, "Diversity performance of multiport dielectric resonator antennas," *Institution of Engineering and Technology,* vol. 4, no. 11, pp. 1735-1745, Nov.2010.

[56] Y. Li and K.-M. Luk, "A Water Dense Dielectric Patch Antenna," *IEEE Access*, vol. 3 pp. 274-280, April, 2015.

[57] L. Xing, Y. Huang, Y. Shen, S. ALja'afreh *et al*, "Broadband U-Shaped Water Antenna for DVB-H Applications," *In Proc. IEEE Antennas and Propagation Society International Symposium*, pp. 1930-1931, July, 2014.

[58] M. Karaboikis, C. Soras *et al.,* "Compact dual-printed inverted-F antenna diversity systems for porable wireless devices," *IEEE Antenna Wireless Propag. Lett*., vol. 8, pp. 9-14, 2009.

[59] H. T. Chattha, Y. Huang, S. J. Boyes *et al.*, "Polarization and pattern diversity-Based dual-feed planar inverted-F antenna," *IEEE Transactions on Antennas and Propagation,* vol. 60, no. 3, pp. 1532-1539, 2012.

[60] H. T. Chattha and Y. Huang, "Low profile dual-feed planar inverted-F antenna for wireless LAN applications," *Microwave Optical Technology Letters,* vol. 53, pp. 1382–1386, 2011.

[61] H. T. Chattha, Y. Huang and X. Zhu, "Dual-feed PIFA diversity antenna for wireless applications," *Electronics Letters,* vol. 46, no. 3, pp. 189-190, 2010.

[62] Y. F. Lin, H. M. Chen, C. Y. Lin, *et al.*, "Planar inverted-L antenna with a dielectric resonator feed in a mobile device," *IEEE Trans. Antennas Propag.,* vol. 57, no. 10, pp. 3342-3346, 2009.

[63] Z. N. Chen, "Impedance characteristics of probe-fed L-shaped plate antenna," R*adio Science*, vol. 36, no. 6, pp. 1377-1384, 2001.

[64] J. Anguera, A. Andujar and . Garcia, "Multiband and small coplanar antenna system for wireless handheld devices," *IEEE Trans. Antennas Propag.,* vol. 61, no. 7, pp. 3782-3789, 2013.

[65] S. Eom, M. Ali, S. O. Park and H. Kim, "Embedded antenna for metallic handheld communication devices," *Progress in Electromagnetics Research B.,* vol. 57, pp. 127-138, 2014.

[66] Y. L. Ban, Y. F. Qiang *et al*, "A dual-loop antenna design for hepta-band WWAN/LTE metal-rimmed smartphone applications," *IEEE Trans. Antennas Propag.*, vol. 63, no. 1, pp. 48-58, 2015.

[67] H. Li, Z. Miers and B. K. Lau., "Design of orthogonal MIMO handset antennas Based on characteristic mode manipulation at frequency bands below 1 GHz," *IEEE Trans. Antennas Propag.,* vol. 62, no. 5, pp. 2756-2766, 2014.

[68] Z. Miers, H. Li and B. K. Kiong., "Design of bandwidth-enhanced and multiban MIMO antennas using characteristcs modes," *IEEE Antenna Wireless Propag. Lett.,* vol. 12, pp. 1696-1699, 2013.

Chapter 2: MIMO Antenna Systems

The introduction of MIMO technology has revolutionized wireless communications over the past decade. Multiple antenna systems are now used at the base station, and have also received a great research attention in the design of compact mobile phones. This chapter starts with an overview about MIMO system; only two important MIMO techniques (spatial multiplexing and spatial diversity) are described with their benefits on the wireless system performance. The third MIMO technique which is called beamforming is not considered as it addresses the signal processing rather than antenna design. Then, as this thesis is focused on the MIMO antenna design based on diversity scheme, mainly on the antenna diversity, the mechanism of antenna diversity, the diversity combining techniques, diversity performance parameters and the decoupling techniques are only discussed and presented in more detail. Also, some of the experimental works of the measurement of both diversity gain and total radiation efficiency are summarized.

2.1 MIMO Systems

The conventional wireless communication system usually uses one antenna element at both the transmitter and the receiver; this system is called single input single output (SISO) system as shown in Fig. 2.1. Although this system is very simple (usually it does not need advanced signal processing), but the received signal quality (SNR) from a severe radio multipath channel is usually an attenuated version of the transmitted one, which makes the system reliability very poor. Also, based on the Shannon-Nyquist criterion [1]; the throughput of SISO depends on both the received signal to noise ratio and the channel bandwidth (usually narrowband). This adds a difficulty in the receiver side to get more data throughput and more reliability.

To enhance the wireless system reliability and to reduce impact of fading, antenna diversity was the effective technique that has been used widely. SISO system was evolved to a single input multiple output (SIMO) system by introducing the receive diversity in 1931 [2, 3], it has been applied in different wireless applications for more than 70 years [4]. By the beginning of 1990s, a new type of multi-antenna techniques was developed by [5], this technique was used transmit diversity to develop a multiple input single output (MISO) system; it has been deployed in the 2G mobile system to enhance the radio coverage of base stations (down link channel).

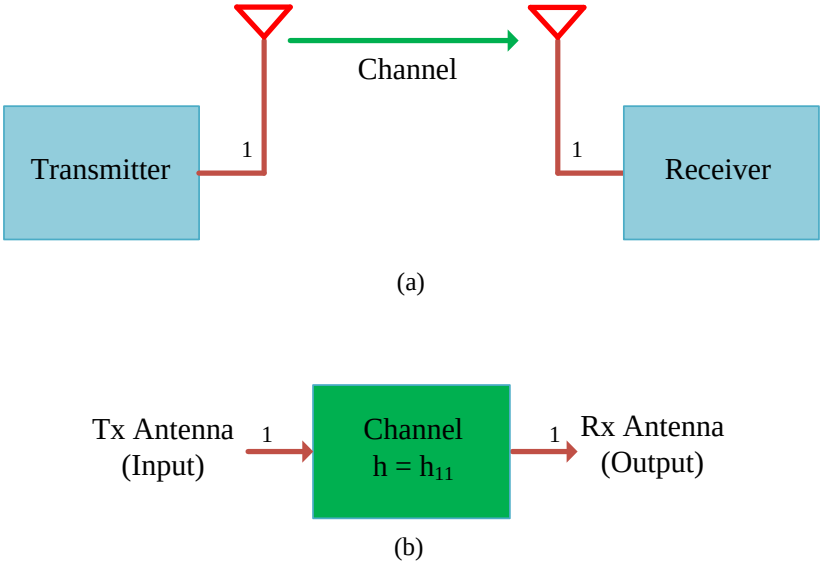

Fig. 2.1: (a) Single input and single output (SISO) system and

(b) SISO from channel perspective

In the late of 1990s, a great breakthrough in the wireless communication system has been conducted with the introduction of the MIMO technology by Foschini [6, 7]. Foschini and his research group not only used spatial diversity to combat the fading, they developed a new way of exploiting fading (spatial multiplexing) to support and enhance the throughput capacity [5]. Since these initial breakthroughs, MIMO technology has been adopted in different commercial wireless applications and standards like: WiMAX in 2005, 4G LTE mobile systems in 2010. Also, both spatial diversity and spatial multiplexing became the most important landmarks and techniques of this new wireless technology (MIMO).

In a MIMO system both the transmitter and the receiver need multiple antenna elements; Fig. 2.2 represents a MIMO system with an M transmit antennas and N receive antennas. It can be seen that the channel response is no longer described by the single channel response as in the case of SISO (see Fig. 2.1(b)); the channel response is now described by a channel matrix H as expressed in Fig. 2.2(b), where h_{ij} is the complex transmission coefficient represents the individual channel between Tx-Rx antennas.

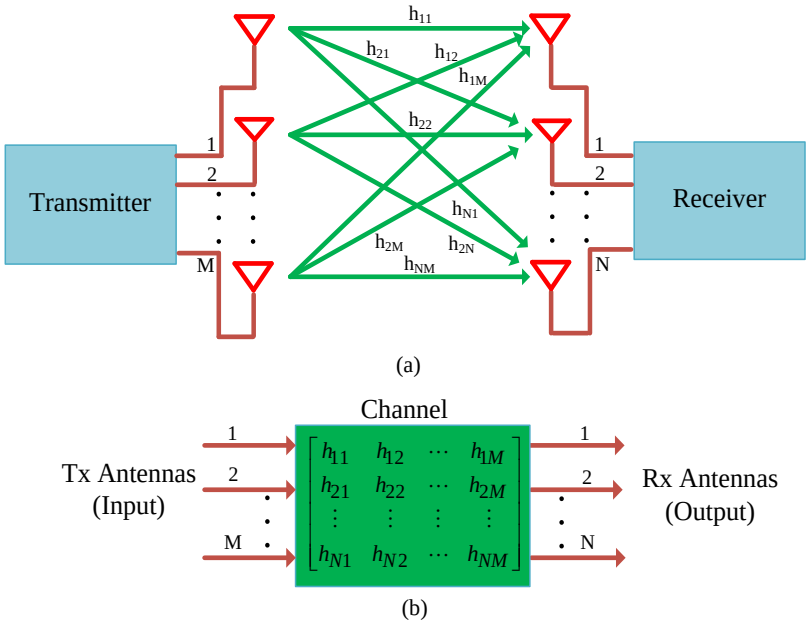

Fig. 2.2: (a) Multiple input multiple output (MIMO) system and

(b) MIMO from channel perspective

2.1.1 Spatial Multiplexing and Channel Capacity

Spatial multiplexing (SM) is one of the most important MIMO techniques. It transmits multiple parallel data streams in multiple data channels over the same frequency band and time slot. One of the most important feature of this technique over other multiplexing techniques (frequency division multiplexing (FDM), time division multiplexing (TDM) and code division multiplexing (CDM)) is that it does not suffer from bandwidth expansion because of assigning multiple signals to different spatial channels [4]. To demonstrate the basic principle of SM, Fig. 2.3 shows a MIMO system with 2×2 elements. As shown, the data bit stream is transformed into parallel sub-streams via serial to parallel (S/P) converter, then the sub-streams are modulated and transmitted simultaneously from each transmit antenna element. If the antennas at both transmitter and receiver are separated far apart,; this means that the propagated channels are uncorrelated and thus the received signals are well separated at the receiver side. After demodulating the original sub-streams, they are combined via P/S converter to produce the original main data stream.

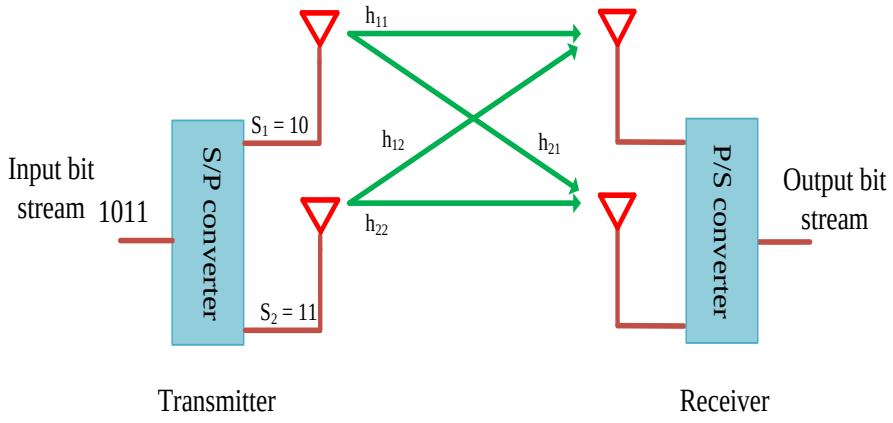

Fig. 2.3: MIMO with spatial multiplexing

Therefore, the SM increases the channel capacity with increasing the number of transmit and receive antennas [6, 7]. For a general case of MIMO system like in Fig. 2.2, with the number of transmit elements M and the number of receive elements N, the maximum number of parallel pipes (data streams) will be:

$$N_{\max} = \min(M, N) \tag{2.1}$$

The resulting channel capacity using SM depends on whether the transmitter has information about the channel state or not, the simplest case which is the case with no information is only discussed. If the channel state is not known at the transmitter, then the transmitter will power all the antennas equally and the resulting channel capacity is [7]:

$$C = \log_2 \det\left[I_N + \frac{\rho}{M} H.H^H \right] \quad \text{[bit/sec/Hz]} \tag{2.2}$$

where ρ denotes the average signal to noise ratio (SNR) at each receiver; *det* is the determinant operator; I_N denotes the identity matrix and H is the normalized channel matrix of $N \times M$ size.

The very interesting benchmark of this technique lies on the exploiting the multipath phenomena in increasing the channel capacity; both the multipath and scattering are very important for SM to work efficiently. This can be shown from Eq (2.3) after applying the eigenvalue decomposition on $H.H^H$ and substituting in Eq (2.2)

$$C = \sum_{i=1}^{r} \log_2 \left[1 + \frac{\rho}{M} \lambda_i \right] \quad \text{[bit/sec/Hz]} \tag{2.3}$$

where *r* is the rank of the channel matrix; represents the positive eigenvalue of $H.H^H$. It is obviously clear from Eq (2.3) that the capacity of MIMO channel is the sum of the capacity of *r* SISO channels. Thus, the multipath channel is no longer an undesirable environment; it is highly demanded for MIMO technology

2.1.2 Spatial Diversity and Diversity Gain

As it has just explained, the SM MIMO technique is used to increase the channel capacity of wireless communication systems. In order to achieve the second aim of MIMO technology (increasing the reliability of wireless systems), diversity techniques are usually used. Different from SM techniques, Fig. 2.4 shows that the spatial diversity (diversity techniques) combat the multipath fading via sending multiple versions of the same transmitted signal to the receiver through the multipath channel. As shown in Fig. 2.4(b), each version of the transmitted signal is received through an independent channel. If the fade in each of these channels is uncorrelated with the other, then the possibility of getting simultaneous (see Fig. 2.4(b)) deep fade in each channel is greatly reduced. Therefore, if one the diversity combining techniques is deployed at the receiver, the receiver can have more freedom in choosing the best received signal quality (best SNR), which will improve the reliability of the wireless system. This improvement is usually called the diversity gain which is the improvement in the received SNR at the output of the diversity combiner relative to the SNR resulted from a reference single antenna at a certain level of performance criterion such as cumulative probability function [8, 9]. If the branch with the best SNR is selected as a reference antenna, the diversity gain at a probability level $P(\gamma_c)$ is called apparent DG as in the following:

$$DG = \left. \frac{\left(\frac{\gamma_c}{\Gamma_c} \right)}{\left(\frac{\gamma_s}{\Gamma} \right)_{best}} \right|_{P(\gamma_c)} \tag{2.4}$$

where γ_c and γ_s are instantaneous SNRs in both the combined and single branch signals, respectively, Γ_c and Γ are mean SNRs and the typical probability $P(\gamma_c)$ usually is 0.01 (0.99 reliability).

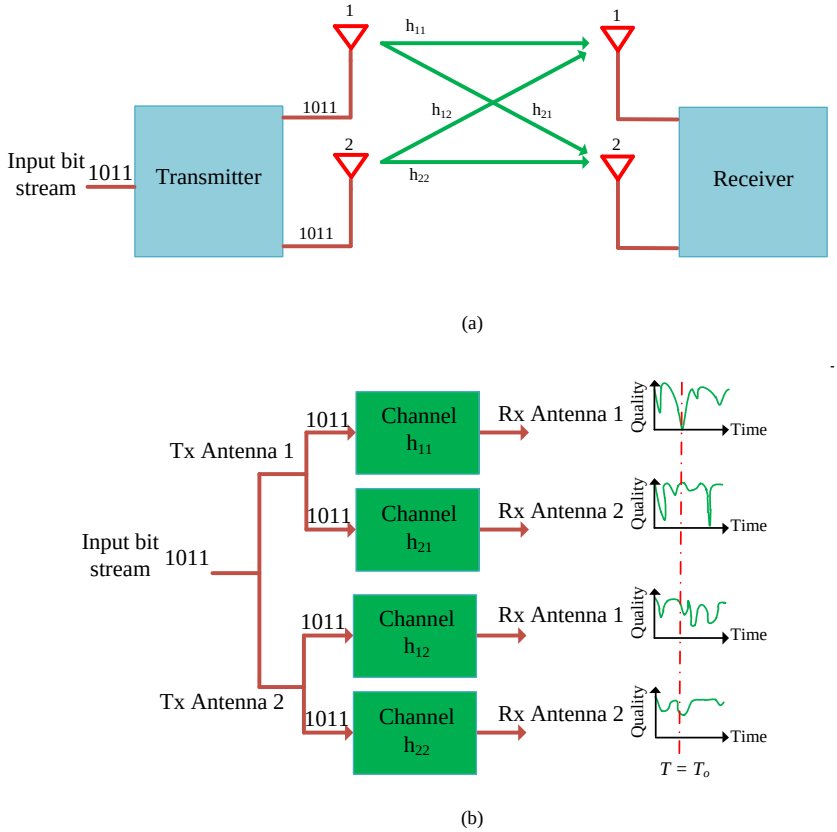

Fig. 2.4: (a) MIMO with spatial diversity and (b) Spatial diversity from a channel perspective (combat fading)

Since the received signal from the multipath radio channel with no line of sight (NLOS) is statistically followed Rayleigh distribution function, the cumulative distribution function (CDF) of a Rayleigh channel is given by

$$P(\gamma \le \gamma_s) = \left[1 - e^{\frac{-\gamma_s}{\Gamma}}\right] \tag{2.5}$$

Let N independent Rayleigh fading channels available at the receiver. Assume each branch has the same SNR mean Γ and the selective combining scheme is used at the receiver, then the probability that all N independent diversity branches receive signals with instantaneous SNR γ and below threshold γ_s is

$$P(\gamma \le \gamma_s) = \left[1 - e^{\frac{-\gamma_s}{\Gamma}}\right]^N \tag{2.6}$$

Equations (2.5) and (2.6) are plotted in Fig. 2.5 to show the probability distributions of relative SNR threshold for N branches with the use of selectivity combining technique. The concept of diversity gain in (2.4) is also illustrated in the graph at 1% probability. The figure shows that there are 10, 13, and 16 dB DGs for two branches, three branches and four branches, respectively.

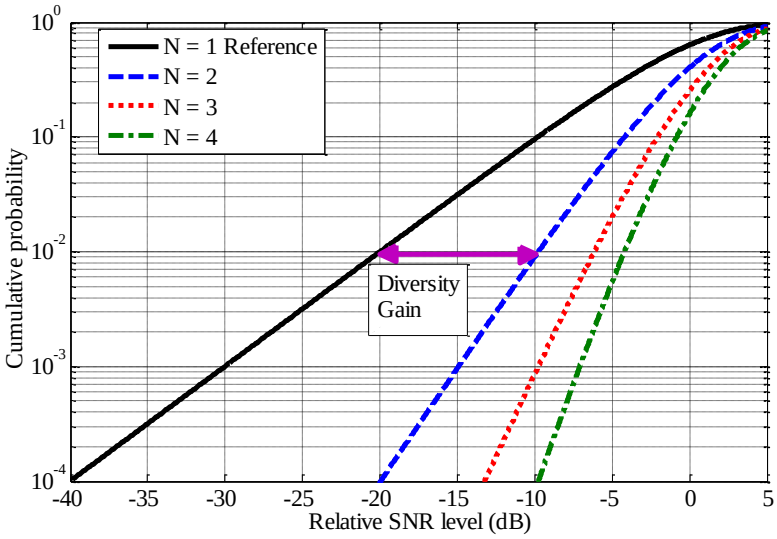

Fig. 2.5: Cumulative distribution functions of relative SNR threshold for N different diversity branches

In this thesis, the work is only focused on the design of MIMO /diversity antennas for mobile phone applications. Therefore, the rest of this chapter addresses the diversity system in detail like: types of diversity techniques; types of diversity combining techniques; diversity system performance parameters and the common decoupling techniques (isolation techniques) used for the design of compact diversity antennas.

2.2 Antenna Diversity Techniques

To reduce the spatial correlation between antennas and to generate replicas of a signal for diversity purposes, the frequency diversity, time diversity and antenna diversity are used widely. As this thesis is concerned on antenna diversity, this section only discusses antenna diversity techniques like: space diversity, angle (pattern) diversity and polarization diversity.

2.2.1 Space Diversity

It is the most common and the simplest diversity technique, it utilizes two or more sufficient spaced antennas as shown in Fig. 2.6. With this separation, the phase delay (difference) will make the multipath received signals arriving at the receive antennas differ in fading depth. For better diversity performance, the received signals by various antenna elements must have a spatial correlation coefficient minimum as much as possible. To address this, several models have been studied the spatial correlation. Initially, Clarke's model studied the spatial correlation caused by only the angular distribution of the received waves [10]; the results showed that for the case of uniformly arrived waves in the azimuth plane (mobile phone scenario), the minimum spacing between antenna elements at a mobile phone should be 0.5 wavelengths, calculated from the zero order Bessel function [8, 11]. Recently, the trend of the mobile phone design is to find a small and compact device; this requires closely spaced antenna elements. However, it has been reported that the spatial diversity performance is enhanced when the multiple antennas are closely spaced down to 0.2 wavelengths and even below this [12, 13]. It is obviously known that the mutual coupling is the effective source of the spatial correlation. To incorporate this, an impedance matrix approach adopted in [14], the correlation under mutual coupling is expressed as a function of the correlation without coupling and the impedance matrix. It has been found that the spatial correlation coefficient can be decreased further with a small distance separation. This difference is linked to the interaction between mutual coupling and the angular distribution of the incoming received wave which could lead to decrease the spatial correlation coefficient with Clarke's model (mobile phone case) [15], or to increase it with circular model [16] that represent base station case. Due to this interaction, the space diversity is no longer considered as the main diversity scheme for the case of closely spaced antennas; the effect of the angle or pattern diversity starts to appear [17]. This and more about the pattern diversity are explained in the next sub-section.

2.2.2 Pattern (Angle) Diversity

The diversity gain can be large if multiple antennas have different patterns. This kind of diversity can guarantee a reception of different sets of multipath wave [18]. Pattern diversity has been used at base stations [19, 20], a similar performance to that of spatial diversity was achieved, especially, in dense urban areas [19, 20]. Referring to mobile handsets, which become smaller and smaller, pattern diversity, is more wanted than spatial one [18]. It has been implemented using different approaches: external circuitry like: a 90^{o}

hybrid was used for combining the output signals from two collocated antennas [21], this yielded two directional patterns with opposite beam maxima directions. To save much space and achieve pattern diversity, switch parasitic techniques has been proposed by Vaughan in [17], it is simply done by making the parasitic antenna switched between two different terminations like open/ground [17], or optimized different load impedances as in [18]. Fig. 2.7 shows an example of a dual-element antenna that utilizes the pattern diversity.

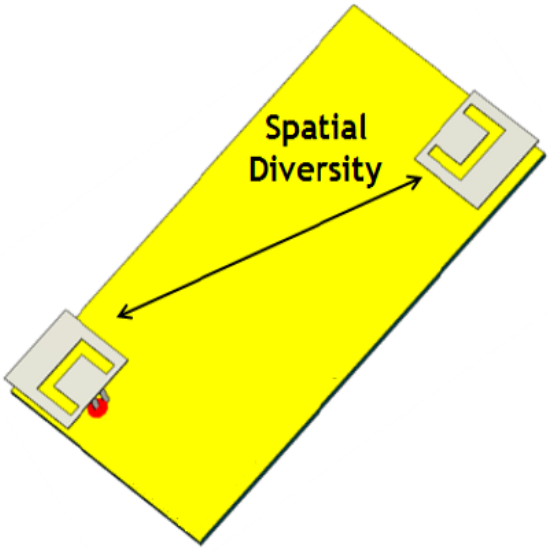

Fig. 2.6: Space (spatial) diversity [22]

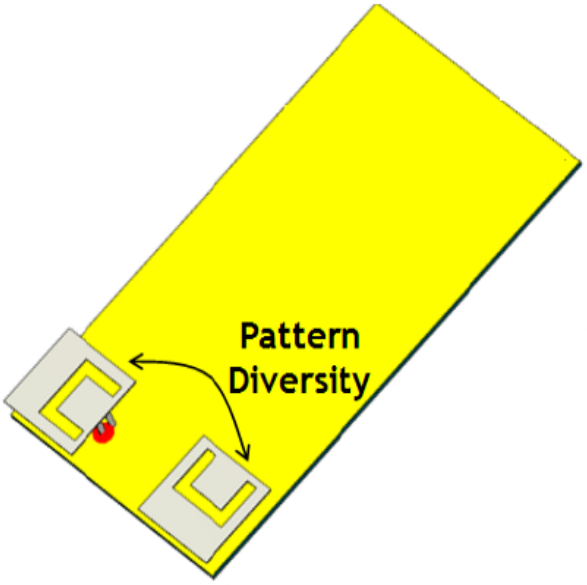

Fig. 2.7: Pattern (angle) diversity [22]

2.2.3 Polarization Diversity

Polarization diversity can be achieved when two or more differently polarized antennas are used as the branch of a diversity receiver or transmitter. It has been shown that the use of polarization diversity at the base stations is very effective in high multipath environments as spatial diversity [23], the space and cost are also can be achieved [21, 22]. Thus, a number of studies have been carried out at the base stations [24-26]. For recent mobile terminals, due to the reduced size of the antenna structures, antenna diversity has been moving toward polarization diversity instead of using conventional spatial diversity [27]. Therefore, a number of recent studies have been deployed polarization diversity to achieve a very compact MIMO antenna system for handset applications [28-30]. Fig. 2.8 shows one example of using the polarization diversity at a mobile terminal, in which one of the elements represents a monopole antenna while the other is a magnetic dipole antenna (loop antenna).

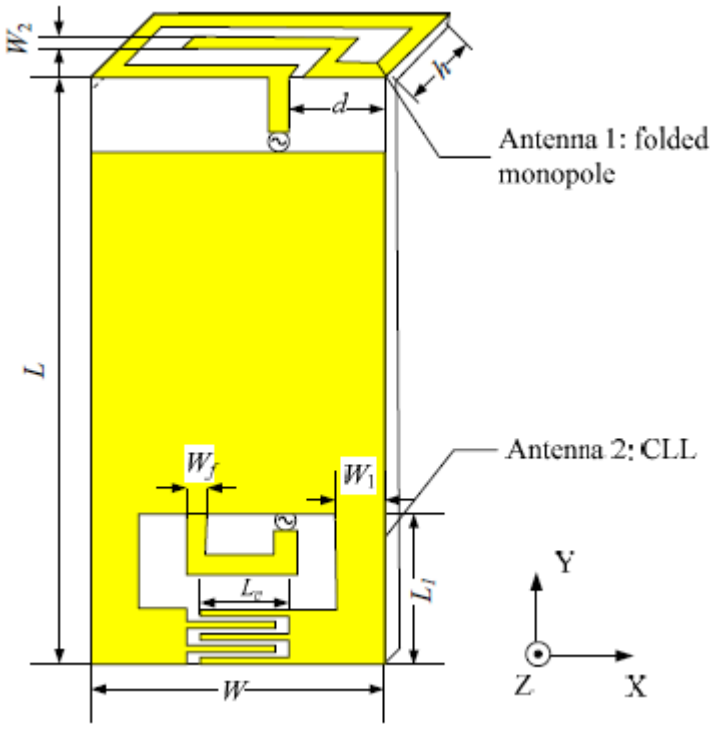

Fig. 2.8: Polarization diversity [27]

2.3 Diversity Combining Techniques

After receiving independent replicas of the signal, diversity combining is required to process signals from different branches and to obtain the best version of the received signal at the output. Four different diversity combining techniques are usually used: Switched combining, selection combining (SC), equal gain combining (EGC) and maximal ratio combining (MRC) [31].

For the switched combining, it uses only one receiver between branches. Based on a predefined threshold, the receiver is switched to other branches only when the SNR of the selected branch is lower than the threshold. In comparison to other combining schemes, this scheme is a cost effective and very suitable for using in mobile devices [32]. However, this method is less efficient method, since it selects one branch a time, and the branch with the highest SNR may not be selected.

SC technique is an improved method relative to the switched combining method. The only difference is in the use of a number of receivers equal to the number of branches. It monitors instantaneous SNRs at all branches and always chooses the one with the highest SNR ratio. In comparison to the other schemes, SC has the simplest signal processing hardware. Therefore, the selection combining (SC) technique has been applied with respect to all diversity gain results in this thesis.

In comparison to the receivers that use either selective or switched combining schemes, receivers with EGC are more smart; this because they have a phase information of the channel of each branch. Signals from all branches are summed coherently. As the signal from each branch is not in-phase with other, phase compensation is added to each branch before combining.

In order to increase the overall SNR at the output, MRC is the optimal combining method. Unlike EGC, MRC makes a good use of the good branches (with high SNR), this is done by multiplying the branches having higher SNRs with high weights. However, this method works efficiently only for high SNR scenarios, since the channel cannot be accurately estimated. Also, compared with other combining schemes, it is very expensive.

2.4 Key Figure of Merits of MIMO Antennas

By the introduction of MIMO technology, the design of multiple antennas at both the mobile terminal and the base station has received a great research attention. In addition to the new design challenges that are brought by implementing multiple antennas in compact mobile devices, this new technology created more performance parameters than those of a conventional single antenna system. While single antenna metrics such as total radiation efficiency, radiation patterns, reflection coefficient and operating bandwidth are required to characterize MIMO antennas [33], new metrics are added such as: S-parameter matrix that contains both the reflection coefficients (S_{ii}) and the transmission coefficients (S_{ij}), diversity conditions like the correlation coefficient and the branch power ratio (power balance), diversity gain, channel capacity and embedded element efficiency [34]. Based on these passive performance parameters, it is worth mentioning that all the designs in this thesis are evaluated.

2.4.1 Impedance Matrix and Scattering Parameter Matrix

The presence of multiple antennas near each other creates an interaction among them, this is called mutual coupling [35]. This coupling can be represented as an induced current flowing on one antenna element from the excitation of the other antenna element. This alters both the input impedance of each antenna element in which the input impedance is defined by both self-impedance and mutual impedance. This change produces an impedance matrix which contains both the self-impedances (Z_{ii}) and the mutual impedances (Z_{ij}) as shown in (2.7).

$$Z = \begin{bmatrix} Z_{11} & \cdots & Z_{1j} \\ \vdots & \ddots & \vdots \\ Z_{i1} & \cdots & Z_{ii} \end{bmatrix} \tag{2.7}$$

As an inevitable result to the creation of the impedance matrix, antenna bandwidth is no longer governed by only the reflection coefficient. It depends on both reflection coefficients and the transmission coefficients in the S-parameter matrix as in (2.8). S_{ii} is the ratio of the reflected wave voltage to the incident one at the port of i^{th} element when all other elements are terminated with matched loads. While S_{ij} represent the ratio of the transferred

voltage from j^{th} element port to the i^{th} element port to the incident voltage at j^{th} element port, S_{ij} is also known as the mutual coupling coefficient.

$$S = \begin{bmatrix} S_{11} & \cdots & S_{1j} \\ \vdots & \ddots & \vdots \\ S_{i1} & \cdots & S_{ii} \end{bmatrix} \tag{2.8}$$

2.4.2 Correlation Coefficient

Up to this point, it has been mentioned many times that in order to achieve a good MIMO and diversity performance, the received signals at the receiver of the diversity system should be independent from each other. This independence can be measured and quantified using the correlation coefficient [34, 36-38].

The correlation coefficient can be described by two forms: complex (ρ_{12}) and envelope (ρ_e) correlation coefficients. These two forms are related to each other as shown from Eq (2.9)

$$\rho_e = \left|\rho_{12}\right|^2 \tag{2.9}$$

The complex correlation coefficient (ρ_{12}) between two antennas can be calculated in the angular domain as follows [37, 39]:

$$\rho_{12} = \frac{\int_0^{\pi}\int_0^{2\pi}\left[XPR.E_{\theta 1}(\theta,\phi).E^*_{\theta 2}(\theta,\phi).P_\theta(\theta,\phi) + E_{\phi 1}(\theta,\phi).E^*_{\phi 2}(\theta,\phi).P_\phi(\theta,\phi)\right].\sin(\theta)d_\phi d\theta}{\sqrt{\sigma_1^2\sigma_2^2}} \tag{2.10}$$

where the variance σ_n^2 is the power of the signal in branch n and it can be calculated as follow:

$$\sigma_n^2 = \int_0^{\pi}\int_0^{2\pi}\left[XPR.E_{\theta n}(\theta,\phi).E^*_{\theta n}(\theta,\phi).P_{\theta n}(\theta,\phi) + E_{\phi 1}(\theta,\phi).E^*_{\phi 2}(\theta,\phi).P_\phi(\theta,\phi)\right]\sin(\theta)d_\phi d_\theta \tag{2.11}$$

where XPR is the cross polarization ratio as in Eq (2.12), it is defined as the ratio of time average vertical power (P_v) to time average horizontal power (P_H) in a multipath fading environment [36]. $E_{\theta n}$ and $E_{\phi n}$ are the far field components. P_θ and P_ϕ are the angular density functions of the vertical and horizontal plane, respectively.

$$XPR = \frac{P_v}{P_H} \tag{2.12}$$

Experimentally, calculation of the correlation coefficient using the pattern approach in the above is time consuming as it needs 3D radiation pattern (which is also hard to obtain accurately in practice). Therefore, the correlation coefficient can be defined in another form which is the envelope correlation coefficient (ECC or ρ_e). This can be done using S-parameters approach [40] as shown below:

$$\rho_e = \frac{\left|S_{11}^* S_{12} + S_{21}^* S_{22}\right|^2}{\left(1-\left|S_{11}\right|^2-\left|S_{21}\right|^2\right)\left(1-\left|S_{22}\right|^2-\left|S_{12}\right|^2\right)} \tag{2.13}$$

where ρ_e is linked to ρ_{12} by the following:

$$\rho_e = \left|\rho_{12}\right|^2 \tag{2.14}$$

Although the S-parameters approach in [40] is a very simple and fast, it is only accurate for the case of loss free antennas. Therefore, the S-parameter method has been modified in which the effect of the radiation efficiency has been taken into account [41]. Eq (2.15) represents this new method which is used widely in the calculation of the ECC [42, 43].

$$\rho_e = \left| \frac{\left|(S_{11}^* S_{12} + S_{22} S_{21}^*)\right|}{\left|(1-\left|S_{11}\right|^2-\left|S_{21}\right|^2).(1-\left|S_{22}\right|^2-\left|S_{12}\right|^2)\eta_{rad1}.\eta_{rad2}\right|^{0.5}} \right|^2 \tag{2.15}$$

For a good diversity gain, the ECC between received signals should satisfy the ECC condition [36, 37] as follows:

$$\rho_e < 0.5 \tag{2.16}$$

2.4.3 Branch Power Ratio and Mean Effective Gain

In addition to the ECC, the amount of reduction in signal fading (good diversity gain) depends on a second condition which is the branch power ratio; it is a measure of the power difference between feeds/ports in the antenna diversity system. This condition can be expressed using the ratio of two branch power levels k as follows:

$$k = \left| \frac{P_1}{P_2} \right| \cong 0dB \tag{2.17}$$

where P_i *[W]* is the power from the i[th] antenna, *k* is the branch power ratio.

An alternative method to obtain the branch power ratio is derived from the mean effective gain (MEG) of the antennas as follows (assuming only two branches) [36, 37]:

$$k = \left| \frac{MEG_1}{MEG_2} \right| \cong 0dB \tag{2.18}$$

where *k* is the branch power ratio and *MEG* is the mean effective gain.

For the ideal case of antenna diversity, *k* should equal to unity (0 dB). Practically, it has been found that for a low *ECC*, *k* should be less than 3 dB to avoid a significant loss in the diversity gain [36, 37].

MEG for an antenna is defined as the ratio of the mean received power to the total mean incident power. It depends on several parameters such as the radiation power pattern, total antenna efficiency and the propagation characteristics of the mobile communication environment [44]; it can be calculated using the following equation:

$$MEG = \int_0^{2\pi} \int_0^{\pi} \left[\frac{XPR}{XPR+1} G_\theta(\theta,\varphi).P_\theta(\theta,\varphi) + \frac{1}{XPR+1} G\varphi(\theta,\varphi).P_\varphi(\theta,\varphi) \right] \sin(\theta).d\theta.d\varphi \tag{2.19}$$

where *XPR* is the cross polarization ratio of average power of incident field in different polarization states, G_θ and G_Φ are θ and Φ components of antenna power gain, and P_θ and P_Φ represent θ and Φ components of angular density functions of the incident power, respectively. All these parameters are strongly dependent on the statistical and propagation characteristics of the communication environment.

Several propagation scenarios have been discussed (indoor, outdoor and isotropic) based on statistical models like Gaussian, Laplacian and uniform distribution models [45, 46]. In this thesis, the value of branch power ratio is calculated in a Gaussian environment with typical statistical values for indoor and outdoor (urban outdoor) environments [45, 46]. Table 2.1 summarizes the values of statistical parameters for each environment

Table 2.1 Propagation models used in this thesis

Environment	Statistical parameters				
	σ_V	σ_H	m_V	m_H	XPR
Gaussian/ Indoor	30^0	30^0	20^0	20^0	1 dB
Gaussian/ Outdoor	15^0	15^0	10^0	10^0	6 dB

* m_V and m_H are mean elevation angles of the vertical and horizontal polarized wave distribution, while σ_V and σ_H are the standard deviation of the vertical and horizontal polarized wave distribution [45,46].

2.4.4 Diversity Gain and Measurement in a Reverberation Chamber

As previously described in Section 2.1.2, the diversity gain (DG) can be expressed as the improvement in the SNR at the output of a diversity combiner compared to the input of the diversity antenna at a given CDF level (usually 1%). Different definitions and types of diversity gain have been proposed like: apparent DG, effective DG and actual DG [47-49]. However, in this thesis, we are interested in the apparent diversity gain with the selection combining technique. Apparent DG is defined as the difference between the power levels in dB scale at a given cumulative probability level between the CDF of a combined signal and the CDF of a signal at the antenna port with the strongest average level [47-49].

As the DG in the MIMO and diversity system can only be achieved in a multipath radio channel, reverberation chambers (RC) are usually used to mimic the multipath channel [49]. The RC is a large metallic cavity with at least a stirrer works in an over mode condition. Due to multiple reflected waves, the RC becomes a rich scattering environment like the urban outdoor and indoor multipath environments. Fig. 2.9 shows the RC at the University of Liverpool. It is constructed from aluminium panels and its dimensions are *3.6 m × 4.0 m × 5.8 m*. It is equipped with two principal sets of mechanical stirring paddles: vertical stirrer and horizontal stirrer to stir vertically polarized waves and horizontally polarized waves, respectively.

The DG can be acquired and calculated from either CDFs or the measured envelope correlation coefficient between two or more antennas in the RC. The following subsections explain these two methods.

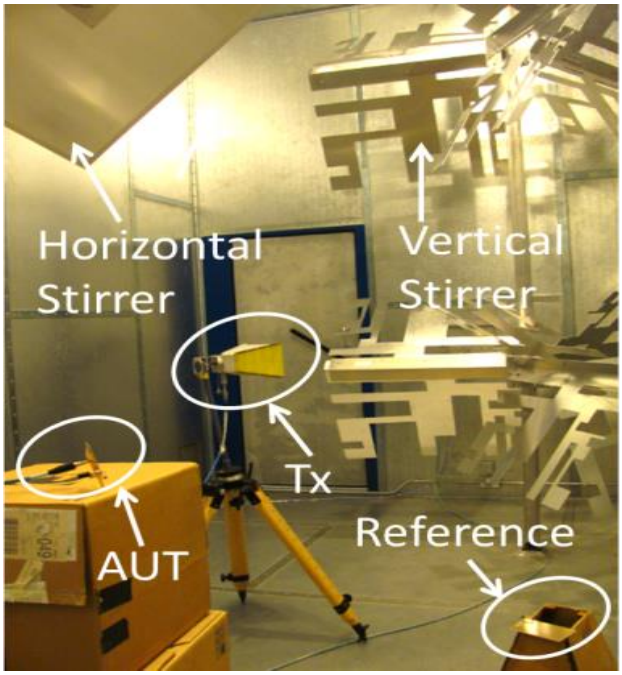

Fig. 2.9: Diversity gain measurement setup in a RC

2.4.4.1 Diversity Gain from CDF's

The general procedure and the post processing of the diversity gain measurement is described here, which was utilized to acquire the results presented in chapters 4, 5 and 6. Table 2.2 details the parameters and types of antennas used in every measurement.

Table 2.2 Measurement parameters for the diversity gain

Parameter	Description
Frequency (GHz)	2.0-4.0 for Chapter 4 1.0-4.0 for Chapter 5 1.0-4.0 for Chapter 6
Stirring sequence	1 degree mechanical stirring
Number of frequency data points	10001
Reference antenna	Satimo SH2000 for Chapter 4 Homemade PILA* for Chapter 5 Homemade PILA* for Chapter 6
Transmitting antenna	R&S HF 906

* The single element planar inverted-L antenna presented in chapter 5 [51]

For every design, the measurement procedure was as follows [52]:

1) Full 2 port calibration of the VNA over the desired frequency band.
2) Place all the antennas (reference, AUT and Tx antennas) inside the chamber to keep the chamber Q factor constant.
3) Connect the Tx antenna to the VNA port 1 and the reference antenna to port 2, load the AUT with a 50 Ohm termination, and collect the full S-parameters (S_{11Tx}, $S_{21\mathrm{Re}f}$, $S_{22\mathrm{Re}f}$) for each stirrer position.
4) Connect the AUT branch *a* to port 2, load the reference antenna and AUT branch b with a 50 Ohm termination, collect S-parameters S_{21a} for each stirrer position.
5) Repeat Step 4) with port 2 connected to the AUT branch b while AUT branch a with a 50 Ohm termination and collect S-parameters S_{21b} for each stirrer position.

After collecting all the S-parameters from each branch (the total number of samples 359 × 10001 = 3590359), a transfer function is established from the reference antenna measurement as follows:

$$T_{\mathrm{Re}f} = \frac{\left\langle \left| S_{21\mathrm{Re}f,s} \right|^2 \right\rangle}{\left(1-\left|\left\langle S_{11Tx}\right\rangle\right|^2\right)\left(1-\left|\left\langle S_{22\mathrm{Re}f}\right\rangle\right|^2\right)} \tag{2.20}$$

where S_{11Tx} is the reflection coefficient of the transmitting antenna, $S_{22\mathrm{Re}f}$ is the reflection coefficient of the reference antenna and $S_{21\mathrm{Re}f,s}$ is the stirred part of the *S*-parameter [51]

$$S_{*,S} = S_* - \left\langle S_* \right\rangle \tag{2.21}$$

where * can be any *S*-parameter combination, $\langle * \rangle$ means the average value of *S*-parameter using any stirring method

Then, the normalised channel samples of both branches are calculated as follows:

$$h_{21a} = \left|S_{21a,s}\right| \sqrt{\frac{\eta_{\mathrm{Re}f}\left(1-\left|\left\langle S_{11Tx}\right\rangle\right|^2\right)}{T_{\mathrm{Re}f}}} \tag{2.22}$$

$$h_{21b} = \left|S_{21b,s}\right| \sqrt{\frac{\eta_{\mathrm{Re}f}\left(1-\left|\left\langle S_{11Tx}\right\rangle\right|^2\right)}{T_{\mathrm{Re}f}}} \tag{2.23}$$

where $\eta_{\mathrm{Re}f}$ is the radiation efficiency of the reference antenna, $T_{\mathrm{Re}f}$ is the chamber transfer function measured by using the reference antenna.

By using the selection combining technique, the combined channel samples are obtained as follows:

$$h_{com} = \max\left(h_{21a}, h_{21b}\right) \tag{2.24}$$

Then, the CDF function for each channel sample is generated with respect to the power level in dB scale. Please note the results in Chapters 4, 5 and 6 are based on this measurement and on the definition of the apparent diversity gain at 1 % CDF level as explained in Section 2.1.2.

2.4.4.2 Diversity Gain from Correlation

Although the diversity gain can be easily predicted from the measured and calculated CDF's, some information such as the frequency range is lost during the post processing and the generation of CDFs. In many cases, it could be important to know how the diversity gain varies as a function of frequency. To achieve this, the envelope correlation coefficient between measured samples from each diversity branch can be calculated using Eq (2.15) and used for the calculation of the diversity gain as in Eq (2.25) [53]. It is worth mentioning that the diversity gain results in Chapter 3 and Chapter 7 are based on this method.

$$DG = 10.48\sqrt{1-\rho^2} \tag{2.25}$$

2.4.5 Far-Field Radiation Patterns and Measurements

The radiation pattern of an antenna is a plot of the radiated field or power as a function of the angle at a fixed distance which should be large enough to be considered as far field [48]. In the area of MIMO and diversity antennas, the embedded element pattern- which is defined as the radiation pattern of antenna element under test (port under test), while other elements (ports) are terminated with matched 50 Ohms loads. It plays an important role in analysis of the diversity antenna [48].

In this thesis, a semi-anechoic chamber (SAC) is used to make the far-field antenna pattern measurements. The chamber is a metallic room whose internal walls and ceiling are

lined with material (made of carbon-loaded polyurethane foam) that absorbs electromagnetic energy in the frequency range of interest. It is intended to simulate an open area test site (OATS). A picture of an anechoic chamber at the University of Liverpool is shown in Fig. 2.10, which has dimensions of $6 \times 3.5 \times 3$ m^3. The source antenna is placed at one end of the chamber acting as a transmitting antenna, and the AUT is put at the other end as a receiving antenna, a separation of 3 m is set to promise the far field criteria. The AUT is usually mounted on a positioner, rotating in the azimuth plane to obtain a two-dimensional (2D) radiation pattern. The embedded pattern for each antenna element or antenna port is collected by the received transmission S-parameters during the rotation, while other antenna elements (ports) are terminated with matched loads. An automatic control system has been set up to record the data, which is given in Fig. 2.11. The turntable positioner, plotter, VNA is all under PC's control. Each time, the PC instructs the positioner to rotate, and triggers a sweep from the VNA, then reads the data into the software. This process is repeated until the measurement is finished.

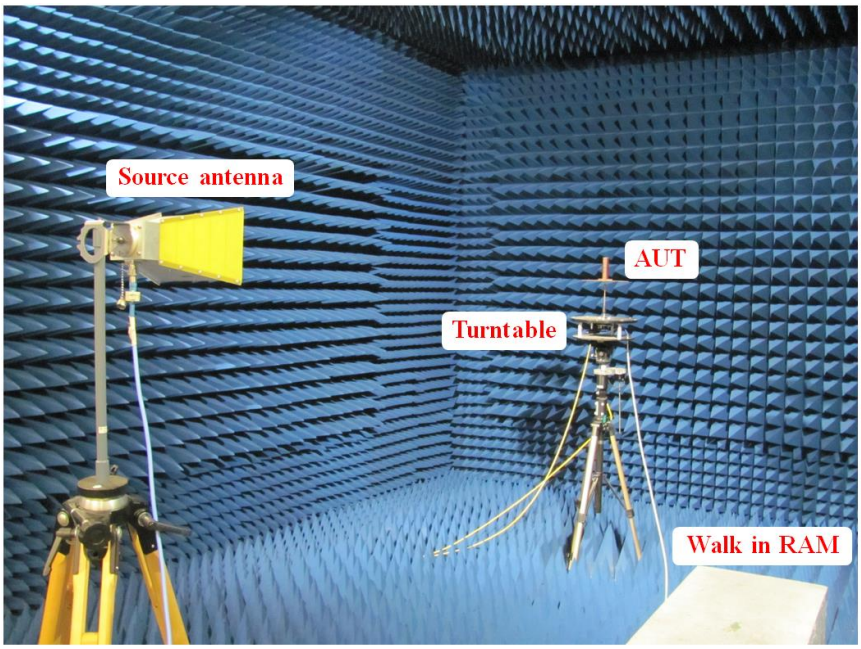

Fig. 2.10: The anechoic chamber at the University of Liverpool

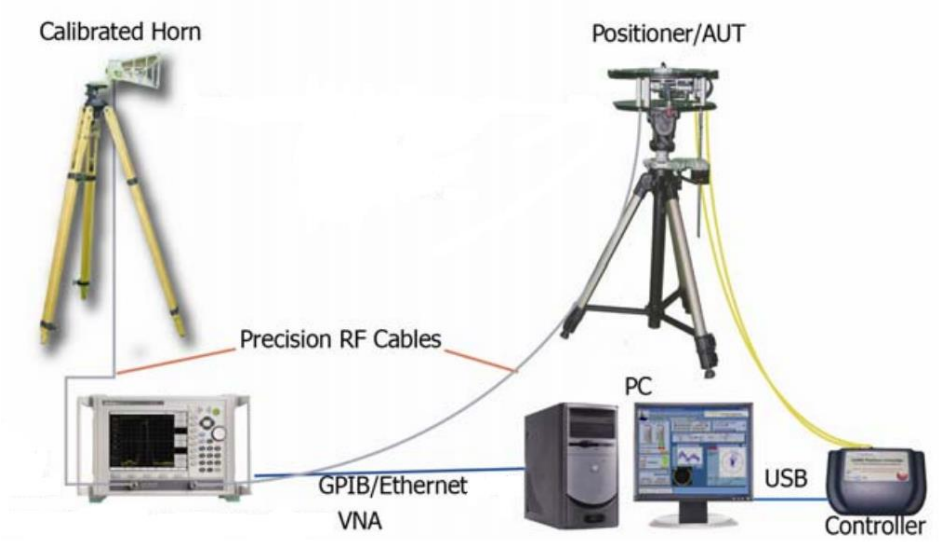

Fig. 2.11: Typical measurement layout.

2.4.6 Total Efficiency and Measurement

In the field of antennas and radiation, the radiation efficiency of an antenna usually is defined as the ratio of the total power radiated by the antenna to the accepted power at its terminal [54]. For the total radiation efficiency, it is defined as the ratio of total radiated power to the total incident power at the input terminal of the antenna; it can be expressed mathematically as a product of the radiation efficiency and mismatch efficiency of an antenna as in the following equation.

$$\eta_{TOT} = \eta_{Rad}\left(1-\left|S_{11AUT}\right|^2\right) \tag{2.26}$$

where η_{TOT} is the total radiation efficiency; η_{Rad} is the radiation efficiency and S_{11AUT} is the reflection coefficient of the antenna under test.

In the area of MIMO antennas, the embedded element efficiency- which is defined as the efficiency of the MIMO antenna when one port is excited and the other unused ports are terminated with matched loads- is one the most important performance parameters; it affects the essential gains (diversity gain and channel capacity) of the MIMO technology [55].

Mathematically, the total embedded element efficiency can be expressed as:

$$\eta_{TOT} = \eta_{Rad}\left(1-\left|S_{11}\right|^2-\left|S_{12}\right|^2\right) \tag{2.27}$$

where the second term in the right hand side usually known as a decoupling efficiency. It is clearly shown from Eq (2.27) that the total embedded radiation efficiency in not only depends on the reflection loss (S_{11}) but also on the mutual coupling loss (S_{12}).

For the radiation efficiency in both Eq (2.26) and (2.27), it can be acquired and calculated using several reverberation chamber (RC) techniques. In this thesis, two techniques are used in the acquiring and the calculation of the radiation efficiency: the conventional three antenna method [48, 56] and the two antenna method reported in [57].

2.4.6.1 Radiation Efficiency Using Conventional Three Antennas Method

The radiation efficiency measurement using this approach usually requires three kinds of antennas to be located inside an RC: transmitter antenna (Tx antenna), known radiation efficiency antenna (REF Antenna) and the antenna under test (AUT antenna). The measurement procedure for this method is the same as the diversity measurement procedure that explained in Section 2.4.4.1. Due to the availability of the reference antenna (SATIMO SH 2000 antenna) for frequencies above 2.0 GHz, three antenna method has been applied for the efficiency measurements of the designs in Chapter 3 and Chapter 4.

Mathematically, after acquiring the data using an RC (the same diversity measurement setup), Eq. (2.28) is applied [56] at the beginning, then for the calculation of the total embedded radiation efficiency Eq. (2.27) is used.

$$\eta_{Rad} = \left\{ \frac{\left\langle \left| S_{21AUT} \right|^2 \right\rangle}{\left\langle \left| S_{21REF} \right|^2 \right\rangle} \times \frac{\left\langle 1 - \left| S_{22REF} \right|^2 \right\rangle}{\left\langle 1 - \left| S_{22AUT} \right|^2 \right\rangle} \right\} \times \eta_{REF} \tag{2.28}$$

where: < > = average of the scattering parameters inside the RC, | | = absolute value, S_{21} = transmission coefficient, S_{22} = reflection coefficient, AUT = antenna under test, REF = reference antenna and $\eta_{\mathrm{Re}f}$ = known reference antenna radiation efficiency.

2.4.6.2 Radiation Efficiency without the Need for Reference Antenna

As the conventional three antennas method has some limitations like its need for three antennas- one of them should have known efficiency, this could cause a problem for some of the laboratories that has no reference antenna. In order to overcome this, Holloway presented interesting approaches for the radiation efficiency measurement in RC chamber [57]. He presented three techniques for determining the efficiency of an antenna without the need for antenna with a known efficiency (reference antenna). In this thesis, due to unavailability of a reference antenna in some frequency bands, the two antenna approach is used in determining the total antenna efficiency for the designs in Chapters 5, 6 and 7.

The measurement procedure of the two antenna method was as follows:

1) Full port calibration of the VNA over the desired frequency band (usually 1 GHz bandwidth is used for better accuracy of the result as there is a transformation from the frequency domain to the time domain via inverse Fourier transform (IFT) to find the chamber time constant τ_{RC} .

2) Place all antennas (AUT and Tx ANT) inside the chamber to keep the chamber Q factor constant.

3) Connect Tx ANT and AUT to ports 1 and 2 of the VNA, respectively, and record S_{11}, S_{22} and S_{21} for each frequency point and stirrer position.

After acquiring the data (total number of samples 359 × 10001 = 3590359) using an RC, Eq. (2.29) is applied [57] to calculate the radiation efficiency, then for the calculation of the total embedded radiation efficiency Eq. (2.27) is used.

$$\eta_{RAD} = \sqrt{\frac{C_{RC}}{e_b.\omega}\frac{\left\langle \left|S_{22s}\right|^2 \right\rangle_{cor}}{\tau_{RC}}} \tag{2.29}$$

where C_{RC} is the chamber constant, τ_{RC} is the chamber time constant, e_b is the enhanced backscatter constant. ω is the angular frequency sample and $\left\langle \left|S_{22,s}\right|^2 \right\rangle_{cor}$ is the correction for S_{22}. Further details about the calculation of all these parameters are presented in Appendix I.

2.5 Decoupling Techniques for MIMO/Diversity Antennas

In a compact and small size MIMO handheld device, the available space to implement multi-element antennas is limited. This would cause a very high mutual coupling level. A strong mutual coupling means a high correlation between the received signals by antenna elements; this high correlation degrades the MIMO/diversity performance such as: the antenna efficiency, channel capacity and diversity gain [58]. Therefore, a number of antennas decoupling techniques (isolation techniques) have been proposed in literature, they can be grouped into two broad categories:

2.5.1 Circuit Level Decoupling Technique

This approach only needs the knowledge of antenna impedances and does not need to modify the antenna structure and the ground plane. For example, a decoupling and matching network (DMN) which is usually done by inserting a transmission line section (that realizes the complex conjugate matching for antenna impedances) between closely coupled antennas [59-61]. For the purpose of size reduction, this decoupling technique can be realized using lumped elements [62]. However, the usefulness of this technique can be limited by the size (the transmission line section), low total efficiency resulted from the ohmic loss in the lumped elements [63, 64]. Furthermore, this decoupling technique is considered as a narrow band solution that increases the detuning sensitivity of the antenna structure [65, 66].

2.5.2 Antenna Level Decoupling Technique

This represents the decoupling techniques that require a modification on the antenna structure or ground plane. Several decoupling techniques fall under this category:

2.5.2.1 Electromagnetic Band Gap Structure (EBG)

Recently, EBG structure which is defined as an artificial periodic structure. It has been utilized in MIMO antenna community to provide antenna isolation. EBG structure (see Fig. 2. 12) can suppress the surface wave between closely spaced antennas and provide a high isolation level, but it suffers from a narrow bandwidth of isolation, a large area and complicated structures [67].

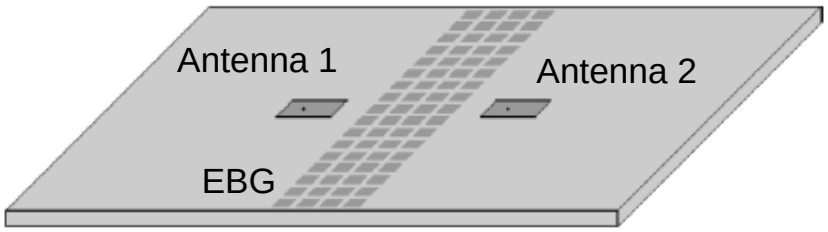

Fig. 2.12: EBG structure between two microstrip antennas [67].

2.5.2.2 Defect Ground plane structure (DGS)

The fabrication of EBG structures is an intricate process (unit cells shorted to the ground through vias) [68]. This excited the researchers to find a simple and planar solution. They found that the surface current on the common ground plane can be altered by making planar modifications on the ground plane. Due to the combination of inductance and capacitance, this modification can produce a band-stop filtering operation to achieve a high isolation level [62]. The modification can have patterned structure as in [68] in which a slit structure on a ground plane was used in reducing mutual coupling between closely-packed antenna elements as shown in Fig. 2.13. Additionally, a simple resonance slot structure on the ground plane can be classified as DGS; a ground plane slot between closely-spaced antennas was used to enhance isolation via trapping the coupling current between antenna elements [68-71]. However, there are three possible drawbacks with DGS: a narrow bandwidth, back radiation, and hard to implement in reality as the ground plane is shared with other components [62].

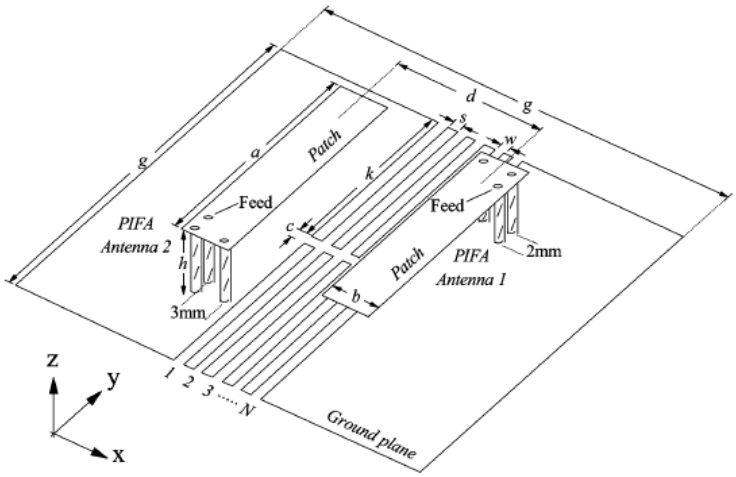

Fig. 2.13: Isolation using DGS structure [68].

2.5.2.3 Neutralization Line

Adding a conducting strip between closely coupled antennas can provide a reverse coupling path that maintains the isolation. Although it has been widely reported in literature [72, 73], the design procedure of this neutralization line differs from analytical formulation of the aforementioned techniques, this makes the final structure sub-optimal in term of the footprint, decoupling level and decoupling bandwidth [74]. Finally, it is worth mentioning this isolation technique is only effective for the case of shorted monopoles [73] and shorted patch antennas like PIFA (as shown in Fig. 2.14) [72].

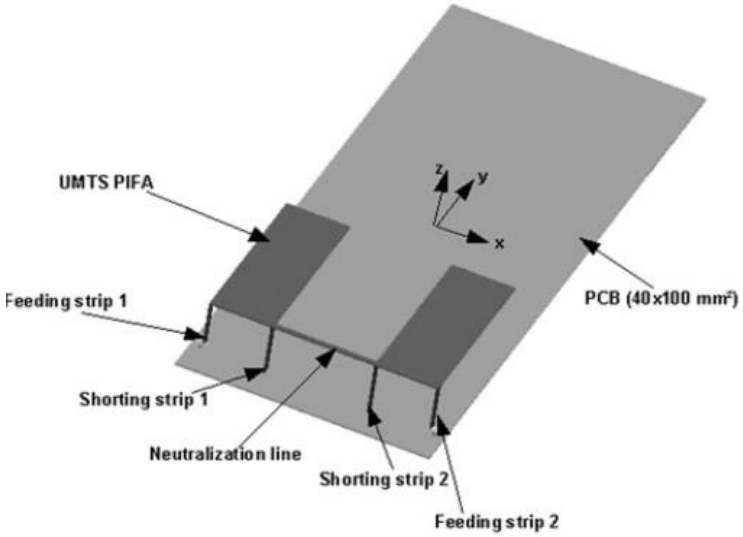

Fig. 2.14: Neutralization line between two PIFA antennas [72].

2.5.2.4 Parasitic Decoupling Element

The possibility of inserting an additional distributed parasitic element has been explored in several projects [75-79]. This solution is to add an additional coupling path between closely coupled antennas by the field cancelation [75] (see Fig. 2.15). Despite this solution has little ohmic loss and it is very suitable for handset integration [80], again there is no general design rule or procedure to obtain optimal results for small footprint, wide isolation bandwidth and acceptable isolation level. Thus, a thorough investigation on the circuit theory has been done in the Chapter 6 where the parasitic decoupling element is designed based on the stepped impedance resonator (SIR) theory.

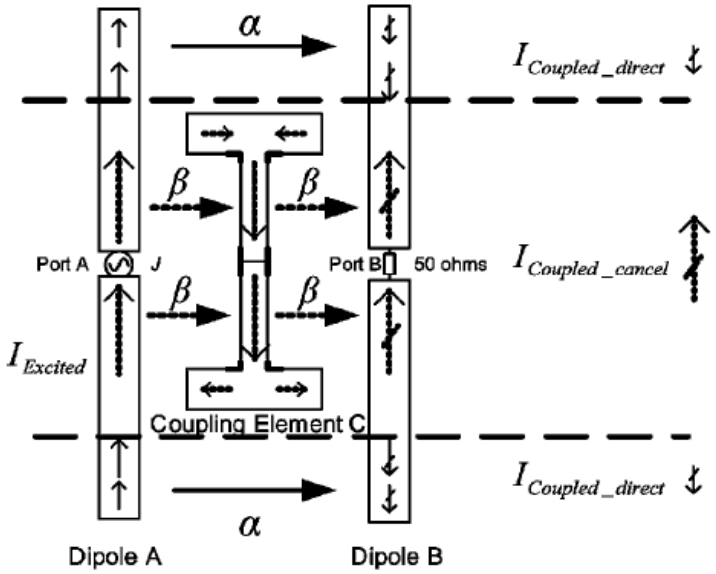

Fig. 2.15: Isolation using parasitic decoupling element [75].

2.6 Summary

In this chapter, a clear overview on the MIMO antenna system has been presented. Both spatial multiplexing technique and spatial diversity technique have been discussed with their gains: enhancement in the channel capacity and the diversity gain, respectively. As this work represents antenna design for MIMO applications based on the antenna diversity scheme, different types of antenna diversity, diversity performance parameters and common decoupling techniques have been explained in detailed. Finally, the chapter is finished with the explanation of the experimental techniques used in acquiring both the total antenna efficiency and the diversity gain.

References

[1] C. E. Shannon, "A mathmatical theory of communication," *Bell Syst Tech.*, vol. 27, pp. 379-423, 623-656, July & Oct. 1948.

[2] H. H. Beverage and H.O. Peterson, "Diversity receiving system of R.C.A. communications, Inc., for radiotelegraphy," *Proceedings of the Institute of Radio Engineers*, vol.19, no. *4*, pp. 529–561, April. 1931.

[3] H. H. Beverage and H.O. Peterson, "Diversity telephone receiving system of R.C.A communications, Inc," *Proceedings of the Institute of Radio Engineers*, vol.19, no. *4*, pp. 562–584, April. 1931.

[4] J. R. Hampton, *Introduction to MIMO communications*, Cambridge University Press, First Published, 2014.

[5] A. Wittneben, "Base station modulation diversity for digital simulcast," *In Vehicular Technology Conference, 1991. Gateway to the Future Technology in Motion 41st IEEE*, pp. 848–853, May 1991.

[6] G. J. Foschini, "Layered space-time architecture for wireless communcation in a fading environmentwhen using multi-element antennas," *Bell Lab Tech J.*, vol. 1, no. 2, pp. 41-59, 1996.

[7] G. J. Foschini and M. J. Gans, "On limits of wireless communications in a fading environment when using multiple antennas," *Wireless Personal Communications*., pp. 311-335, Mar. 1998.

[8] R. G. Vaughan and J. B. Anderson, "Antenna diversity in mobile communicstions," *IEEE Trans.Veh. Thecnol.*, vol. VT-36, no. 4, pp. 149-172, Nov. 1987.

[9] V. Plicanic,"Antenna diversity studies and evaluation," M.S. thesis, Dept, of Electroscience, Lund University, May. 2004 [Online]. Avialable: htttp:// www,es.lth.se/teorel/publications/TEAT-500-se-ries/TEAT-5064.pdf.

[10] W. C. Jakes, *Microwave mobile communications*, IEEE Press Classis Reissue, Piscataway, NJ IEEE Press 1994

[11] A. Khaleghi, "Diversity techniques with parallel dipole antennas: Radiation pattern analysis," *Progress in Electromagnetics Research (PIER).*, vol. 64, pp. 23-42, 2006.

[12] T. Taga,"Characteristics of space-diversity branch using parallel dipole antennas in mobile radio communications," *Electron. Commun. Jpn.*, pt.I, vol. 76, no. 9, pp. 55–65, 1993.

[13] R. G. Vaughan and N. L. Scott, "Closely spaced monopoles for mobile communications," *Radio Sci*, vol. 28, no. 6, pp. 1259–1266, Nov-Dec 1993.

[14] R. Janaswamy, *Handbook of antennas in wireless communications*, IEEE Press CRC Press, 2002.

[15] R. H. Clarke, "A statistical theory of mobile-radio reception," *Bell Syst Tech.*, vol. 47, no. 6, pp. 957-1000, July-Oct. 1968.

[16] P. Petrus, J.H. Reed, and T.S. Rappaport, "Geometrically based statistical channel model for macro cellular mobile environments," *Proc. IEEE Globecommun.*, pp. 1197–1201, 1996.

[17] R. G. Vaughan,"Switched parasitic elements for antenna diversity," *IEEE Trans. Antennas Propag*, vol. 47, no. 2, pp. 399-405, Feb. 1999.

[18] P. Mattheijssen, M. H. A. J. Herben *et al*,"Antenna-pattern diversity versus space diversity for use at handhelds," *IEEE Trans. Vehicular Tech*, vol. 53, no. 4, pp. 1035-1042, July. 2004.

[19] P. L. Penry, C. L. Holloway,"Angle and space diversity comparison in defferent mobile radio environments," *IEEE Trans. Antennas Propag*, vol. 46, no. 6, pp. 764-775, June. 1998.

[20] R. G. Vaughan,"Pattern translation and rotation in uncorrelated source distributions for multiple beam antenna design ," *IEEE Trans. Antennas Propag*, vol. 46, no. 7, pp. 982-990, July. 1998.

[21] C. B. Dietrich *et al*,"Spatial, polarization, and pattern diversity for wireless handheld terminals," *IEEE Trans. Antennas Propag*, vol. 49, no. 9, pp. 1271-1281, Sept. 2001

[22] http://www.cst-korea.co.kr/Application/MIMO-Antenna-Simulation-CSTMWS.pdf.

[23] R. G. Vaughan,"Polarization diversity in mobile communications," *IEEE Trans. Antennas Propag*, vol. 39, no. 3, pp. 177-186, Aug. 1990.

[24] A. M. D. Turkmani, A. A. Arowojolu *et al*,"An experimental evaluation of the performance of two-branch space and polarization diversity schemes at 1800 MHz," *IEEE Trans. On Vehicular Technology*, vol. 44, no. 2, pp. 318-326, May. 1995.

[25] K. Cho, T. Hori and K, Kagoshima,"Effectiveness of four-branch height and polarization diversity configuration for street microcell," *IEEE Trans. Antennas Propag*, vol. 46, no. 6, pp. 776-781, June. 1998

[26] C. Beckman and U. Wahlberg,"Antenna system for polarization diversity," *Microwave Journal*, pp. 330-334, May. 1997

[27] T. W. C. Brown, S. R. Saunders *et al*,"Charctrization of polarization diversity at the mobile," *IEEE Trans. Antennas Propag,* vol. 56, no. 5, pp. 2440-2447, Sept. 2007

[28] H. Li, B-K. Lau *et al*,"Angle and polarization diversity in compact dual-antenna terminals with chassis excitation," *In Pro of General Assembly and scientific Symposium,* vol. 1, no. 4, pp. 13-20, Aug. 2011.

[29] Q. Rao and D. Wang,"A compact dual-port diversity antenna for long-term evolution handheld devices," *IEEE Trans. Antennas Propag,* vol. 59, no. 3, pp. 1319-1329, March. 2010

[30] H. T. Chattha, Y. Huang, S. J. Boyes *et al.*, "Polarization and Pattern Diversity-Based Dual-Feed Planar Inverted-F Antenna," *Antennas and Propagation, IEEE Transactions on,* vol. 60, no. 3, pp. 1532-1539, 2012.

[31] M. Tarkiainen and T. Westman, "Predictive switched diversity for slow speed mobile terminals," *IEEE Vehicular Technology Conference,* vol. 3, pp. 2042-2044, 1997.

[32] R. G. Vaughan and J. B. Anderson, "Channels, propagation and antennas for mobile communications," *IEEE Electomagnetic Waves,* series. 50, London, Uk, 2003.

[33] L. J. Foged and A. Scannavini, "Efficient testing of wirless devices from 800 MHz to 18 GHz," *Radioengineering,* vol. 50, no. 4, pp. 460-466, Dec 2009.

[34] P. S. Kildal and K. Rosengren, "Correlation and capacity of MIMO systems and mutual coupling, radiation effeciency and diversity gain of their antennas: simulations and measurements in a reverbration chamber," *IEEE Communications Magazine,* vol. 42, no. 12, pp. 104-112, 2012.

[35] P. B. Fletcher, M. Dean and A. R. Nix, "Mutual coupling in multi-element array antennas and its influnance on MIMO channel capacity," *Electronics Letters,* vol. 39, no. 12, pp. 342-344, 2003.

[36] R. G. Vauchan and J. B Anderson, "Antenna diversity in mobile communications," *IEEE Trans. Vehicular Technology,* vol. 36, no. 4, pp. 149-172, Nov. 1987.

[37] S. C. K. Ko and R. D. Murch, "Compact Integrated diversity antenna for wireless communications," *IEEE Trans. Antennas Propagation* , vol. 49, no. 6, pp. 954-960, June. 2001.

[38] M. K. Ozdemir, E. Arvas *et al.*, "Dynamic of spatial correlation and implications on MIMO systems," *IEEE. Communications Magazine,* vol. 42, no. 6, pp. 514-519, June. 2004.

[39] G. F. Pedersen and J. B. Andersen, "Handsets antennas for mobile communications, integration, diversity and performance," *URSI Review of Radio Science*, pp. 119-139, 1996.

[40] S. Blanch, J. Romeu, and I. Corbella,"Exact representation of antenna system diversity performance from input parameter description," *Electronics Letters,* vol. 39, no. 9, pp. 705-707, 2003.

[41] P. Hallbjorner,"The significance of radiation effeciencies when using S-parameters to calculate the received signal correlation from two antennas," *IEEE Antenna Wireless Propag. Letter,* vol. 4, pp. 97-100, 2005.

[42] T. C. Tang, K. H. Lin ,"MIMO antenna design in thin-film integrated passive devices," *IEEE Trans. Components, Packaging and manufacturing Tech* , vol. 4, no. 4, pp. 648-655, April. 2014.

[43] J. F. Li, Q. X. Chu *et al.*,"Compact dual band-notched UWB MIMO antenna with high isolation," *IEEE Trans. Antennas Propag,* vol. 61, no. 9, pp. 4759-4766, Sept. 2013.

[44] T. Taga,"Analysis for mean effective gain of mobile antennas in land mobile radio environments," *IEEE Trans. Vehicular Tech,* vol. 39, no. 2, pp. 117-131, 1990.

[45] Y. Ding, Z. Du *et al.*,"A novel dual-band printed diversity antenna for mobile terminals," *IEEE Trans. Antennas Propag,* vol. 55, no. 7, pp. 2088-2096, July, 2007.

[46] V. Plicanic, "Antenna diversities studies and evaluaton," *M.Sc. Thesis ,Dept. of Electrosience,* Lund University, May, 2004.

[47] P.-S. Kildal, K. Rosengren *et al.*,"Definition of effective diversity gain and how measure it in a reverbration chamber," *Microwave and Optical Technology Letters,* vol. 34, pp. 56-59, 2002.

[48] P.-S. Kildal, K. Rosengren ,"Correlation and capacity of MIMO systems and mutual coupling, radiation effeciency, and diversity gain of their antennas: simulations and measurements in a reverbrastion chamber," *IEEE Communications Magazine,* vol. 42, pp. 104-111, Dec. 2004.

[49] K. Rosengren and P.-S. Kildal,"Definition of effective diversity gain and how measure it in a reverbration chamber," *IEEE Proceedings on Microwave, Antennas and Propagation,* vol. 152, no. 1, pp. 7-16, Feb. 2005.

[50] E. Genender, C. L. Holloway, K. A. Remley *et al.*, "Simulating the multipath channel with a reverberation chamber: application to bit error rate measurements," *IEEE Trans. Antennas Propagat.*, vol. 42, no. 4, pp. 766-777, Nov. 2010.

[51] S. Alja'afreh, Y. Huang and L.Xing,"Compact, wideband and low profile planar inverted-L antenna," *Proc.of the European Conference. On Antenna and Propagation (EuCAP 2014),* The Hague, Netherlands, 2014.

[52] Q. Xu, Y. Huang, X. Zhu, S. Alja'afreh and L. Xing,"A new antenna diversity gain measurement method using a reverbration chamber," *IEEE Antenna Wireless Propag. Letter,* vol. 14, pp. 935-938, 2015.

[53] J. Yang, S. Pivnenko, T. Laitinen, J. Carlsson, and X. Chen, "Measurements of diversity gain and radiation efficiency of the Eleven antenna by using different measurement techniques," *in Antennas and Propagation (EuCAP), 2010 Proceedings of the Fourth European Conference on, 2010, pp. 1-5*.

[54] "IEEE Standard Definitions of Terms for Antennas," *IEEE Std.145-1993.*

[55] J. F. Valenzuela, N. A. Garcia-Fernandez, *et al*,"The influence of effeciency on receive diversity and MIMO capacity for rayleigh fading channels," *IEEE Trans. Antennas Propag.,* vol. 65, no. 5, pp. 1444-1450, May. 2008.

[56] S. J. Boyes, P. J. Soh, Y. Huang, G. A. E. Vandenbosch, "Measurement & Performance of Textile Antenna Efficiency on Human Subjects in a Reverberation Chamber", *IEEE Transactions Antennas & Propagation,* vol. 61, no. 2, 2013.

[57] C. L. Holloway, H. A. Shah, *et al.,* "Reverbration chamber techniques for determinating the radiation and total efficiency of antennas", *IEEE Transactions Antennas & Propagation,* vol. 60, no. 4, 2012.

[58] S. C . Ko, R. Murch,"Compact integrated diversity antenna for wireless communications," *IEEE Trans. Antennas Propag.,* vol. 49, no. 6, pp. 954-960, June. 2001.

[59] J. Anderson and H. Rasmussen,"Decoupling and descattering networks for antennas," *IEEE Trans. Antennas Propag.,* vol. 24, no. 6, pp. 841-846, Nov. 1976.

[60] J. W. Wallace, and M. A. Jensen, "Mutual coupling in MIMO wireless systems: a rigorous network theory analysis," *IEEE Trans. Antennas Propag,* vol. 3, no. 4, pp. 1317-1325, 2004.

[61] L. Zhao, L. K. Yeung and K. L. Wu., "A Coupled Resonator Decoupling Network for Two-Element Compact Antenna Arrays in Mobile Terminals. " *IEEE Trans. Antennas Propag,* vol. 62, no. 5, pp. 2267-2276, May, 2014.

[62] Y. L. Ban, C. L. Liu, J. L. W. Li *et al.*,"Multiple Antenna Systems with Inherntly Decoupled Radiators," *IEEE Trans. Antennas Propag,* vol. 60, no. 2, pp. 503-515, Feb. 2012.

[63] A. Sibille, C. Oestges and A. Zanella.,"Multiple Antenna Terminals; in MIMO from Theory to implemetation," Acabemic Press, pp. 267-298, 2010.

[64] Y. L. Ban, C. L. Liu, J. L. W. Li *et al.*,"A decoupling techniques for increasing the port isolation between two strongly coupled antennas," *IEEE Trans. Antennas Propag*, vol. 56, no. 12, pp. 3650-3658, Dec. 2008.

[65] B. K. Lau, J. B. Anderson *et al.*,"Impact of Matching Network on Bandwidth of Compact Antenna Arrays," *IEEE Trans. Antennas Propag,* vol. 54, no. 11, pp. 3225-3238, 2006.

[66] M. A. Moharram and A. A. Kishk,"General decoupling network design between two coupled antennas for MIMO applications," *Progress in Electromagnetics Research Letters,* vol. 37, pp. 133-142, 2013.

[67] F. Yang, Y. Rhmat. Samii.,"Microstrip antennas integrated with electromagnetic band gap EBG strucutures: a low mutual coupling design for array applications," *IEEE Trans. Antennas Propag,* vol. 51, no. 10, pp. 2936-2946, Oct. 2003.

[68] C. C-Yuk, C. C. Ho *et al.*,"Reduction of mutual coupling between closely-packed antenna elements," *IEEE Trans. Antennas Propag*, vol. 55, no. 6, pp. 1732-1738, June. 2007.

[69] S. Zhang, J. Xiong *et al.*,"MIMO antenna system of two closely-positioned PIFAs with high isolation," *Electronic.Lett.*, vol. 45, no. 15, pp. 771-773, 2009.

[70] S. Zhang, S. N. Khan *et al*., "Reducing mutual coupling for an extremly closley-packed tunable dual-element PIFA array through a resonance slot antenna formed in-between," *IEEE Trans. Antennas Propag.*, vol. 58, no. 8, pp. 2771-2776, Aug. 2010.

[71] S. Zhang, B. Kiong *et al*., "Mutual coupling reduction of two PIFAs with a T-shaped slot impedance transformer for MIMO mobile terminals ," *IEEE Trans. Antennas Propag*., vol. 60, no. 3, pp. 1521-1531, March. 2012.

[72] A . Diallo, C. Luxey, P. Le Thuc *et al.*,"Enhanced two-antenna structures for universal mobile telecommunications system diversity terminals," *IET Microwaves, Antennas & Propagation*, vol. 2, no. 1, pp. 93-101, 2008.

[73] Y. Wang and Z. Du.,"A Wideband Printed Dual-Antenna System with A Novel Neutralization Line for Mobile Terminals," *IEEE Antennas and Propagation Letters,* vol. 12, pp. 1428-1431, 2013.

[74] M. Pelosi, M. B. Knudsen and G. F. Pederson.,"Multiple antenna asystems with inherently decoupled radiators," *IEEE Trans. Antennas Propag,* vol. 60, no. 2, pp. 503-515, Feb. 2012.

[75] A. C. K. Mak, C. R. Rowell and R. D. T. Murch.,"Isolation enhancement between two closely packed antennas," *IEEE Trans. Antennas Propag,* vol. 56, no. 11, pp. 3411-3419, Nov. 2008.

[76] Z. Li, Z. Du, M. Takahashi *et al.*,"Reduction mutual coupling of MIMO antennas with parasitic elements for mobile terminals," *IEEE Trans. Antennas Propag*, vol. 60, no. 2, pp. 473-480, Feb. 2012.

[77] K. Payandehjoo. and R. Abhari," Investigation of parasitic elements for coupling reduction in multiantenna hand-set devices," *Int J RF and Microwave Comp Aid Eng,* vol. 24, no. 1, pp. 1-10, Jan, 2014.

[78] T. Y. Wu, S. T. Fang and K. L. Wong,"Printed diversity monopole antenna for WLAN operation," *Electronics Letters,* vol. 38, no. 25, pp. 1625-1626, Dec. 2002.

[79] G. Chi, B. Li and D. Qi,"Dual-band printed diversity antenna for 2.4/5.2- GHz WLAN application," *Microwave and Optical Technology Letters,* vol. 45, no. 6, pp. 561-563, june 2005.

Chapter 3: Water Antenna for Diversity Applications

3.1 Introduction

Recently, liquid antennas like mercury antennas [1, 2], liquid crystal antennas [3, 4] and water antennas [5] have received a great research attention because of the special properties of the liquids such as: liquidity, transparency [6] and reconfigurability as their electrical properties can be changed easily by the addition of some solvent solutions [7, 8]. Among these antennas, water antennas become the most popular due to low cost, easy access, less toxicity. Furthermore, the very interesting property that makes water more popular material than the other is its very high dielectric constant ($\varepsilon_r = 81$); this benefits the use of water either as a dielectric resonator antenna (DRA) [9] or as a loading material that helps in reducing the size of an antenna by a factor of $1/\sqrt{\varepsilon_r}$ [10-12].

In the literature, several water antenna solutions have been proposed. Some of them were made from salty water or sea water in which the water worked as a conductor antenna that support current flow [8, 10, 13-14]. Other designs used pure water to make DRA antennas [15, 16]. However, the high dielectric loss at high frequency bands usually affects the radiation efficiency of these antennas; and this forced most of researchers and antenna designers to find water antenna solutions for frequency applications less than 1GHz [4, 5, 15, and 16]. Interestingly, in the area of MIMO and antenna diversity technology, there is no work presents water antenna (or DRA with very high dielectric constant) solution for recent MIMO applications in small handheld devices. However, the use of the pure water in the design of DRA antennas benefits on producing of transparent antennas with a high detuning resistance. Consequently, this motivates this work to find a novel water-based antenna for handset MIMO applications.

In this chapter, the dielectric characteristics of pure water are discussed at the beginning. Then, a brief overview on DRA antenna types, design and feeding is presented. After that, two water-based antenna designs are proposed. A single feed water antenna is proposed first. Due to the high dielectric loss over the frequency range of interest (2.4-2.7 GHz), the design has low antenna efficiency. To address this, and to continue for finding a water antenna for MIMO applications, a dual-feed water based antenna is proposed, with the aid of a parasitic decoupling element, the design achieved acceptable antenna efficiency. Both antennas are simulated, fabricated and tested. The results demonstrate that water can be a good candidate for transparent antenna design in the future.

3.2 Pure Water Characteristics

Fig. 3.1 shows the dielectric characteristic of pure water at the room temperature 25 C^o as a function of frequency in the range 2-4 GHz. The measured dielectric properties are collected using Agilent Dielectric Probe 85070 as shown in Fig. 3.2, while the theoretic values are calculated using the first order Debye model [17], which is imported from the CST Microwave Studio [18]. It can be seen that both the measured and the theoretic values are in a good agreement. Further, the loss tangent is also calculated as a ratio between the imaginary and the real part of the permittivity using Eq. (3.1) and presented in the Fig. 3.1(b), it shows that the water has a high dielectric loss over the frequency band of interest.

$$\tan(\delta) = \frac{\varepsilon''}{\varepsilon'} \tag{3.1}$$

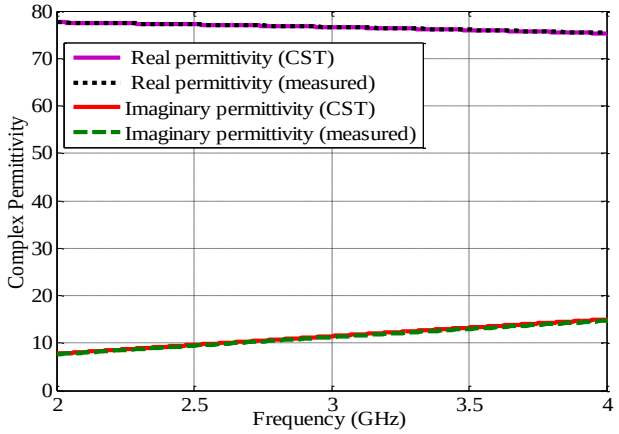

(a)

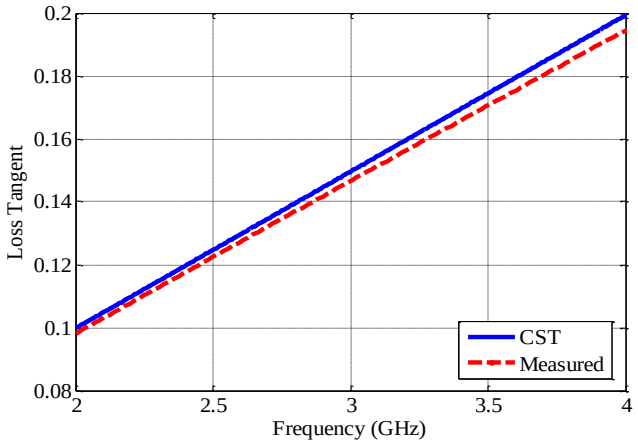

(b)

Fig. 3.1: Pure water dielectric characteristics at 25 C^0 (a) Complex permittivity (b) Loss tangent

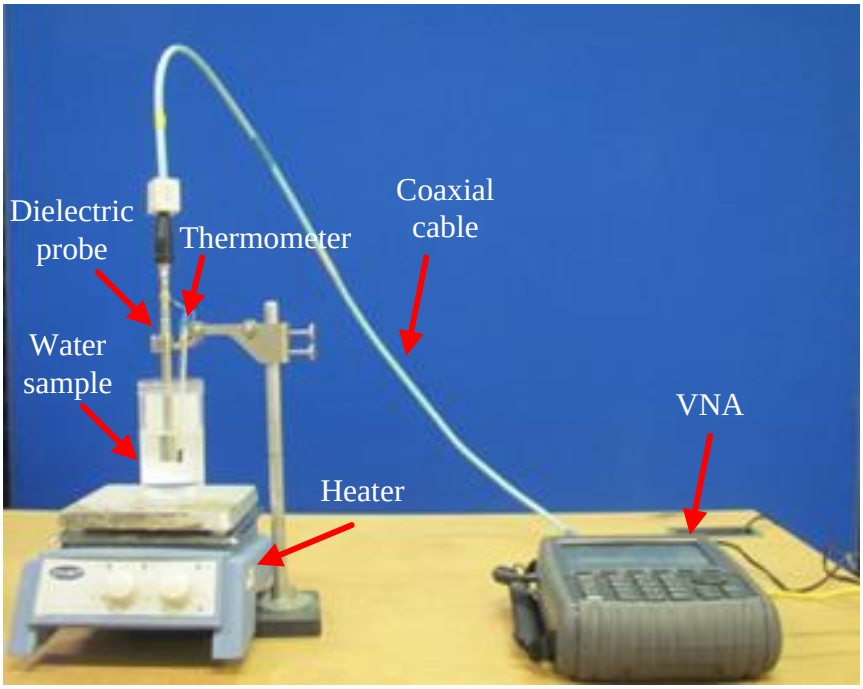

Fig. 3.2: Complex permittivity measurement setup

3.3 Rectangular Dielectric Resonator Antennas

At the beginning of 1980s, the first study on the use of dielectric resonators as antenna was done by Long [19]. Since then, DRA antennas have witnessed extensive research efforts in both academic and industry fields. Different shapes of DRA have been examined and studied such as: cylindrical [19], spherical [20], and rectangular [21]. Among these, rectangular shape is chosen for this work as it has more practical advantages over other shapes. Such advantages are like:

1) The mode degeneracy can be controlled and avoided by properly adjusting the three dimensions of the resonator [22]. Thus, the level of cross polarization can be minimized.
2) Unlike other basic shapes like, cylindrical and spherical, rectangular dielectric resonator antennas (RDRA) have three dimensions (length, width and height), which gives more flexibility in controlling the resonance frequency and the operational bandwidth [22].

This section looks at the fundamental mode of the isolated RDRA and the common feeding or excitation schemes that are usually used. Then, the design equation for estimating the resonance frequencies for different modes of isolated RDRA is discussed.

3.3.1 RDRA Fundamental Mode and the Design Equation

Since the RDRA is not a body of revolution, it can only support TE modes [22] (non-confined mode). The fundamental mode is the TE_{111}. As the three dimensions of the RDRA are independent, the TE modes can be along the three directions: x, y and z. Referring to Fig. 3.3(a), if the dimensions of RDRA are such as a>2b>g (2b instead of b because it represents an isolated RDRA without a presence of a ground plane), then, the modes in the order of increasing resonant frequency are $TE^{y}_{1\delta 1}$, $TE^{z}_{11\delta}$ and $TE^{x}_{\delta 11}$, which radiate like short magnetic dipole in the y-, z- and x- directions, respectively. The lowest mode is usually called the fundamental mode, Fig. 3.3 (b) shows the fundamental mode of the RDRA in Fig. 3.3(a) which is $TE^{y}_{1\delta 1}$.

The resonant frequency of the fundamental mode of the isolated RDRA can be predicted by solving the following transcendental equation resulted from the dielectric waveguide model (DWM) [22]. This predicted value usually has a slight deviation from the measured one; this is due to the effect of the feeding scheme that is not included in DWM.

$$k_y \tan\left(\frac{k_y g}{2}\right) = \sqrt{(\varepsilon_r - 1)k_0^2 - k_y^2} \tag{3.2}$$

where

$$k_o = \frac{2\pi f_0}{c},\ k_x = \frac{\pi}{a},\ k_z = \frac{\pi}{2b} \tag{3.3}$$

where k_x, k_y and k_z are the wavenumbers, k_o denotes the free space wave number, f_o is the resonant frequency.

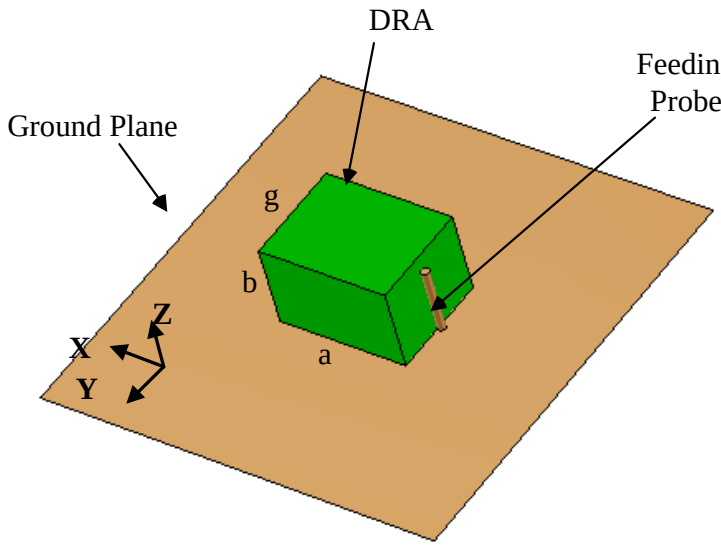

(a)

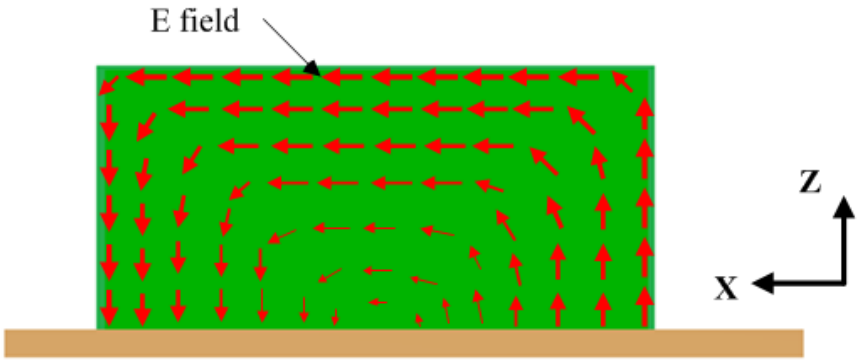

(b)

Fig. 3.3: Rectangular dielectric resonator antenna(a) RDRA antenna, (b) Electric field lines of the fundamental mode ($TE^{y}_{1\delta1}$)

3.3.2 RDRA Feeding Methods

Different feeding schemes were employed to excite different DRA modes. Both the type of the feed and its location play an important role in determining the excited mode, the radiation quality factor, the input impedance and other radiation characteristics [23]. Such feeding schemes like: coaxial probe feed, aperture feed, microstrip feed and coplanar waveguide feed. In this work, the coaxial probe feed is only discussed because it is the most

suitable one for the shape of the proposed water-based antenna design (tile shape). More details on other feeding schemes can be found in [23].

As the probe feed has an electric current with a density **Js**, it behaves like an electrical source. Thus, based on the coupling theory of resonator circuits and Lorenz reciprocity theory with boundary conditions [24], strong coupling can be obtained using a probe feed if the source is located in a position with a strong electric field inside the DRA. It is clearly shown in Fig. 3.3 (b) that the field configuration of the fundamental mode ($TE^{y}_{1\delta1}$) inside the RDRA that is shown in Fig. 3.3 (a), it shows that the electric field components (E_x and E_z) reach their maximum value near the edges of the RDRA (based on the size of the arrows). Thus, for a strong coupling of the fundamental mode, the probe should be located near the edges of the RDRA with a suitable height as shown in Fig. 3.4.

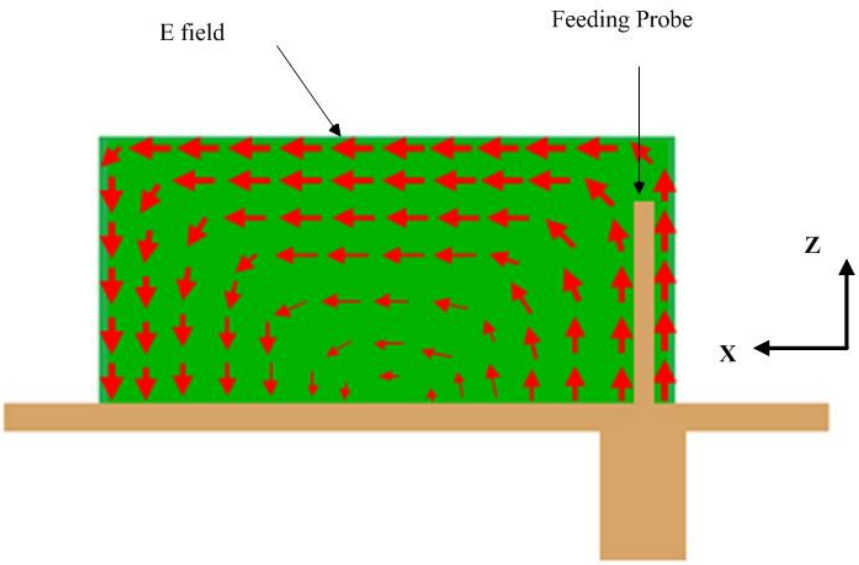

Fig. 3.4: Coaxial probe feed coupling for $TE^{y}_{1\delta1}$ RDRA mode

3.4 Single Feed Water-Based Antenna

3.4.1 Antenna Configuration

The geometry of the proposed water-based RDRA antenna is shown in Fig. 3.5. Pure water is filled inside a PVC tube having a rectangular shape with a wall thickness of 1 mm. The whole structure is placed on a ground plane with a thickness of 0.5 mm, length L_g, and width W_g. The RDRA antenna dimensions without PVC thickness are; length a, width g and height b. The position of the antenna is taken along the top edge of the ground plane to

decrease the resonant frequency toward the desired frequency band, while it is positioned on a distance X_{dr} from the side edge. The antenna is fed using a coaxial probe feed with a height L_{probe} which is attached to the shorted side of the RDRA antenna to excite the fundamental mode $TE^{y}_{1\delta1}$.

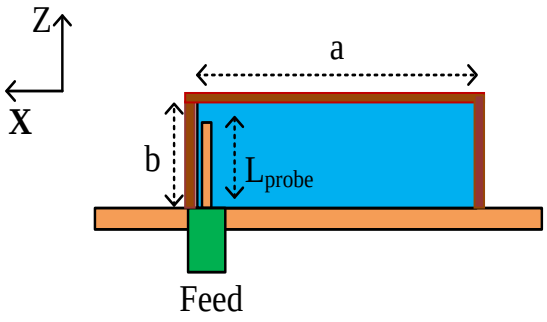

(a)

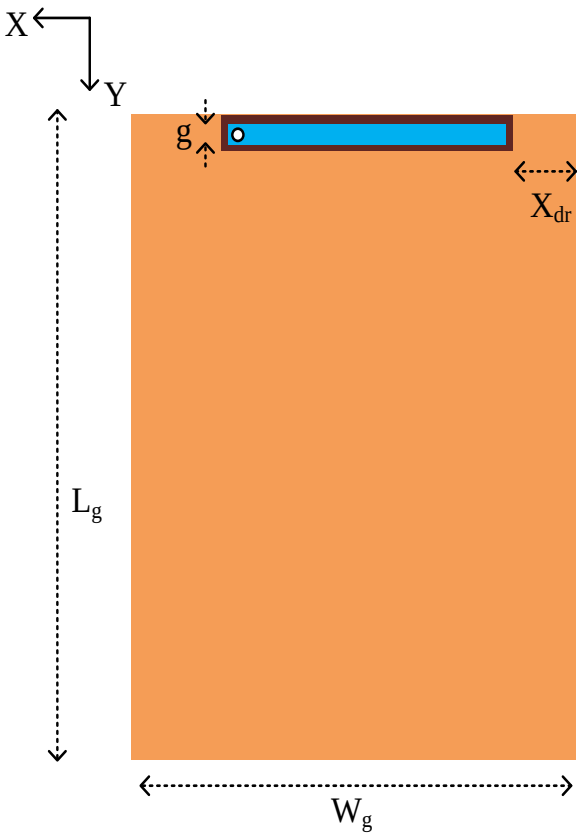

(b)

Fig. 3.5: Single-feed water antenna configuration (a) side view and (b) top view

3.4.2 Prototype and S-parameters

The simulations are performed using CST Microwave Studio to optimize the antenna parameters for the desired operation band. A prototype (see Fig. 3.6) was fabricated using the following optimized parameters: a =26 mm, b = 10 mm, g = 1.5 mm, L_g = 70 mm, W_g = 40 mm, X_{dr} = 12 mm, L_{probe} = 9 mm. Initially, the PVC tube was formed in a mechanical workshop; it is opened from the bottom side to keep a direct contact between the water and the PEC or the ground plane. In order to inject the water inside the tube, a small hole was made on the top of the tube. After that, the fabricated tube and the ground plane (copper plate with thickness 0.5 mm) were pasted together using a super glue. The antenna was fed by SMA connector in which the inner was passed through the water along the shorted edge of the PVC tube.

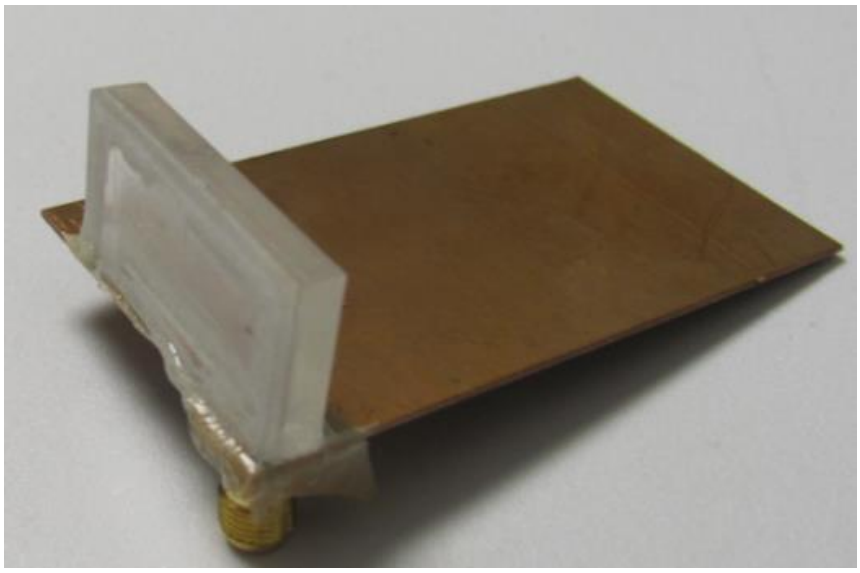

Fig. 3.6: Single-feed water-based antenna prototype

After injecting the pure water having a temperature of 25 C° inside the tube, the reflection coefficient was measured inside an anechoic chamber. The measured results were compared with the simulated results as shown in Fig. 3.7. From the simulated results, it can be seen that the antenna can achieve a bandwidth (S11< -10 dB) about 0.715 MHz (2.4-3.15 GHz). However, the measured results bandwidth is about 1 GHz (2.35-3.35 GHz). This discrepancy is mainly due to the fabrication error and an additional loss added by the use of the glue material which is not included in the simulation. Nevertheless, the design still can cover the desired frequency band applications in the range of 2.4-2.7 GHz.

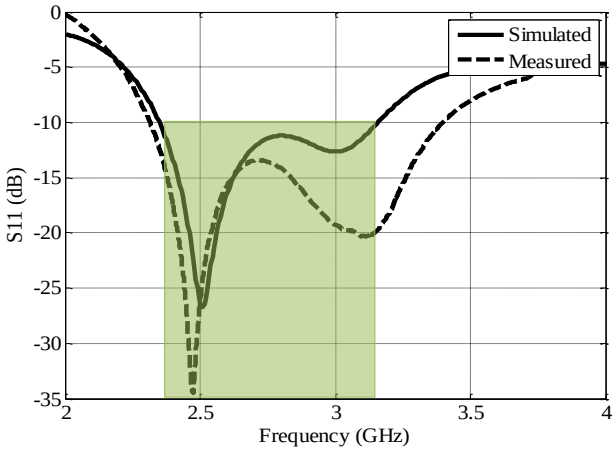

Fig. 3.7: Measured and simulated reflection coefficients

To better understand the achieved results, both the input impedance and the electrical field distribution inside the RDRA are evaluated using CST Microwave studio. Fig. 3.8 shows that the antenna has a parallel resonance around 2.5 GHz, this means that the radiation is contributed to the dominant mode inside the RDRA ($TE^{y}_{1\delta1}$) as it behaves like a magnetic dipole [23]. This can be also confirmed from the electric field distribution inside the proposed antenna (see Fig. 3.9) at 2.5 GHz; the excited field line represents $TE^{y}_{1\delta1}$ mode.

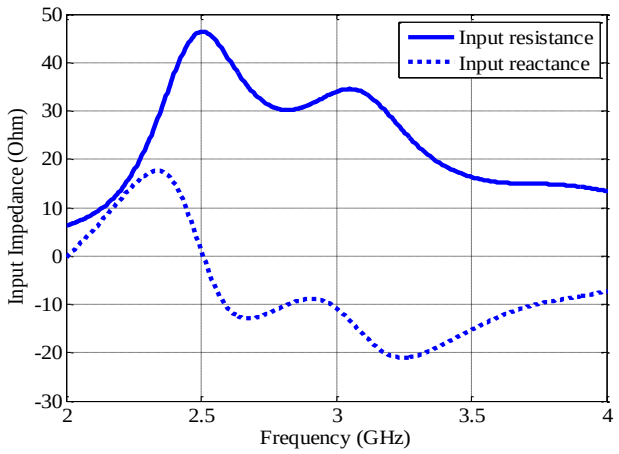

Fig. 3.8: Input impedance of the single feed water antenna

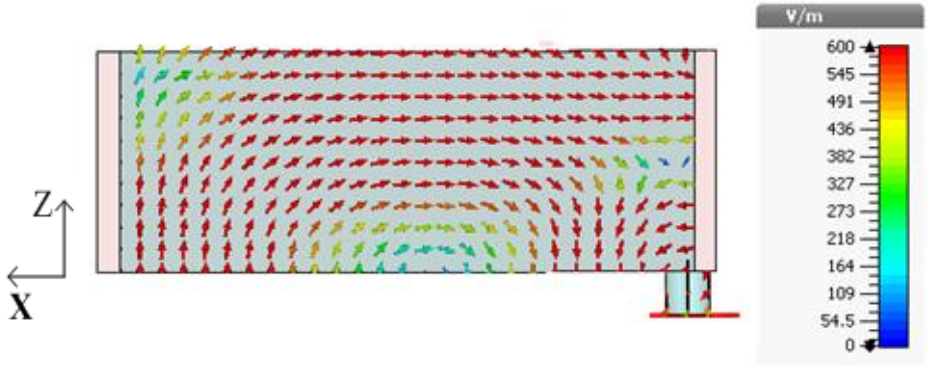

Fig. 3.9: Electric field distribution of the excited $TE^{y}_{1\delta 1}$ mode at 2.5 GHz

3.4.3 Parametric Study

This section gives the effects of some of the design parameters on the resonant frequency (based on the resonance dip) and the impedance bandwidth of the proposed water-based antenna. The simulations are carried out using CST Microwave Studio. The study is done by varying the parameter of interest, while other design parameters are held constant.

In Fig. 3.10, the variation of the reflection coefficient is shown as the RDRA length is varied from 20 mm to 26 mm. It can be seen that the increase in the length of the RDRA decreases the resonance frequency. While the impedance bandwidth increases with the length; this can be interpreted from the reduction of the radiation quality factor, which results from the reduction of the volume to surface ratio as in Eq.(3.4) [25]. In this context, the height of the proposed antenna also has the same trend on both the resonant frequency and the operational bandwidth.

$$Q = 2\omega_0 \frac{Stored.Energy}{Radiated.Power} \propto 2\omega_0 \varepsilon_r^p \left(\frac{Volume}{Surface} \right)^s \tag{3.4}$$

where ω_0 is the resonant angular frequency, $p \geq s \geq 1$

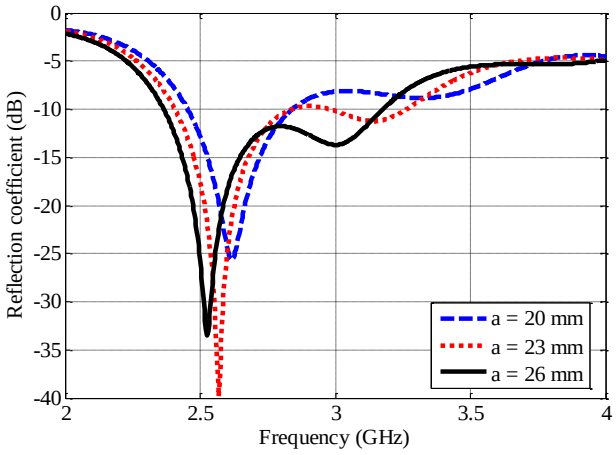

Fig. 3.10: The effect of the length

Unlike other dimensions (the length and the height), the width of the proposed antenna has a significant effect on both the resonant frequency and the bandwidth fraction as shown in Fig. 3.11. The resonant frequency decreases with the increase in the width because this dimension is in the y-dimension which is the dominant dimension for the excited mode $TE^{y}_{1\delta 1}$. For the operational bandwidth, it is obviously shown from Eq.(3.4) that increasing the width will increase the volume and thus increases the quality factor which means a reduction on the operational bandwidth.

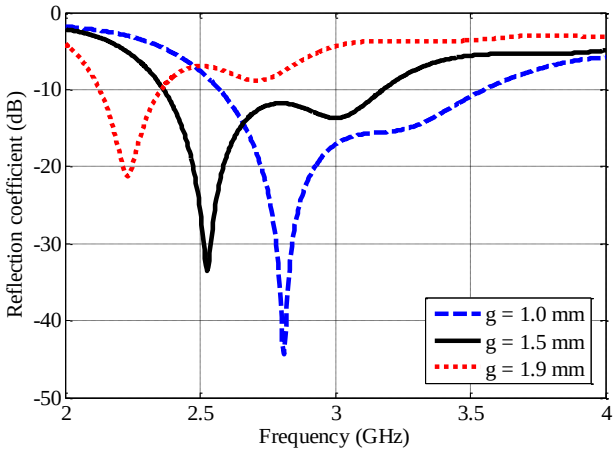

Fig. 3.11: The effect of the width

In addition to the geometric dimensions of the RDRA, probe feed length play an importance role in tuning the resonant frequency. Fig. 3.12 shows that the resonant frequency is shifted down with the increasing of the probe length. This can be interpreted from the perturbation theory of microwave cavities and resonators, the probe feed represents

an inward perturbation on the RDRA and as long as it is located at a position of a large electric field the resonant frequency decreases with increasing the inward perturbation [26].

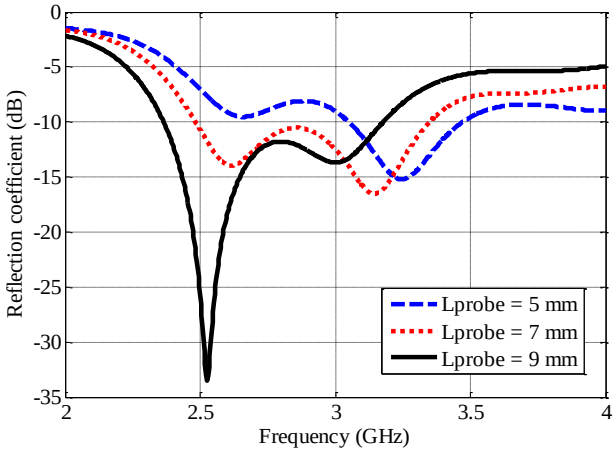

Fig. 3.12: The effect of the probe length

3.4.4 Far Field Radiation Patterns

Fig. 3.14 shows the measured and the simulated normalized radiation patterns. It is clearly shown that in both XZ and YZ planes, the antenna has a maximum radiation toward the positive z-direction; this can be explained from the nature of the excited resonator mode which is $TE^{y}_{1\delta1}$, it has a maximum electric field line along the top of the RDRA antenna. For better understanding, the 3D simulated far field pattern is shown in Fig. 3.13.

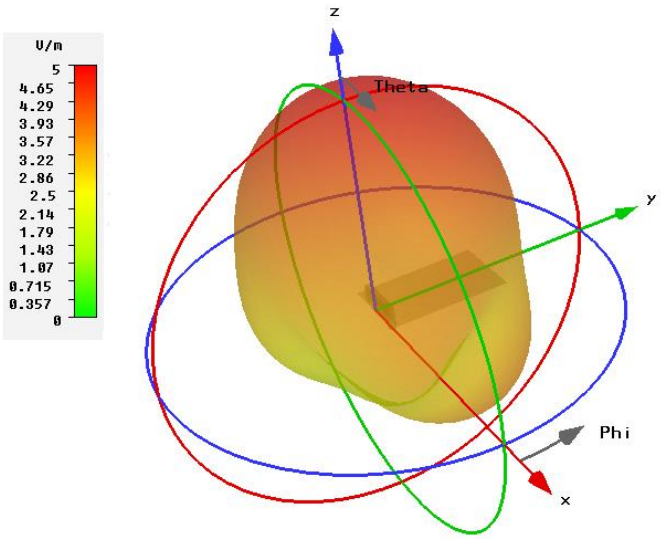

Fig. 3.13: 3D simulated far field radiation pattern at 2.5 GHz

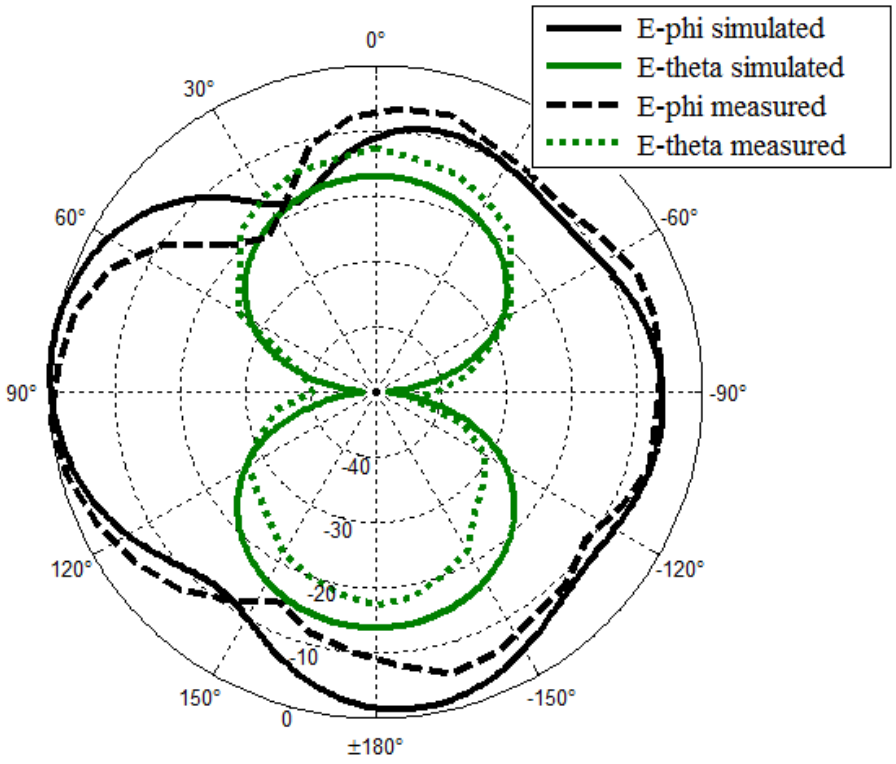
E-phi simulated
E-theta simulated
E-phi measured
E-theta measured
0°
30°
60°
90°
120°
150°
±180°
-30°
-60°
-90°
-120°
-150°
-40
-30
-20
-10
0

(a)

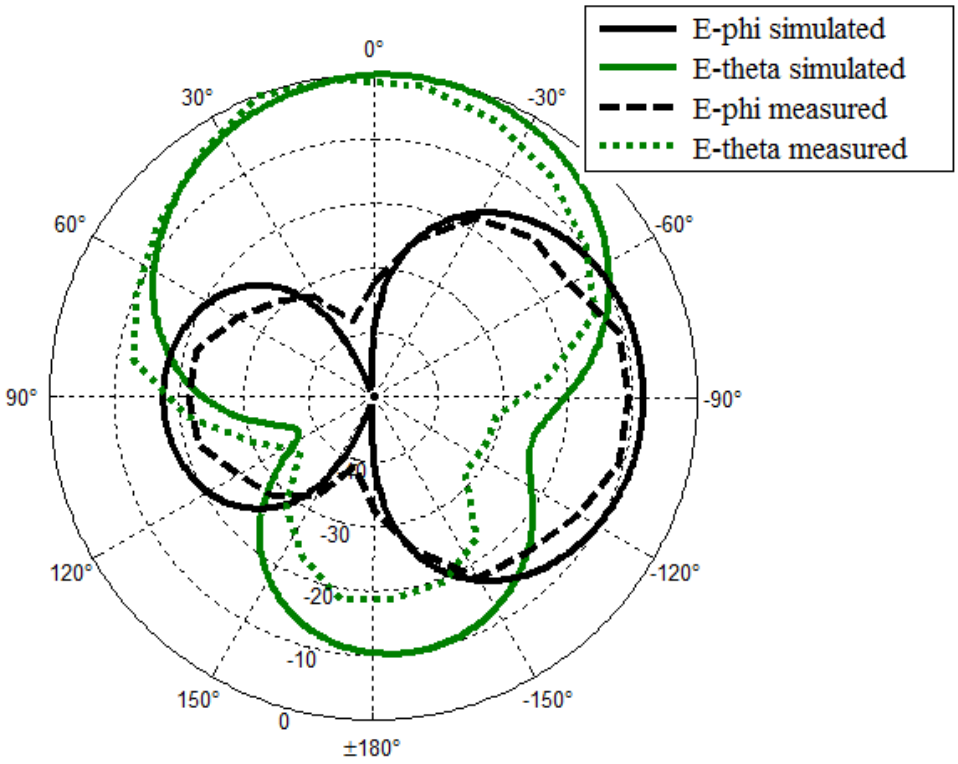
E-phi simulated
E-theta simulated
E-phi measured
E-theta measured
0°
30°
60°
90°
120°
150°
±180°
-30°
-60°
-90°
-120°
-150°
-40
-30
-20
-10
0

(b)

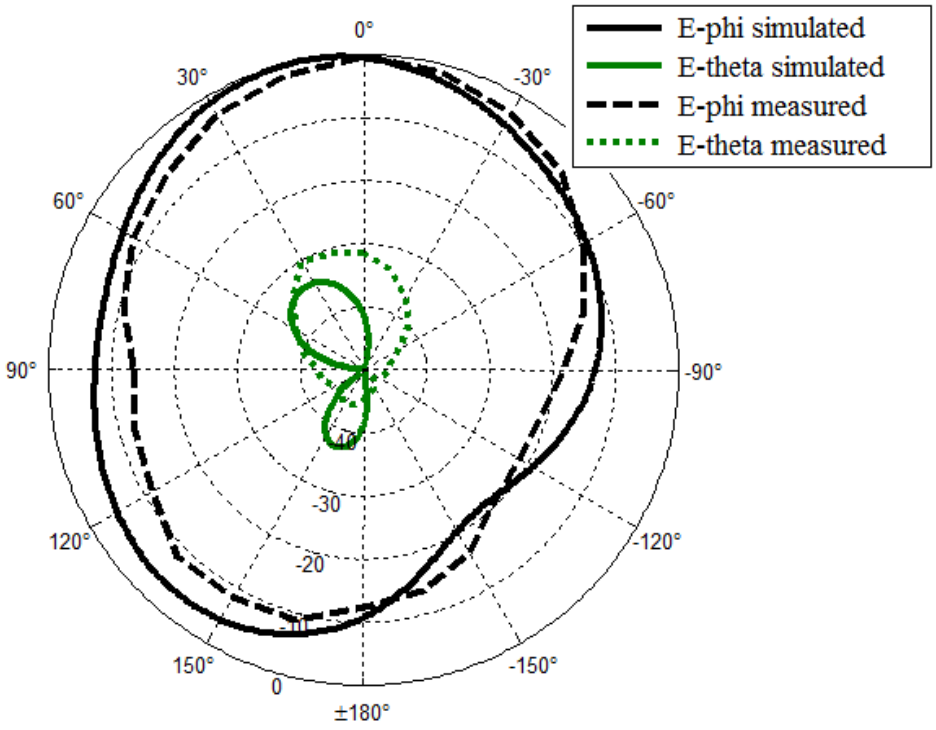

(c)

Fig. 3.14: Measured and simulated radiation patterns at 2.5 GHz

(a) XY plane, (b) XZ plane and (c) YZ plane

3.4.5 Total Efficiency

The total radiation efficiency measurement was conducted inside a reverberation chamber. After acquiring the data using the three antenna method that is discussed in Section 2.4.5, the total radiation efficiency is calculated using Eq. (2.28) and Eq. (2.26), respectively. Fig. 3.15 shows that both the measured and the simulated efficiencies are in a good agreement. However, the proposed water-based antenna has a low total radiation efficiency (between 35 % to 40 %) over the frequency band (2.4-2.7 GHz); this can be linked to the high dielectric water loss for the frequencies above 2 GHz as discussed at the beginning of this chapter. The question may arise now is to what extend can this water-based antenna be used in MIMO applications? The answer of this question can be found in the next section.

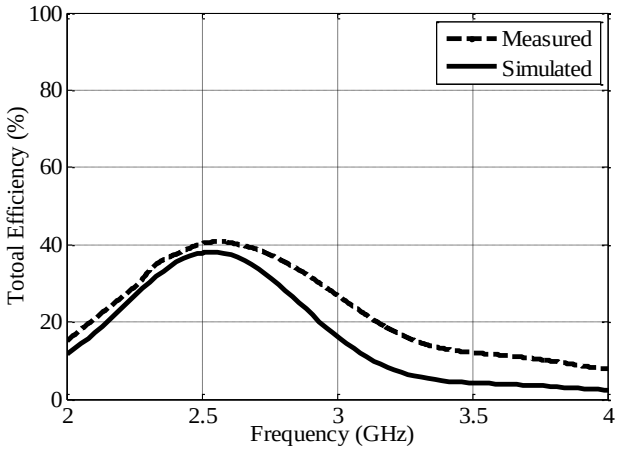

Fig. 3.15: Measured and simulated total efficiency

3.5 Dual-Feed Water-Based Antenna

In the literature, most of handset MIMO antenna designs are based on conductor antennas like planar antenna structures (PIFA, microstrip and planar monopole antennas), but very few designs have employed DRAs for MIMO applications [27-29]. Furthermore, even the existing MIMO DRA designs are only with equal-dimension structures like cylindrical and cube shape [27-29]. Equally-dimensions DRAs are preferred because the ground surface current is confined underneath structures with dimensional aspect ratios around one and this will increase the level of feeds isolation [27]. However, there is no existing design for a compact multiport RDRA with unequal-dimensions (different dimensional aspect ratios) although these structures offer an attractive feature like large bandwidth that can be achieved.

Regarding the material type of DRA, most of DRA materials are solid, low loss dielectric materials which require a special cutting to get the exact dimensions of a resonator; moreover, the cost of dielectric materials with a very high dielectric constant like BaTiO3 ceramic powder ($\varepsilon_r = 79$) is very expensive. Therefore, water antenna might be a cost-effective antenna and could be a very attractive alternative as a MIMO diversity antenna. However, it has been shown in the previous section that the single feed water-based antenna has a poor radiation efficiency. Consequently, this creates an obstacle for the design of MIMO antennas from water because it is already known that the radiation efficiency is one of the most important performance parameters of MIMO antennas [30]. To manage this, the

ground plane of a small handset mobile is taken usually as a part of the antenna system and it can radiate energy as the antenna element [31]. Hence it can change some of the radiation characteristics like: resonant frequency, impedance bandwidth and radiation patterns.

Thus, the ground plane can be utilized to achieve a dual-feed water-based antenna with acceptable radiation efficiency; this can be done by employing a suitable decoupling technique that can help both the radiation and feeds isolation. Among the decoupling techniques that have been discussed in the previous chapter, the parasitic decoupling element technique is the best candidate as it can enhance both the radiation and the isolation.

In this section, a very cheap, dual-feed water-based antenna is proposed and investigated. It can operate over the frequency range of 2.4-3.4 GHz for such applications like: 2.4 WLAN, Bluetooth, LTE (bands 7, 38, 41) with acceptable total radiation efficiency (over 50 % in the frequency range of 2.4-2.7 GHz).

3.5.1 Antenna Configuration

The geometry of the proposed dual-feed water-based antenna is depicted in Fig. 3.16. The water is filled inside a PVC tube having a rectangular shape with a wall thickness of 1 mm. The whole structure is placed on a ground plane with a thickness of 0.5 mm, length L_g and width W_g. The antenna dimensions without including the PVC wall thickness are: length *a*, width *g* and height *b*. The position of the antenna is taken along the ground plane top edge for two purposes: one is to increase the operational bandwidth and the second one is to simplify the design of the isolation circuitry by employing a parasitic element decoupling technique. The decoupling element consists of two back to back L-shaped strip with total length *L+Ys*. In order to further tune both the stop band and the impedance bandwidth, two rectangular-shaped ground pads are added around each port. The two ports are fed by probe feeds, each one has a height b to excite the fundamental RDRA mode ($TE^{y}_{1\delta1}$).

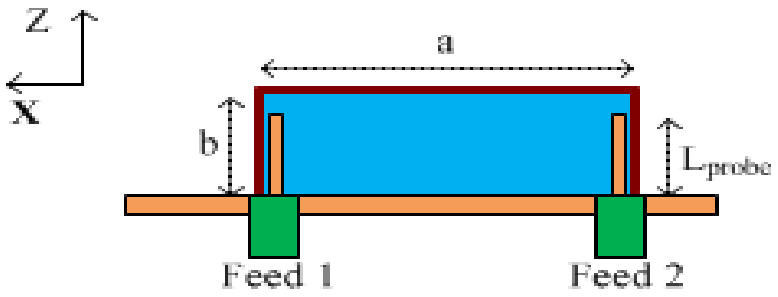

(a)

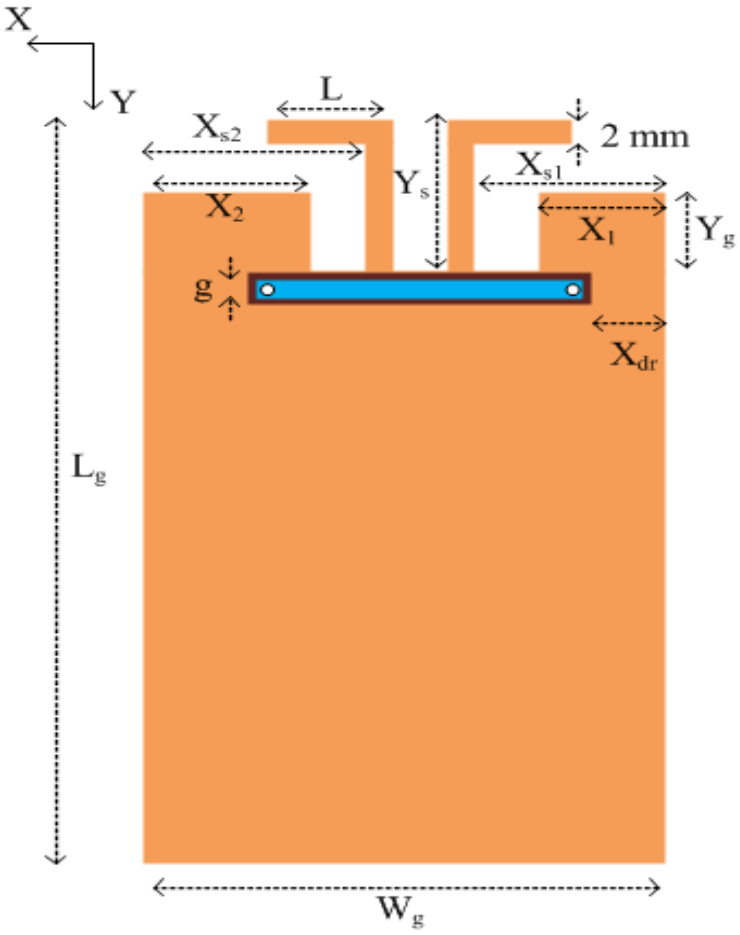

(b)

Fig. 3.16: Geometry of the dual-feed water antenna: (a) side view, (b) top view

3.5.2 Prototype and S-parameters

The simulations are performed using CST Microwave Studio to optimize the antenna parameters for the desired operation band and isolation. Fig. 3.17 depicts the fabricated antenna prototype that is constructed using the following design parameters: a =25 mm, b = 10 mm, g = 1.5 mm, L_g = 100 mm, W_g = 40 mm, X_{dr} = 9 mm, L_{probe} = 9.5 mm, Y_g = 13 mm, X_1 = 9 mm, X_{s2} = 19 mm, X_{s1} = 14 mm, Y_s = 18 mm, L = 9 mm and X_2 = 10 mm. The simulated and measured S-parameter results are acquired inside an anechoic chamber at the University of Liverpool. Fig.3.18 shows that both the simulated and the measured results, which are in a good agreement and the design can cover a 10 dB reflection loss bandwidth about 1 GHz for the frequency band between 2.4 to 3.4 GHz, and with isolation level better than 13 dB on average. Also, compared to the results before decoupling (see Fig. 3.19), both the impedance bandwidth and the isolation level are enhanced in which the former is doubled and the latter is enhanced by around 8 dB.

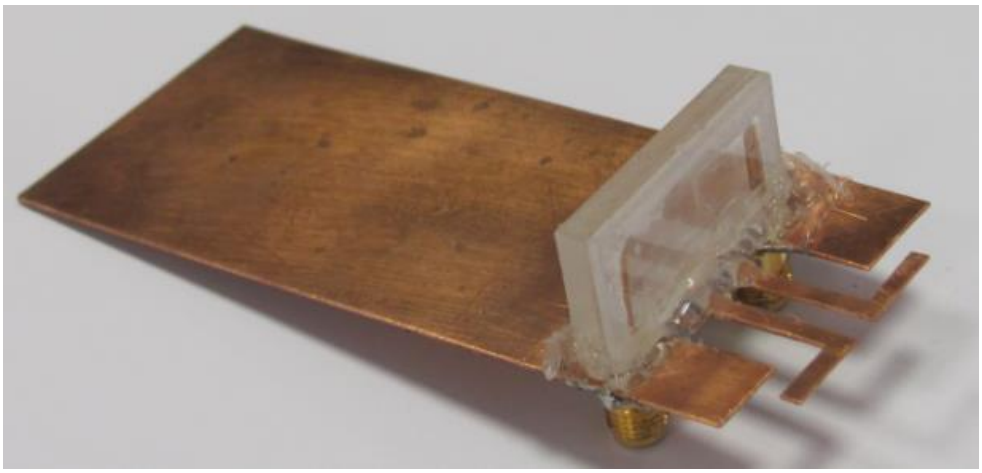

Fig. 3.17: Dual-feed water antenna prototype

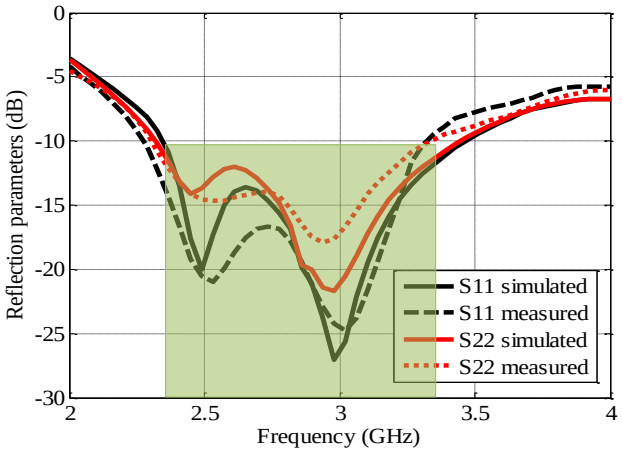

(a)

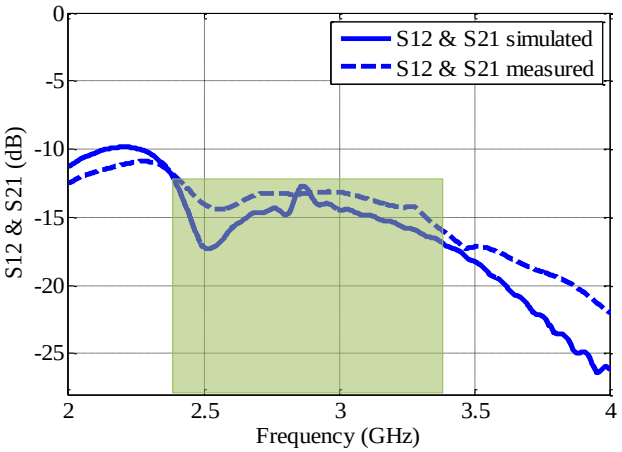

(b)

Fig. 3.18: Measured and simulated S-parameter results (a) Reflection parameters and (b) mutual coupling parameters

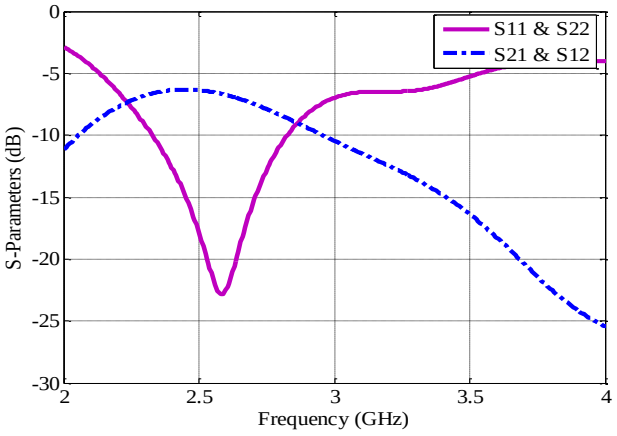

Fig. 3.19: S-parameters of the dual-feed water antenna without the decoupling element

To better understand the achieved results, CST Microwave Studio was used to generate images of the surface current distributions when one feed is excited and the other is terminated with a matched load. Fig. 3.20 shows the current distribution on the ground plane at 2.5 GHz. It can be seen the two different current paths; the surface current resulted from Feed 2 is concentrated on both L-shaped strip and underneath the right part of RDRA, while Feed 1 has a current on both L-shaped strip and underneath the left half of the RDRA. These two different current modes can provide the low mutual coupling level and enhance the radiation by the radiation from the strips.

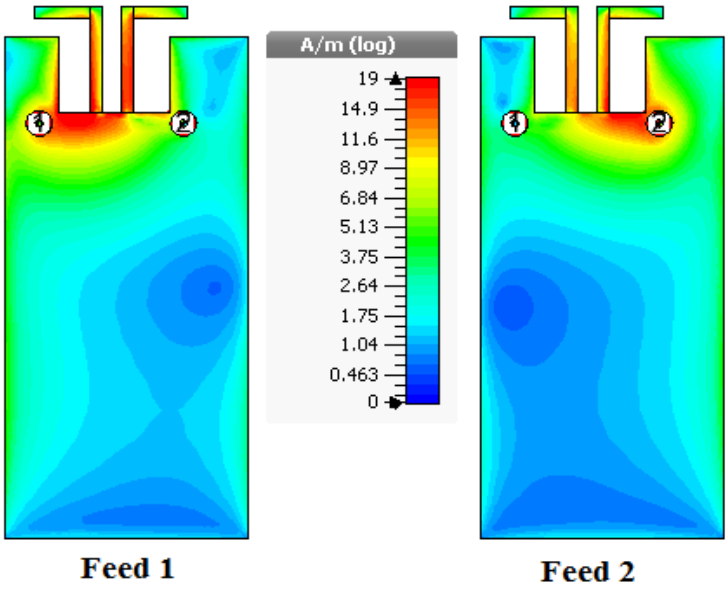

Fig. 3. 20: Surface current distribution at 2.5 GHz

3.5.3 Parametric Study

The length of the decoupling strips is varied to observe its effect on the S-parameters, whereas all other parameters are held constant. Fig. 3.21 shows that both the reflection coefficients and the isolation coefficients are affected by the length; both resonant frequency and the stop band frequency are shifted down with increasing of the strip length. It is evident that the parasitic strips play important role in both the radiation and the isolation between the antenna feeds.

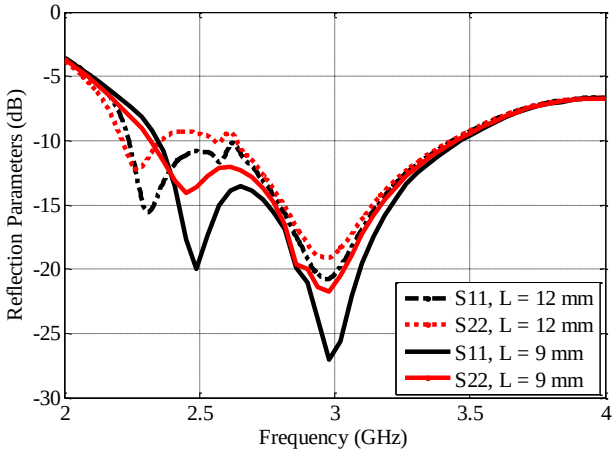

(a)

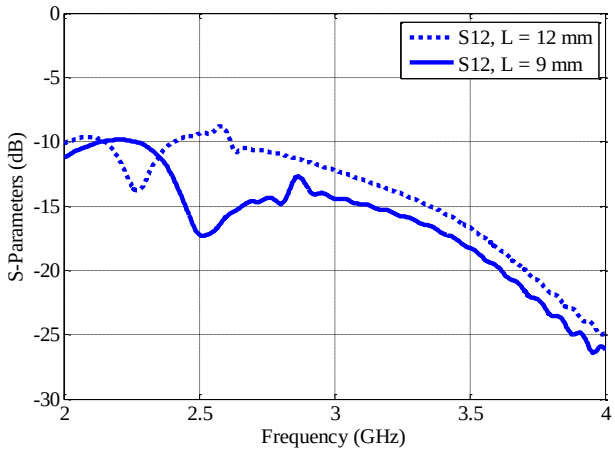

(b)

Fig. 3. 21: Effect of L-shaped strip length (a) S11 and S22, (b) S21 and S12

To investigate the effect of the ground plane pads, further simulations are conducted using CST Microwave Studio. Fig. 3.22 shows the resulted S-parameters with and without the pads. It can be seen that the introduction of the pads tunes the isolation bandwidth down to the desired frequency band, while the reflection bandwidth is slightly affected.

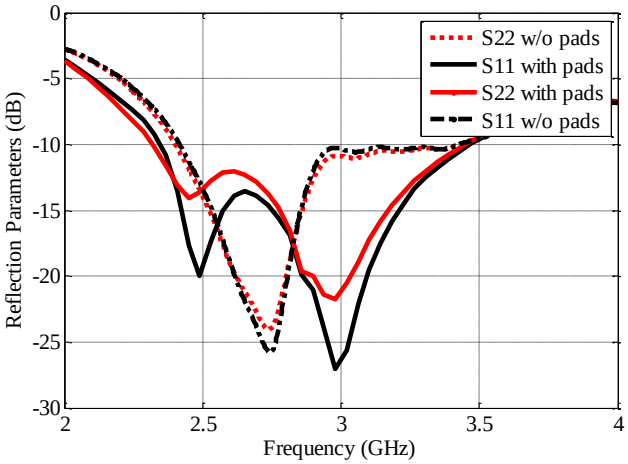

(a)

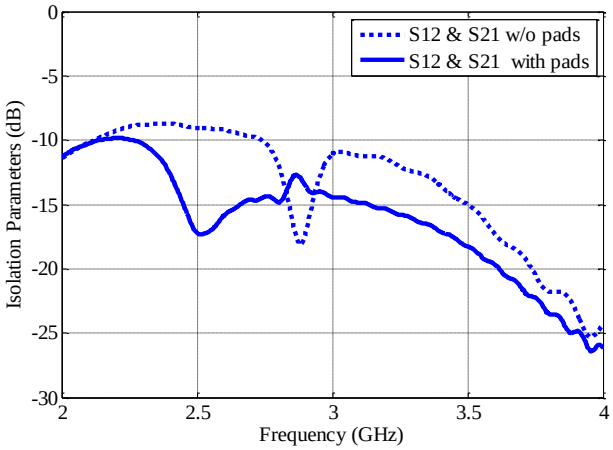

(b)

Fig. 3. 22: Effect of the added ground plane pads (a) S11 and S22, (b) S21 and S12

3.5.4 Far Field Radiation Patterns

Fig. 3.23 shows the measured and simulated XY plane radiation patterns for both feeds at 2.5 GHz. It can be observed that the radiation patterns of the two ports are comparatively different enough to achieve pattern diversity. Regarding other planes (XZ and YZ), the radiation patterns of both feed are similar because of the structure symmetry on these planes. For these planes, the pattern diversity is also achieved, but in oblique planes (and). This can be seen from the 3D simulated far field patterns as in Fig. 3.24.

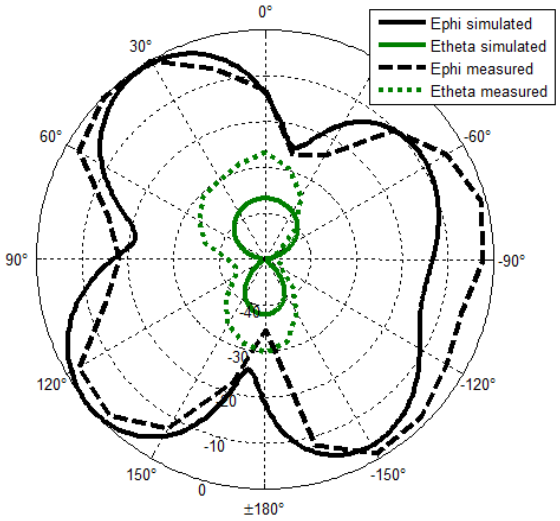

(a)

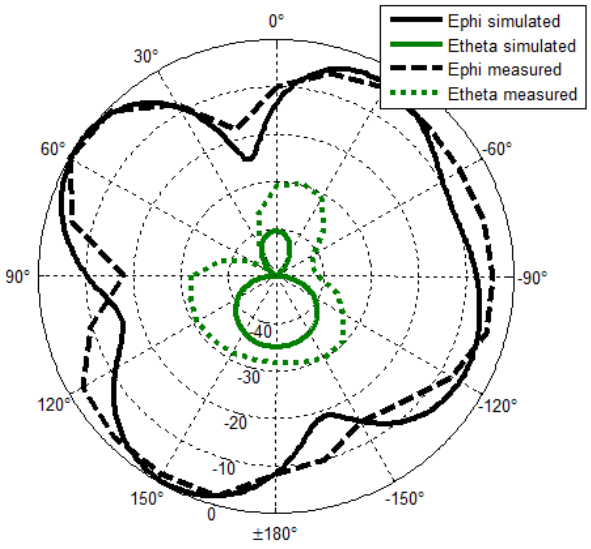

(b)

Fig. 3. 23: Radiation patterns in XY plane at 2.5 GHz (a) Feed 1, (b) Feed 2

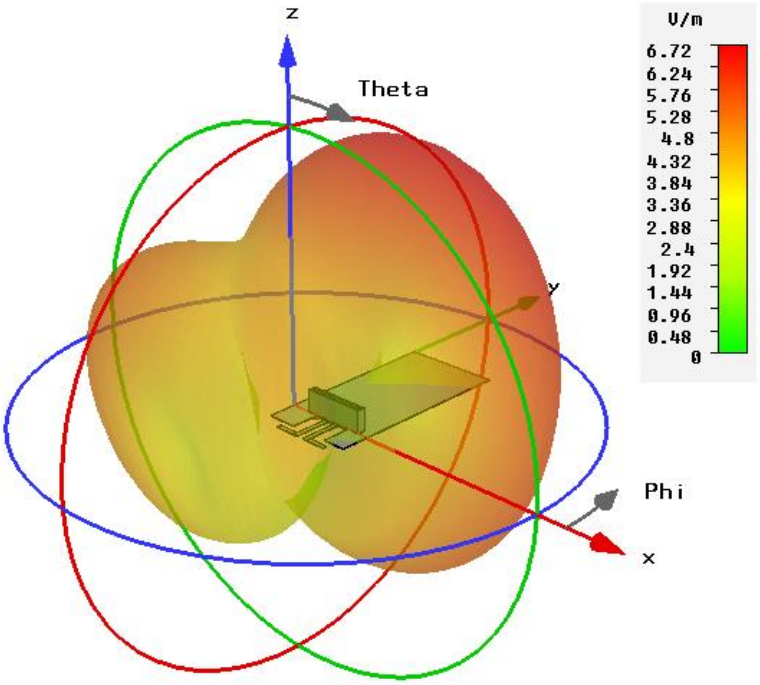

(a)

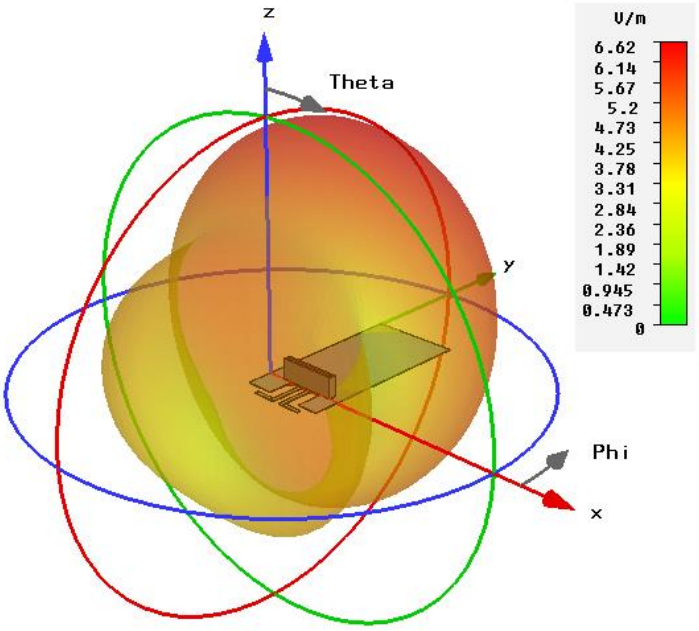

(b)

Fig. 3. 24: Simulated 3D radiation patterns at 2.5 GHz (a) Feed 1, (b) Feed 2

3.5.5 Diversity Performance Parameters

The diversity performance parameters of the proposed dual-feed antenna are also studied and quantified based of the values of ECC, MEG ratio, diversity gain and the total efficiency.

The MEG condition is evaluated from the 3D simulated gain patterns using Eq (2.19). Table 3.1 summarizes the results over the predefined Gaussian model for both indoor and urban outdoor environments. It can be seen that the MEG ratios satisfy the branch power ratio condition (less than 3 dB).

Table 3.1: MEG in different environments at 2.5 GHz

Environment	Mean Effective Gain (dB)		k
	Feed 1	Feed 2	
Indoor	-2.97	-3.23	0.26
Outdoor	-5.26	-6.31	1.05

Fig. 3.25 shows the measured and simulated ECC between the antenna feeds using Eq. (2.15), a good agreement is clearly shown. The figure shows that the ECC of less than (0.13) have been achieved, which is also less than the critical limit (ECC< 0.5).

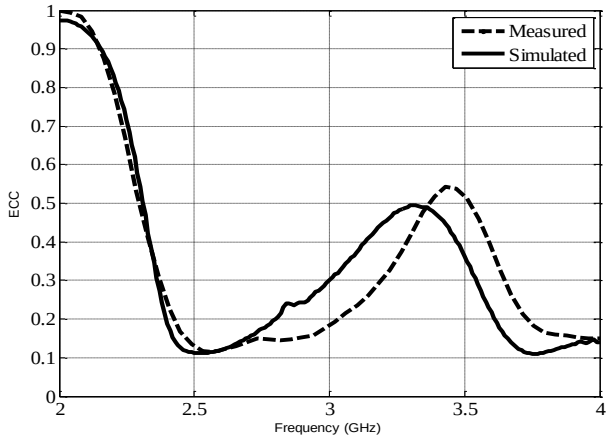

Fig. 3. 25: Measured and simulated envelope correlation coefficient

The measured diversity gain is calculated based on the measured ECC-that is presented in Fig. 3.25- using Eq. (2.24). Fig. 3.26 shows the measured and simulated

diversity gain, it shows that both results are in a good agreement with an average value about 8.5 dB over the covered frequency band.

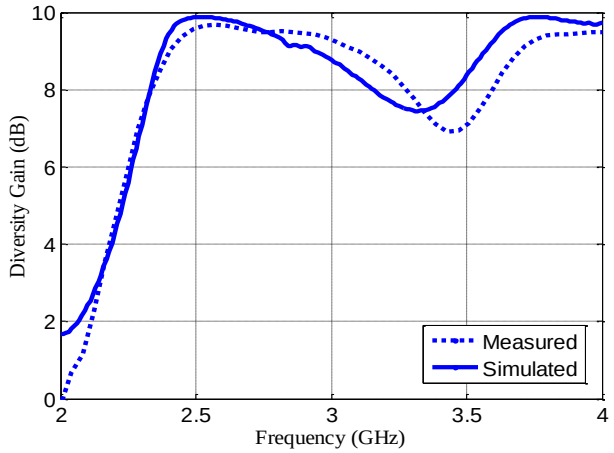

Fig. 3. 26: Measured and simulated diversity gain using ECC

Initially, the measurement of the total radiation efficiency is conducted inside a reverberation chamber at the University of Liverpool. The three antenna method that is discussed in Section 2.4.5.1 is employed over the frequency band of interest (2.0-4.0 GHz). After acquiring the measured data, the total radiation efficiency is calculated using Eq.(2.28) and then Eq.(2.27). Fig.3.27 shows a good agreement between the measured and the simulated total efficiencies of each feed. For frequencies between 2.4 and 2.7 GHz, the total efficiencies are over 50 % on average. Also, compared to the single-feed water-based antenna (see Fig. 3.15), the total efficiency is doubled with the dual-feed design.

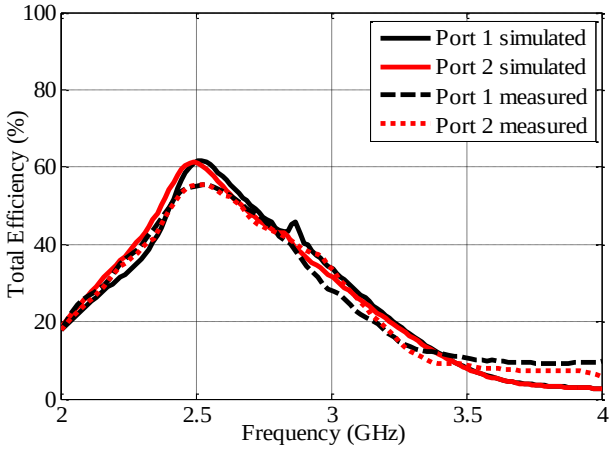

Fig. 3. 27: Measured and simulated total efficiency

3.6 Dual-Feed RDRA with a Very High Dielectric Constant

Up to this point, two cost-effective water based RDRA designs have been proposed and investigated. Both designs have been presented for wireless applications over the frequency range of (2.4-3.4 GHz). Due to the lossy nature of the pure water over microwave frequencies, the resulted radiation efficiencies are quite low, especially, for the case of the single feed antenna (Section 3.4). The question may arise now, what is the benefit behind using pure water as a dielectric material? It has been stated at the beginning of this chapter that the pure water represents a very cheap material with a very high dielectric constant ($\varepsilon_r = 81$). Also, its liquidity state makes the fabrication process very simple.

Further simulations are also conducted for the case of a pure dielectric material having the same dielectric constant of water ($\varepsilon_r = 81$) and zero dielectric loss. The study demonstrates the following key points:

1) For the single feed case, the proposed antenna structure covers the frequency band from 2.5 GHz to 2.7 GHz having a bandwidth of 200 MHz for S_{11}< -10 dB. Furthermore, the interesting finding can be shown from Table 3.2 is that the antenna structure has the lowest antenna profile compared to the previous works-having equivalent dielectric constant in the literature.

Table 3.2 Single-feed loss-free RDRDA compared to other work

Ref	ε_r	Frequency band (GHz)	Height (mm)	Shape
[25]	80	2.4-2.5	24	C-shaped
[32]	79	2.1-2.8	23	RDRA
This Work	81	2.4-3.4 for lossy 2.5-2.7 for lossless	10	RDRA

2) The dual-feed design is also simulated with a free loss material having a relative permittivity equal to $\varepsilon_r = 81$. Fig. 3.28 shows that the proposed antenna

structure has a 10 dB return loss bandwidth about 300 MHz (2.4-2.7 GHz), it also has an acceptable isolation level better than 11 dB over the covered frequency band. Also, Fig. 3.29 shows the resulted total efficiency for both feeds is greater than 80 %.

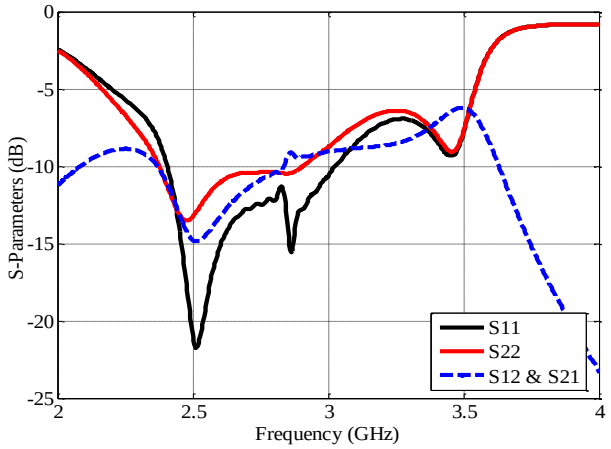

Fig. 3. 28: S-parameters of the proposed dual-feed RDRA antenna with a loss-free material having a dielectric constant $\varepsilon_r = 81$

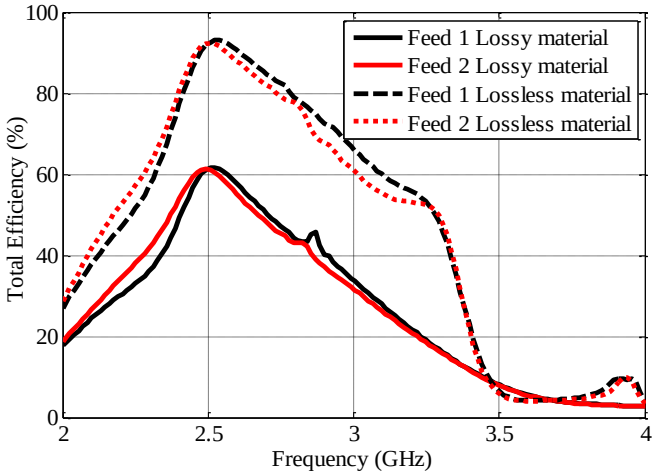

Fig. 3. 29: Radiation efficiency comparison between RDRA with a lossless material of $\varepsilon_r = 81$ and a lossy material of $\varepsilon_r = 81$

3.7 Summary

In this chapter, two new RDRA antennas have been presented. Both designs utilized pure water as a cost effective liquid dielectric material having a very high dielectric constant.

The first design was a single-feed RDRA antenna. A coaxial feed has been used to excite the fundamental mode ($TE^{y}_{1\delta1}$). A broadband operation has been achieved over the frequency range of (2.4-3.4 GHz) but with a low total radiation efficiency due to the high dielectric water loss.

To manage and solve the radiation deficiency appeared in the single-feed design; a dual-feed water based RDRA antenna has been proposed and investigated. The proposed antenna can operate with pattern diversity over the frequency range of 2.34-3.43 GHz with a wide impedance bandwidth. It covers 2.4 GHz WLAN, Bluetooth and three LTE bands (band 7, band 38 and band 41). A parasitic decoupling element has been used to help both feeds isolation and radiation. Finally, it has been shown that if the dielectric loss of the water is neglected, then both the single feed and the dual feed water antennas gave good results over the frequency range of 2.4-2.7 GHz.

References

[1] Y. Kosta and S. Kosta, "Liquid antenna systems," *In Proc. IEEE Antennas and Propagation Society International Symposium*, vol. 3, pp. 2392-2395, June, 2004.

[2] Y. Kosta and S. Kosta, "Realization of a microstrip-aperture-coupled-passive liquid antenna," *In Proc. IEEE International RF and Microwave Conference*, pp. 135-138, Dec, 2008, Kuala Lumpur.

[3] P. Yaghmaee, O. H. Karabey *et al*, "Electrically tuned microwave devices using liquid crystal technology," *International Journal on Antenna and Propoagation*., vol. 2013, Article ID: 824214, 2013.

[4] J.-C. S. Chieh and A.-V. Pham, "A bidirecetional microstrip X-band antenna array on liquid crystal polymer for beamforming applications," *IEEE Transactions on Antennas and Propagation*., vol. 61, no. 6, pp. 3364-3368, June. 2013.

[5] L. Xing, Y. Huang, Y. Shen, S. ALja'afreh *et al*, "Broadband U-shaped water antenna for DVB-H applications," *In Proc. IEEE Antennas and Propagation Society International Symposium*, pp. 1930-1931, July, 2014.

[6] Y. Li and K.-M. Luk, "A water dense dielectric patch antenna," *IEEE Access*, vol. 3 pp. 274-280, April, 2015.

[7] C. Hua, Z. Shen and J. Lu, "High effeciency sea-water monopole antenna for maritime wireless communications," *IEEE Transactions on Antennas and Propagation*., vol. 62, no. 12, pp. 5968-5973, December. 2014.

[8] L. Xing, Y. Huang, S. Aljaafreh and S. J. Boyes, "A monopole water antenna," In *Proc. Loughborough Antennas Propagation Conference*., pp. 1-4, Nov. 2012.

[9] S. Aljaafreh, Y. Huang and L. Xing, "A compact dual-feed water-based diversity antenna," In *Proc. Loughborough Antennas Propagation Conference*., pp. 1-4, Nov. 2013.

[10] L. Xing, Y. Huang *et al*, "Further investigation on water antennas," *IET Microwaves, Antennas and Propagations*, vol. 9, no. 8, pp. 735-741, 2014.

[11] L. Xing, Y. Huang *et al*, "Reconfigurable 3D folded monopole Antenna Design," In *Proc. Loughborough Antennas Propagation Conference*., pp. 1-4, Nov. 2014.

[12] L. Xing, Y. Huang *et al*, "Wideband hybrid rectangular water antenna for DVB-H applications," Microwave and Optical Technology Letters., vol. 57, no. 9, pp. 2160-2164, April. 2015.

[13] H. Fayad and P. Record, "Broadband liquid antenna," *Electronics Letters*, vol. 42, no.. 3, pp. 133-134, Feb. 2006.

[14] Z. Hu, Z. Shen, W. Wu "Reconfigurable leaky-wave antenna based on periodic water grating," *IEEE Antenna and Propagation Letters*, vol. 13, pp. 134-137, 2013.

[15] Z. Hu, Z. Shen, W. Wu "Reconfigurable water antennas," *In Pros. IEEE Conference on Antennas Measurements and Applications*, Nov, 2014, Antibes Juan-les-Pins.

[16] R. Zhou, H. Zhang and H. Xin, "A compact water based dielectric resonater antenna," *In Proc. IEEE Antennas and Propagation Society International Symposium*, pp. 1-4, June, 2009.

[17] R. Zhou, H. Zhang and H. Xin, "Liquid-based dielectric resonator antenna and its applications for measuring liquid real permittivities," *IET Microwaves, Antennas and Propagations*, vol. 8, no. 4, pp. 255-262, March. 2014.

[18] www.cst.com

[19] S. A. Long, M. W. Mcallister, L. C. Shen, "The resonant dielectric cavity antenna," *IEEE Transactions on Antennas and Propagation* , vol. 31, no. 3, pp. 406-412, May. 1983.

[20] K. W. Leung, K. Y. A. Lai, K. M. Luk *et al.*, "Input impedance of aperture coupled hemispherical dielectric resonator antenna," *Electronics Letters*, vol. 29, no. 13, pp. 1165-1167, 1993.

[21] M. W. Mcallister, S. A. Long, and G. L. Conway, "Rectangular dielectric resonator antenna," *Electronics Letters*, vol. 19, no. 6, pp. 218-219, 1983.

[22] R. K. Mongia, and A. Ittipiboon, "Theoretical and experimental investigations on rectangular dielectric resonator antennas," *Antennas and Propagation, IEEE Transactions on*, vol. 45, no. 9, pp. 1348-1356, 1997.

[23] A. Petosta, *Dielectric resonator antenna handbook*, Norwood, MA, Artech House, 2007.

[24] E. R. Collin, *Foundation for microwave engineering*, NewYork, McGraw, 1966.

[25] M. Rotaru and J. K, Sykulski, "Numerical investigation on compact multimode dielectric resonator antennas of very high permittivity," *Science, Measurement & Technology, IET*, vol. 3, no. 3, pp. 217-228, 2009.

[26] R. F. Harrington, *Time harmonic electromagnetic fields*, NewYork, McGraw-Hill, 1961.

[27] K. Ishimiya, J. Langbacka, Y. Zhinong *et al.*, "A compact MIMO DRA antenna.", *International workshop on antenna technology. IWAT 2008*, pp. 286-289.

[28] C. Oikonomopoulos-Zachos, and B. Rembold, "A 4-Port antenna for MIMO channels.", *EuCAP 2007*, pp. 1-4.

[29] L. Z. Thamae, and Z. Wu, "Diversity performance of multiport dielectric resonator antennas," *Institution of Engineering and Technology*, vol. 4, no. 11, pp. 1735-1745, Nov.2010.

[30] P. Vainikainen, J. Ollikainen, O. Kivekas and I. Lelander, "Resonator-based analysis of the combination of mobile handset antenna and chassis, " *IEEE Transactions on Antennas and Propagation*, vol. 50, no. 10, pp. 1433-1444, Oct. 2002.

[31] J. F. Valenzuela, N. A. Garcia-Fernandez, *et al*,"The influence of effeciency on receive diversity and MIMO capacity for rayleigh fading channels," *IEEE Trans. Antennas Propag.*, vol. 65, no. 5, pp. 1444-1450, May. 2008.

[32] G. Bit-Babik, C. Di Nallo, and A. Faraone. "Multimode dielectric resonator antenna of very high permittivity," *IEEE Antennas and Propagation Society International Symposium*, 2004

Chapter 4: A Low Profile Dual-Feed PIFA Antenna

4.1 Introduction

Nowadays, there is a strong demand for a higher data rate and better reliability in wireless communication systems. The MIMO technology [1] has become a core technology to meet this demand. This is related to its ability in increasing the channel capacity with the number of antennas at both communication ends without using the conventional techniques likes increasing transmitted power or using more spectrum [2]. Also with multiple antenna schemes, the antenna diversity plays an important role in increasing the reliability of wireless systems.

MIMO antenna design can be conducted normally using either multiple element antennas (MEA) or isolated mode antenna technology (IMAT). It has been shown that MEA arranged in a pattern or polarization diversity configuration with sufficient antenna spacing can offer a large diversity gain [3]. However, recent trends in mobile market require small, slim handset terminals for multisystem; these increase the demand for low profile, small size, and multiband/wideband antennas. The design of MIMO antenna systems for small mobile terminals becomes very challenging because saving space means increasing the level of mutual coupling that will degrade MIMO and diversity system performance. In order to meet the compactness requirement for MIMO antenna systems, IMAT was introduced as a new design approach [4] in which a single antenna element with more than one feed can be used as a compact MIMO antenna scheme. However, the compact MIMO antenna is normally achieved at the expense of a large mutual coupling level, thus isolation techniques are required.

The isolation between MIMO antenna elements or ports is a critical design parameter. Strongly coupled antennas have very poor radiation efficiency and MIMO system performance, because an antenna element or port will act as a load for the other elements or ports [5]. Up to now, several decoupling techniques have been proposed to reduce the antenna mutual coupling in small portable devices. Changing the spacing of antennas is one of the oldest techniques to decrease the mutual coupling level [5], but this technique is not suitable for small portable devices because of the limited space. Matching networks have been used as decoupling networks and applied to several antenna structures like monopoles [6], dipoles [7], patch antennas [8] and planar inverted-F antennas (PIFA) [9]. But this technique has several drawbacks: the first one lies in the resulted ohmic losses from the matching network components; the second issue is the large utilized space; and the third

problem is that the resulted antenna bandwidth usually is narrow [6]. Decoupling the current path known as the neutralization line has been proposed for different antenna structures [10-12]. A neutralization line with an optimized shape and dimensions provides a reverse current path of the original path between antenna elements [10]. In addition, a defect ground plane structure [13-15] is one of the popular isolation techniques, and it has been widely used for closely spaced and coupled antennas.

Among various antenna structures like monopoles, patches, and slots, the PIFA is the most widely used structure in the portable wireless devices due to its excellent features (low profile, ease to design, low cost and reliable performance). It has also received a lot of attention for MIMO antenna systems [16-18]. Recently, compact dual-feed diversity PIFA antennas were proposed for MIMO applications [19-21]. Although these designs were novel, they have several drawbacks like: the height of these antennas is relatively large [19-21] and the bandwidth is relatively narrow [19-21], thus it is difficult to use them in real applications. Table 4.1 summarizes all the published dual-feed PIFA works.

In this chapter, a new wideband and very low profile PIFA antenna with a new feed arrangement is proposed for handset wireless applications over the frequency range of 2.35-3.25 GHz. It employs polarization diversity that is achieved using a coplanar feed. The work presented in this chapter can be considered as the continuation of the work reported in [19-21] in the sense of using the dual-feed to form a MIMO and diversity antenna. It presents a new PIFA feed arrangement (coplanar feed) that has two excellent features to overcome the aforementioned drawbacks of other feed arrangements in [19-21]: it offers lower mutual coupling level and, at the same time, it allows the use of waveguide slots to achieve the radiation and isolation. Finally, the structure of this PIFA antenna can be modified and scaled down to cover the lower handset's frequency band applications in the range of (1.7-2.7 GHz) for recent smartphones.

The rest of this Chapter is organized as follows: Section 4.2 is about the new feed arrangement based on the output of a comparative study on the mutual coupling between different feed arrangements. Section 4.3 presents the new design configuration. In Section 4.4, the prototype, scattering parameters, current distributions and far-field radiation patterns are provided and discussed. Section 4.5 deals with diversity characteristics and MIMO performance of the prototype; the envelope correlation coefficient, mean effective gains, total radiation efficiency and the diversity gain of the antenna are obtained and discussed. Finally, the summary is drawn in Section 4.6.

Table 4.1 Summary of dual-feed PIFAs

Ref	Modified ground plane	Feed Arrangement	Frequency band (GHz)	Height (mm)
19	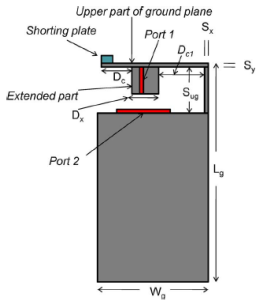	Orthogonal	2.4-2.6	10
20	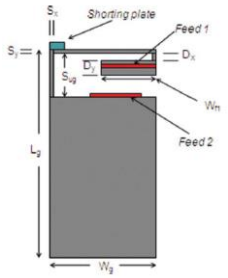	Parallel	2.425-2.475	5
21	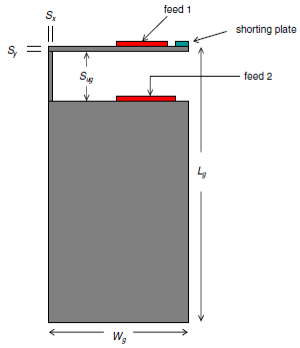	Parallel	2.35-2.55	10
29	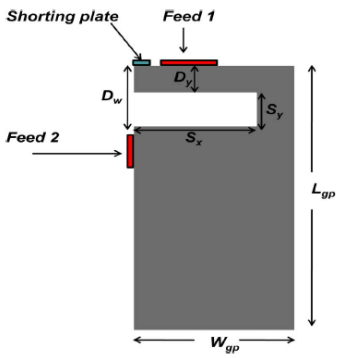	Orthogonal	2.1-2.9	5

4.2 Feed Arrangement Comparative Study

Recently, three multi-port PIFA antennas were proposed [19-21]. However, they have drawbacks such as, high profiles relatively narrow bandwidths and large top plate size which are impractical for real applications. Here, a comparative study on the mutual coupling between PIFA feed arrangements is conducted with the aim to find a solution for the aforementioned drawbacks.

It is well-known that the mutual coupling between MEAs depends on several factors, such as element radiation pattern, array geometry or relative orientation of array elements. In this context, three PIFA feed arrangements are given in Fig. 4.1, a coplanar feed case, parallel feed case and orthogonal feed case. It is worth mentioning that in these cases all parameters are the same except the feed arrangement and shorting pin positions. Fig. 4.2 shows the mutual coupling coefficients obtained using a simulation tool (CST Microwave Studio). We can see that the orthogonal feed exhibits the lowest mutual coupling level; this is obviously due to the utilization of the polarization diversity between the orthogonal feeds. However, the coplanar feed case is selected as the main feed arrangement due to the following reasons:

1) It has about 2.5 dB less mutual coupling level than the parallel feed case by an average. Also, it has a similar mutual coupling level in the orthogonal feed for frequencies above 2.5 GHz.
2) It is a new feed arrangement that has not been employed in the previous designs of a dual-feed PIFA.
3) It offers a geometry of a parallel plate waveguide, which permits the use of the slot waveguide theory to produce either radiation or isolation

From this result, we can ask two questions: why the coplanar feed provides less coupling level? and how to optimize this arrangement for MIMO applications? The answers can be found from the electric field distribution on the top plate and from the geometry of the structure with coplanar feed case, respectively.

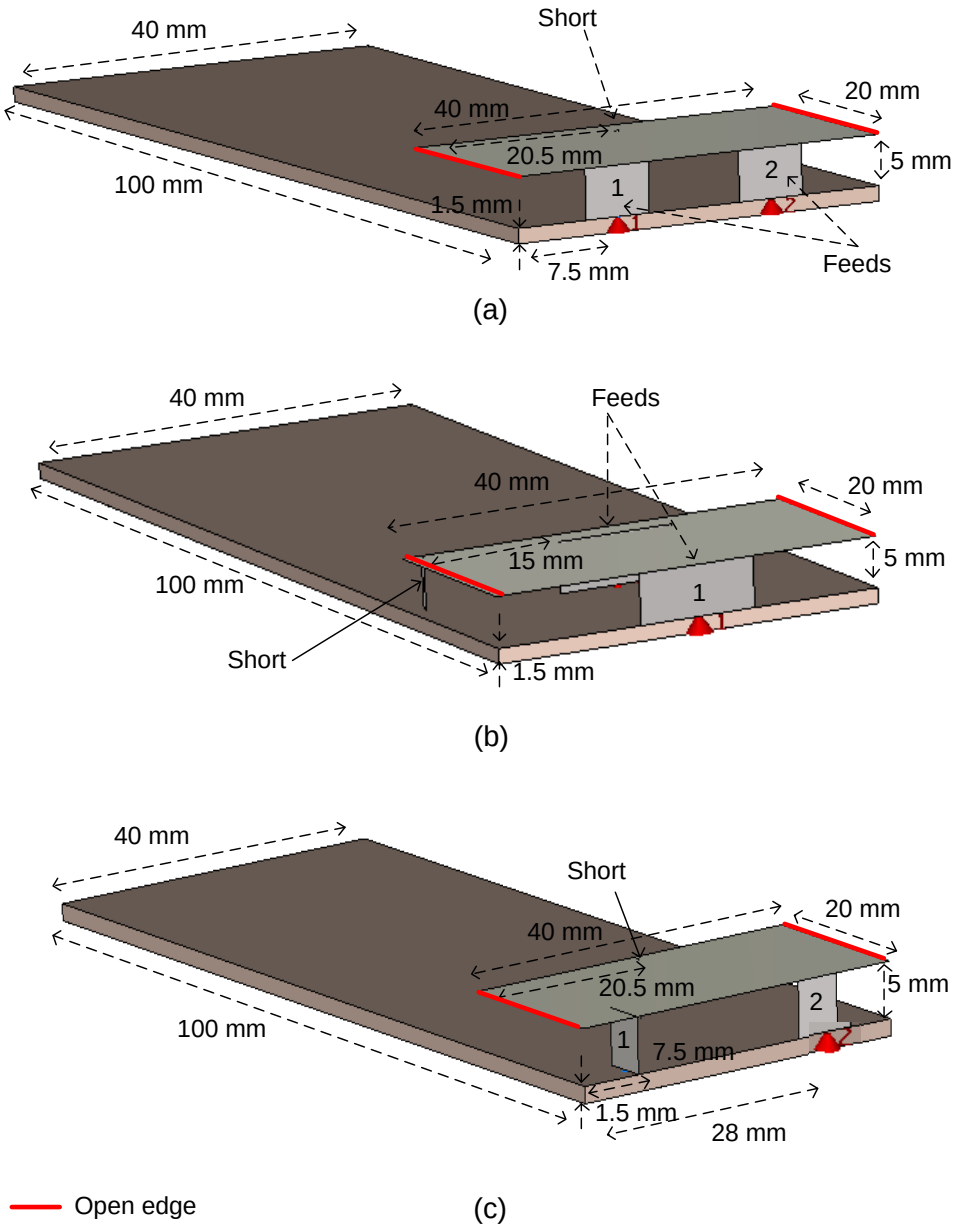

Fig. 4.1: PIFA antenna with different feed arrangements (a) coplanar feed, (b) parallel feed and (c) orthogonal feed

The first issue can be explained from the electric field distribution as shown in Fig. 4.3. It can be seen that both feeds share the same open edge of PIFA in the case of parallel feed, while for the coplanar case, each feed has its own open edge. In another word, this means that the mutual coupling in parallel feed case has two sources: the near field coupling and the surface current coupling, while in the case of coplanar feed, there is only one source of mutual coupling, and it is the surface current. According to this, the equivalent PIFA array [22] for each feed arrangement is drawn in Fig. 4.4.

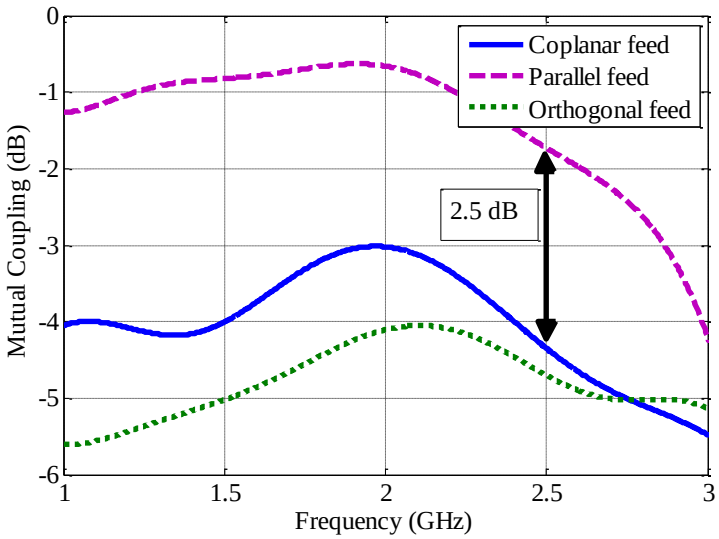

Fig. 4.2: Mutual coupling between PIFA feeds

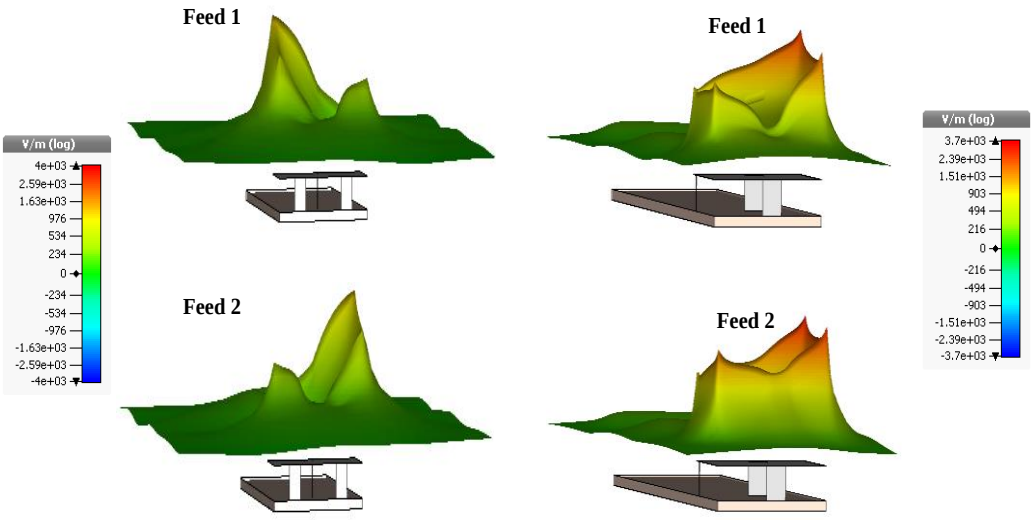

(a)Coplanar feed **(b) Parallel feed**

Fig. 4.3: Electric field distributions on top plate at 2.5 GHz (a) coplanar feed and (b) parallel feed

To deal with the second issue, it is worth noting that the surface current is the effective source of mutual coupling; this can be found from the theory of characteristic mode [23]. The chassis of size (*40 mm ×100 mm*) is selected as an example and it has a full wave characteristic mode around 2.5 GHz as shown in Fig. 4.5. Since both coplanar feeds represent a capacitive coupling element (CCI) (electric source) aligned on the top edge of the chassis; both feeds share the same characteristic mode at 2.5 GHz. However, an important feature of this feed arrangement is that the geometry of the PIFA and ground plane

represents a parallel plate waveguide excited by an electric source (coplanar feed), this waveguide supports transverse electromagnetic (TEM) mode in y-direction – this can be seen from the excited electric and magnetic fields between the top plate and the ground plane as shown in Fig. 4.6 where the arrows on the top plate and ground plane represent the direction of the surface current. Thus, the slot waveguide theory can be employed to analyze and optimize the feed isolation (longitudinal to direction of the surface current), also the radiation can be enhanced if a transverse slot is used [24].

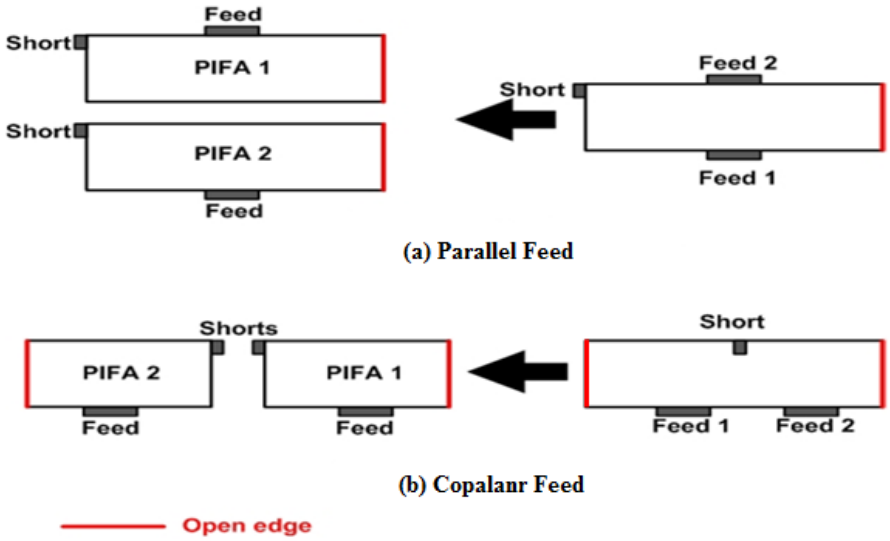

Fig. 4.4: Equivalent array representation of dual-feed PIFA antenna (a) parallel feed and (b) coplanar feed

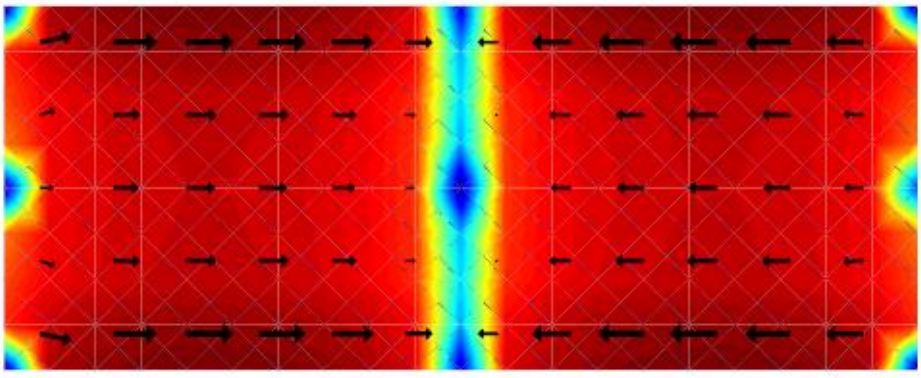

Fig. 4.5: Characteristic mode of a rectangular 40 mm ×100 mm ground plane computed at 2.5 GHz [23].

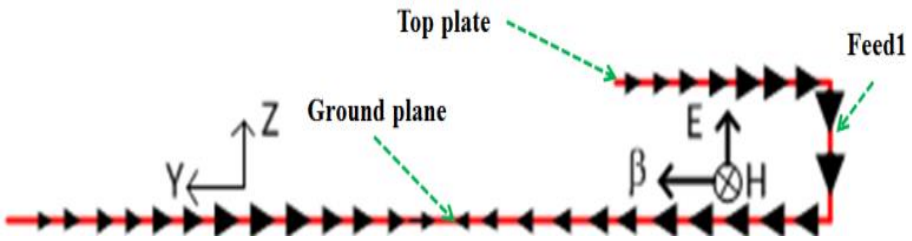

Fig. 4.6: Side view of dual-coplanar-Feed PIFA over ground plane with surface current distribution and excited fields between parallel plates at 2.5 GHz

4.3 Antenna Configuration

Based on the conclusion drawn from the comparative study, a dual coplanar-feed PIFA is proposed and depicted in Fig. 4.7. The top radiating plate of dimensions $W \times L$ is placed at height h over a PCB substrate of dimensions $L_g \times W_g$. In order to improve the impedance matching for Feed 2 without the need for increasing the height, the top plate is modified by creating a small strip with a width W_t, a length L_t, x-position X_t and y-position Y_t. The ground plane has a FR-4 substrate with a thickness $t = 1.5\ mm$ and a relative permittivity $\varepsilon_r = 4.4$. The radiating plate has three legs, two of them are the feeds, the dimensions of Feed 1 and Feed 2 plates are $W_{f1} \times h$ and $W_{f2} \times h$, respectively. The third leg is the shorting pin with dimensions $W_s \times (h + t)$. The horizontal distance of shorting pin from ground plane side edge is X_{sh} and the vertical distance from top edge is Y_{sh}, while the horizontal distances to Feed 1 and Feed 2 from the side edge are X_{f1} and X_{f2}, respectively.

Fig. 7(b) shows the modified ground plane which contains two main types of slots. An L-shaped slot is formed by Slot 1 and Slot 3 with dimensions $W_{s1}\times L_{s1}$ and $W_{s3}\times L_{s3}$, respectively, this slot represents a band stop resonator to provide the isolation between the feeds. Slot 2 is created with dimensions $W_{s2}\times L_{s2}$ to improve the impedance matching for Feed 1 and it will show later that it also radiates the energy from Feed 1.

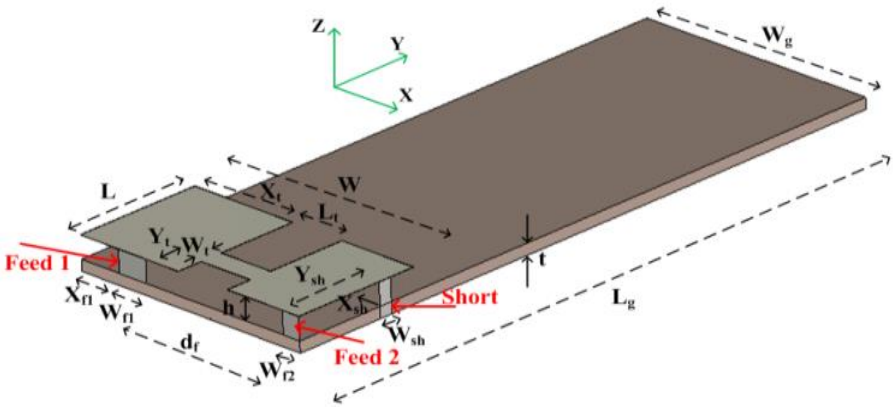

(a)

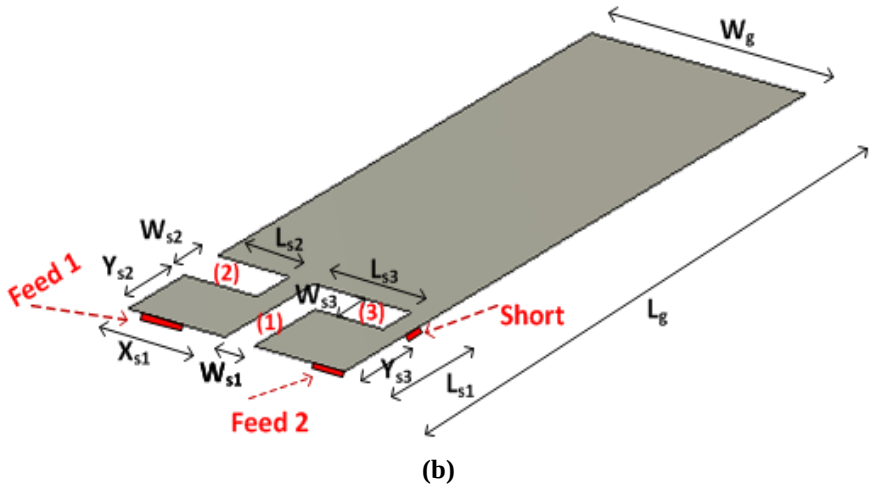

(b)

Fig. 4.7: Structure of dual-coplanar feed PIFA antenna (a) structure and (b) modified ground plane

4.4 Simulated and Measured Results

4.4.1 Prototype and S-parameters

The simulations are performed using CST Microwave Studio to optimize the antenna parameters for the desired operation band and isolation. A prototype (see Fig. 4.8) is constructed using the following optimized design parameters: L_g = 100 mm, W_g = 40 mm, L = 16 mm, W = 40 mm, X_{f1} = 7 mm, X_{f2} = 38 mm, W_{f1} = 5 mm, W_{f2} = 2 mm, d_f = 26 mm, X_{sh} = 40 mm, Y_{sh} = 15.5 mm, W_{sh} = 0.5 mm, h =3 mm, t = 1.5 mm, L_t = 9 mm, W_t = 2.5 mm, Y_t = 4 mm, X_t = 18 mm, X_{s1} = 18 mm, W_{s1} = 5 mm, L_{s1} = 15 mm, W_{s2} = 6 mm, L_{s2} = 14 mm, Y_{s2} = 9

mm, L_{s3} = 18 mm, W_{s3} = 6 mm and Y_{s3} = 9 mm. The simulated and measured S-parameter results are depicted in Fig. 4.9. They are mostly in a good agreement and a slight discrepancy between them is likely due to the effect of soldering and fabrication errors. The design can cover a wide bandwidth 2.35-3.25 GHz (simulated) with a fractional bandwidth of 32 %.

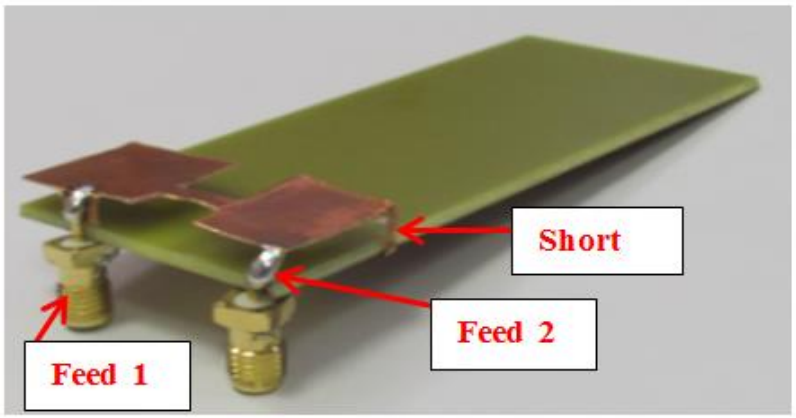

(a)

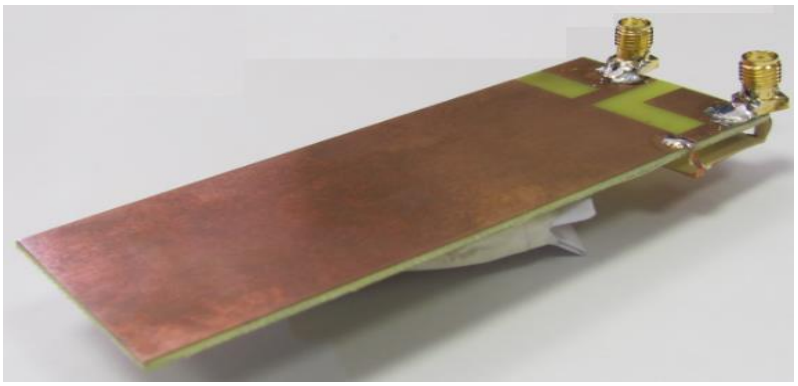

(b)

Fig. 4.8 Prototype of the proposed antenna (a) top view and (b) back view

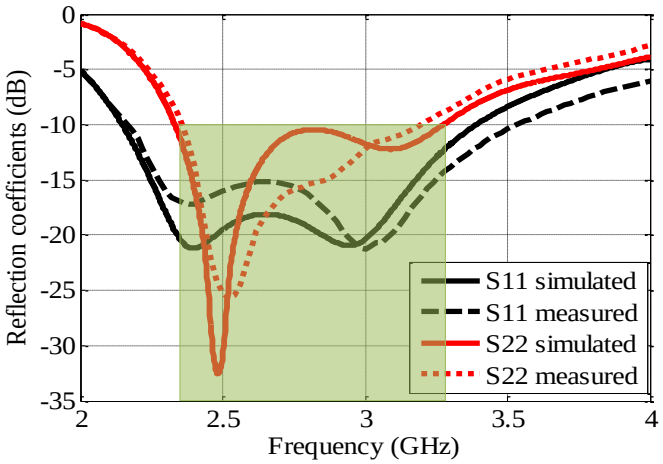

(a)

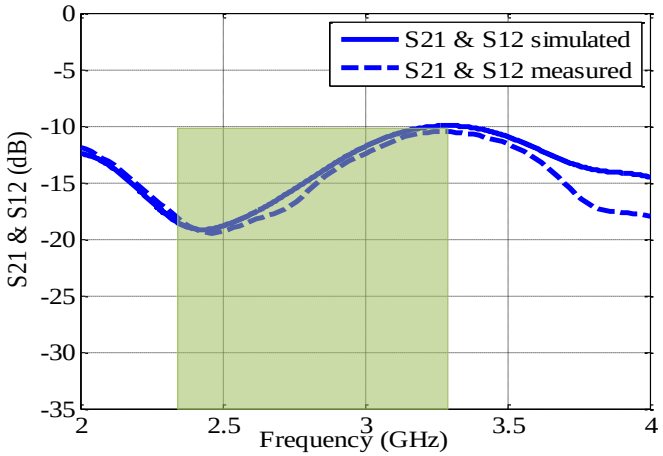

(b)

Fig. 4.9: Measured and simulated S-parameters (a) Reflection coefficients, (b) Transmission coefficients

4.4.2 Current Distributions and Impedance Characteristics

To better understand the achieved results, CST Microwave Studio was used to generate images of the surface current distributions when one feed is excited and the other is terminated with a matched load. Fig. 4.10 shows the current distribution on both the ground plane and the top plate, it can be seen that Feed 1 has a strong current on the open ground plane slot, while Feed 2 has a strong current on the top plate. This means that the antenna fed by Feed 1 is the ground plane slot while the radiation of Feed 2 is mainly from PIFA. Another interesting finding that can give extra evidence on this claim is the current modes on the ground plane; Feed 1 has distributed current mode (usually slot antenna has this kind of

mode [25]) while Feed 2 has a localized current mode underneath the top plate (usually PIFA antenna has this kind of mode [25]). Furthermore, to gain more insight into the achieved results, Fig. 4.11 shows the direction of currents on the top plate fed by Feed 1 and Feed 2 at 2.5 GHz; the arrows represent the direction of current modes. It can be seen that the two feeds have orthogonal current modes. This leads to the production of both polarization and pattern diversities.

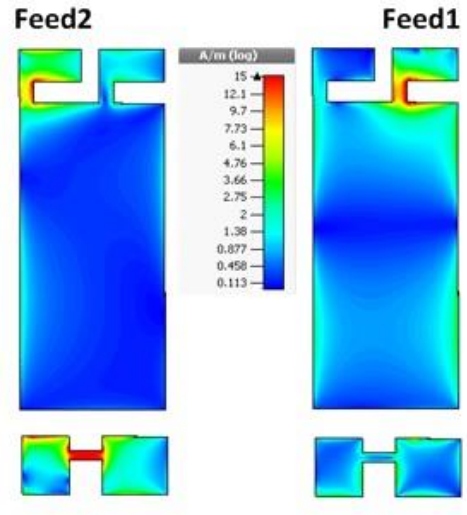

Fig. 4.10: Current distributions at 2.5 GHz

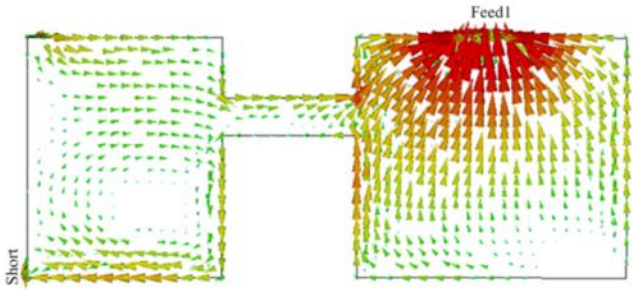

(a)

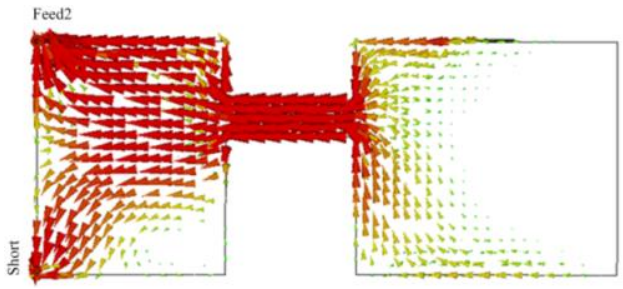

(b)

Fig. 4.11: Directions of currents on the top plate at 2.5 GHz (a) Feed 1 and (b) Feed 2

Furthermore, impedance characteristics can give extra evidence on the operation of the proposed antenna. Fig. 4.12 shows the real and imaginary components of the impedance at feeding Port 1 and Port 2, it shows that Port 2 has a series resonance around 2.5 GHz. This means that Port 2 is connected to a PIFA antenna. On the other hand, Port 1 has a parallel resonance and is linked to a slot antenna (Slot 2) as stated earlier. Also, the wide bandwidth is achieved due to the slow change in the impedance around the resonant frequency.

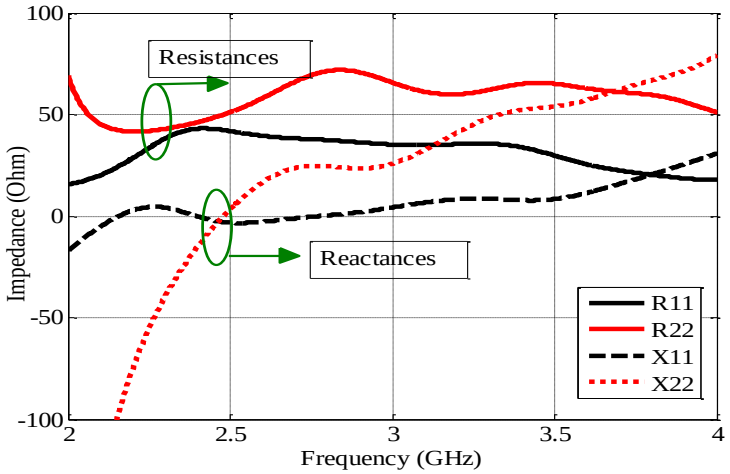

Fig. 4.12: Input impedance as a function of frequency

4.4.3 Far-field Radiation Patterns

The radiation patterns are produced at 2.5 GHz under the condition that one feed is excited while the other one is terminated with a matched load. The simulated and measured normalized radiation patterns in XZ-plane, YZ-plane and XY-plane at 2.5 GHz are shown in Fig. 4.13. It is apparent that the radiation patterns of the two feeds have pattern and polarization diversities. Furthermore, the polarization diversity can be in both XZ and YZ planes, the co-polarization radiation patterns of each feed represent the cross polarization radiation pattern of the other feed. This can also be observed from the 3D simulated radiation patterns at 2.5 GHz in Fig. 4.14. Therefore, these properties lead to good antenna diversity in severe fading environments.

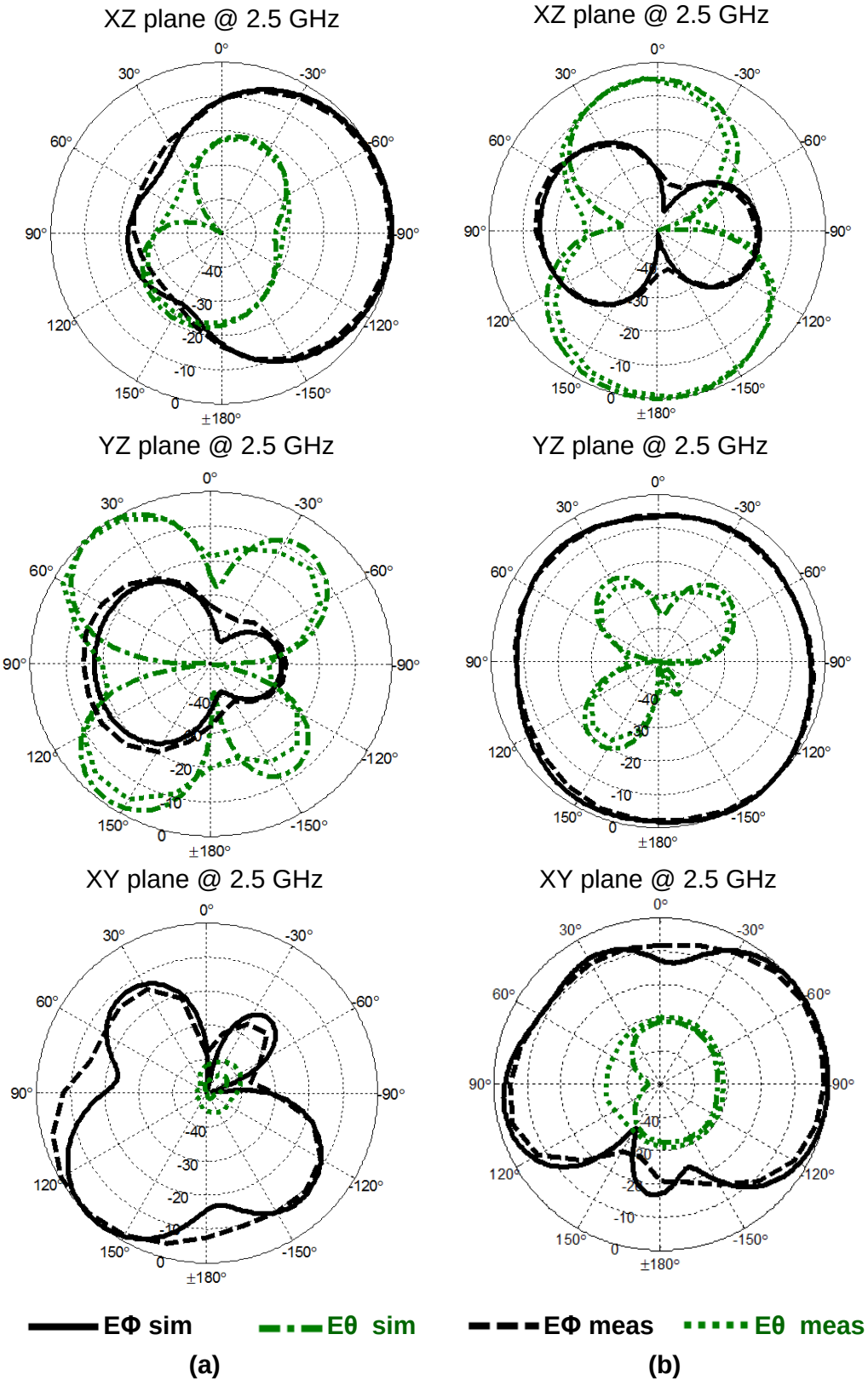

Fig. 4.13 Measured and simulated radiation patterns at 2.5 GHz

(a) Feed 1 and (b) Feed 2

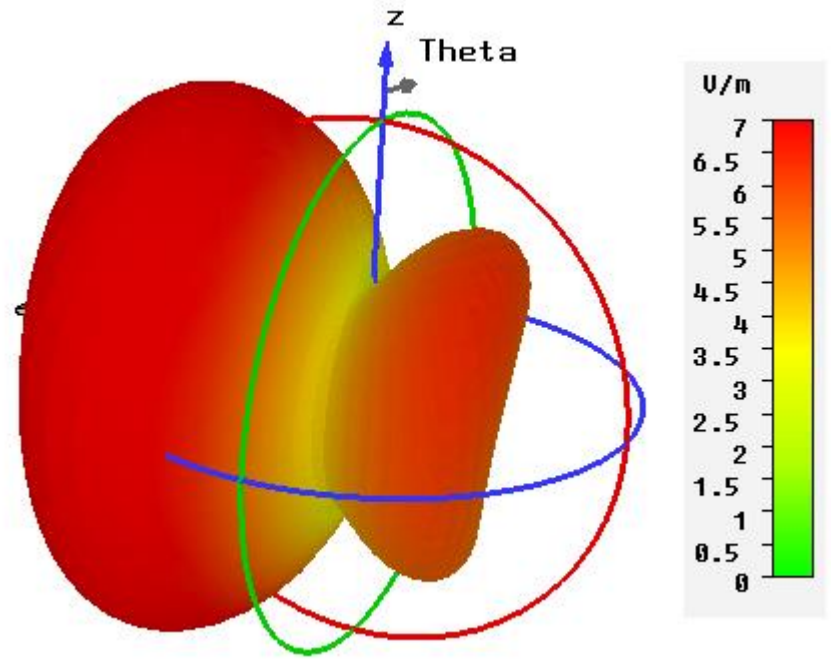

(a)

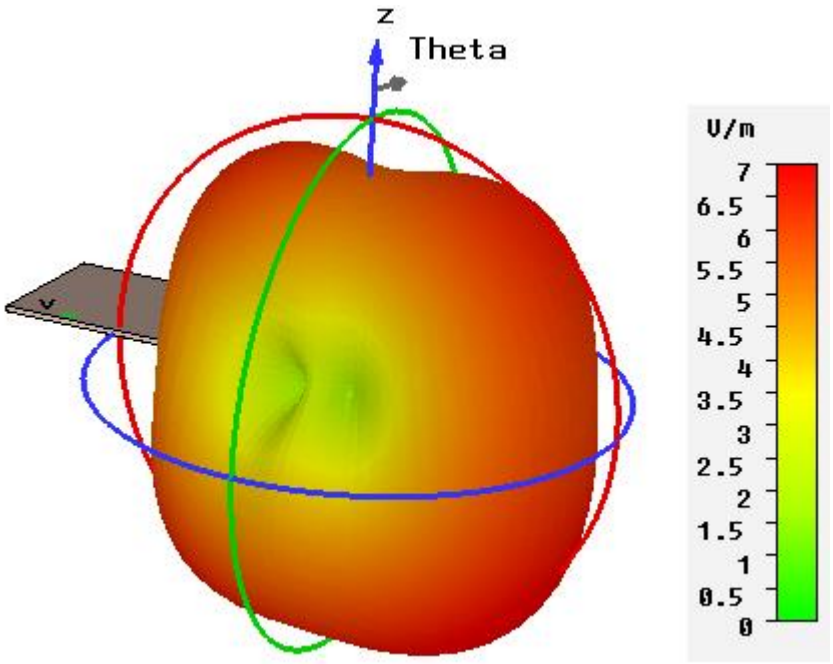

(b)

Fig. 4.14: 3D simulated radiation patterns at 2.5 GHz

(a) Feed 1 and (b) Feed 2

4.4.4 Parametric Study

To gain better insight into the influence of some important design parameters on the frequency response of the reflection coefficients and the mutual coupling coefficients, a parametric study was conducted using CST Microwave Studio. It was done by varying the parameters of interest, while keeping the other design parameters fixed.

1) **Effects of the open ground plane slot** (Slot 2): Fig. 4.15 examines the impact of Slot 2 length (L_{s2}) on the reflection coefficient and impedance matching of Feed 1. It can be seen that S_{11} is sensitive to the length of Slot 2. Furthermore, the study showed that both the length and width of Slot 2 have no effect on Feed 2 response and the isolation level between feeds; because this slot represents a transverse slot in a parallel plate waveguide, which in-turn can help in radiation only [24].

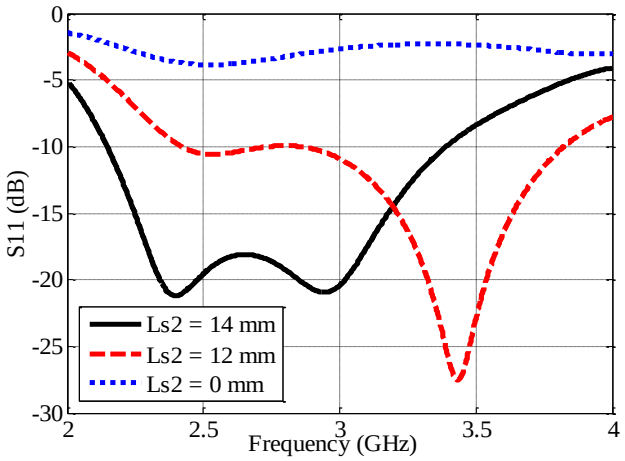

Fig. 4.15: Effect of Slot 2 length on S_{11}.

2) Effects of L-shaped Slot (Slot 1+Slot 3): Fig. 4.16 shows the influence of the L-shaped slot lengths on the mutual coupling coefficients (S_{21} and S_{12}). It can be observed: as the lengths increased, the stop band frequency is decreased (dips on the curves). This can be interpreted from the theory of the transmission line resonators [26]; the L-shaped slot represents a band stop transmission resonator formed from Slot 1 that represents a shunt open-circuit quarter wavelength stub, and Slot 3 which works as a series short-circuit quarter wavelength stub. Although the isolation can be improved, the creation of this slot structure has a negative effect on the level of matching of Feed 2. This is because the position of the slot is located between Feed 2 and the shorting pin.

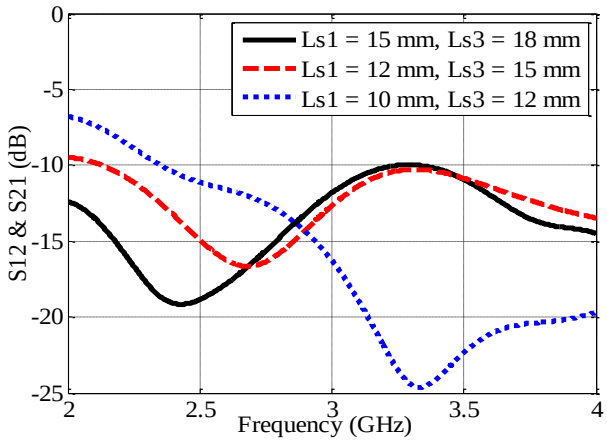

Fig. 4.16: Effect of different L-slot lengths on mutual coupling coefficients

3) Effects of top plate strip: It can be seen from Fig.4.17 (a), the effect of varying the width of the top plate strip is on the level of the impedance matching of Feed 2. This can be interpreted as a simple matching circuit is formed from a series inductance (small width strip) and a shunt capacitance (capacitance between the left hand side of the top plate and the ground plane) [27]. There is no need to increase the antenna profile, thus the proposed antenna has the lowest profile compared the other designs in [19-21, 29].

A question now is how much this strip will affect the feed isolation. To answer this question, a further parametric study has been done on the parameters of the strip; such as: the strip width, strip position and strip length. The results demonstrate that the top plate strip affects only the level of matching of Feed 2. Fig.4.17 (b) shows that the width of the strip has little effect on the level of isolation. This leads to the conclusion that the small strip on the top plate is to improve the impedance match, not the isolation, thus it is different from the neutralization line in [28].

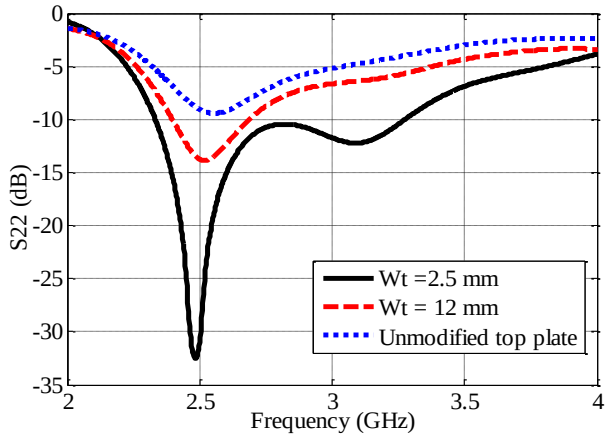

(a)

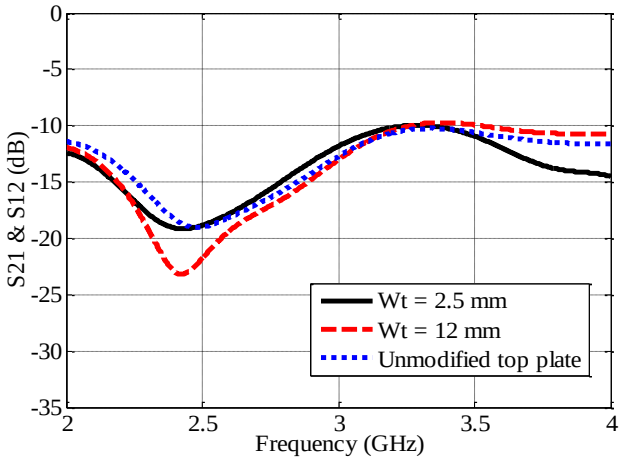

(b)

Fig. 4.17: Effect of top plate strip width on (a) Reflection coefficient of Feed 2 and (b) Mutual coupling coefficient

4.5 Diversity Performance Parameters

The diversity characteristics and MIMO performance parameters of the proposed antenna are simulated, measured, and evaluated in free space; the parameters like envelope correlation coefficient, antenna branch power ratio in terms of the mean effective gain (MEG) ratio, the total efficiencies and the diversity gain are presented in this section.

4.5.1 Mean Effective Gain and Envelope Correlation Coefficient

As there is a lack of facility to conduct the measurement of 3D gain patterns. The MEG of each feed within the different environments explained in Chapter 2 is evaluated from the 3D simulated gain patterns using Eq (2.19). The results are tabulated in Table 4.2, it can be seen that the calculated values over the defined Gaussian model in both indoor and urban outdoor environments have satisfied the acceptable diversity criteria of branch power ratio (less than 3 dB [5]).

Table 4.2: MEG in different environments at 2.5 GHz

Environment	Mean Effective Gain (dB)		K
	Feed 1	Feed 2	
Indoor	-3.23	-3.33	0.1
Outdoor	-6.12	-5.89	0.27

As the proposed antenna has a small loss dielectric substrate, ECC is calculated using S-parameters and radiation efficiency method (Eq (2.15)). Fig. 4.18 shows the simulated and measured values are in a good agreement; also the values of ECC are less than 0.02 within the whole operation band. Based on (2.16), ECC satisfies the condition and this is another good metric for MIMO system.

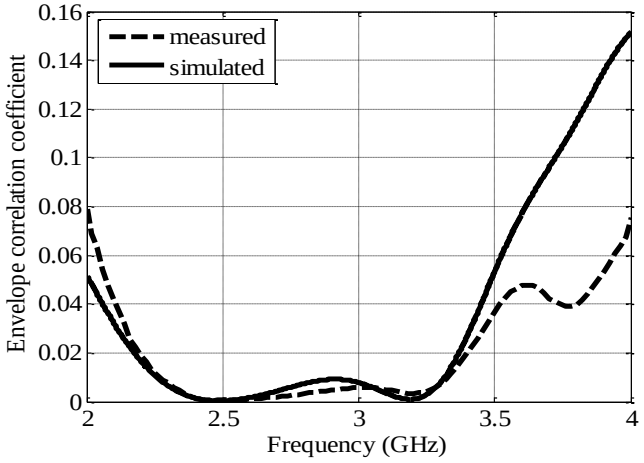

Fig. 4.18: Envelope correlation coefficient

As the proposed diversity antenna has a very low ECC and an acceptable MEG ratio over different environments, this will lead to a high diversity gain. The measured diversity gain is presented in the next sub-section.

4.5.2 Diversity Gain

The diversity gain of the proposed antenna is measured in a reverberation chamber. The measurement utilizes the reverberation chamber at the University of Liverpool. The apparent diversity gain result is calculated using the CDF method explained in Section 2.4.4.1. Fig. 4.19 shows the proposed antenna has a diversity gain around a 0.01 CDF level is about 9.95 dB. Furthermore, Table 4.3 compares the top plate dimensions, antenna profile, modified ground plane area, feed arrangement, frequency bandwidth and diversity gain of the proposed design with some recently published results. It shows that the proposed design has achieved excellent performance with the lowest profile, smallest modified ground plane area (256 mm^2) and largest bandwidth. Thus, the antenna is a good candidate for modern handset applications. Thus, the antenna is a good candidate for modern handset applications.

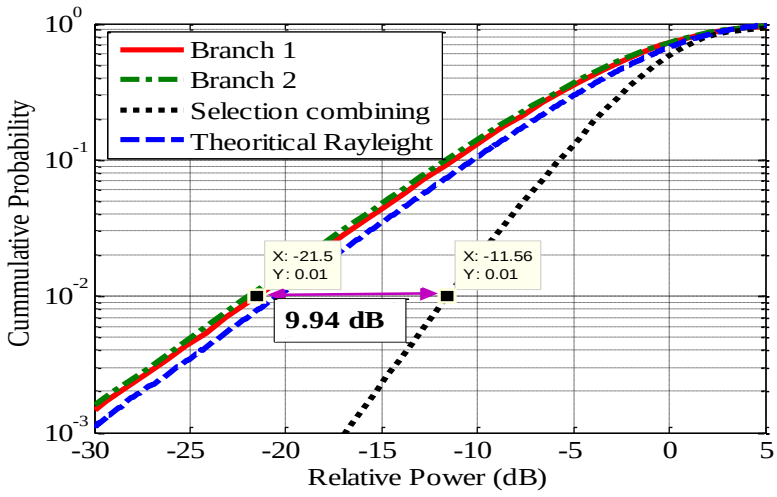

Fig. 4.19: CDF functions and apparent diversity gain

Table 4.3: Comparison the proposed design with previous works

Ref	Feed arrangement	Diversity scheme	Frequency band (GHz)	Modified ground area (mm^2)	Height (mm)
[19]	Orthogonal	Pattern and polarization	2.35-2.6	772	10
[20]	Parallel	Pattern	2.425-2.475	711	5
[21]	Parallel	Pattern	2.4-2.6	644	10
[29]	Orthogonal	Pattern and polarization	2.1-2.9	700	5
Work	Coplanar	Pattern and polarization	2.35-3.2	256	3

4.5.3 Total Radiation Efficiency

The same collected data from the diversity gain measurement is used in calculating the total efficiencies. The simulated and measured total efficiencies are calculated using Eq (2.28) and (2.27) are depicted in Fig. 4.20. It shows that the proposed antenna has a high total radiation efficiency (> 80%) over the frequency band of interest.

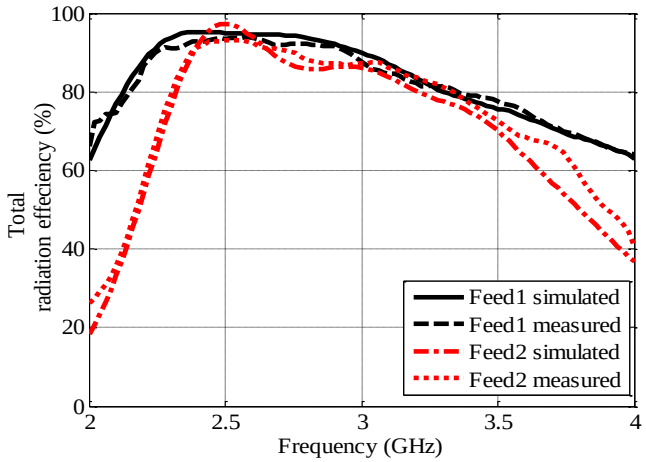

Fig. 4.20: Measured and simulated total efficiency

4.6 Summary

In the literature, several dual-feed PIFA designs have been proposed for diversity and MIMO applications. But all of them share several drawbacks like: a high antenna profile, a narrow operational bandwidth and unreliable use. In this Chapter, a new wideband, low profile (height = 3 mm) dual-coplanar-feed PIFA antenna has been presented as a diversity and MIMO antenna for wireless applications over the frequency band 2.35-3.25 GHz. The key of this design lies in the use of a new feed arrangement that exhibits a lower mutual coupling level compared to other feed arrangements. Both pattern and polarization diversities have been achieved by exciting two orthogonal modes; Feed 1 radiation is mainly from the open ground plane slot, while Feed 2 radiation is from PIFA loop mode. The feeds isolation has been achieved via L-shaped ground plane slot. Both simulated and measured results have been presented in a good agreement. The results also show that this antenna has a good diversity performance across the whole operational bandwidth.

It should be pointed out that the frequency band can be easily scaled up or down to cover the desired frequencies using the same design since the width of the mobile for this investigation is just *40 mm* while most of the latest smart phones have a width of *70 mm*. As an example: if we increase the width to *55 mm* (a scaling factor of 1.33), Fig. 4.21 shows that the design can cover about 1 GHz 6-dB bandwidth (1.70 to 2.70 GHz). Also, a dual-element antenna can be installed to cover the lower frequency applications below 1 GHz; this can be easily done with the aid of metallic frame as one antenna element and other antenna element at the lower edge of PCB [30].

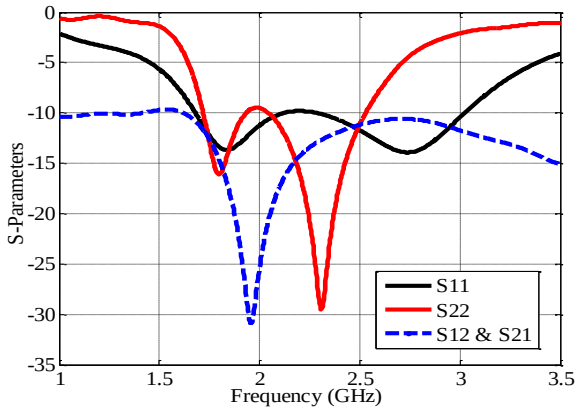

Fig. 4.21: Modified design response for *55 mm* × *100 mm* smartphone PCB

References

[1] G. J. F and M. J. Gans, "On limits of wireless communications in a fading environment when using multiple antennas," *Bell Labs Technical Journal,* vol. 1, no.2, pp 41-59, 1996.

[2] S. Zhang, B. K. Lau, Y. Tan, Z. Ying and S. He., "Mutual coupling reduction of two PIFAs with a T-shape slot impedance transformer for MIMO mobile terminals," *IEEE Transactions on Antennas and Propagation,* vol. 60, no. 3, pp. 1521-1531, 2012.

[3] C. B. Dietrich, Jr., K. Dietze, J. R. Nealy *et al.*, "Spatial, polarization, and pattern diversity for wireless handheld terminals," *IEEE Transactions on Antennas and Propagation,* vol. 49, no. 9, pp. 1271-1281, 2001.

[4] F. M. Caimi, M. Mongomery and P. Tornatta, "Isolated mode antenna technology (IMAT)," SkyCross, Inc, Jan, 2008.

[5] R. G. Vaughan, and J. B. Andersen, "Antenna diversity in mobile communications," *IEEE Transactions on Vehicular Technology,* vol. 36, no. 4, pp. 149-172, 1987.

[6] J. Andersen, and H. Rasmussen, "Decoupling and descattering networks for antennas," *IEEE Transactions on Antennas and Propagation,* vol. 24, no. 6, pp. 841-846, 1976.

[7] J. W. Wallace, and M. A. Jensen, "Mutual coupling in MIMO wireless systems: a rigorous network theory analysis," *IEEE Transactions on Wireless Communications, ,* vol. 3, no. 4, pp. 1317-1325, 2004.

[8] S. Dossche, J. Rodriguez, L. Jofre *et al.*, "Decoupling of a two-element switched dual band patch antenna for optimum MIMO capacity." *IEEE Antennas and Propagation Society International Symposium 2008,* pp. 325-328, July. 2008.

[9] C. Volmer, J. Weber, R. Stephan *et al.*, "Mutual coupling in multi-antenna systems: figures-of-merit and practical verification.", *in Proc. 3rd European Conference on Antennas and Propagation (EuCAP 2009),* pp. 1114-1118, March. 2009, Germany.

[10] A. Diallo, C. Luxey, P. Le Thuc *et al.*, "Enhanced two-antenna structures for universal mobile telecommunications system diversity terminals," *IET Microwaves, Antennas & Propagation,* vol. 2, no. 1, pp. 93-101, 2008.

[11] A. M. Han, J. Choi, " Small-size printed strip MIMO antenna for next generation mobile handset application," *Microw. Opt. Technol. Lett,* vol. 53, pp. 348-352, 2011.

[12] J. Holopainen, O. Kivekas, C. Icheln *et al.*, "Internal broadband antennas for digital television receiver in mobile terminals," *IEEE Transactions on Antennas and Propagation,* vol. 58, no. 10, pp. 3363-3374, 2010.

[13] F. Zhu, J. Xu and Q. Xu, "Reduction of mutual coupling between closely-packed antenna elements using defected ground structure," *In Proc. 3rd IEEE International Symposium on Microwave, Antenna Propagation and EMC Technologies for Wireless Communications*, Oct. 2009.

[14] C. Chi-Yuk, C. Chi-Ho, R. D. Murch *et al.*, "Reduction of mutual coupling between closely-packed antenna elements," *IEEE Transactions on Antennas and Propagation*, vol. 55, no. 6, pp. 1732-1738, 2007.

[15] Y. Gao, X. Chen, Z. Ying *et al.*, "Design and performance investigation of a dual-element PIFA array at 2.5 GHz for MIMO terminal," *IEEE Transactions on Antennas and Propagation*, vol. 55, no. 12, pp. 3433-3441, 2007.

[16] Y. Yao, X. Wang, X. Chen *et al.*, "Novel diversity/MIMO PIFA antenna with broadband circular polarization for multimode satellite navigation," *IEEE Antennas and Wireless Propagation Letters*, vol. 11, pp. 65-68, 2012.

[17] S. C. Chen, Y. S. Wang, and S. J. Chung, "A decoupling technique for increasing the port isolation between two strongly coupled antennas," *IEEE Transactions on Antennas and Propagation*, vol. 56, no. 12, pp. 3650-3658, 2008.

[18] S. Blanch, J. Romeu, and I. Corbella, "Exact representation of antenna system diversity performance from input parameter description," *Electronics Letters*, vol. 39, no. 9, pp. 705-707, 2003.

[19] H. T. Chattha, Y. Huang, S. J. Boyes *et al.*, "Polarization and pattern diversity-based dual-feed planar inverted-F antenna," *IEEE Transactions on Antennas and Propagation*, vol. 60, no. 3, pp. 1532-1539, 2012.

[20] H. T. Chattha and Y. Huang, "Low profile dual-feed planar inverted-F antenna for wireless LAN applications," *Microwave Optical Technology Letters*, vol. 53, pp. 1382–1386, 2011.

[21] H. T. Chattha, Y. Huang and X. Zhu, "Dual-feed PIFA diversity antenna for wireless applications," *Electronics Letters*, vol. 46, no. 3, pp. 189-190, 2010.

[22] H. Carrasco, H. D. Hristov, R. Feick, and D. Cofré, " Mutual coupling between planar inverted-F antennas," *Microwave Optical Technology Letters*, vol. 42, no. 3, pp. 224–227, 2004.

[23] J. Rahola and J. Ollikainen., "Optimal antenna placement for mobile terminals using charactristic mode analysis," *In Proc. First Europian Conference on Antennas and Propagation (EUCAP 2006)*, Nov. 2009, France.

[24] S. Silver, Microwave antenna theory and design, McGraw-Hill, 1949 (Volume.12 of Radiation Laboratory Series, reprinted 1984).

[25] L. Hui, T. Yi, L. Buon Kiong *et al.*, "Characteristic mode based tradeoff analysis of antenna-chassis interactions for multiple antenna terminals," *IEEE Transactions on Antennas and Propagation,* vol. 60, no. 2, pp. 490-502, 2012.

[26] David M. Pozar, *Microwave engineering*, John Wiley & Sons, 3rd Edition,1998.

[27] Paul H. Young, *Electronic communications techniques*, Prentice Hall, 5th Edition, 2003.

[28] A. Diallo, C. Luxey *et al.*, "Study and reduction of the mutual coupling between two mobile phone PIFAs operating in the DCS 1800 and UMTS bands," *IEEE Transactions on Antennas and Propagation,* vol. 54, no. 11, pp. 3063-3074, Nov. 2006.

[29] H. T. Chattha, M. Nasir *et al.*, "Compact low-profile dual-port single wideband planar inverted-F MIMO antenna," *IEEE Antenna and Propagation Letters*, vol. 12, pp. 1673-1675, 2013.

[30] H. Li, Z. Miers and B. K. Lau., "Design of orthogonal MIMO handset antennas based on the charactristic mode manipulation at frquency bands below 1 GHz," *IEEE Transactions on Antennas and Propagation,* vol. 62, no. 5, pp. 2756-2766, May. 2014.

Chapter 5: A Wideband Dual-Element PILA Antenna

5.1 Introduction

Over the last 25 years, mobile communications industry has enjoyed a rapid growth: it has been evolved from 1G to digital 2G, then to 3G and now to 4G systems [1]. This induces the development of multiple input and multiple output (MIMO) technology, which improves the communication quality and increases the system capacity. Thus, to take the advantage of this new technology, multiple antennas should be integrated at both communications ends. In conjunction to this evolution, the market trend is now moving to smart phones that include other wireless technologies like WiFi, NFC (near field coupling), GPS and Bluetooth (2.45 GHz). Moreover, some new features are added to handset design such as a slim design and a large display [2]. Thus, the integration of small footprint antennas, low profile, multi-elements and multi-standards handset antennas is a subject of huge interest.

However, to meet the above requirements and to gain MIMO advantages, the antenna correlation should be minimized by decreasing the level of mutual coupling. Despite several isolation techniques have already been proposed, the practical implementation in commercial products is still very challenging [3]; this increases the importance of conventional diversity techniques like spatial, pattern and polarization diversities, especially, when they are employed with small footprint, low profile and multi-standard antennas.

Unlike other antenna structures (loop antenna [4], planar inverted-F antenna [5] and printed monopole antenna [6]) that are widely used as internal antennas in handset devices, the PILA is rarely used; this is because it suffers from high impedance mismatch loss resulted from the low input resistance and high input reactance. In literature, several techniques have been employed to deal with this problem, e.g., modifying the radiator structure by adding another shorted inverted-L (convert to PIFA), or modifying the feed by using a dielectric resonator antenna (DRA) as a feed [7]. To our knowledge, there is no work dealt with the interaction between the PILA top plate and the ground plane underneath. Also, based on a very recent work on the interaction between the handset antenna and the ground plane in [2], this Chapter proposes a low profile and wideband PILA diversity antenna for mobile applications in the frequency range from 1.7 to 2.85 GHz.

In this Chapter, a study on this antenna is conducted to gain a better understanding on the antenna and the working mechanism behind the single element design. A two-element MIMO antenna based on the developed PILA is then proposed, simulated, optimised, fabricated and measured. The diversity performance parameters are obtained from the simulation and measurement results.

5.2 Single Element Design

5.2.1 Antenna Configuration

The proposed element antenna is depicted in Fig. 5.1. The top plate with dimensions of 5×15 mm^2 is placed 5 mm above the ground plane with a FR-4 substrate of dimensions $55\times100\times1.5$ mm^3, relative permittivity of $\varepsilon_r = 4.3$ and a loss tangent of tan $\delta = 0.025$. The radiating top plate has a feed strip with dimensions 2×5 mm^2. To reduce the electrical length and provide capacitive loading, a vertically bended plate with dimensions of 11×5 mm^2 is added to the end of the top plate. To enhance the radiation resistance and the impedance bandwidth, a ground plane notch is created by partially removed the ground plane underneath the top plate; the dimensions of the removed area are 9×39 mm^2. Finally, a very small parasitic ground plane strip with dimensions of 15×2 mm^2 is added to the notch to reduce the lower edge frequency down to 1.7 GHz.

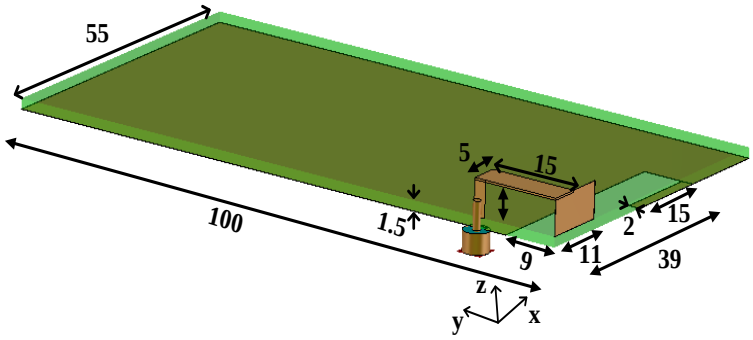

Fig. 5.1: Geometry of the proposed element antenna (unit: mm)

5.2.2 Design Process

To reveal the operational mechanism of the proposed antenna, an evolutional design process including five stages is drawn in Fig. 5.2 and the resulted reflection coefficient S11 after each design stage is also presented (linked by colour). It shows how much improvement

is made on the antenna impedance matching after each stage. In stage 2, part of the ground plane was removed which caused a reduction in the reactance – this in turn increased the resonant frequency of the PILA and created a new resonance dip related to the resulted ground plane notch. Stage 3 was to add an additional length at the end of top plate; this provided an inductive load that shifted the resonant frequencies downwards. Although the operating band was shifted down in stage 3, the top plate size was increased and the resulting antenna impedance at both resonance dips suffered from capacitive reactance (as shown in Fig. 5.3 (a)). Consequently, a capacitive loading was employed in stage 4 by bending the added section; this reduced the antenna size and created a pure resonance at both resonant frequencies. Fig. 5.3 (b) clarifies the effectiveness of capacitive loading introduced by bending the end plate; a simple matching circuit represents a self-matching circuit resulted from both inductive loading by meandering (series inductor) and capacitive loading by bending (shunt capacitor). To shift the lower edge frequency down to 1.7 GHz, stage 5 was conducted by loading ground notch with a small strip. With this addition the design has dual resonance; the first resonance related to the ground plane notch, it is about 0.25 wavelength at 1.95 GHz, while the second one is linked to PILA with a total length equal 0.25 wavelength at 2.64 GHz). Finally, the design utilizes a small footprint area over the ground (about 351 mm^2 which is less than the element size in [6] which is about 375 mm^2) and covers a wide frequency bandwidth 1.7- 2.85 GHz for S11 < -10 dB.

To further understand the wideband operation, simulated surface current distributions at the frequencies 1.95 GHz and 2.64 GHz are given in Fig. 5.4. When the antenna operates at 1.95 GHz, most of the currents are concentrated along the ground plane notch, while at 2.64 GHz the currents are concentrated on the PILA top plate.

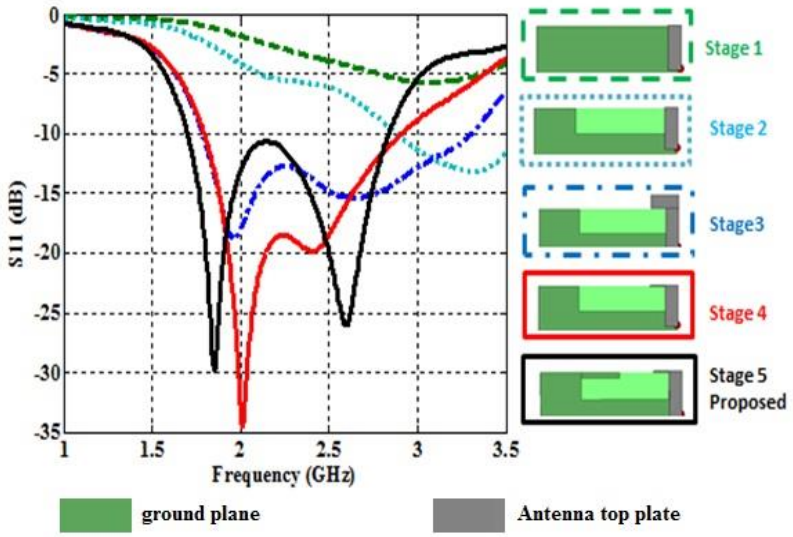

Fig. 5.2: The step by step change on geometry and S_{11} evolutions

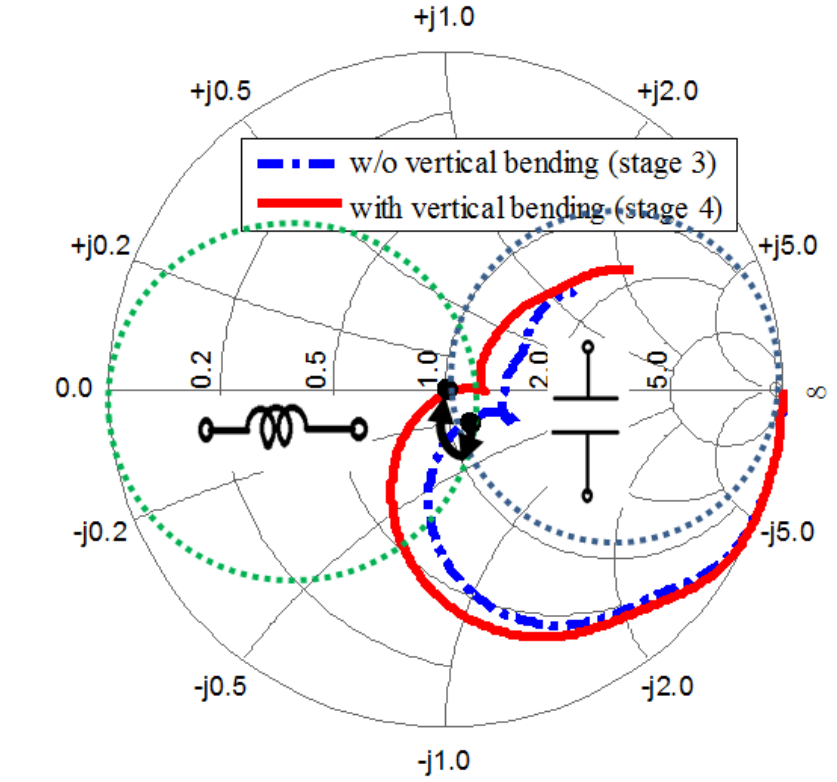

(a)

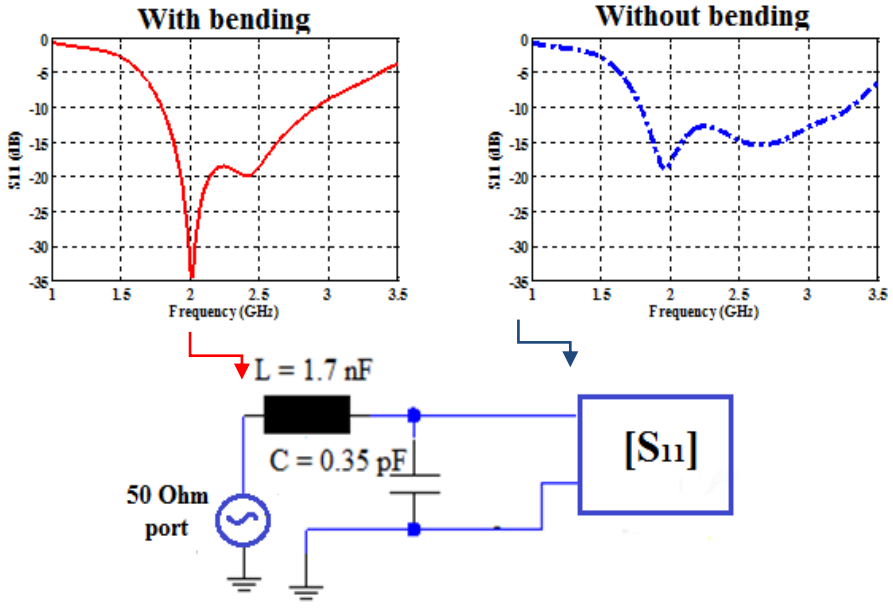

(b)

Fig. 5.3. Effect of the bended plate (a) Smith chart of normalized input impedance, (b) S_{11} and equivalent matching circuit

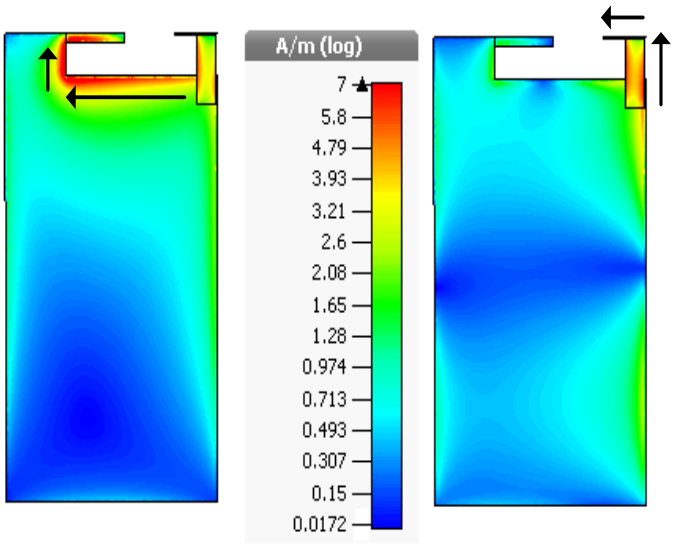

(a) **(b)**

Fig. 5.4: Simulated surface current distributions (a) at 1.95 GHz and (b) at 2.64 GHz

5.2.3 Prototype and S-parameters

In order to validate the simulation results, a prototype antenna shown in Fig 5.5 was fabricated and tested. It can be seen from Fig. 5.6 that the measured results show a similar trend as the simulated results and exhibit almost the same behaviour. It is evident that the proposed antenna covers DCS1800, PCS1900, UMTS2100, LTE2300, LTE2500, WiFi and Bluetooth frequency bands based on the -10 dB bandwidth criterions.

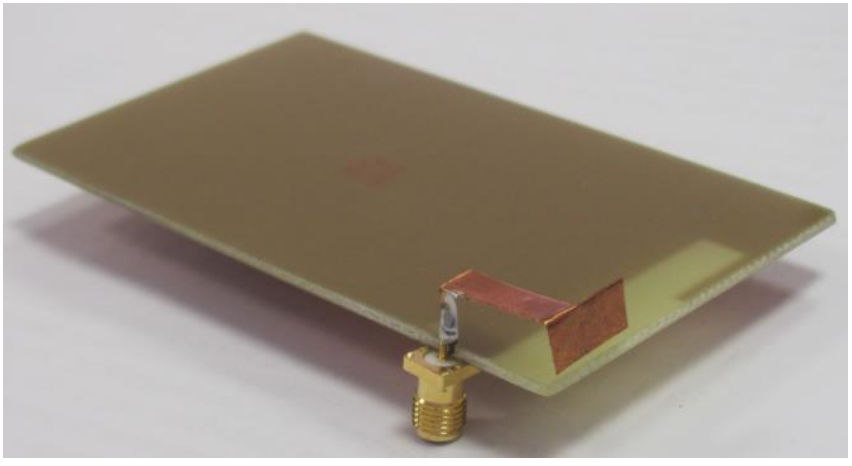

Fig. 5.5. Single element PILA prototype

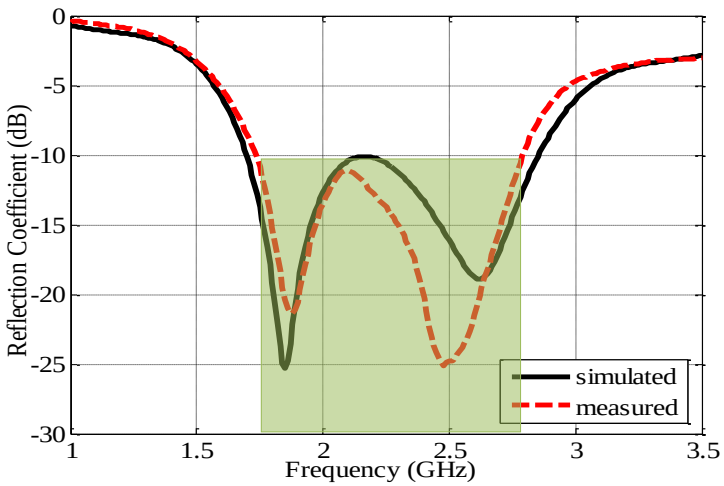

Fig. 5.6: Measured and simulated reflection coefficients of single element

5.2.4 Far-field Radiation Patterns

The radiation patterns of the prototype antenna were measured inside an anechoic chamber at the University of Liverpool. The 2D polar plots of the measured and simulated radiation patterns of this antenna at 1.95 GHz and 2.64 GHz in dB scale are show in Fig. 5.7, Fig. 5.8 and Fig. 5.9 for XY, XZ and YZ planes, respectively. The discrepancies on XZ and YZ plane patterns are mainly due to the inclination of the prototype while it was in the vertical positions (XZ and YZ planes). Furthermore, the simulated 3D radiation pattern at both resonant frequencies are attached to Fig. 5.10.

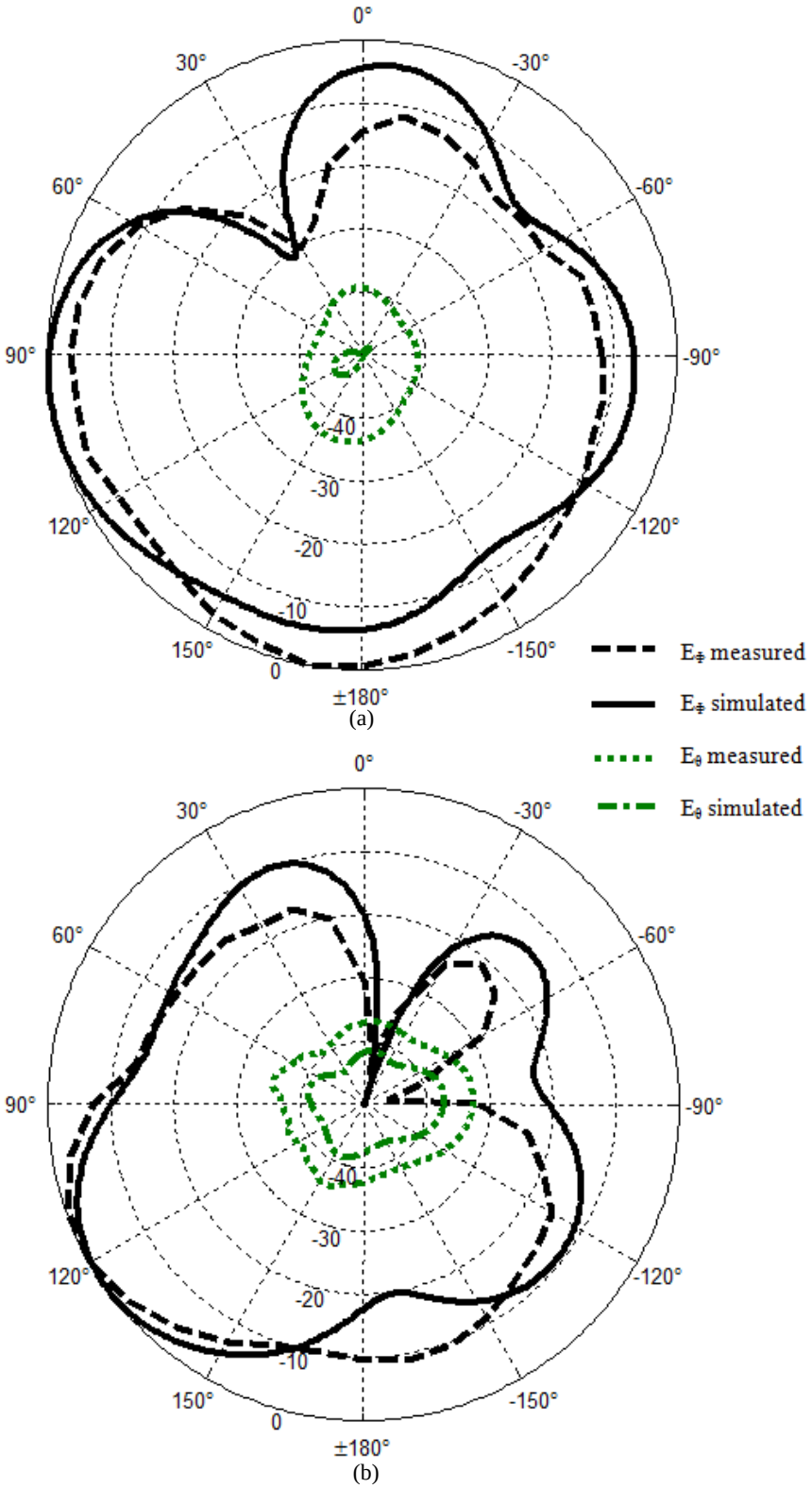

Fig. 5.7 Measured and simulated radiation patterns in XY plane

(a) at 1.95 GHz and (b) at 2.64 GHz

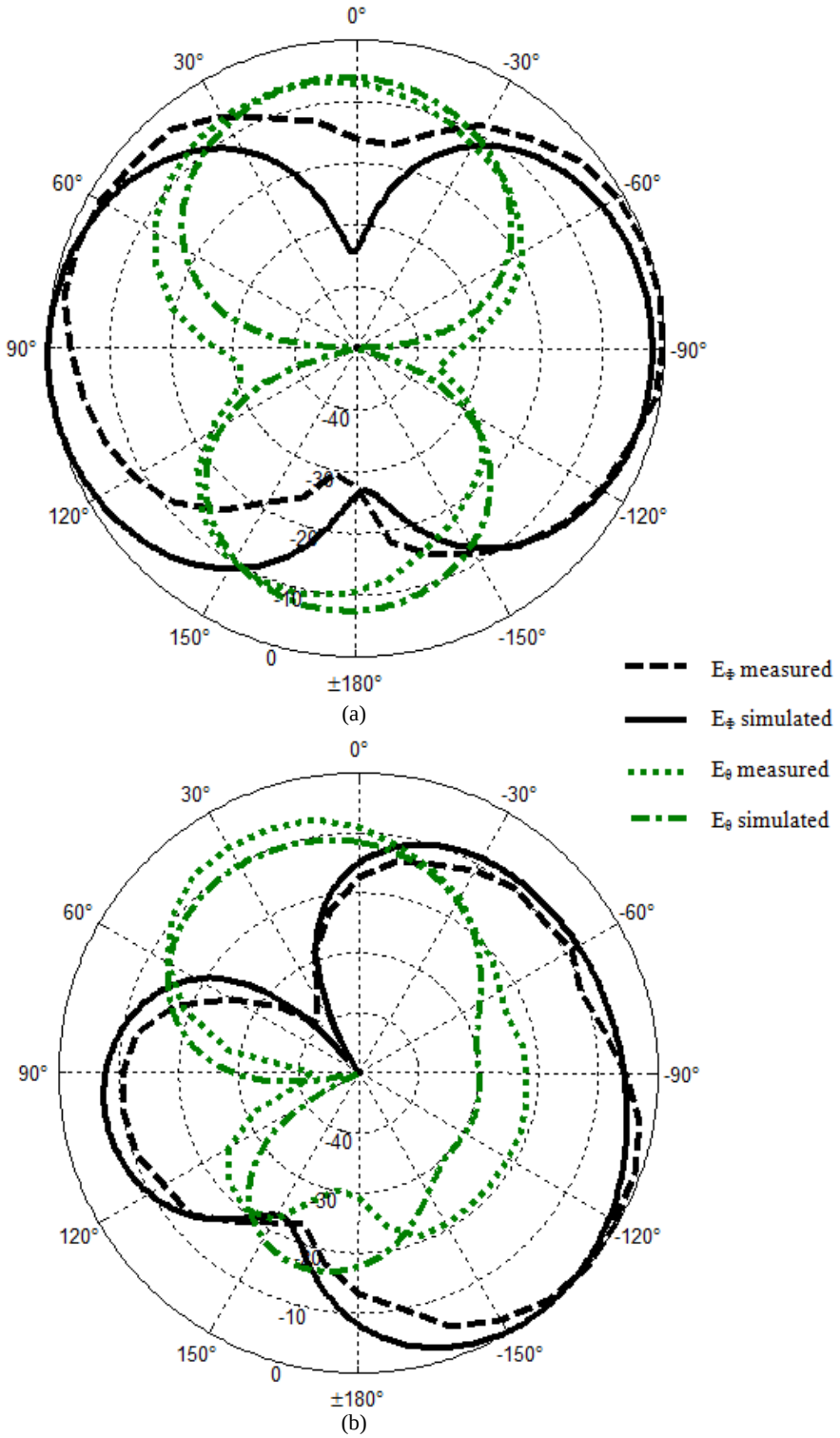

Fig. 5.8 Measured and simulated radiation patterns in XZ plane

(a) at 1.95 GHz and (b) at 2.64 GHz

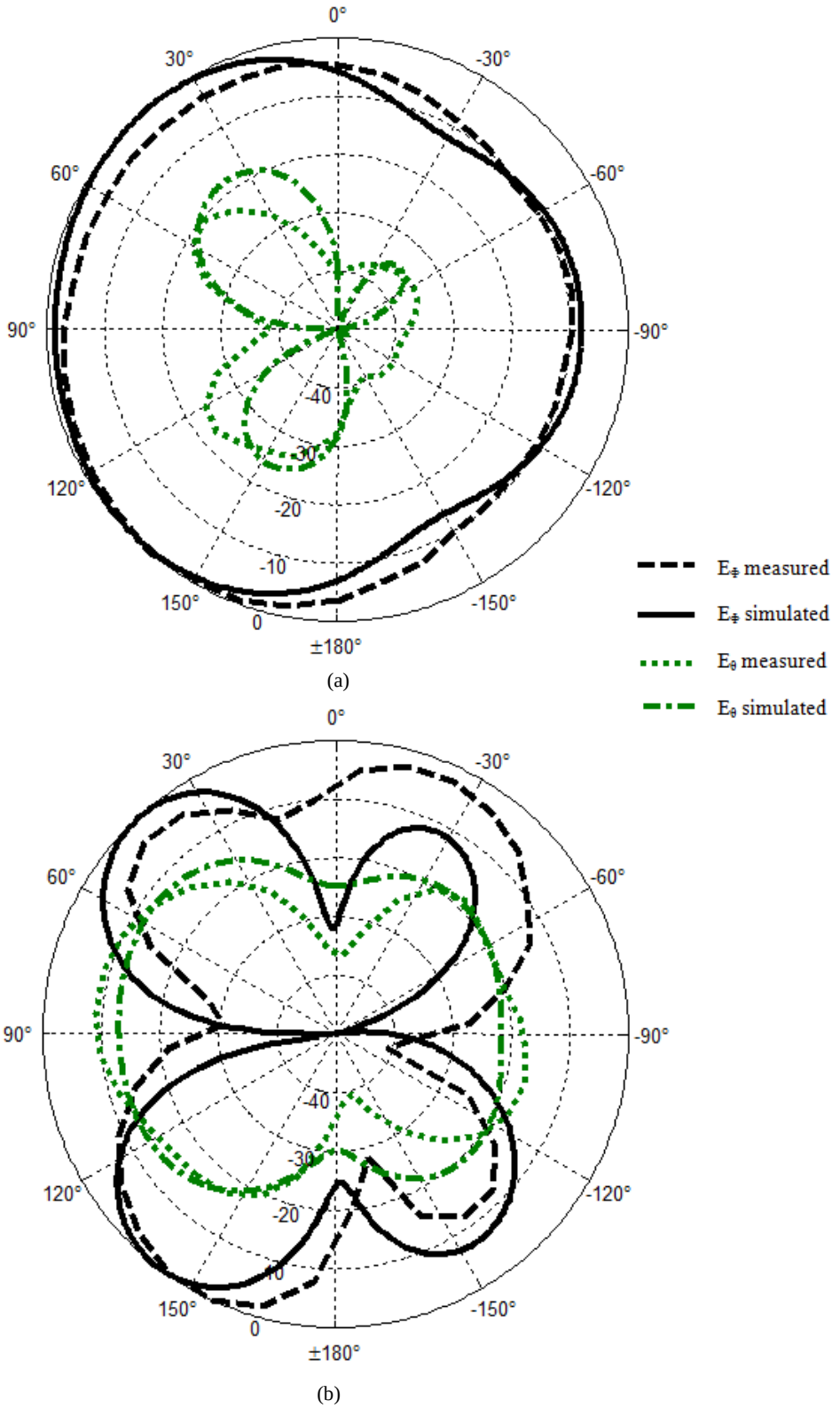

Fig. 5.9 Measured and simulated radiation patterns in YZ plane

(a) at 1.95 GHz and (b) at 2.64 GHz

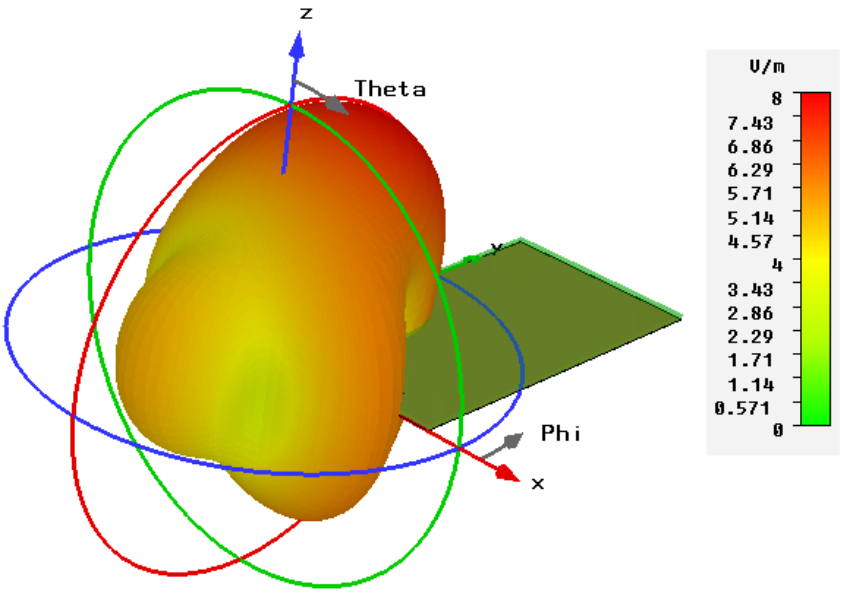

(a)

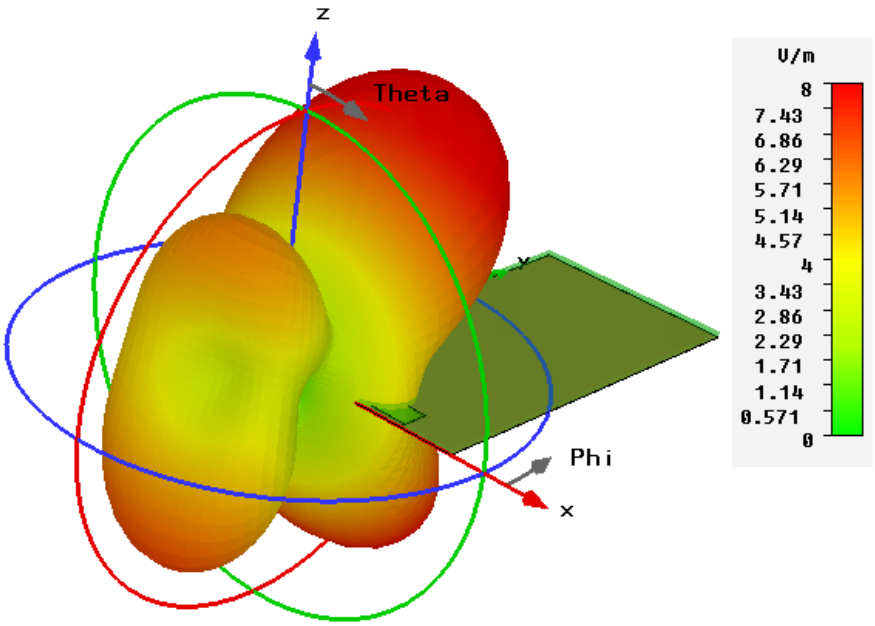

(b)

Fig. 5.10: 3D simulated radiation patterns (a) at 1.95 GHz and (b) at 2.64 GHz

5.2.5 Total Radiation Efficiency

The two antenna method explained in Chapter 2 was used in acquiring the measured S-parameter samples inside an RC chamber. Then Eq. (2.29) and Eq. (2.26) were applied to calculate both the radiation efficiency and the total radiation efficiency, respectively. The simulated and measured total efficiencies are depicted in Fig. 5.11. It shows that the proposed antenna has high total radiation efficiency (> 90%) over the frequency band of interest. Below 1.7 GHz, there is a 40% disagreement between the simulated and the measured value, which is probably due to the measurement errors resulted the very wide bandwidth that was used in collecting the data (1-3.5 GHz), which made the collected samples are sparse in the frequency domain. More accurate results can be collected if the overall bandwidth is spilt into two bands; each one has a wide of 1.25 GHz. Nevertheless, a good agreement is achieved over the frequency band of interest (1.7-2.85 GHz).

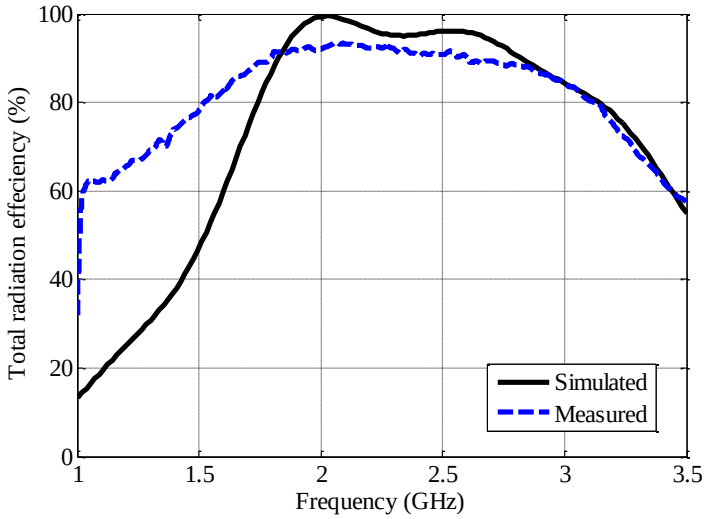

Fig. 5.11: Simulated and measured total radiation efficiency

5.3 Dual-Element PILA Antenna

To maximize both the channel capacity and diversity performance, another copy of the element is placed on the lower edge of the PCB at the left hand corner as shown from the fabricated two-element prototype in Fig. 5.12, the PCB has the same material, thickness and

dimensions as in the single element design. The design has utilized a ground plane area of 702 mm^2 which is less than that in [6] (900 mm^2).

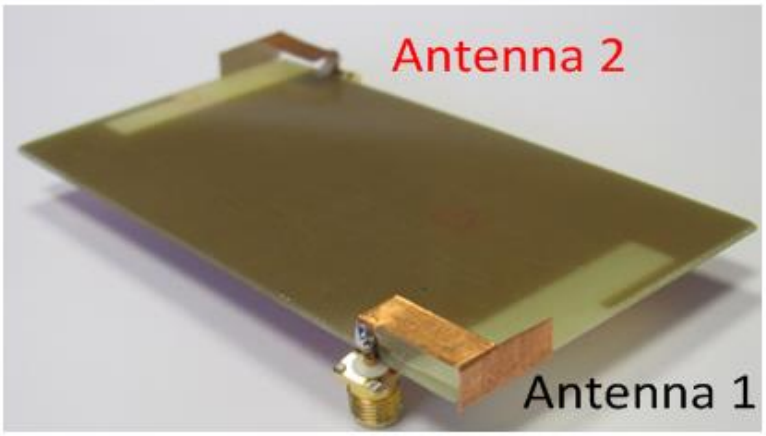

Fig. 5.12: Dual-element PILA Antenna

5.3.1 Measured and Simulated S-Parameters

The S-parameters are measured and presented in Fig. 5.13. It shows that the simulated -10 dB impedance bandwidth is 1.15 GHz (1.7-2.85 GHz) and the isolation level is higher than 13 dB. The measured -10 dB impedance bandwidth is 1.1 GHz (1.75-2.85 GHz), while the measured isolation level is not as good as the simulated result, but still acceptable. The difference is most likely resulted from the soldering and fabrication errors since the top plates are hand-made.

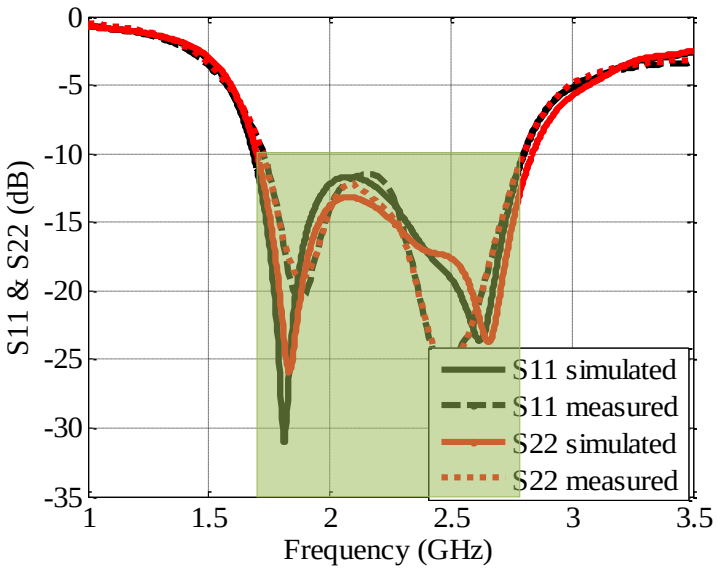

(a)

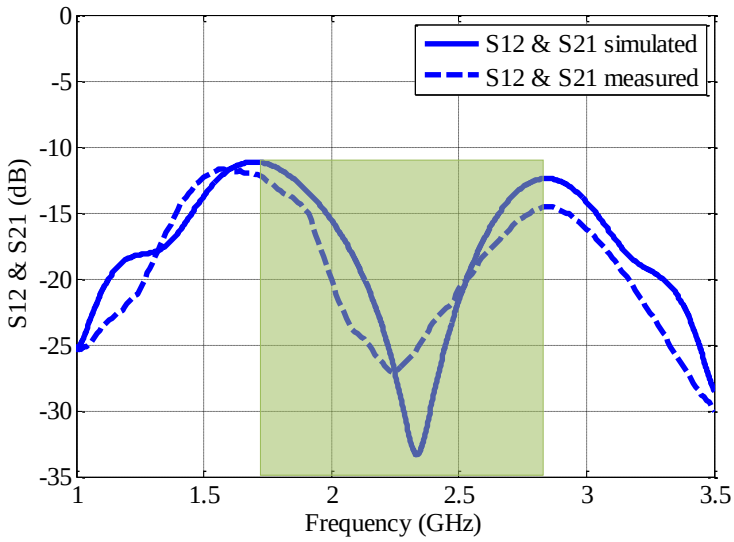

(b)

Fig. 5.13 Simulated and measured S-parameters (a) Reflection parameters and (b) isolation parameters

5.3.2 Far-Field Radiation Patterns

Fig. 5.14 shows the simulated and measured co-polarized and cross-polarized normalized radiation patterns of the fabricated antennas at 1.95 GHz and 2.64 GHz, the radiation patterns have good complementary in the space, especially in XY-plane and XZ-plane. These properties can provide a good diversity gain in sever fading channels. This can also be cleared from the 3D simulated radiation pattern at both resonant frequencies, Fig. 5. 15 shows that the two elements has a different radiation pattern over the space. It can be seen how much the patterns are different, which also an evident for a good diversity performance.

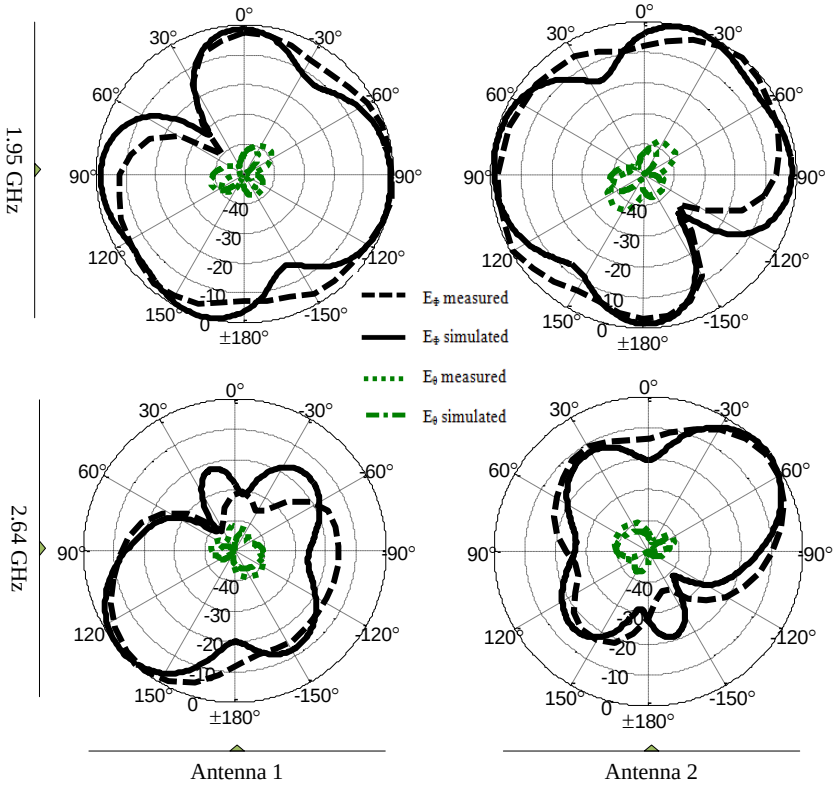
1.95 GHz
2.64 GHz
Eφ measured
Eφ simulated
Eθ measured
Eθ simulated
Antenna 1
Antenna 2

(a)

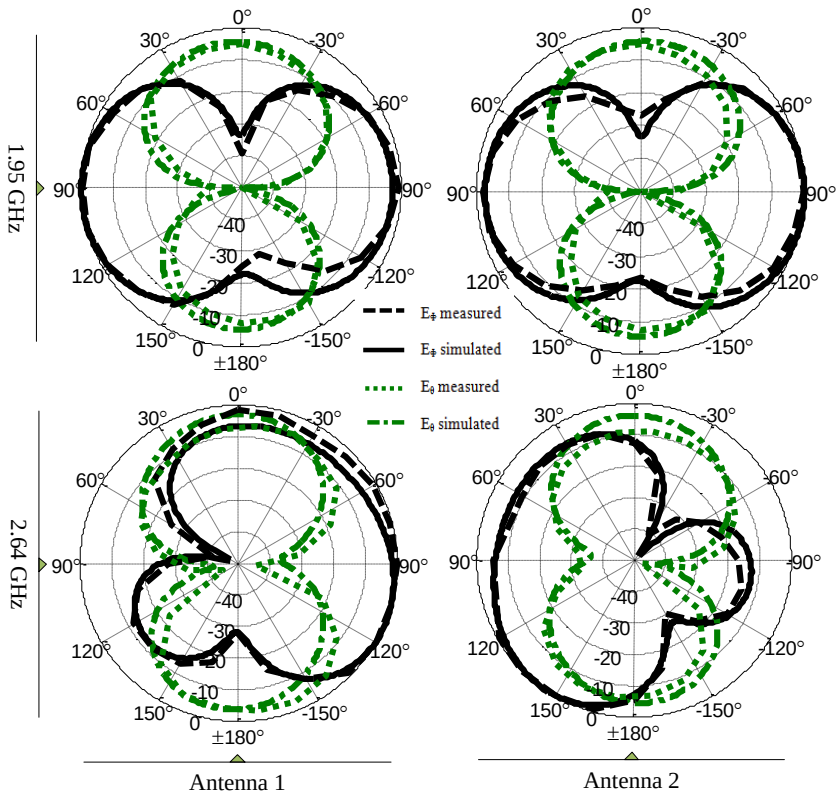
1.95 GHz
2.64 GHz
Eφ measured
Eφ simulated
Eθ measured
Eθ simulated
Antenna 1
Antenna 2

(b)

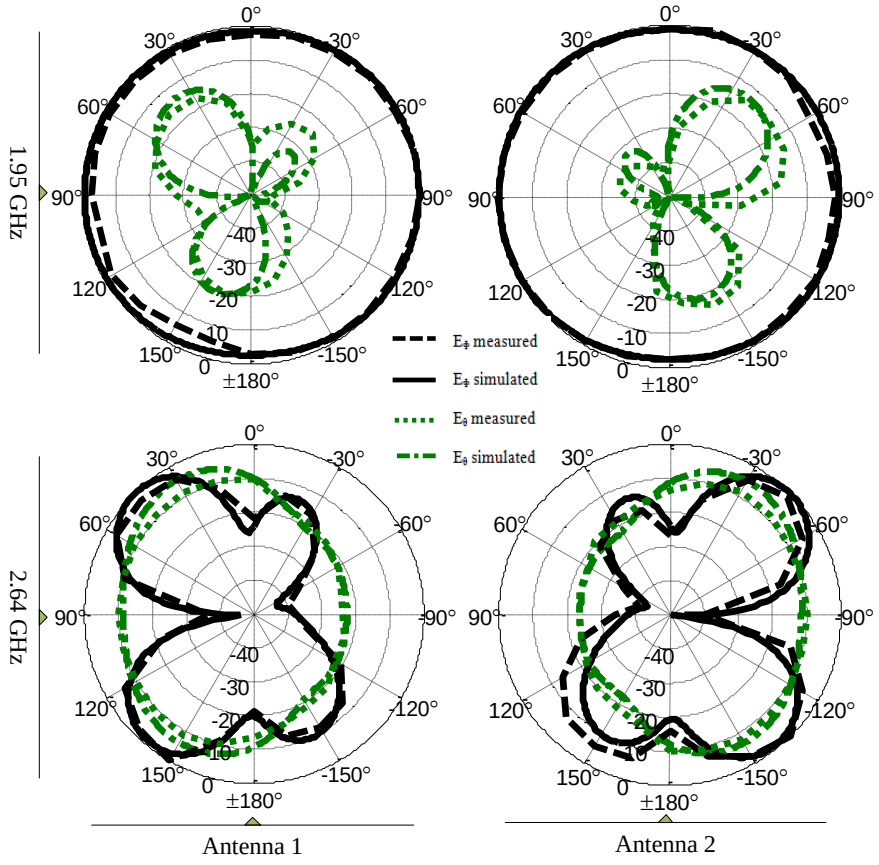

(c)

Fig. 5.14: Simulated and measured radiation patterns (a) XY plane;

(b) XZ plane and (c) YZ plane

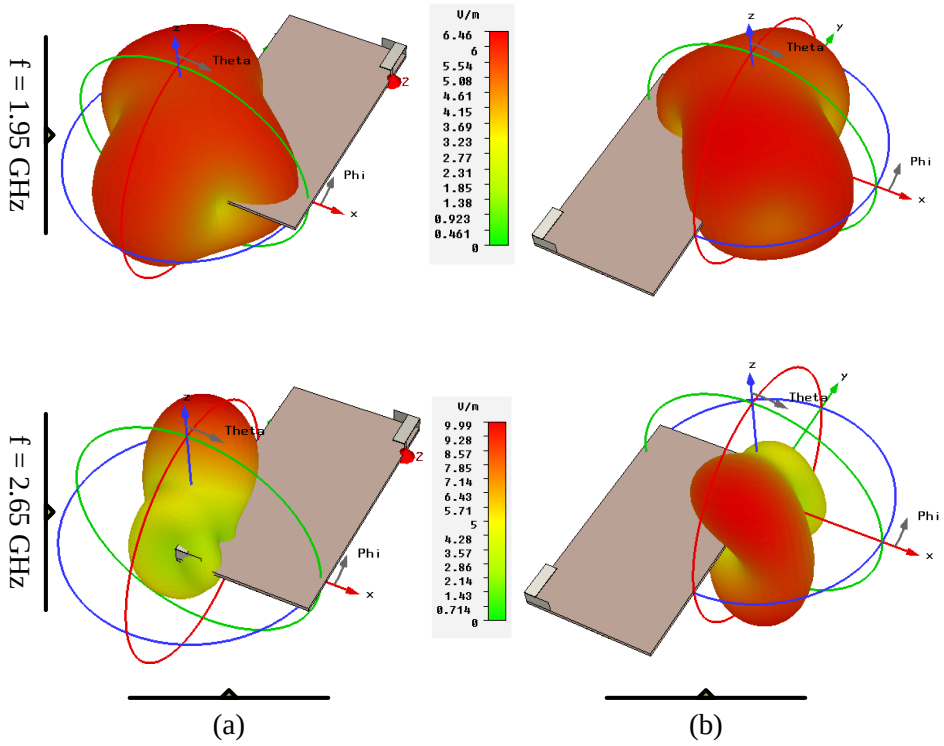

Fig. 5.15: 3D simulated radiation patterns (a) Antenna 1 and (b) Antenna 2

5.3.3 Diversity Performance Parameters

The diversity performance of the proposed dual-element antenna is also studied and quantified based of the values of ECC, MEG ratio, diversity gain and the total effeciency.

The MEG condition is evaluated from the 3D simulated gain patterns using Eq (2.19). Table 5.1 summarizes the results over the defined Gaussian model for both indoor and urban outdoor environments. It can be seen as the MEG ratios for both resonance frequencies are less than the critical limit (3 dB), thus, the design satisfies the branch power ratio condition.

The correlation between antenna elements is evaluated using Eq (2.15). Fig. 5.16 shows the measured and simulated ECC, a good agreement is clearly shown. The figure shows that the ECC of less than (0.1) have been achieved and this also ensures that the proposed design is a good antenna for diversity applications.

Table 5.1: MEG in different environments

Environment	Frequency (GHz)	Mean Effective Gain (dB)		k
		Ant1	Ant2	
Indoor	1.95	-3.72	-3.65	0.07
	2.64	-3.45	-3.5	0.05
Outdoor	1.95	-6.23	-6.18	0.05
	2.64	-5.6	-5.55	0.05

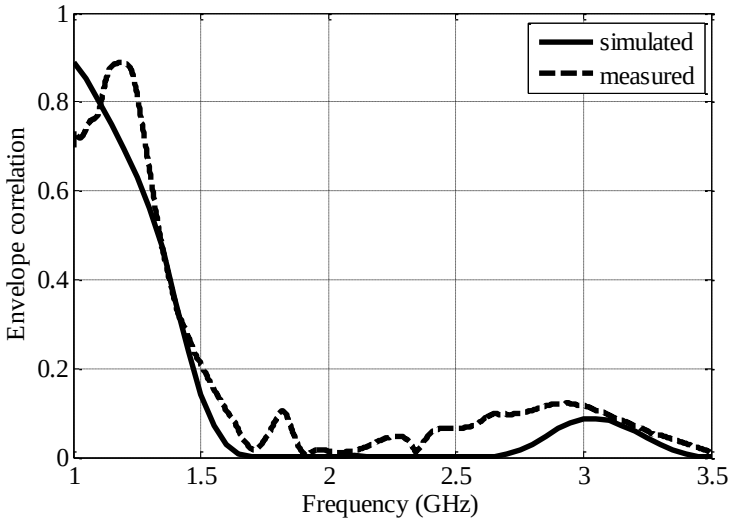

Fig. 5.16: Envelope correlation coefficient

As the proposed diversity antenna has a very low ECC and an acceptable MEGs ration over different environments, this will lead to a high diversity gain. In order to quantify the diversity performance, the measurement of apparent diversity gain was conducted inside the reverberation chamber at the University of Liverpool. The selection combining technique was used to obtain the measured diversity gain at 1 % CDF level and is found to be about 10.19 dB as shown in Fig. 5.17. This is higher than other similar designs in the literature [6]; this is because of good pattern diversity and very low ECC achieved as in Fig. 5.16 and Fig. 5.17, respectively. Therefore, it has demonstrated that the proposed antenna can provide a large diversity gain and is a very good candidate for modern mobile handset applications.

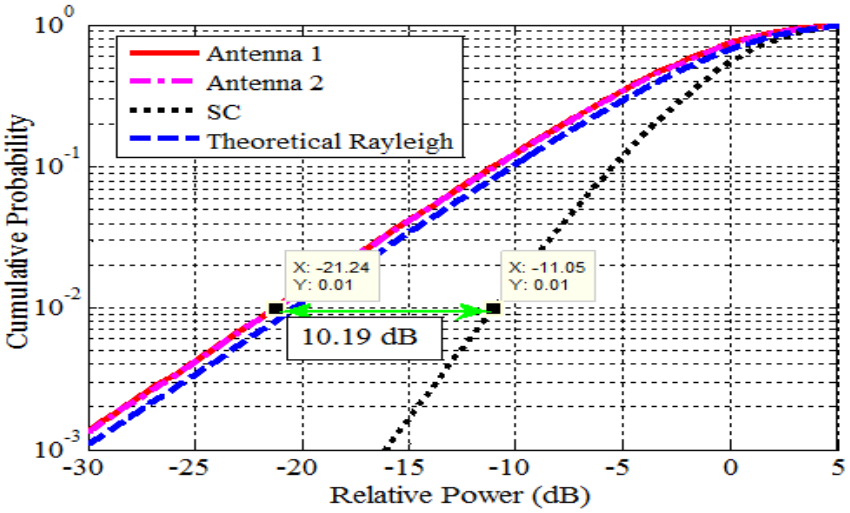

Fig. 5.17: CDF functions and apparent diversity gain

Finally, using two antenna methods in Chapter 2 and after applying the data post-processing, the measured total radiation efficiency of each antenna element is calculated using Eq. (2.27). The simulated and measured total efficiencies are shown in Fig. 5.18. It shows that both antenna elements have high total radiation efficiency (> 87%) over the frequency band of interest. It can be seen the discrepancy between the measured and the simulated values outside the frequency band of interest, it is might be due to the measurement errors resulted from either cable movement or the very wide bandwidth that was used in collecting the data (1-3.5 GHz).

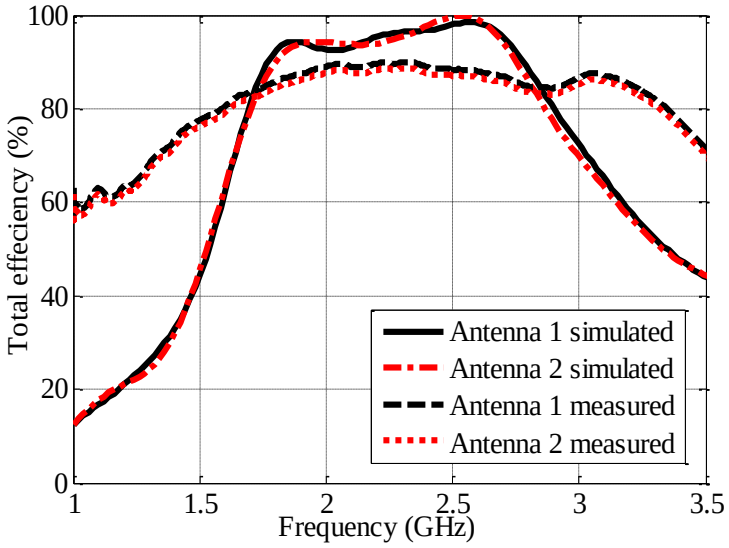

Fig. 5.18: Total efficiency of the proposed antenna

5.4 Summary

Despite the PILA is one of the earliest low profile antenna structures, it is rarely used as an internal antenna in handset devices. In the chapter, a low profile and wideband PILA-based antenna has been proposed for handset diversity and MIMO applications. The working mechanism and design principle of the antenna have been presented; the design principle can be summarized in the following four techniques:

1) Partially cleared ground plane area was used to enhance the input impedance characteristic.
2) Inductive loading has been applied by adding an additional length at the end of the top plate; this was to decrease the resonance frequency.
3) To decrease the occupied size, a capacitive loading was also applied by bending the added length on the top plate by 90^0.
4) Merging both the PILA resonance (2.64 GHz) and the resulted ground plane notch resonance (1.95 GHz) by loading the ground plane notch with a small strip.

Both prototypes for a single element and dual elements have been designed, fabricated and measured, the results have shown that the design can cover the frequency range of 1700-2850 MHz with S_{11}< -10 dB. The diversity parameters have also been measured and presented. The measured apparent diversity gain from the CDF function is about 10.19 dB. The results have demonstrated that this design is a very good candidate for handset MIMO and diversity antenna. Furthermore, it utilizes a small area of the ground plane on both the top and bottom PCB edges (about 702 mm^2, which is smaller than that in [6] 900 mm^2) and is easy to facilitate the integration of other handset components.

References

[1] J. Anguera, A. Andújar et al, "Advances in antenna technology for wireless handheld devices ," *International Journal on Antenna and Propagation*., vol. 2013, Article ID: 838364, 2013.

[2] J. Anguera, A. Andújar, and C. García, "Multiband and small coplanar antenna system for wireless handheld devices ," *IEEE Trans. Antennas Propag.*, vol. 61, no. 7, pp. 3782–3789, Jul. 2013.

[3] M. Pelosi, M. B. Knudsen, and G. F. Pederson, "Multiple antenna systems with inherently decoupled radiators ," *IEEE Trans. Antennas Propag.*, vol. 60, no. 2, pp. 503–515, Jul. 2012.

[4] H. W. Hsieh, Y. C. Lee, K. K. Toing *et al.*, "Design of a multiband antenna for mobile handset operations," *IEEE Antennas and Wireless Propag. Lett.,* vol. 8, pp. 200-203, 2009.

[5] J. Anguera, I. Sanz, J. Mumbru *et al.*, "Multiband handset antenna with a parallel excitation of PIFA and slot radiators," *IEEE Trans. Antennas Propag.*, vol. 58, no. 2, pp. 348-356, 2010.

[6] Y. Wang, and Z. Du, "A wideband printed dual-antenna system with a novel neutralization line for mobile terminals," *IEEE Antennas and Wireless Propag. Lett.*, vol. 12, pp. 1428-1431, 2013.

[7] Y. F. Lin, H. M. Chen, C. Y. Lin, *et al.*, "Planar inverted-L antenna with a dielectric resonator feed in a mobile device," *IEEE Trans. Antennas Propag.*, vol. 57, no. 10, pp. 3342-3346, 2009.

[8] S. S. Alja'afreh, Y. Huang and L. Xing., "A compact, wideband and low profile planar inverted-L antenna. ", *in Proc. 8th European Conference on Antennas and Propagation*, April. 2014, Netherlands.

[9] P. Hallbjorner, "The significance of radiation efficiencies when using S-parameters to calculate the received signal correlation from two antennas," *IEEE Antenna Wireless Propag. Lett.*, vol. 4, pp. 97-100, 2005.

[10] R. G. Vaughan, and J. B. Andersen, "Antenna diversity in mobile communications," *IEEE Trans. Veh. Tech.*, vol. 36, no. 4, pp. 149-172, 1987.

[11] T. Taga.,"Analysis of mean effective gain of mobile antennas in land mobile radio environments," *IEEE Trans. Veh. Tech.*, vol. 39, no. 2, pp. 117-131, 1990.

[12] Y. Ding, Z. Du *et al.*,"A novel dual-band printed diversity antenna for mobile terminals," *IEEE Trans. Antennas Propag.,* vol. 55, no. 7, pp. 2088-2096, July. 2007.

[13] S. C. K. Ko and R. D. Murch, "Compact integrated diversity antenna for wireless communications," *IEEE Trans. Antenna and Propag.*, vol. 49, no. 6, pp. 954-960, 2001.

[14] Rosengren, and P. S. Kildal, "Radiation efficiency, correlation, diversity gain and capacity of a six-monopole antenna array for a MIMO system: theory, simulation and measurement in reverberation chamber," *IEE Proc. Microwaves, Antennas and Propag.,* vol. 152, no. 1, pp. 7-16, 2005.

Chapter 6: Multi-Element PILA Antennas Using A New Approach for Parasitic Element Design

6.1 Introduction

Although the proposed design in the previous chapter has a small footprint area over the PCB, the design utilized both the upper the bottom edges of the mobile device PCB. This adds a difficulty in integrating other antennas for frequency applications below 1 GHz. Thus, there is a need to place both PILA antenna elements on the same edge of the PCB. However, this could be very challenging due to a strong mutual coupling between closely spaced antennas. A strong mutual coupling means a high correlation between the received signals by antenna elements which in turns deteriorates the MIMO performance such as: the antenna efficiency, channel capacity and diversity gain. Thus, decoupling the antenna elements is a critical issue in MIMO technology and antenna diversity systems [1]. A lot of isolation (decoupling) techniques have been proposed in literature such as: decoupling and matching network (DMN) [2], defect ground plane structures (DGS) [3], electromagnetic band gap structure (EBG) [4], neutralization line [5] and parasitic decoupling element (PDE) [1]. Among these techniques, PDE has been deployed in several works as it has a small Ohmic loss and it is very suitable for handsets integration [1, 6, and 7]. Despite of this, there is no general design rule or procedure to obtain optimal results for a small footprint PDE, a wideband isolation bandwidth and an acceptable isolation level. Thus a thorough investigation on the circuit theory is needed.

This chapter firstly presents a new, small footprint and low profile dual-element PILA antenna for wideband handset diversity applications over the frequency range of (1.7-2.7 GHz). This design is based on a novel design approach for a PDE element inserted between two coupled antennas. It is based on the stepped impedance resonator (SIR) circuit theory. Using this approach, the following features can be achieved: 1) A small footprint decoupling element can be achieved; 2) It provides a wideband decoupling solution; 3) It offers a tradeoff between the decoupling bandwidth and isolation level; 4) It offers two functions for the parasitic element; it can work as a decoupling element that enhances the isolation level or as a decoupling and a radiation element which enhances both the impedance bandwidth and the decoupling bandwidth. In the second part of this chapter, a new four-element PILA antenna is proposed by adding another copy of the dual-element antenna at the lower edge of the ground plane.

6.2 Compact Dual-Element PILA Antenna with a Parasitic Decoupling Element

6.2.1 Antenna Configuration

The proposed mobile antenna is depicted in Fig. 6.1. The antenna includes two symmetrically modified- planar inverted-L antenna (PILA) elements [8]. The top plate with dimensions of 5×15 mm^2 is placed 5 mm above the ground plane with an FR-4 substrate of dimensions 55×100×1.5 mm^3, relative permittivity of ε_r = 4.3 and a loss tangent of tan δ = 0.025. Each antenna element is fed by a feeding strip of dimensions 2×5 mm^2. To reduce the electrical length of each element, both capacitive loading (bending) and inductive loading (meandering) are employed by creating a vertically bended plate of dimensions 5×9 mm^2. To enhance the radiation resistance, the ground plane is partially removed underneath the top plate; the dimensions of the ground free area are 7×55 mm^2. All these dimensions are optimized via computer simulations. In order to reduce the mutual coupling between the two elements, a parasitic decoupling element is added, designed and optimized based on the proposed approach in Section 6.2.3. The decoupling element is located right in the middle of the two elements, it represents a three-section SIR band stop filter, the length of each section is 6.5 mm while the widths are 1 mm, 3 mm and 23 mm, respectively.

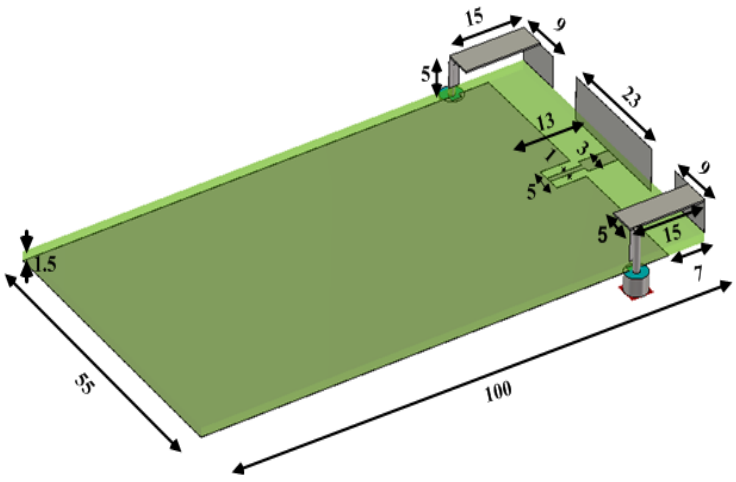

Fig. 6.1: The proposed dual-element antenna with dimensions in [mm].

6.2.2 Prototype and S-Parameters

The simulated scattering parameters are depicted in Fig. 6.2, and for comparison, the simulated performance without the parasitic decoupling element is also added to Fig. 6.2. It is found that by adding the parasitic decoupling element, the mutual coupling is improved: S_{21} is decreased from -6 dB to less than -12 dB. Also, since the design has a dual resonance: the first one is linked to the parasitic element while the second one refers to antenna element; the -6 dB S_{11} bandwidth is increased from about 1700 – 2800 MHz to 1700 – 3500 MHz.

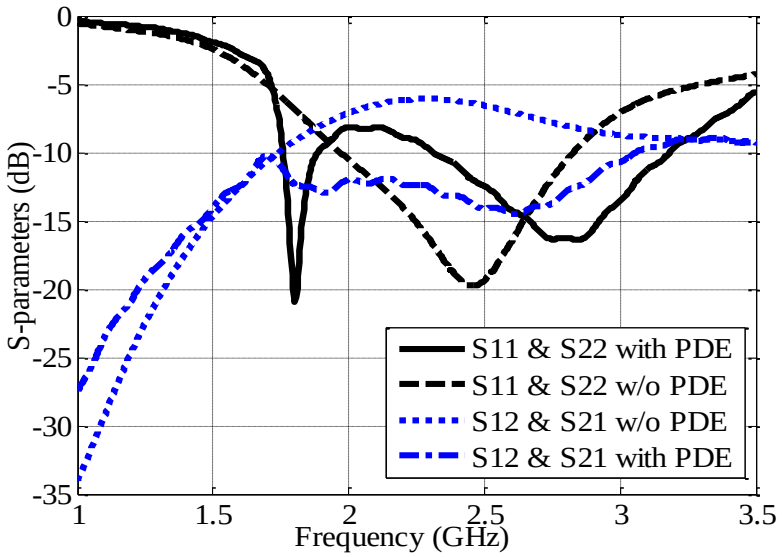

Fig. 6.2: Simulated scattering parameters (PDE: mean, parasitic decoupling element).

To validate the proposed design, a prototype is fabricated and presented in Fig. 6.3. The measured S-parameters are depicted in Fig. 6.4. It can be observed that the measured results are very similar to the simulated ones in Fig. 6.2, and exhibit almost the same behaviour.Thus, based on the -6 dB bandwidth criteria, the design covers handset wireless applications over the frequency range (1700-2700 MHz), such applications like: DCS 1800 (1710-1880 MHz), PCS 1900 (1850-1990 MHz), UMTS (1920-2170 MHz), LTE and LTE-advanced between 1700 MHz and 2700 MHz. Furthermore, WiFi /Bluetooth (2400-2485 MHz), and S-DMB (Satellite Digital Multimedia Broadcasting 2170 – 2200 MHz) frequency bands are also covered by this antenna.

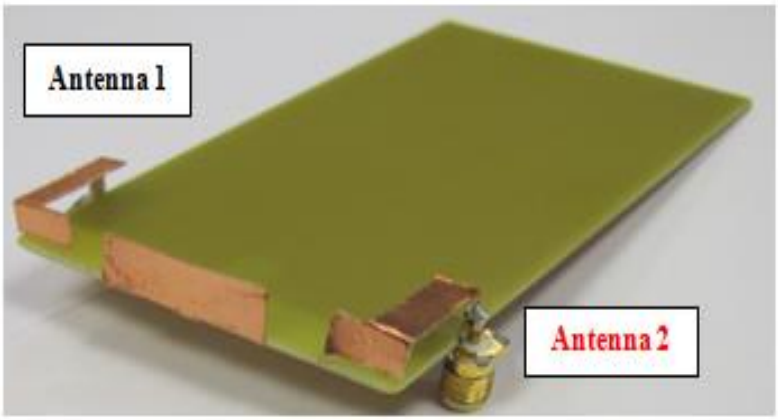

(a)

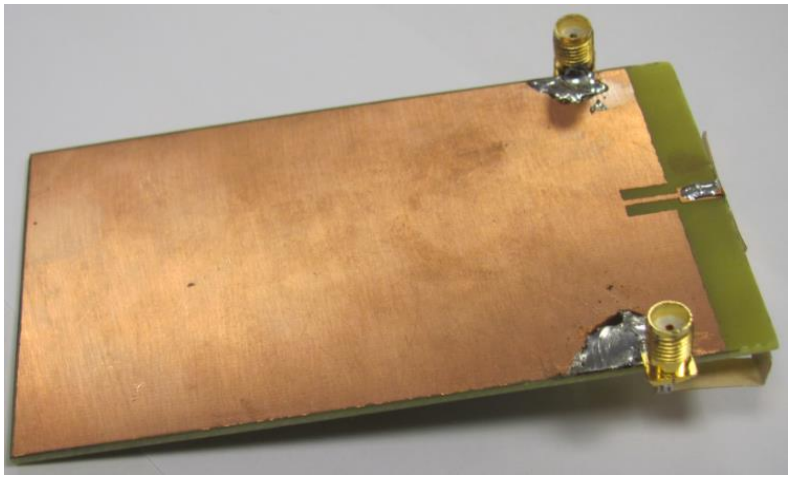

(b)

Fig. 6.3: Prototype of the proposed antenna (a) top view and (b) back view

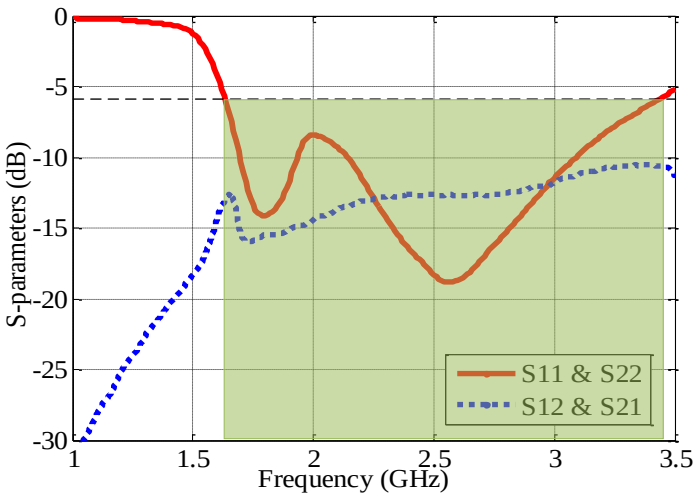

Fig. 6.4: Measured scattering parameters

6.2.3 Decoupling Element Design Approach Using SIR

6.2.3.1 SIR Theory

Fig. 6.5 shows a basic structure of a quarter-wavelength SIR. It represents a transmission line with two different characteristic impedances Z_1 and Z_2 and two different electrical lengths θ_1 and θ_2, respectively.

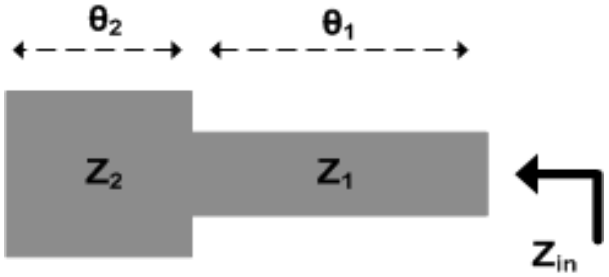

Fig. 6.5: Layout of a conventional two-section quarter wavelength SIR

As the structure represents an open circuit transmission line (from Z_2 end), the resonance condition for any odd multiple of quarter wavelength can be obtained when the input impedance to be zero:

$$Z_{in} = jZ_1 \frac{Z_1 \tan(\theta_1)\tan(\theta_2) - Z_2}{Z_1 \tan(\theta_2) + Z_2 \tan(\theta_1)} = jZ_1 \frac{\tan(\theta_1)\tan(\theta_2) - R_z}{\tan(\theta_2) + R_z \tan(\theta_1)} = 0 \quad (6.1)$$

Yielding the resonance condition as follows:

$$\tan(\theta_1)\tan(\theta_2) - R_z = 0 \Rightarrow R_z = \frac{Z_2}{Z_1} = \tan(\theta_1)\tan(\theta_2) \quad (6.2)$$

where R_z is the impedance ratio Z_2 / Z_1.

It can be seen from the above resonance condition that SIR resonance frequency can be controlled by more than one design parameter; both electrical length and impedance ratio play important roles in determining the resonance frequency of SIR [9]. Furthuremore, one interesting property of SIR over the uniform impedance resonator (UIR) is the compactness; SIR can have a minimum length at the same resonance frequency when the impedance ratio $R_z < 1$, while it can have a maximum length when $R_z > 1$ [9].

In order to enhance the resonator bandwidth and achieve a more compact design, a multi-step resonator is usually employed over a two-step resonator. As an example, a three-step SIR is created in Fig. 6.6, a new section with a charactristic impedance Z_3 and electrical length θ_3 is inserted between original sections 1 and 2. Similar to the analysis of a two-section SIR, the resonance condition of a three-section SIR can be drawn after letting the

input impedance be zero. For simplicity of both design and analysis, let the three sections have the same electrical length θ, thus

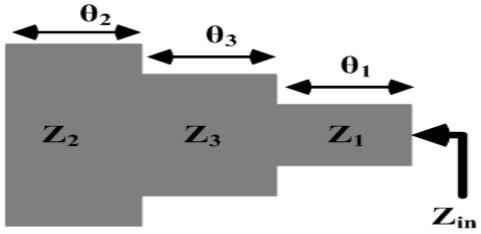

Fig. 6.6: Layout of tri-section quarter wavelength SIR

$$Z_{in} = jZ_1 \frac{Z_3^2 \tan^2(\theta) - Z_2 Z_3 + Z_1 Z_3 \tan^2(\theta) + Z_1 Z_2 \tan^2(\theta)}{Z_1 Z_3 \tan(\theta) + Z_1 Z_2 \tan(\theta) - Z_3^2 \tan^3(\theta) + Z_2 Z_3 \tan(\theta)} = 0 \quad (6.3)$$

Let the impedance ratios be

$$K_1 = \frac{Z_2}{Z3} \quad , \; K_2 = \frac{Z3}{Z_1} \quad (6.4)$$

Then, the resonance condition is:

$$\theta = \tan^{-1}\left(\sqrt{\frac{K_1 K_2}{1 + K_1 + K_2}}\right) \quad (6.5)$$

Eq (6.5) can be further simplified using (6.4) and (6.2) as:

$$\theta = \tan^{-1}\left(\sqrt{\frac{R_z}{1 + K_1 + K_2}}\right) \quad (6.6)$$

For the case of two-section SIR with equal length, using (6.2), we have:

$$\theta = \tan^{-1}\left(\sqrt{R_z}\right) \quad (6.7)$$

It can be seen that the argument in (6.6) is scaled by $(1 + K_1 + K_2)^{1/2}$ which makes the multi-section SIR more compact than the two-section SIR.

6.2.3.2 Design Approach

Fig. 6.7 represents a general geometry of dual-element monopole antenna with a parasitic decoupling element. For simplicity, the decoupling element is symmetrical between antennas. Referring to the transmission line theory and SIR theory, one can see the following: 1) the general configuration of the structure similar to the configuration of transmission line stop band filter. The decoupling element represents an open circuit electrically coupled shunt stub (a shunt series LC resonator). This stub (decoupling element) represents a centre strip of coplanar waveguide (CPW) while the antenna elements act as the CPW ground strips. 2) The shape of the decoupling element reflects that this stop band resonator is a kind of SIR stop band resonator (two-section SIR). From aforementioned SIR

theory, the stop band resonance frequency, isolation level and the isolation bandwidth can be tuned by changing the characteristic impedance ratio between sections, this can be done by changing the widths (W_1 and W_2) and the gaps (g_1 and g_2) without increasing the total length of the decoupling element. Using this theory, a compact parasitic decoupling element can be found with wideband isolation characteristics.

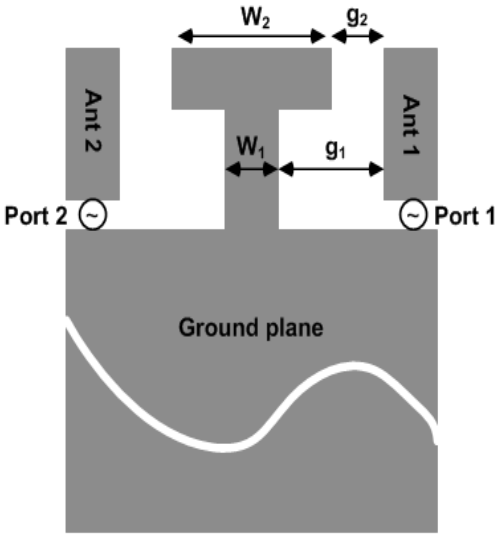

Fig. 6.7: General geometry of dual-element monopole antenna with a parasitic decoupling element

For the proposed design, the following steps summarized the design and optimization procedure for the parasitic decoupling element parameters:

1) Extraction of SIR Equivalent Structure: Referring to Fig. 6.8(a), it can be seen that the decoupling element represents a three-section CPW SIR Structure, Fig. 6.8(b) shows the equivalent CPW for each section. Thus, the decoupling element represents a parallel coupled quarter wavelength SIR between antenna feeds. In order to use the SIR theory, the calculation of the characteristic impedance for each SIR section is needed, and this requires a calculation of the effective permittivity.

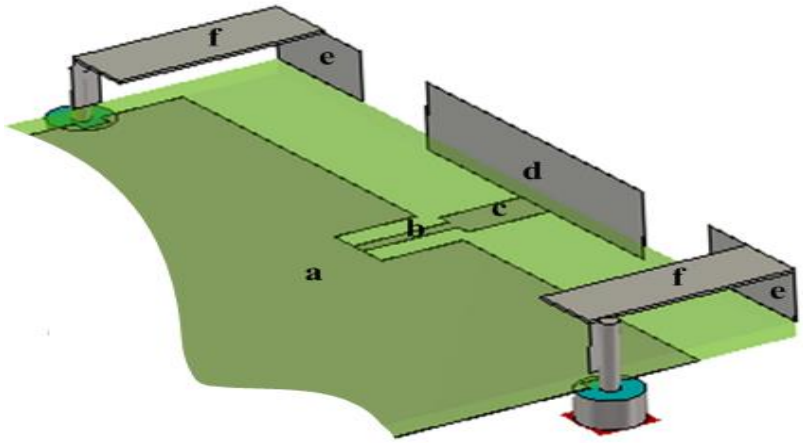

(a)

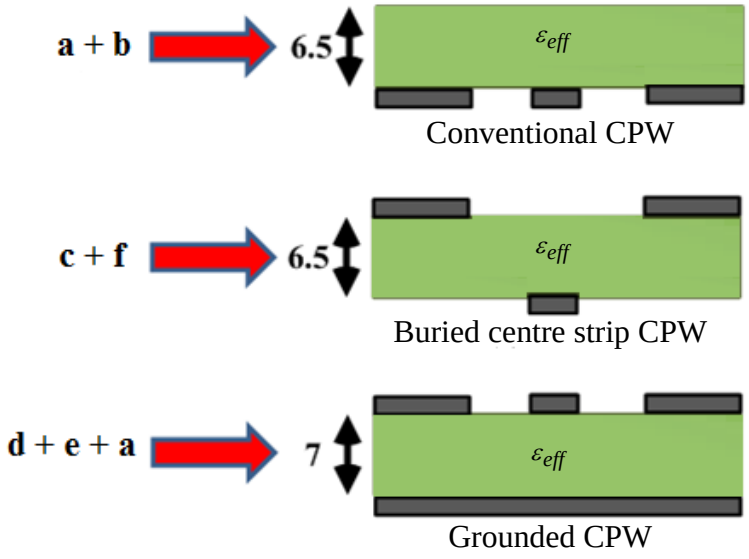

(b)

Fig. 6.8: Equivalent CPWs from the proposed structure(a) Proposed structure and (b) the equivalent CPW schemes

2) Calculation of the Effective Permittivity: As the proposed structure represents a parallel plate capacitor (parallel antenna feeds) filled with two dielectric layers (vacuum and FR-4) parallel to the normal direction of the parallel plates as shown in Fig. 6.9 (a), the effective permittivity of the equivalent layer can be calculated based on the following relation [10]:

$$\varepsilon_{eff} = \sum_{i=1}^{N} \rho_i \varepsilon_i \qquad (6.8)$$

where ρ_i represents the volume density of the i_{th} layer and ε_i represents the relative permittivity of the i_{th} layer.

A question may arise now is how accurate this calculation is. Fig. 6.9(b) gives a clear answer where the S-parameter results in both cases are about the same (the original structure with FR-4 substrate and the case with the equivalent layer with effective relative permittivity equal to 1.75). This effective permittivity represents the permittivity of the equivalent layer in CPW schemes in Fig. 6.8 (b) and is used for the calculations of characteristic impedance for each SIR section.

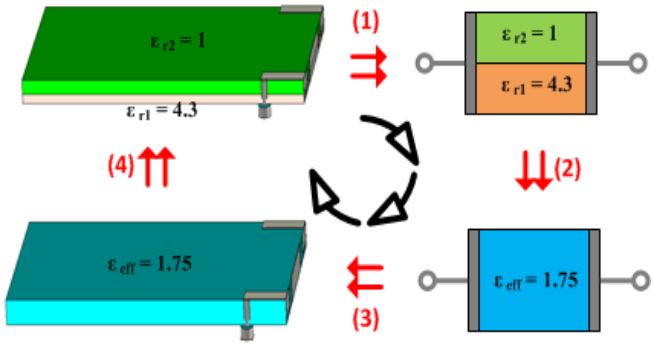

(a)

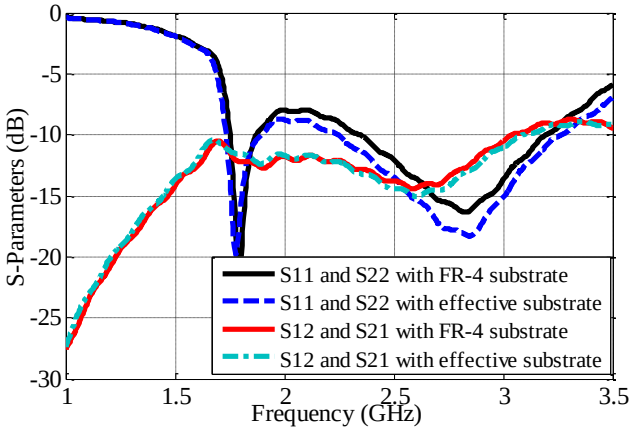

(b)

Fig. 6.9: Effective permittivity (a) Parallel capacitance theory and (b) Validation of the calculation

3) Two-Section SIR: By creating only one discontinuity on the decoupling element, it represents a two-section SIR structure formed from two coplanar waveguides: the first section represents conventional CPW with characteristic impedance Z_1 while the second section represents a grounded CPW with characteristic impedance Z_2 [11]. Fig. 6.10 and Fig. 6.11 show the effects of changing Z_1 and Z_2 on the level of the mutual coupling and the stop-band bandwidth, respectively, the total length of SIR has been kept constant. It can be seen that the mutual coupling impedance curve has behaviour similar to the input impedance of the two-section SIR shown in Eq. (6.1). Furthermore, the most important point can be concluded from both figures is that: as the impedance ratio reduces, the stop band frequency moves downwards. Beside this, Fig. 6.12 shows the effect of tuning the impedance ratio on the operational bandwidth. It can be seen that the operational bandwidth can be enlarged from the upper edge when the impedance ratio goes high, while for a low ratio, it is enlarged from the lower edge frequency. This leads to the conclusion that the decoupling element indeed works as a decoupling and a parasitic element. Also, the compactness can be achieved when the impedance ratio is low. Table 6.1 summarizes the SIR analysis of simulation and theoretical point of views: it can be seen that the values of simulated resonance frequencies are in a good agreement with the theoretical values obtained using (6.1). In the analysis, CPW line structure is employed, the discontinuities in the step junctions and changes of the effective dielectric constant due to width and gap variations are all considered.

Table 6.1 Summary of the two-section SIR analysis

Z_1 (Ω)	Z_2 (Ω)	ε_{e1}	ε_{e2}	R_z	$f_{z,\ Simulated}$ (GHz)	$f_{z,\ Theory}$ (GHz)
156	48	1.38	1.525	0.307	2.1	2.14
156	73.3	1.38	1.52	0.47	2.57	2.53
92	73.3	1.384	1.52	0.797	2.93	3.02
156	148	1.38	1.47	0.95	3.15	3.2
71.5	73.3	1.388	1.52	1.03	3.22	3.26

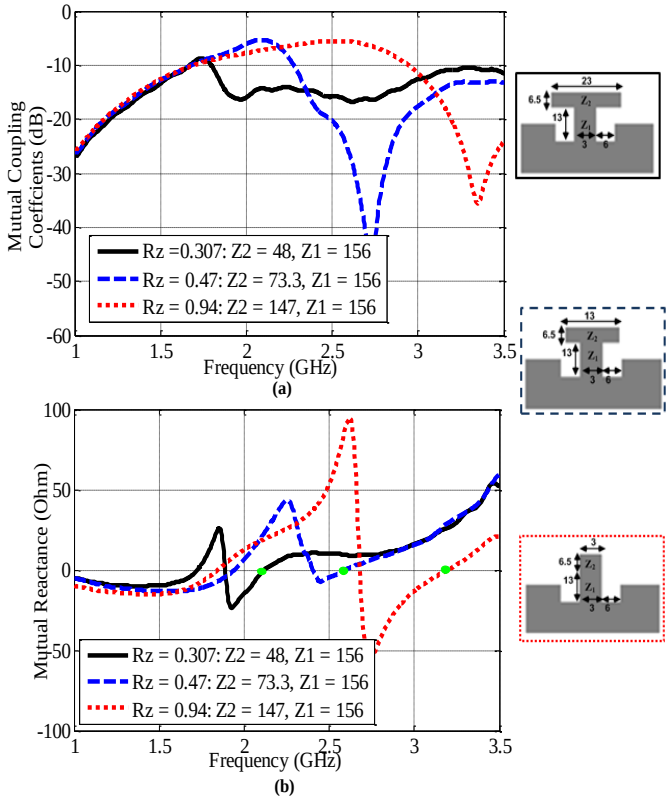

Fig. 6.10: Effect of changing Z_2 (a) mutual coupling coefficient and (b) mutual coupling impedance

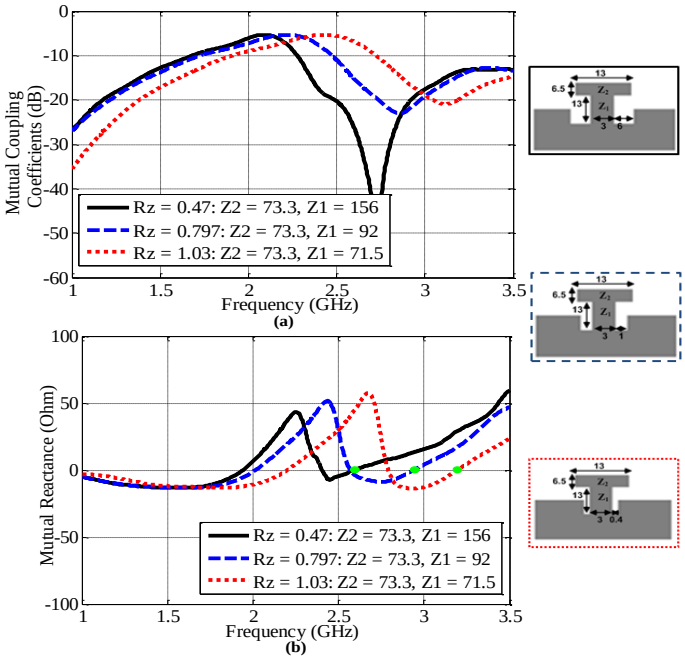

Fig. 6.11: Effect of changing Z_1 (a) mutual coupling coefficient and (b) mutual coupling impedance

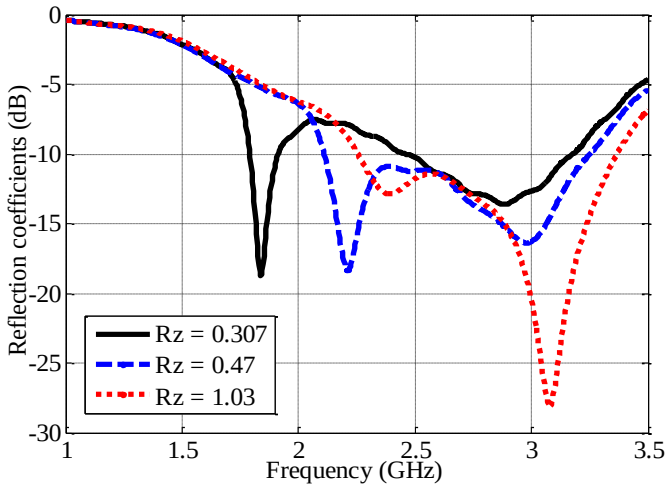

Fig. 6.12: Effect of changing impedance ratio on the reflection coefficients

3) Three-Section SIR: From the two-section SIR analysis, it can be seen that the level of mutual coupling around 1.7 GHz is quite high (Z_2 = 48 Ω and Z_1 = 156 Ω). To reduce this level, there are two possible solutions; the first one, which is not preferable, is to increase the total length or width of the gap between the ground plane and Section 1 in the decoupling element; the second one, which is preferable, is to upgrade the two-section SIR into three-section SIR by creating two width discontinuities. By deploying the second solution, the total length of the decoupling element is kept the same and the ground plane gap around Section 1 is small, also both the decoupling element and antenna elements can have a small footprint over the PCB (55 mm ×13 mm). Fig. 6.13(a) shows the three equal lengths of the SIR; the first section is equivalent to the conventional CPW, the second section represents a buried CPW while the third section represents a grounded CPW [11]. The equivalent characteristic impedance for each of the three sections are Z_1 = 156 Ω, Z_2 = 212 Ω, Z_3 = 48 Ω, respectively. By substituting these values in (6.4) and (6.5), the resonance frequency of this structure is found to be 2.0 GHz. The simulation result obtained using CST Microwave Studio has also verified this calculation as shown from the mutual impedance curve in Fig. 6.13(c): the simulated stop-band resonance frequency is also around 2.0 GHz. Furthermore, another advantage of using the three-section SIR shown in Fig. 6.13(b) is that the level of mutual coupling around 1.7 GHz is decreased to lower than -12 dB. Table 6.2 compares the total electrical lengths for the two-section and three-section SIRs; it shows that the design with three-section is more compact than the two-section case. It is worth mentioning that

during the calculation, the changes of the effective dielectric constant due to width and gap variations have been considered.

Table 6.2 Total electrical length comparison

	Two-section SIR	Three-section SIR
Frequency (GHz)	2.1	2.0
Total electrical length (rad)	$\theta_1 + \theta_2 = 1.03$	$3\theta = 3(0.3) = 0.9$

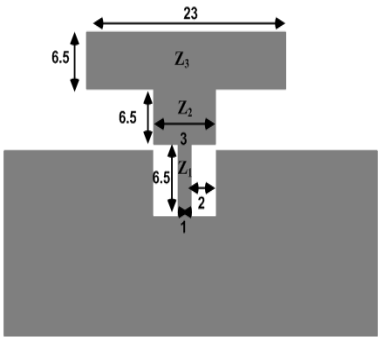

(a)

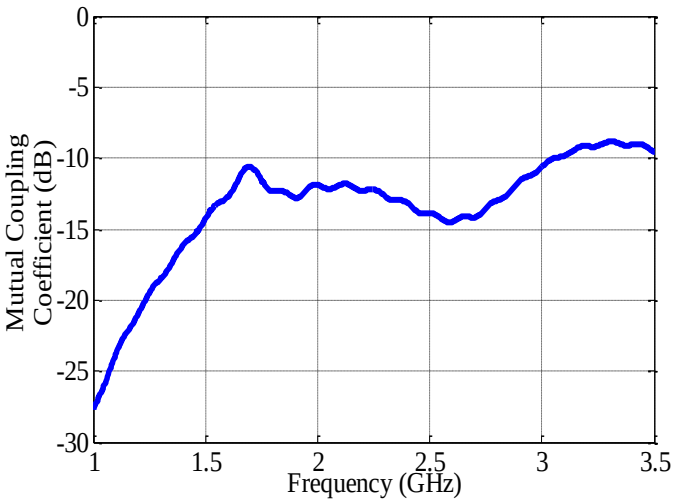

(b)

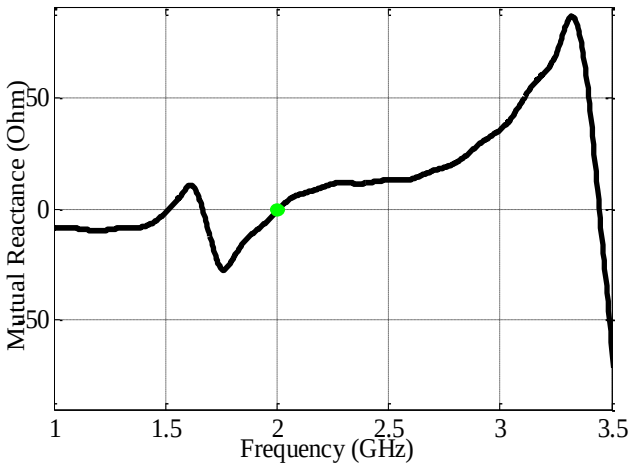

(c)

Fig. 6.13: Three sections SIR (a) Structure, (b) mutual coupling coefficient and (c) mutual coupling impedance

6.2.4 Far-Field Radiation Patterns

The radiation pattern measurement was also conducted inside an anechoic chamber with one port excited and the other terminated with a 50 Ohm load. Fig. 6.14 shows the measured and simulated far field normalized patterns at two resonance frequencies 1.75 GHz and 2.7 GHz. The pattern diversity can be observed in both XY and XZ plane while due to the symmetry of the structure, the radiation patterns in YZ plane look the same. Due to the limited measurement facilities, only the simulated 3D radiation patterns are shown in Fig. 6.15. It can be seen that the patterns are complementary to each other in both XY and XZ plane, while they are symmetrical around YZ axis. However, the difference in both XY and XZ planes is sufficient to achieve a good diversity performance.

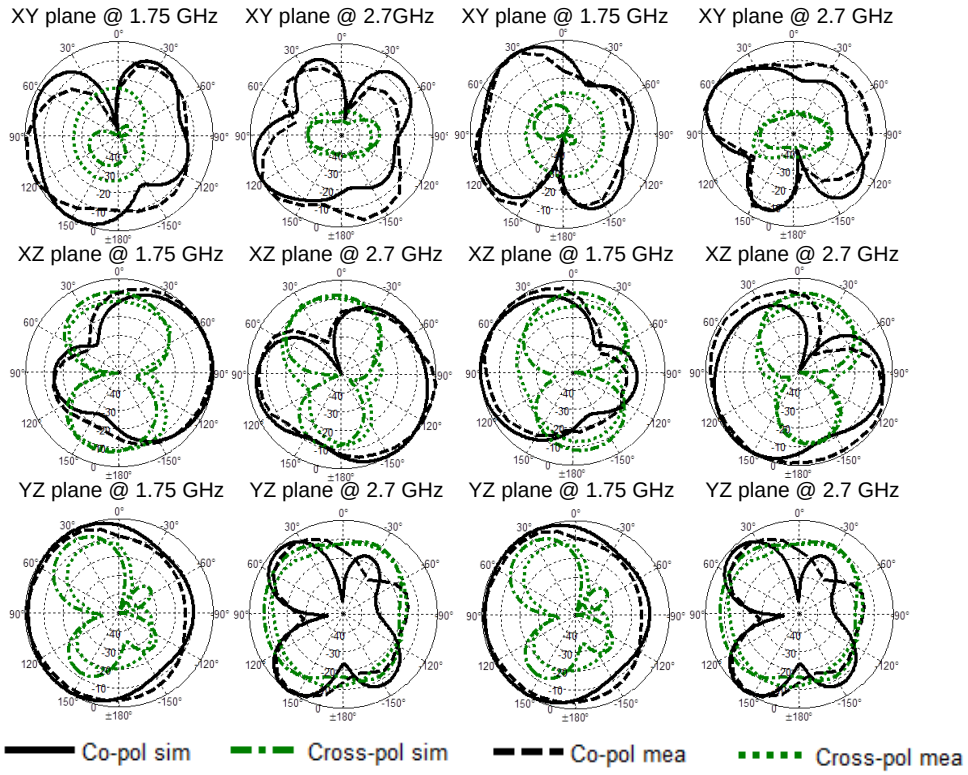

Fig. 6.14: Measured and simulated radiation patterns (a) Element 1 and (b) Element 2

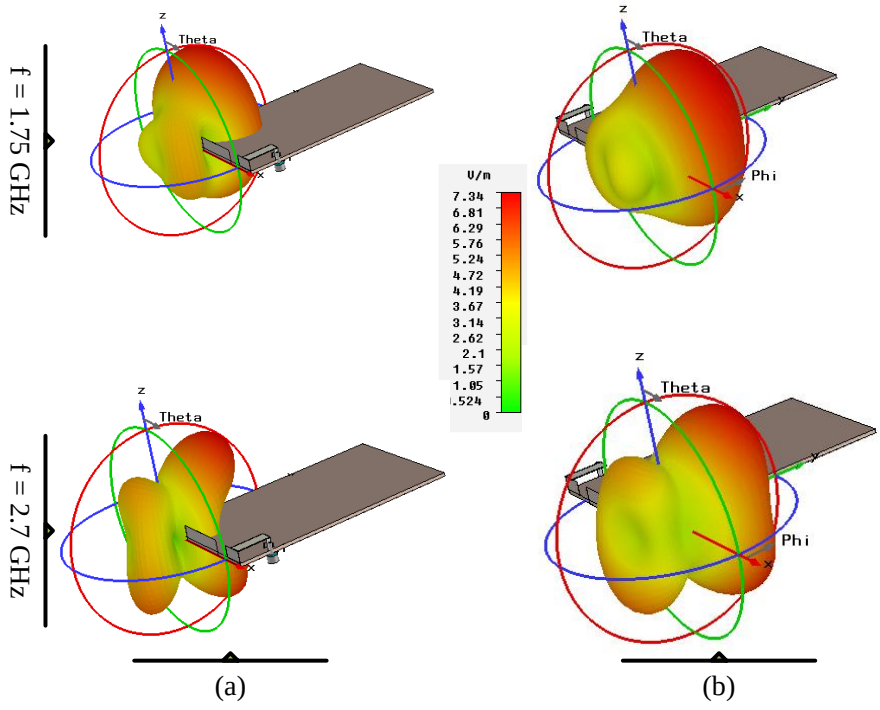

Fig. 6.15: 3D simulated radiation patterns (a) Element 1 and (b) Element 2

6.2.5 Diversity Performance Parameters

In order to characterize the antenna diversity performance, the diversity performance parameters of the proposed antenna are simulated, measured and evaluated.

The antenna branch power ratio in-terms of MEGs ratio is calculated using Eq.(2.18) in which the MEG of each antenna element is calculated using Eq.(2.19) over the different environments explained in Chapter 2. Table 6.3 reflects that the proposed antenna satisfies the energy balance condition as both ratios are less than 3 dB.

Fig. 6.16 shows the simulated and measured ECC, the results have a good agreement and both of them satisfy the ECC condition (ECC < 0.5). As both diversity conditions are satisfied, then the proposed compact dual-element PILA can be used as a MIMO and diversity antenna.

Table 6.3 MEG in different environments

Environment	Frequency (GHz)	Mean Effective Gain (dB)		k
		Ant1	Ant2	
Indoor	1.75	-3.02	-3.32	0.3
	2.7	-3.9	-3.7	0.2
Outdoor	1.75	-5.05	-5.36	0.31
	2.7	-6.0	-6.45	0.95

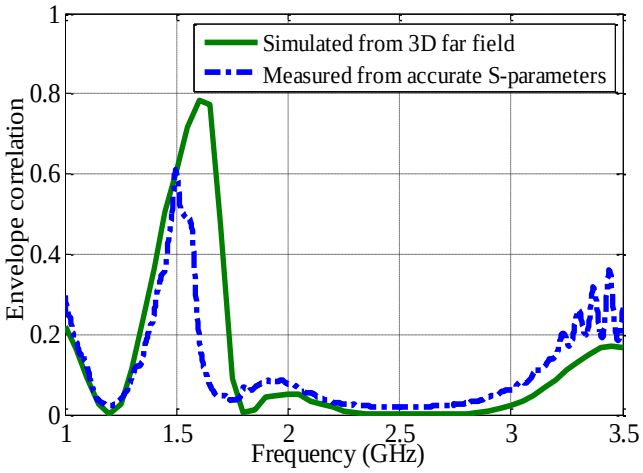

Fig. 6.16: Envelope correlation coefficient

The diversity gain measurement was performed in conjunction with a double ridged waveguide horn antenna (R&S®HF906) and a homemade PILA [12] with known radiation efficiency calculated via one-antenna approach inside the RC [13]. After acquiring and processing the data, the SC diversity scheme was applied and the corresponding CDF for each channel was calculated. As the diversity gain is defined as the ratio of the output power of the diversity combiner to the power of the reference branch at a specified CDF probability level (usually is 0.01), the apparent diversity gain @ 0.01 CDF is depicted in Fig. 6.17, and it is about 10 dB. This value is also verified from the measured ECC using Eq.(2.25), it is about 9.75 dB on average over the frequency band of interest.

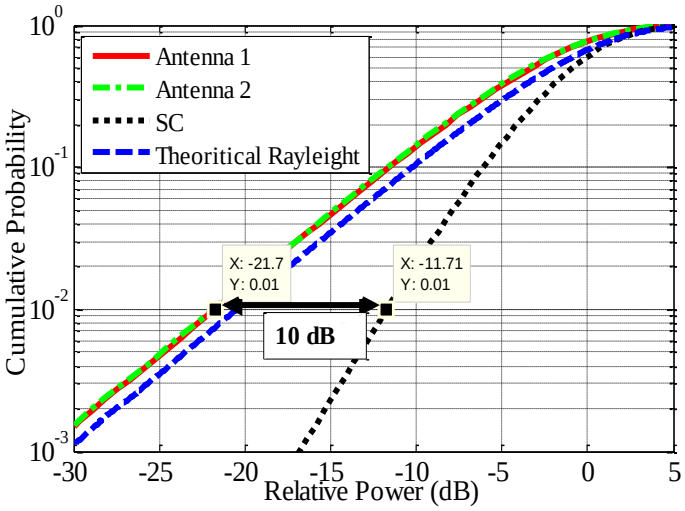

Fig. 6.17: CDF function and measured apparent diversity gain

The same collected data from the diversity gain measurement was used in calculating the total efficiencies using Eq. (2.29) and Eq. (2.27). The simulated and measured total efficiencies are depicted in Fig. 6.18. Despite the discrepancy outside the desired bandwidth, the figure shows that the proposed antenna has a high total radiation efficiency (> 80%) over the frequencies of interest (1.7 2.7 GHz).

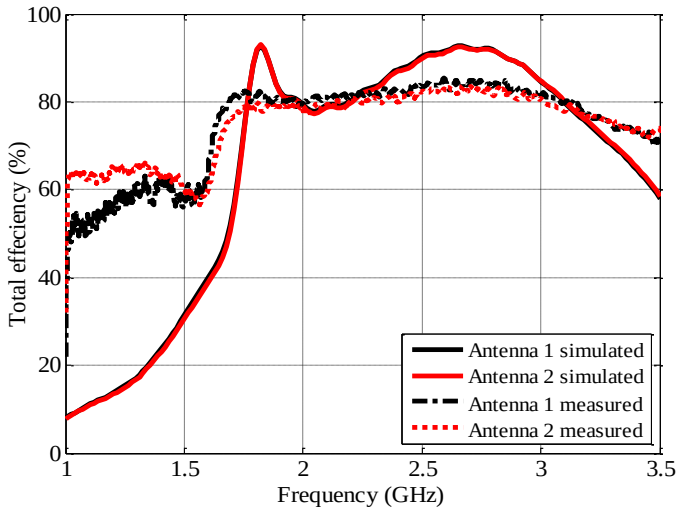

Fig. 6.18: Total radiation efficiency

6.3 Four-Element PILA Antenna

In order to meet the increasing demand for more data capacity and system reliability, the number of antennas should be increased at both communication system ends. In this context, the literature includes a huge number of dual-element MIMO antennas for small handsets applications, but the use of four-element MIMO antennas has not widespread yet. Even the published ones, some of them were a narrow band design [14-16]. Other designs were not suitable for handset integration as they utilized the ground planes for both radiating elements and isolation circuitry [17-20]. In [18], a tri-band four-element MIMO antenna has been proposed, but it covered high frequency application (above 2.4 GHz). Table 6.4 summarizes the aforementioned 4-element designs.

As explored in the previous section, the dual-element PILA has a wide bandwidth operation with a small footprint over the PCB. Therefore, this section presents a four-element PILA antenna for handset MIMO and diversity applications over the frequency range of (1.7-2.7 GHz)

Table 6.4 Summary of 4-element MIMO antenna published designs

Ref	Antenna configuration	Antenna Structure	Size (mm^2)	Frequency band (MHz)	Comments
[14]	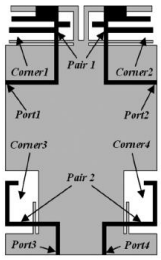	Printed monopoles	95×60	1880-2200	Single band design + Not suitable for handset integration
[15]	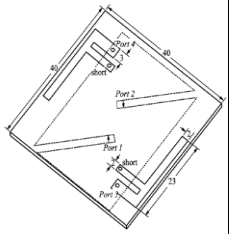	Printed-F monopoles and printed ground plane slots	40×40	2400-2448	Not suitable for handset devices due to small ground plane + Narrow band design
[16]	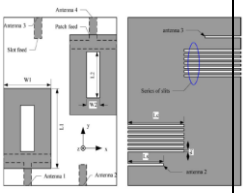	Two quarter wavelength slots and two square ring patch antennas	80×60	2400-2448	Multi-layer substrates with different thicknesses + Narrow band design
[17]	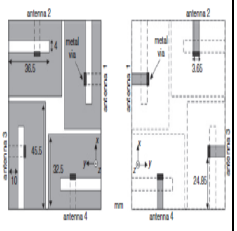	Printed slot antennas	70×70	1630-2050	The size of PCB is not suitable for real handset

[18]	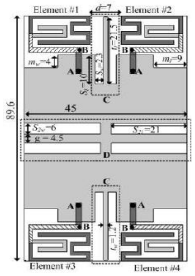	Printed monopoles	90×45	2340-2950 3380-3750 4400-6700	High frequency applications + Not suitable for handset integration
[19]	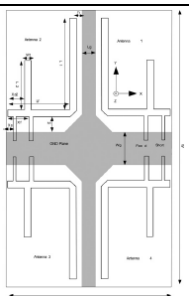	Printed monopoles with modified ground plane	110×58	734-790 2307-2475	Not suitable for handset integration + Very poor isolation
[20]	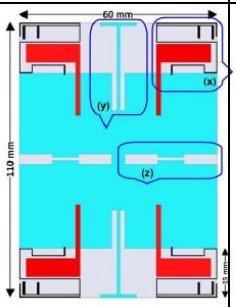	Printed monopole	110×60	1680-2180 2290-3000	Not suitable for handset integration

6.3.1 Prototype and S-Parameters

The four-element PILA antenna is made by creating another copy of the dual-element PILA, which is placed on the lower edge as shown in the fabricated prototype in Fig. 6.19; the PCB is the same as for the dual-element antenna. The simulated and measured S-parameters are in a good agreement as shown in Fig. 6.20, the design covers the frequency band between 1.7 to 2.7 GHz with an $S_{ii} < -6$ dB and $S_{ij} < -10$ dB. It covers DCS (1710-1880 MHz), PCS (1850-1990 MHz), UMTS (1920-2170 MHz) and the 4G LTE bands in the range of (1700-2700 MHz). Also, this design covers other wireless communication systems that are integrated with recent smart phones like WiFi (2400-2484 MHz) and Bluetooth. It can been seen from Fig. 6.20 that the mutual coupling coefficient between elements (1 and 3) and elements (2 and 4) reach -10 dB at some frequencies; this is mainly due to the strong chassis current mode along the edges of the ground plane. Despite of this, the design is very suitable for handset integration as there is no modification on the system ground plane. Also,

the level of the mutual coupling can be further decreased after integration of an LCD display and a battery.

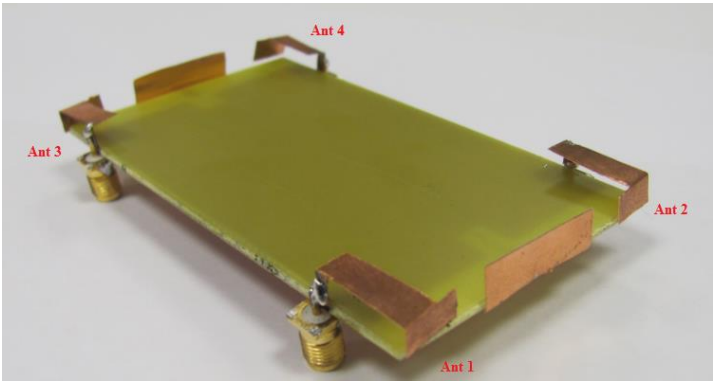

Fig 6.19: Four-element PILA prototype

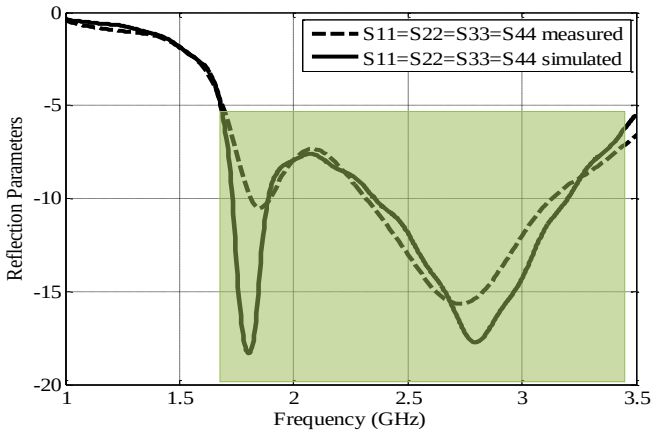

(a)

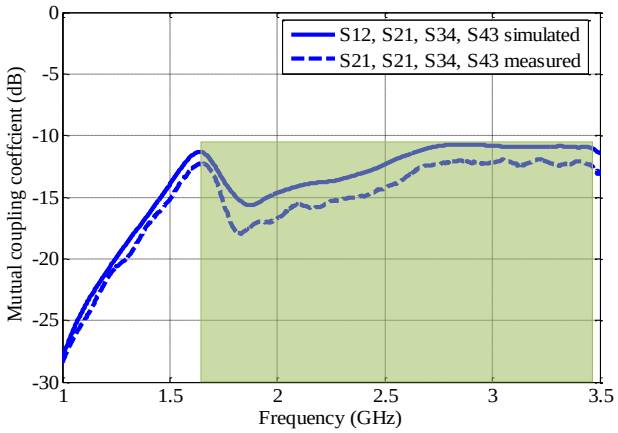

(b)

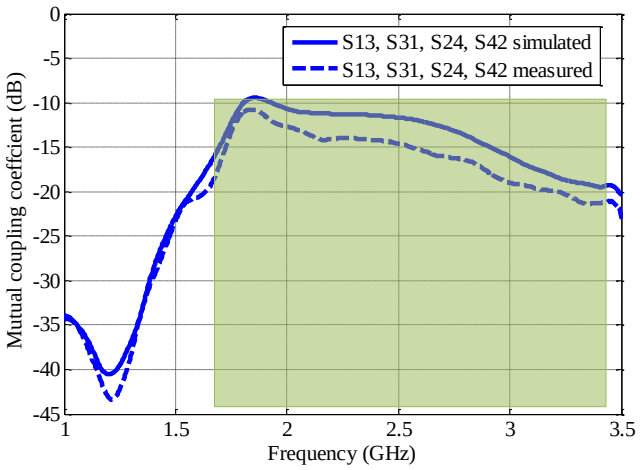

(c)

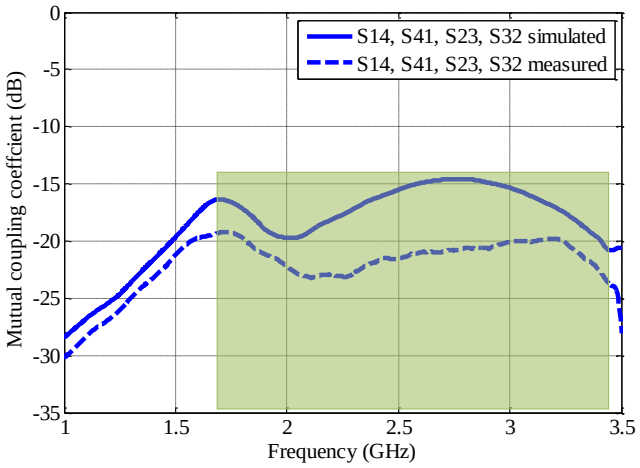

(d)

Fig. 6.20: Measured and simulated S-parameters (a) Reflection coefficients, (b), (c) and (d) Mutual coupling coefficients

6.3.2 Far-Field Radiation Patterns

The 2D far-field radiation pattern measurement was conducted inside an anechoic chamber in which the element under test is connected to a VNA while the others are terminated by 50 Ohm loads. Fig. 21 shows the simulated and measured normalized radiation patterns of the fabricated antennas at 1.75 GHz and 2.7 GHz, the radiation patterns of these four elements tend to cover complementary space regions, especially in XY-plane (all the patterns). For XZ and YZ planes, the patterns have a good complementary but

between different antenna pairs. These properties can provide a good diversity gain in severe scattering fading channels.

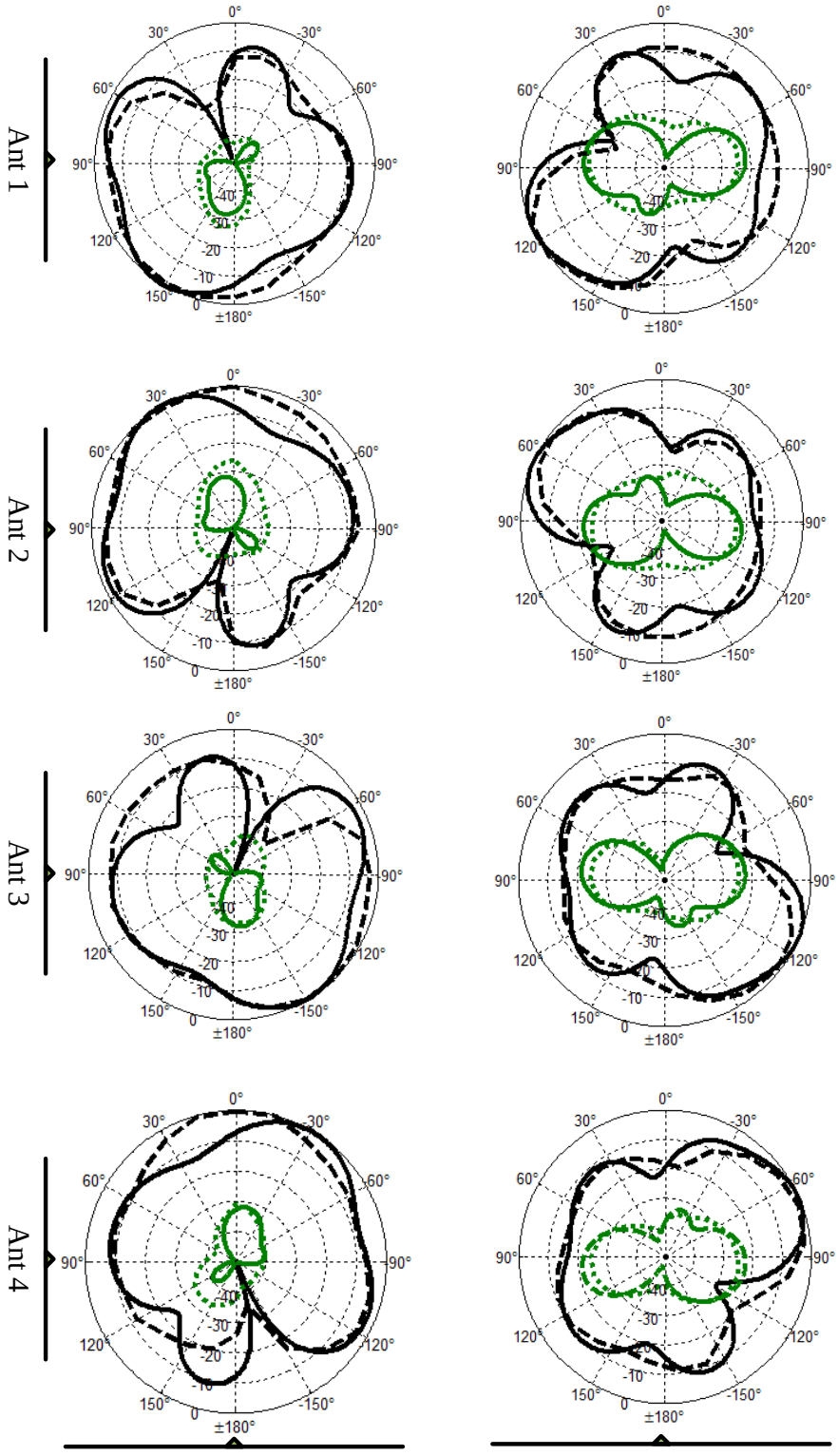

(a)

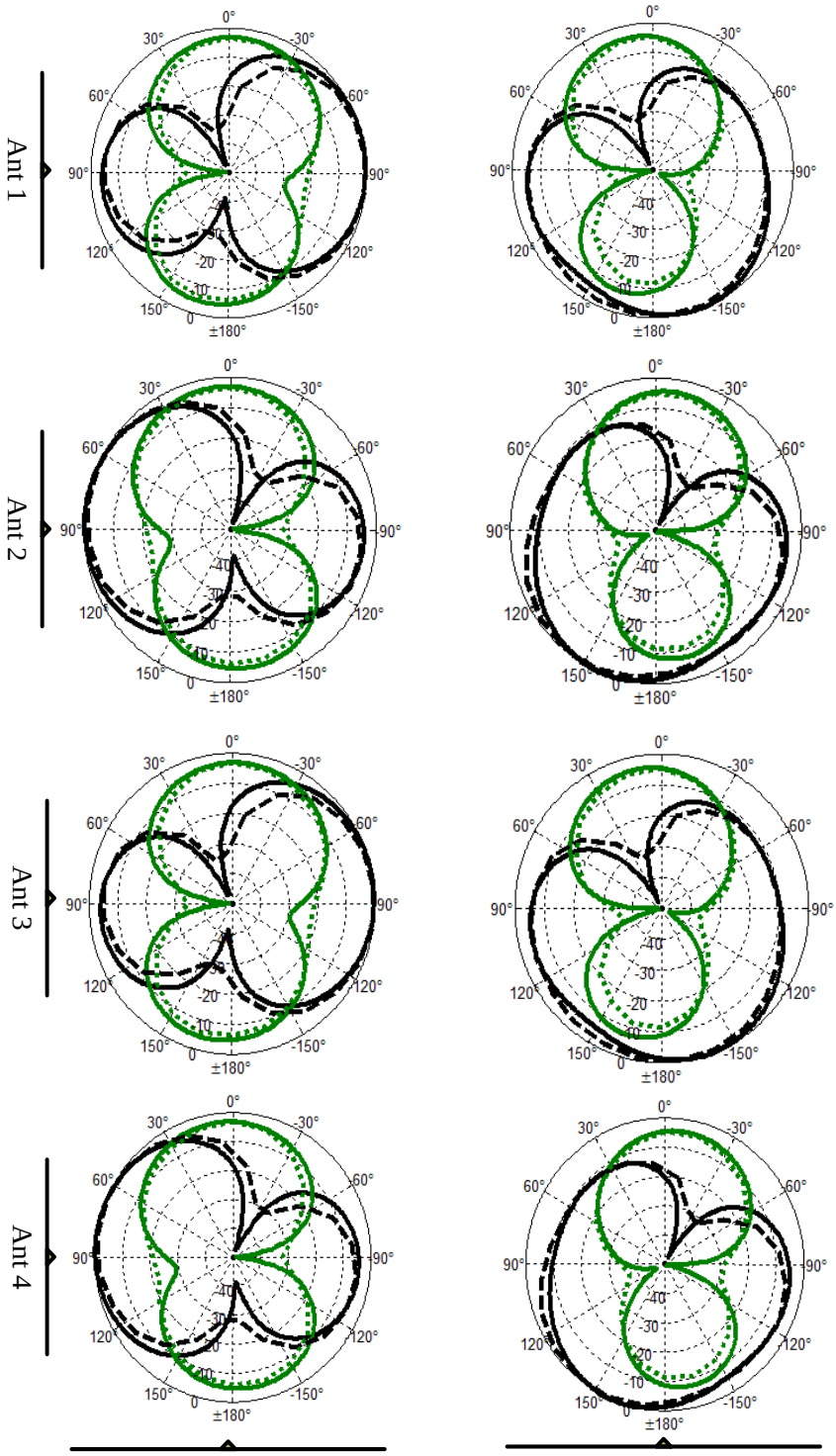

(b)

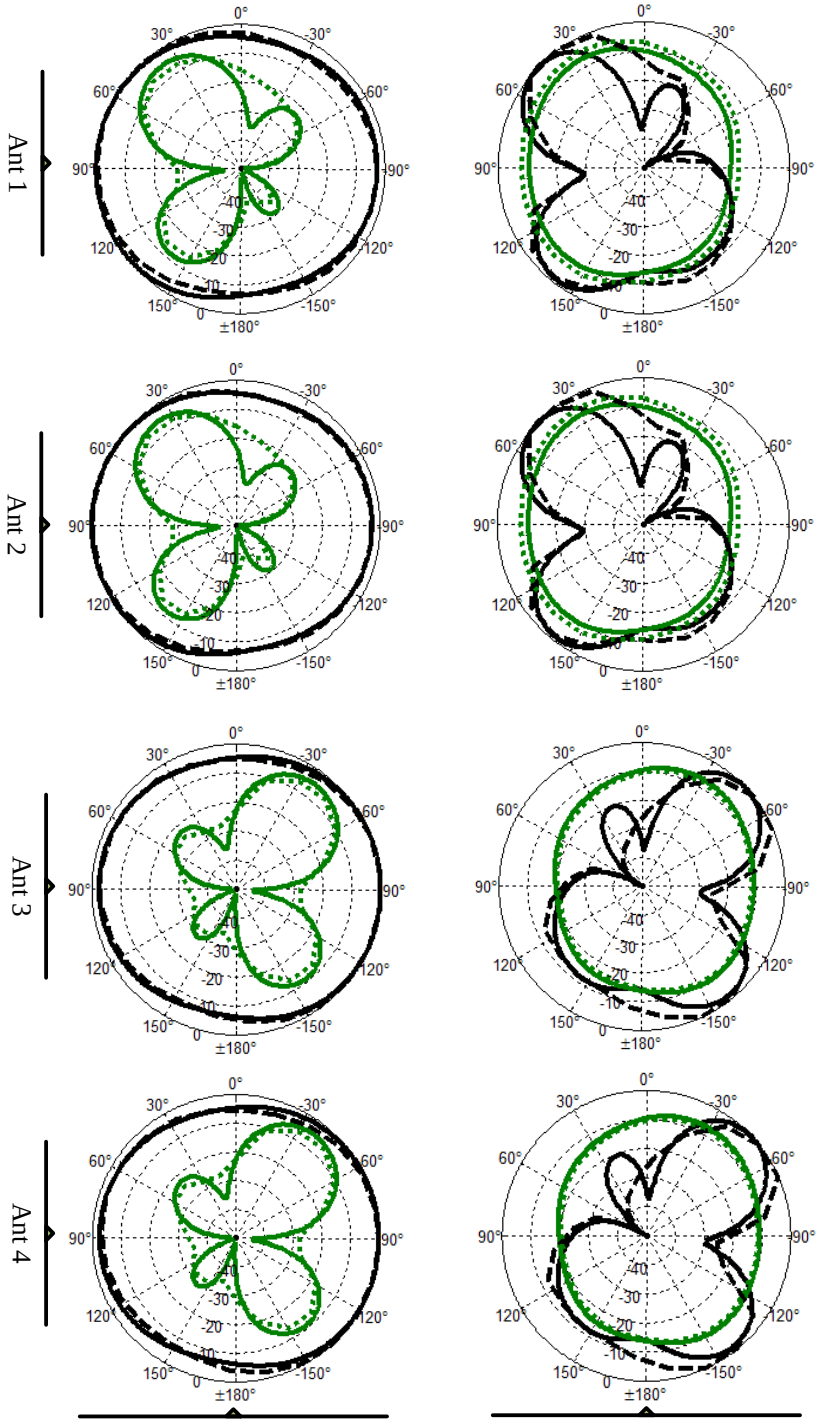

(c)

Fig. 6.21: Measured and simulated far-field normalized radiation patterns (a) XY plane (b) XZ plane and (c) YZ plane (Black E_ϕ, Green E_θ, the solid lines represent the simulated results, while the dashed and dotted lines are the measured patterns)

6.3.3 Diversity Performance Parameters

The proposed antenna satisfies the ECC diversity condition. Fig. 6.22 shows a good agreement between all the measured and the simulated ECC values, it shows also that the maximum value among ECC curves is about 0.1 which is already less than the critical limit (ECC < 0.5). This can be explained from the results of the radiation pattern in the previous section in which both pattern diversity and spatial diversity already exist between antenna element pairs (top and bottom pairs).

For the second diversity condition (power balanced condition), values for MEGs computed by Eq.(2.19) and their ratios over the defined indoor and urban outdoor environments are tabulated in Table 6.5. It can be seen that the maximum MEG ratios in both environments are all below 3 dB limit.

Table 6.5 MEG in different environments

Environment	Frequency (GHz)	Mean Effective Gain (dB)				Max (k)
		Ant1	Ant2	Ant3	Ant4	
Indoor	1.75	-2.9	-3.25	-3.3	-3.4	0.5
	2.75	-2.74	-3.41	-3.55	-3.74	1.0
Outdoor	1.75	-5.38	-5.3	-6.12	-5.95	0.82
	2.75	-3.86	-5.35	-5.85	-5.5	1.99

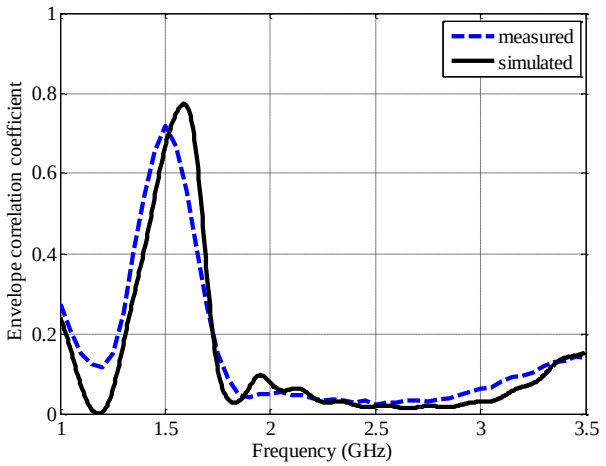

(a)

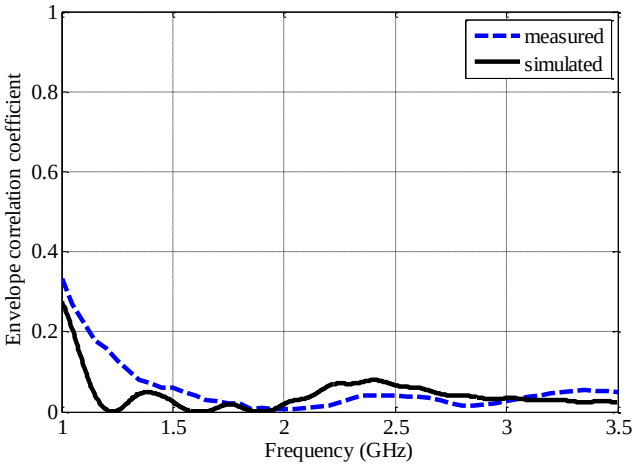

(b)

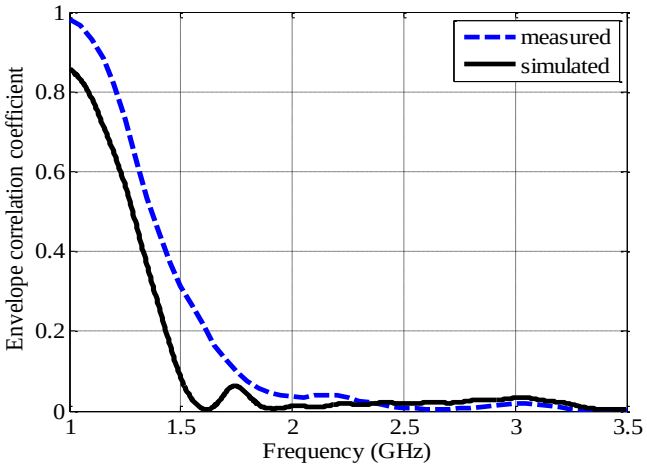

(c)

Fig. 6.22: Measured and simulated ECCs (a) ρ_{12}, ρ_{34} ; (b) ρ_{13}, ρ_{24} and (c) ρ_{14}, ρ_{23}

As the proposed design satisfied both diversity conditions, the diversity gain measurement was performed inside a reverberation chamber. Fig. 6.23 shows the resulted CDF curves from the post processing of the measured data. Using the selection combining scheme, the design has an apparent diversity gain about 15.5 dB, this can give an indication on how much the effectiveness of increasing the number of antenna elements on the system reliability.

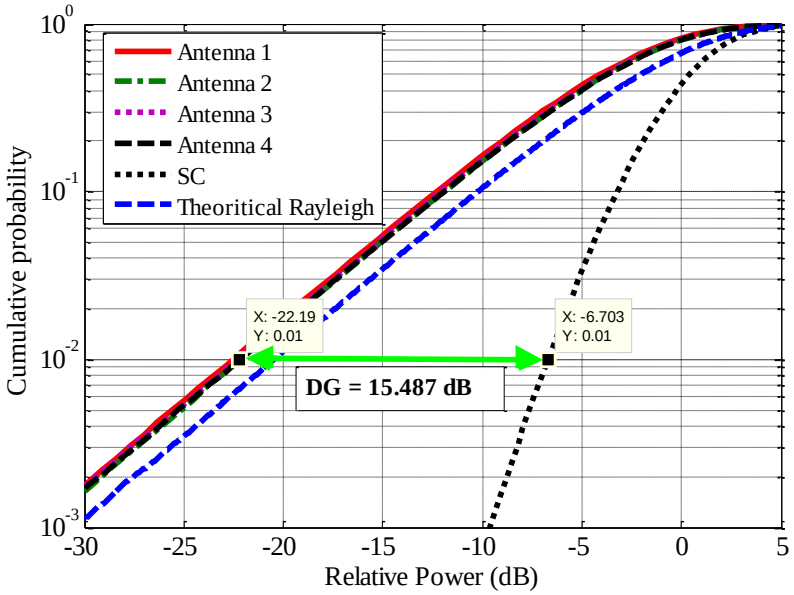

Fig. 6.23: Measured diversity gain from CDF

Finally, both the measured and simulated total efficiencies are calculated and depicted in Fig. 6.24 which shows that the four-element antenna has a free space total efficiency between 73 % and 82 % over the frequency band of interest. The slight discrepancy between the measured and the simulated curves is probably due to measurement errors inside RC chamber. Such source of errors like, the multiple calibration and the swapping process that changed the position of the used cables in the measurement.

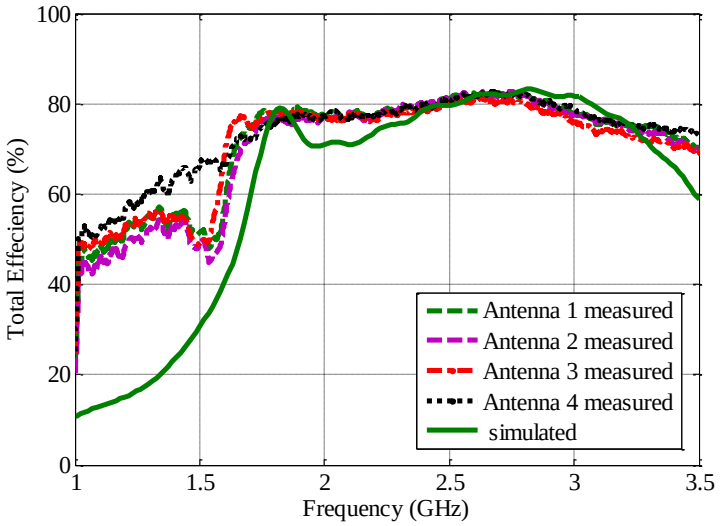

Fig. 6.24: The total radiation efficiency

6.4 Summary

This chapter has presented two compact MIMO antenna designs (a dual-element PILA antenna and a four-element PILA antenna) using a small footprint parasitic decoupling element which has been designed and optimized based on a new design approach. The main contributions are summarized below:

1) A low profile, small footprint and wideband dual-PILA-element antenna with a parasitic decoupling element has been presented for handset applications in the frequency range 1700-3500 MHz, the calculated and measured results of the antenna have shown that it can be a very good candidate for MIMO and diversity systems. Moreover, the design is compatible with the recent handset antenna design industry trend (handset with metallic frame ID) as both the decoupling element and antenna element can be considered as a part of the metal frame.

2) A new approach for designing a parasitic decoupling element between two-element MIMO antennas has been proposed. It is based on the stepped impedance resonator circuit theory. It offers some excellent features such as: I) small footprint decoupling elements; II) wide bandwidth; III) controllability of

the functionality of the decoupling element which can work as decoupling element or parasitic radiator or both. Table 6.6 compares the total length of the proposed decoupling element with some recently published work, and it shows that using this new approach, an optimal size can be achieved.

Table 6. 6: Comparison with the previous work

Ref	Total length	Lowest frequency (GHz)
[1]	$0.26\lambda_0$	2.4
[13]	$0.31\lambda_0$	1.92
[16]	$0.21\lambda_0$	2.4
work	$0.18\lambda_0$	1.7

3) To take the advantage of the compactness of the design, a four-element PILA antenna has been proposed in which another copy of the dual-element PILA was placed on the lower edge of the PCB. Unlike other four-element antennas in the literature, this design has the following features: I) as the ground plane between antenna elements is not modified, this design is very suitable for the real time use in handset devices. II) It has a wideband response over the frequency range 1700-3500 GHz with an acceptable isolation level. III) It has a very good diversity gain (15.5 dB) over a wide frequency range.

References

[1] A. C. K. Mak, C. R. Rowell and R. D. T. Murch.,"Isolation enhancement between two closely packed antennas," *IEEE Trans. Antennas Propag*, vol. 56, no. 11, pp. 3411-3419, Nov. 2008.

[2] J. Anderson and H. Rasmussen.,"Decoupling and descattering networks for antennas," *IEEE Trans. Antennas Propag.*, vol. 24, no. 6, pp. 841-846, Nov. 1976.

[3] C. Chi-Yuk, C. Chi-Ho, R. D. Murch *et al.*,"Reduction of mutual coupling between closely-packed antenna elements," *IEEE Trans. Antennas Propag* vol. 55, no. 6, pp. 1732-1738, 2007.

[4] C. Chi-Yuk and Z. Du.,"Microstrip antennas integrated with electromagnetic band gap EBG strucutures: a low mutual coupling design for array applications," *IEEE Trans. Antennas Propag*, vol. 51, no. 10, pp. 2936-2946, Oct. 2003.

[5] A. Diallo, C. Luxey, P. Le Thuc *et al.*,"Enhanced two-antenna structures for universal mobile telecommunications system diversity terminals," *IET Microwaves, Antennas & Propagation*, vol. 2, no. 1, pp. 93-101, 2008.

[6] Z. Li, Z. Du, M. Takahashi *et al.*,"Reduction mutual coupling of MIMO antennas with parasitic elements for mobile terminals," *IEEE Trans. Antennas Propag*, vol. 60, no. 2, pp. 473-480, Feb. 2012.

[7] G. Chi, B. Li and D. Qi,"Dual-band printed diversity antenna for 2.4/5.2- GHz WLAN application," *Microwave and Optical Technology Letters*, vol. 45, no. 6, pp. 561-563, june 2005.

[8] S. Alja'afreh, Y. Huang and L.Xing, Q. Xu and X. Zhu,"A low profile and wideband PILA-based antenna for handset diversity applications," *IEEE Antenna Wireless Propag. Letter*. [Online]. Avialable: doi: 10.1109/LAWP.2014.2384834.

[9] M. Sagawa, M. Makimoto and S. Yamashita.,"Geometrical structures and fundamental characteristics of microwave stepped-impedance resonators," *IEEE Trans. Mirowave Theory*, vol. 45, no. 7, pp. 1078-1084, July. 1997.

[10] T. Nakamura, M. Shimizu and H. Kimura *et al*,"Effective permittivity of amorphous mixed materials," *Electronics and Communications in Japan*, vol. 88, no. 10, Oct. 2005.

[11] R. N. Simons, *Coplanar waveguide circuits, components and systems*, John Wiley & Sons, Inc., New York, USA, 2001.

[12] S. Alja'afreh, Y. Huang and L.Xing,"Compact, wideband and low profile planar inverted-L antenna," *Proc. of the Europian Conference. On Antenna and Propagation (EuCAP 2014)*, The Hague, Netherlands, 2014.

[13] C. L. Holloway, H. A.Shah, R. J. Pirkl *et al.*,"Reverbration chamber techniques for determining the radiation and total efficiency of antennas," *IEEE Trans. Antennas Propag*, vol. 60, no. 4, pp. 1758-1770, April. 2012.

[14] Y. Ding, Z. Du and Z. Feng,"A four-element antenna system for mobile phones," *IEEE Antennas and Wireless Propagation Letters*, vol. 6, pp. 655-658, 2007.

[15] C-Y. Chiu and R. D. Murch,"Compact four-port antenna suitable for portable MIMO devices," *IEEE Antennas and Wireless Propagation Letters,* vol. 7, pp. 142-144, 2008.

[16] H.Li, J. Xiong and S. He,"A compact planar MIMO antenna system of four elements with similar radiation characteristics and isolation structure," *IEEE Antennas and Wireless Propagation Letters*, vol. 8, pp. 1107-1110, 2009.

[17] S. Zhang, P. Zetterberg and S. He,"Printed MIMO antenna system of four closely-spaced elements with large bandwidth and high isolation," *Electronic Letters,* vol. 46, no. 15, pp. 344-345, July.2010.

[18] J.-F. Li, Q.-X. Chu and X.-X. Guo,"Tri-band four-element MIMO antenna with high isolation," *Progress In Electromagnetics Research*, vol. 24, pp. 235-249, 2011.

[19] M. S. Sharawi, M. A. Jan and D. N. Aloi,"Four-shaped 2x2 multi-standard compact multiple input-multiple output antenna system for long –term evolution mobile handsets," *IET Microwave, Antennas and Propagation,* vol. 6, no. 6, pp. 685-696, 2012.

[20] F. Ahmad, Y. Feng and R. Li,"Dual wide-band four-unit MIMO antenna system for 4G/LTE and WLAN mobile phone applications," *Proc. of Loughborough Antennas and Propagation Conference (LAPC 2013)*, Loughborough, United kingdom, 2013.

Chapter 7: Multiband MIMO Antenna for Smartphones

7.1 Introduction

Over the last three decades, the mobile communication system has witnessed a great evolution started from single band 1G into dual band 2G then 3G and now 4G systems. Particularly, by releasing 4G systems, a new wireless standard is added (LTE). This increased the complexity of antenna design for small handset devices by two ways: 1) Mobile handset devices should support various wireless standards like: LTE, GSM, DCS, PCS and UMTS; 2) The new wireless standard (LTE) needs an integration of multiple antennas at both communication system ends, the implementation of the MIMO technology in a limited space at handset devices is a full of challenge. In particular, for frequencies below 1 GHz, antenna elements share the same chassis that works as a main radiator. This increases the mutual coupling which leads to degradation on the performance parameters of the MIMO antenna system such as: envelope correlation coefficient, diversity gain and total antenna efficiency. Thus, integration of a multi-element antenna with a multiband operation is a subject of huge interest.

Many decoupling methods have been proposed to cope the mutual coupling between closely spaced antenna elements. Such techniques are like: decoupling and matching networks [1], defect ground plane structures [2], electromagnetic band gap structures [3], parasitic decoupling elements [4] and neutralization lines [5]. However, all of them are effective only for the high frequencies (above 1.8 GHz) [6]. Even if they are applied for applications below 1 GHz, the final structures usually have a very narrow bandwidth and a single band operation [7-9]. In [6], a very interesting and powerful decoupling approach has been proposed to design an uncorrelated dual-element antenna at frequencies below 1 GHz. The basic principle behind this technique was to excite orthogonal chassis modes below 1 GHz, these two modes were the conventional chassis dipole mode and the T-strip mode that was resulted from a manipulation on the mobile chassis (Loading the chassis by two T-shaped strips as a metal frame).

On the other hand, smartphones have dominated mobile markets and are still enjoying a rapid growth. A current trend in smartphone design is to use a metallic frame in housing for adding more mechanical strength and nice cosmetic appearance [10]. Another

advantage of the metallic frame lies in the integration with the antenna circuitry. Metal frame antennas are very attractive as they occupy a narrow space with the casing of portable devices; this can save more space for other handset components such as the large display, battery, etc.

In this context, several promising designs have been proposed. For example, a low-profile metal frame antenna was reported in [11] but lumped elements were used to provide impedance matching which affected the radiation efficiency. In [12-15], several multiband designs were proposed, but all of them shared the same drawback: the same chassis mode was used for frequencies below 1 GHz, which usually increases the difficulty of installing other handset antennas and made them not suitable for the recent MIMO technology. To overcome this problem, interesting design solutions have been reported in [6, 16] where a new characteristic mode (orthogonal to the conventional chassis dipole mode below 1 GHz) has been excited by a metal frame antenna. This facilitated the introduction of a dual-element antenna for MIMO applications. However, these proposed solutions are high profile designs and can only cover single band [6] or dual band [16].

This chapter presents a low profile dual-element antenna capable of providing hexa-band WWAN/LTE MIMO operation. It consists of a modified metal frame antenna (covers six frequency bands) and a multiband modified (PILA) coupled with a meandered parasitic monopole (covers seven frequency bands). Both single element designs are presented firstly, and then the dual-element antenna is proposed. The performance of the dual-element antenna is evaluated in the free space and the results demonstrate that it is a promising design for multiband and MIMO smartphone applications. This followed by the effect of integrating with other components like LCD touch screen and battery. Finally, the summary is drawn in the last section.

7.2 Hexa-Band Metallic Frame Antenna for Smartphone Applications

7.2.1 Antenna Configuration

The geometry of the proposed frame antenna is depicted in Fig. 7.1 with the optimized dimensions. The design uses a *1 mm* thick FR4 substrate of dimensions *60×130* mm^2 relative permittivity *4.4* and loss tangent *0.025* as the system printed circuit board (PCB) and the substrate material for the metal frame antenna. The metal frame is composed of two parts segment 1 (the main radiator) and segment 2. For ease of fabrication, each segment is printed on a *1 mm* thick FR4 substrate of dimensions *8×130* mm^2. Unlike [6, 16] that have high profiles (8 mm height above PCB), the frame is positioned vertically, next to the system PCB with *4 mm* above and *4 mm* below the ground plane; this will keep the total thickness of the resulting handset device within the limit (thickness ≤ 8 *mm*), even after the integration of both the LCD display and the battery. The gaps between the ground plane and the frame antenna segments are *3.5 mm* and *1 mm* from segment 1 and segment 2, respectively. The area without the ground at the top edge of the PCB is *60×13* mm^2; this cleared area can be used to install another antenna element as it will excite the conventional dipole chassis mode below 1 GHz [6, 16] and this will simplify the design of MIMO antenna. A narrow plate parallel (*3.5×20* mm^2) to the system PCB, is used to create a capacitive coupling that can excite the frame mode properly. It is connected to segment 1 and fed by a vertical feeding plate connected to a feeding probe (not shown for the clarity of the figure). As shown by Fig. 7.1(b), the feeding plate is placed at a *55 mm* from the top edge of the PCB with dimensions *4×10* mm^2; also the shorting plates (Short 1 and Short 2) with dimensions 4×*5* mm^2 are used to connect the frame segments to the ground plane. Fig. 7.1(c) shows the detailed dimensions of the main segment. The frame is loaded with stubs to provide the multiband operation. Segment 2 (see Fig. 7.1(d)) is added to enhance the operational bandwidth at the lower frequency band (GSM850).

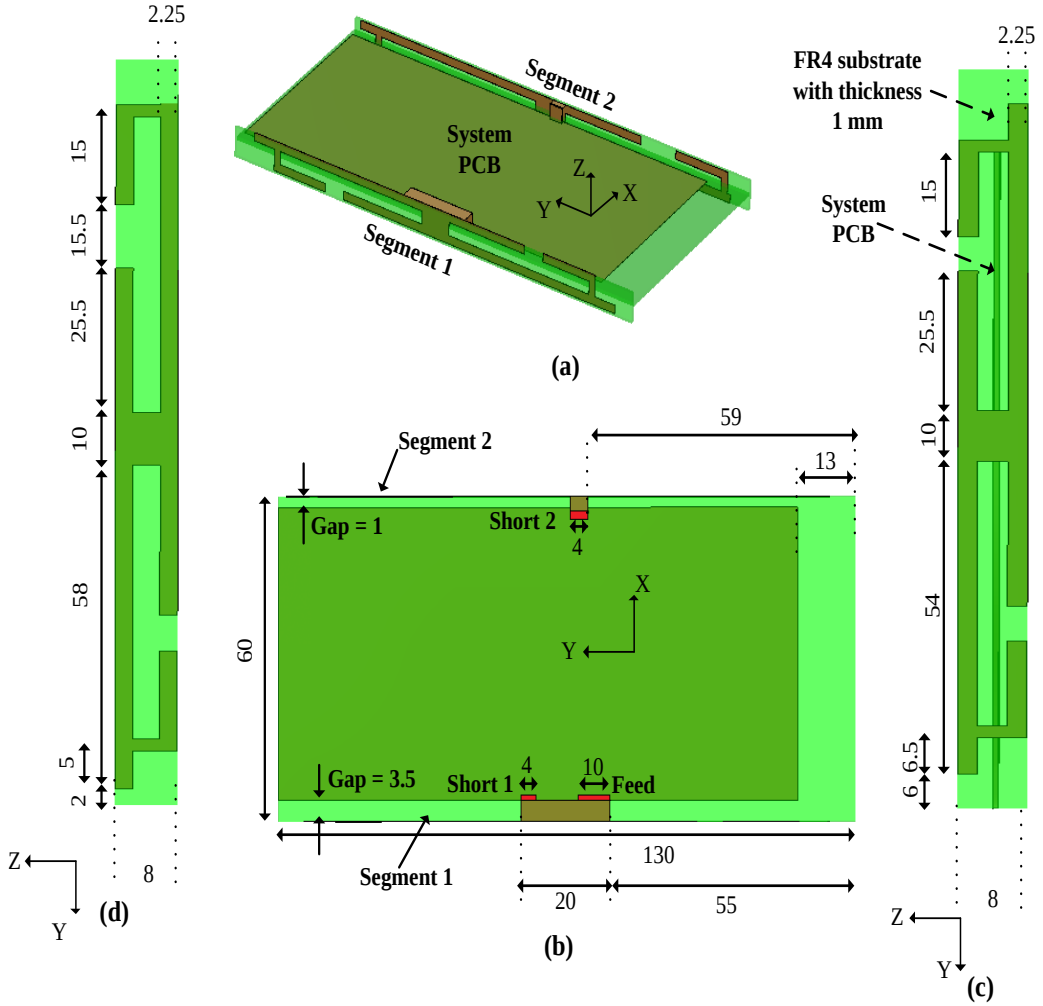

Fig. 7.1: Geometry of the proposed design: (a) 3D antenna geometry, (b) the top view with detailed dimensions, , (c) Segment 1 with detailed dimensions and (d) Segment 2 with detailed dimensions. (Unit: mm)

7.2.2 Antenna Design Process

To reveal the operational mechanism of the proposed antenna, an evolutional design process, including four stages is shown in Fig. 7.2 (b) and the resulted reflection coefficient S11 after each design stage is presented in Fig. 7.2 (a). Initially, the design was like a dual-branch shorted monopole as shown in Stage I. It is clearly shown that the design in Stage I has three resonance modes at 0.99 GHz, 2.1 GHz and 3.18 GHz, corresponding to the 0.25λ (branch #1), 0.25λ (branch #2) and 0.75λ (branch #1), respectively. Stub 1 (inverted-L shape) was added in Stage II for two reasons: the first one is to provide an inductive loading for branch #1 resonance modes (0.25λ and 0.75λ), both were shifted down to 0.85 GHz

and 2.55 GHz. The second one is to create a new resonant frequency at the higher frequency bands, this can be seen from Fig. 7.2(a) where a new resonance deep appears at 3.75 GHz which is linked to 0.25λ mode of the added Stub. In order to achieve a wideband operation in the frequency range 1.7 GHz to 2.2 GHz, a new resonance mode (f = 1.85 GHz) was created in Stage III by the addition of Stub 2 (0.25λ), it was tuned to 1.85 GHz to merge with 2.1 GHz resonance. Thus, DCS1800, PCS1900 and UMTS2100 all were covered by Stage 3 as shown in Fig. 7.2(a). It is worth mentioning that the rest metallic part of segment 1 was added to provide more mechanical strength and a nice appearance. Finally, the second frame segment (segment 2) was added in Stage IV to work as a wavetrap that can enhance impedance bandwidth at 0.85 GHz as shown in Fig. 7.2(a). Thus, for the 6-dB return loss bandwidth, the design covers six frequency bands ranging from GSM850 to LTE3600.

To further understand the multiband operation, the simulated surface current distributions at five resonant frequencies are given in Fig. 7.3. Obviously, for the lowest frequency band (0.85 GHz), the largest surface current density is observed along the frame segments, which represents a 0.25λ PIFA-like fundamental mode. It can be seen also how is the chassis current is trapped by segment 2, which helps in enhancing the impedance bandwidth. For the second (1.85 GHz) and third (2.1 GHz) resonances, the current distributions become more concentrated on Stub 2 and branch #2, respectively, Both of them represent 0.25λ resonance modes (see Fig. 7.3(b) and (c)). For the higher resonant frequencies, it is clearly shown by Fig. 7.3 (d) that the resonance at 2.55 GHz is linked to the 0.75λ resonance of branch #1 while at 3.7 GHz it is related to a 0.25λ Stub 1 (inverted-L) mode.

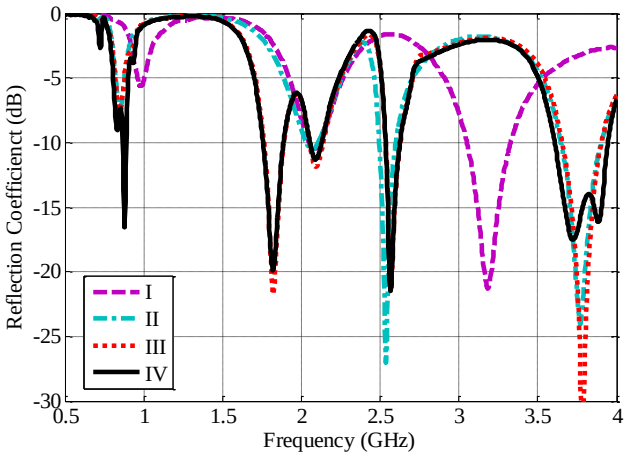

(a)

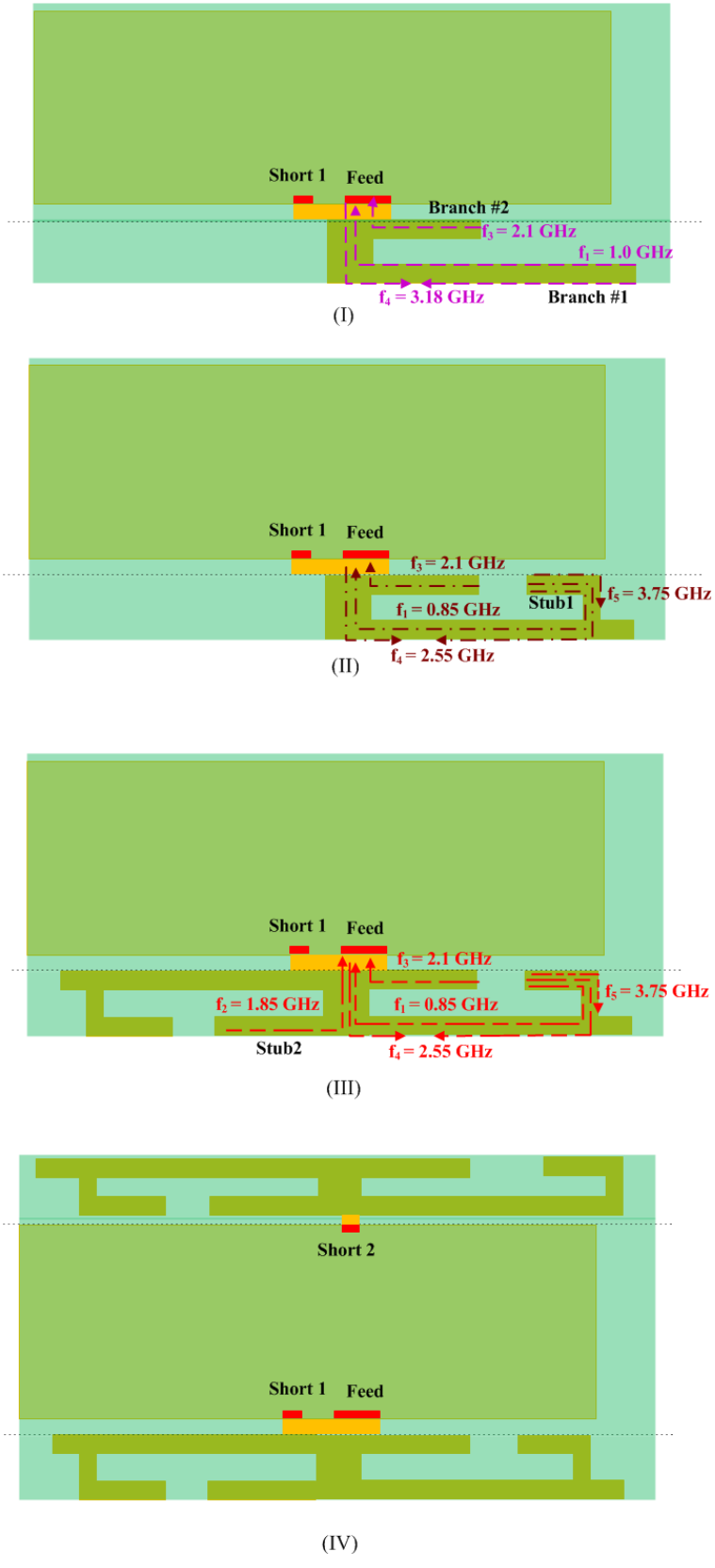

(b)

Fig. 7.2: (a) S_{11} evolutions, (a) the step by step change on the frame geometry (planar form)

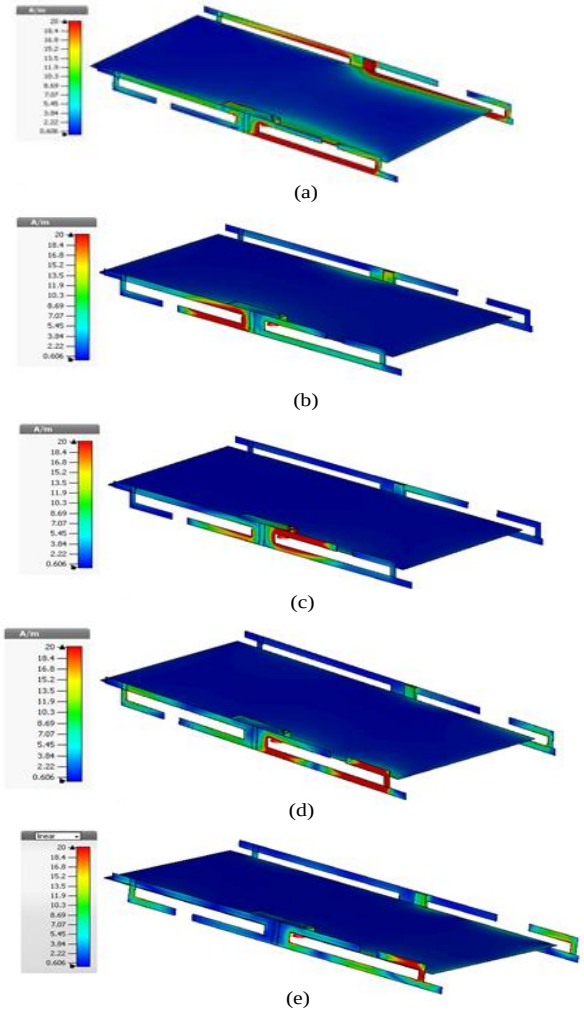

Fig. 7.3: Simulated surface current distributions (a) 0.85 GHz, (b) 1.85 GHz, (c) 2.1 GHz, (d) 2.55 GHz and (e) at 3.75 GHz.

7.2.3 Simulated and Measured Results

Simulations were performed using CST Microwave Studio to optimize the antenna parameters for the desired frequency bands. A prototype of the optimized design (shown in Fig. 7.4) was fabricated and tested. Fig. 7.5 shows the measured and the simulated reflection coefficients. A good agreement can be seen, a small discrepancy between them in the high frequency bands is due the effect of soldering and structure assembling. Based on the 6 dB return loss bandwidth, the proposed frame antenna covers six operating bands which are GSM850/ DCS1800/ PCS1900/ UMTS2100 /LTE2500/ LTE3600.

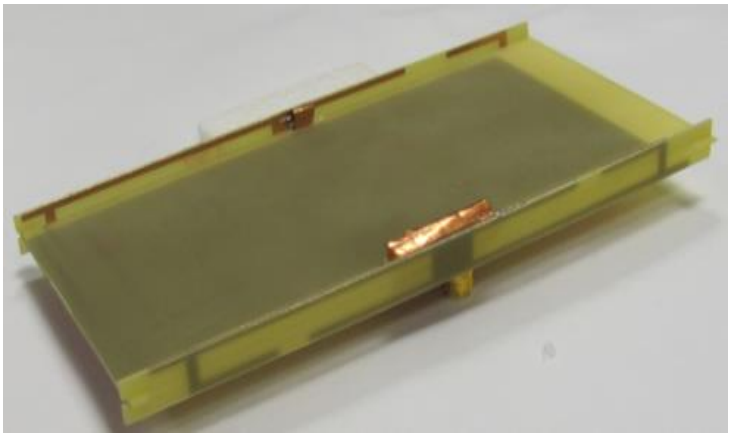

Fig. 7.4: The fabricated prototype

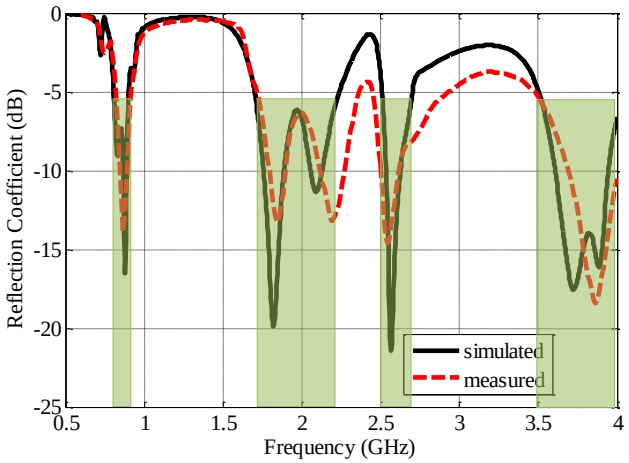

Fig. 7.5: Measured and simulated reflection coefficients

Fig. 7.6 shows the simulated and measured normalized radiation patterns of the proposed antenna. It can be seen the big advantage of this design over other multiband designs [11-15] at the lower frequency 0.85 GHz, the design has orthogonal patterns to the common and conventional chassis mode; also this can be understood from the 3D simulated radiation pattern at 0.85 GHz as shown in Fig. 7.7. This can facilitate the design of a MIMO antenna below 1GHz. As mentioned earlier, this design presents a multiband solution over [6. 16], the radiation patterns at the higher resonant frequencies are also included in Fig. 7.6. The simulated and the measured results are in good agreements, slight difference occurs in higher frequency results, which corresponds to the feeding cable and the orientation (some inclination may exist) of the antenna during the measurement, especially, on the vertical planes (XZ and YZ planes).

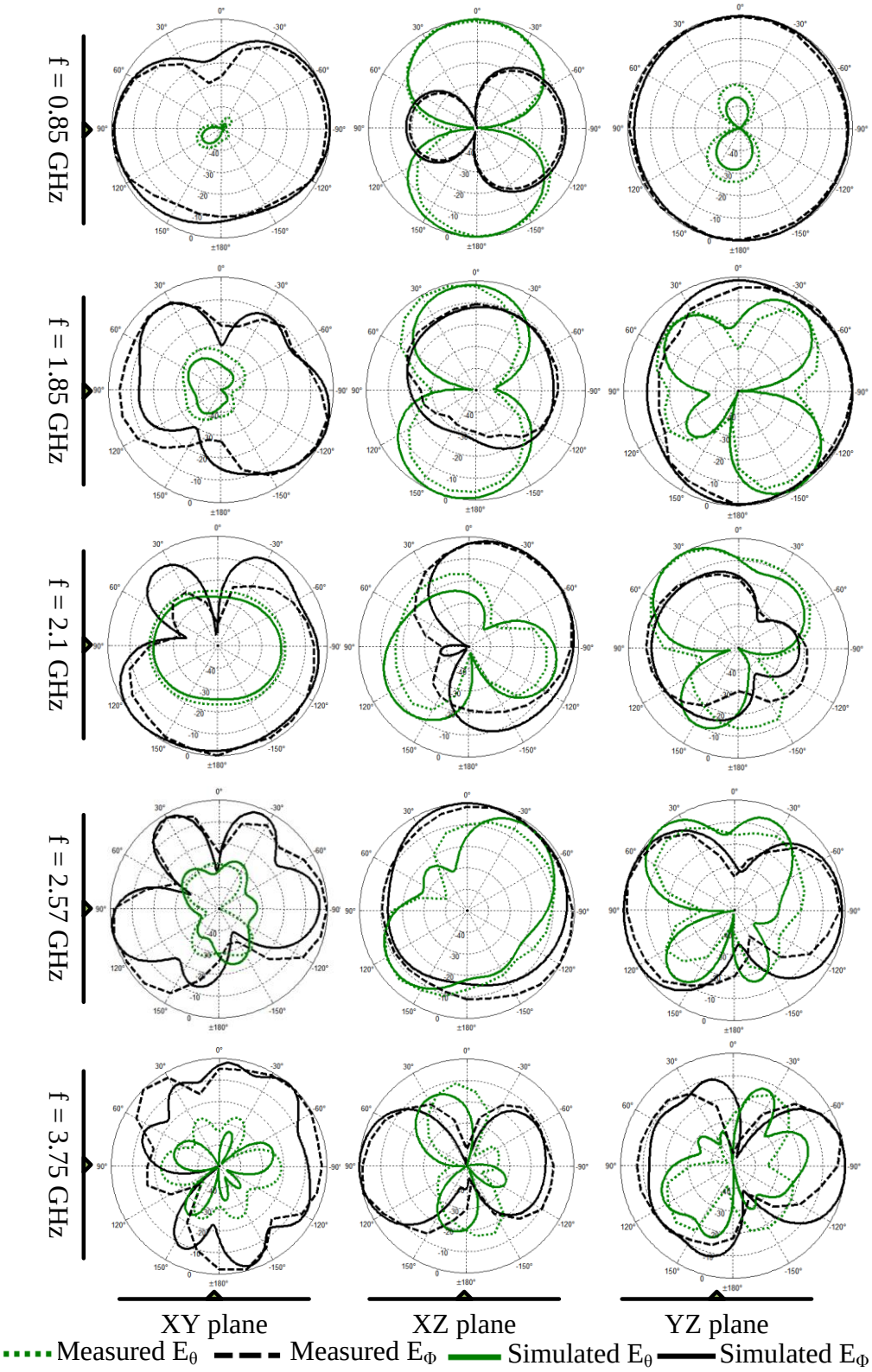

Fig. 7.6: Simulated and measured normalized far field radiation patterns

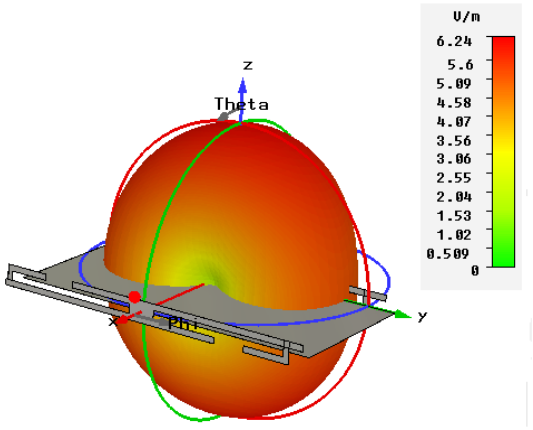

Fig. 7.7: 3D simulated far field pattern at 0.85 GHz

Finally, the total efficiency of the fabricated antenna was measured inside our reverberation chamber. The two antenna method presented in Chapter 2 was used for the measurement. Table 7.1 shows the measured and simulated total efficiency obtained at resonant frequencies 0.85, 1.8, 2.1, 2.55 and 3.75 GHz. The results are in a good agreement (the measured ones are slightly smaller) and the discrepancy between the results is likely due to the fabrication errors and the material property variations.

Table 7.1 Simulated and measured total efficiency

Frequency (GHz)	Simulated	Measured
0.85	83%	79%
1.8	90%	82%
2.1	85%	80%
2.55	87%	82%
3.75	86%	83%

7.3 Hepta-Band Internal Antenna for Smartphone Applications

7.3.1 Antenna Configuration

This section presents the second multiband antenna design, which is a commonly used antenna structure in mobile phones. Fig. 7.8 represents a hepta-band PILA antenna coupled with a meandered parasitic monopole. The design has a ground plane with dimensions *60 mm x 130 mm*, it is loaded by an FR4 substrate with a thickness of *1 mm*. As any internal antenna (electrical antenna), the proposed antenna is placed on the top shorted edge of the mobile PCB to achieve better impedance matching and frequency bandwidth. It has a total volume of *28 x 15 x 4.5 mm*^{3}. As shown in Fig. 7.8, it is compromised of three main parts: the PILA plate as the main coupling element, which is fed by a feeding strip with dimensions *2 mm x 3.5 mm*, the coupled meandered monopole as a parasitic radiator and the thick FR4 substrate (permittivity of 4.4 and loss tangent 0.025) that works as a carrier and a loading material.

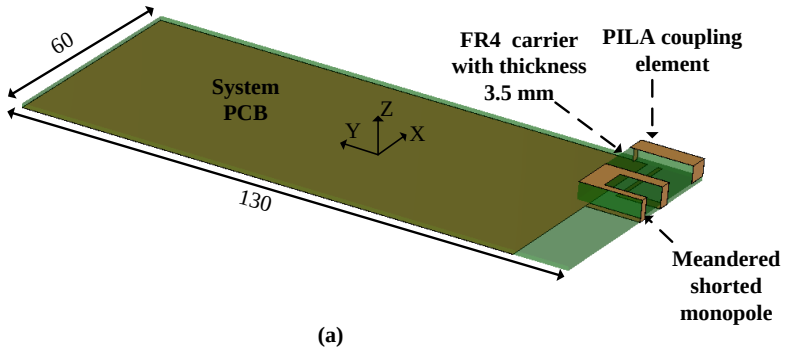

(a)

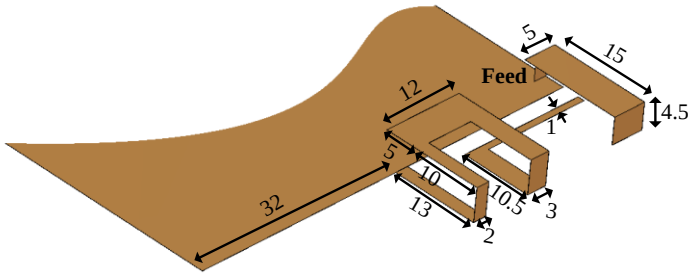

(b)

Fig: 7.8: Antenna configuration (a) Whole configuration and (b) Detailed dimensions (unit: mm)

7.3.2 Antenna Design Process

This section demonstrates the effect of the introduction of each part of the proposed antenna in an evolutionary process. Fig. 7.9 shows the resulted resonance deep around 3.2 GHz after the creation of the PILA plate with a total length around *22 mm* (equal to $\lambda/4$ of 3.2 GHz). In order to move the frequency band down to 1.7-2.7 GHz band, the FR4 carrier is added as a loading material. Finally, the parasitic meandered monopole structure with a total length of *86 mm* is capacitively coupled with the PILA plate antenna. This adds two resonant frequencies: one is linked to the quarter wavelength resonance mode and it is around 0.85 GHz, and the other is a higher order mode resonance which is around 3.45 GHz. Thus, based on the 6 dB return loss bandwidth; the design covers seven frequency bands which are: GSM850, DCS1800, PCS1900, UMTS2100, LTE2500, 2.4 GHz WiFi and LTE3600.

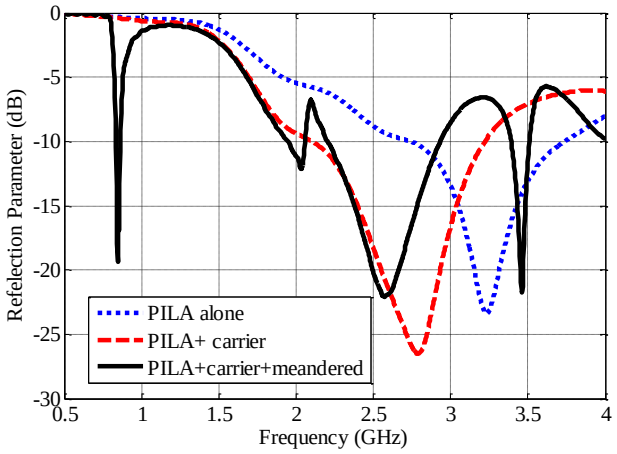

Fig. 7.9: Reflection coefficient evolutions

To further understand the multiband operation, the simulated surface current distributions at the three resonant frequencies (0.85 GHz, 2.55 GHz and 3.45 GHz) are given in Fig. 7.10. It is clearly shown that the lowest resonance is linked to a quarter wavelength resonance mode of the meandered monopole, while the wideband operations from 1.7 GHz to 4.0 GHz is resulted from merging the resonance of PILA at 2.55 GHz (see Fig. 7.10(b)) with the higher order mode of the meandered monopole at 3.45 GHz (see Fig. 7.10(c)).

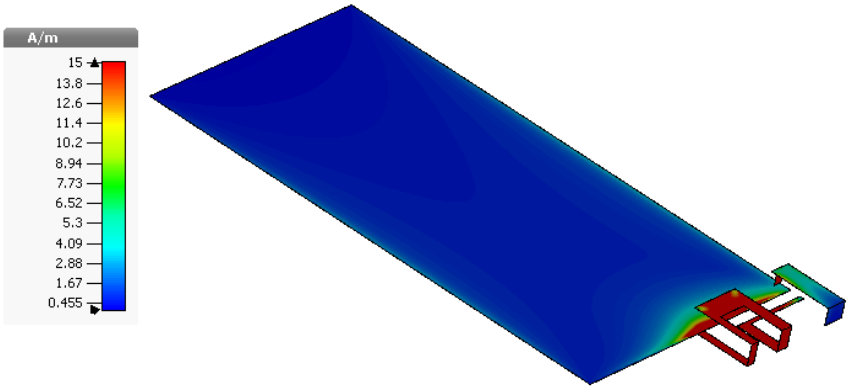

(a)

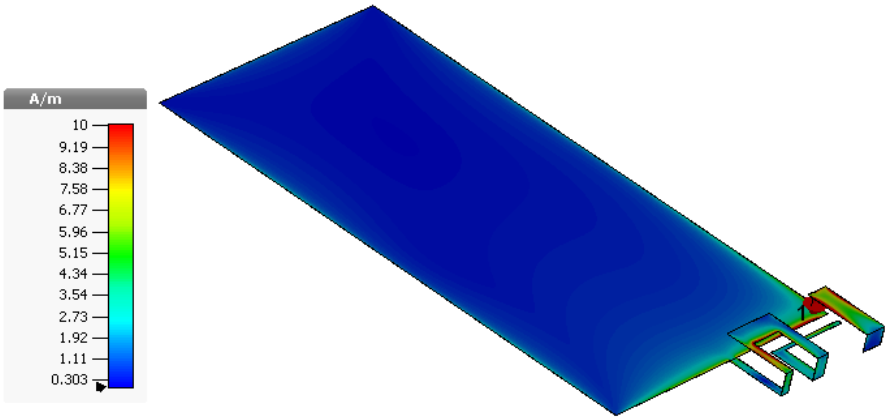

(b)

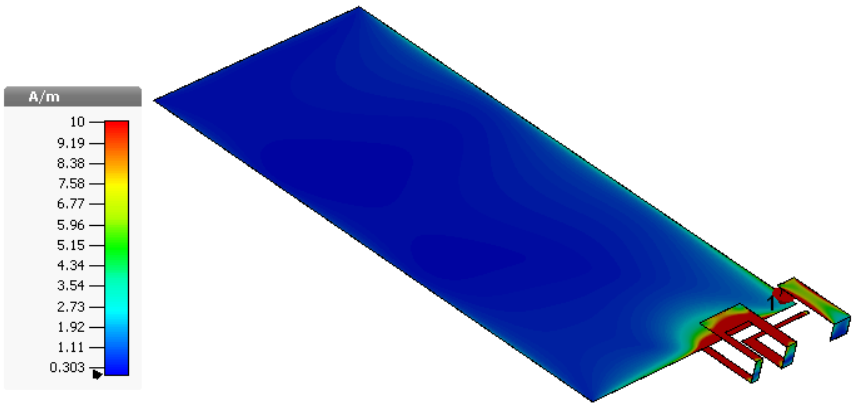

(c)

Fig. 7.10: Simulated surface current distributions (a) f = 0.85 GHz,

(b) f = 2.55 GHz and (c) f = 3.45 GHz

7.4 Dual-Element Antenna System for Multiband Smartphone Applications

As mentioned in the beginning, the main challenge in antenna design for mobile phones MIMO applications is mainly for the frequencies below 1 GHz. This due to severe mutual coupling between antenna elements as the common ground plane works as the main radiator. The best and the most reliable technique to implement multi-element antenna for such frequency applications is to excite orthogonal chassis characteristic modes. The two antenna designs in the previous have this orthogonality at 0.85 GHz, this can be seen from the resulted 3D radiation patterns as shown in Fig. 7.11. The resulted pattern from the multiband PILA design (Section 7.3) is similar to the fundamental dipole chassis mode, while the metal frame antenna design in Fig. 7.11(a) has an orthogonal pattern. Thus, the mutual coupling problem below 1 GHz can be managed if both antennas are integrated together as a MIMO antenna. This section presents the resulted dual-element multiband antenna.

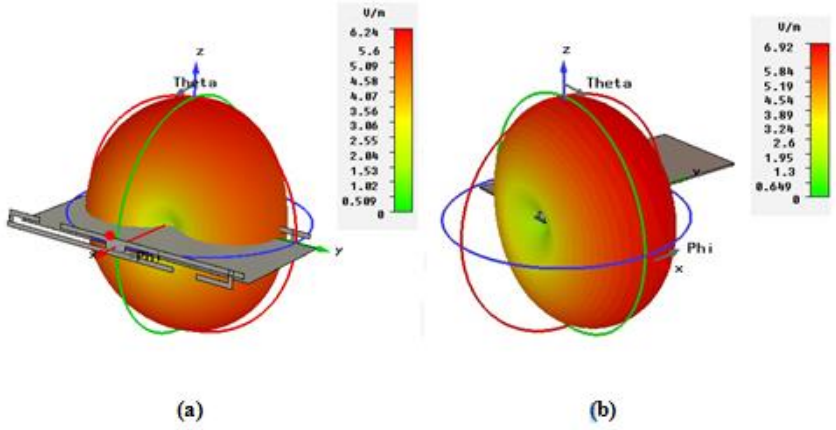

Fig. 7.11: Far field 3D radiation patterns at 0.85 GHz (a) Hexa-band metal frame antenna and (b) Hepta-band PILA antenna

7.4.1 Antenna Configuration

Fig. 7.12 shows a dual-element multiband antenna system, consisting of a hexa-band metal frame antenna and a hepta-band PILA antenna coupled with a meandered parasitic shorted monopole. Both antennas shared the same PCB board, which is a *1mm* thick FR4 substrate of dimensions *60 mm x 130 mm*, relative permittivity 4.4 and loss tangent 0.025, it has a cleared ground plane area of dimensions *13 mm x 60 mm* for installing the PILA antenna. As the PILA antenna is located on the top edge of the mobile chassis, it can effectively excite the fundamental chassis dipole mode. It occupies a total volume of *28 x 4.5 x 15 mm*^{3}. It includes three parts: : the PILA plate as the main coupling element, which is fed by a feeding strip with dimensions *2 mm x 3.5 mm*, the coupled meandered monopole as a parasitic radiator and the thick FR4 that works as a carrier and a loading material. The metal frame antenna is composed of two segments, the mainframe (right one) and the auxiliary frame (left one). Each frame is printed on a 1mm thick FR4 substrate of dimensions. It is worth mentioning that the same optimized dimensions of both antennas (as described in section 7.2 and 7.3) are used here.

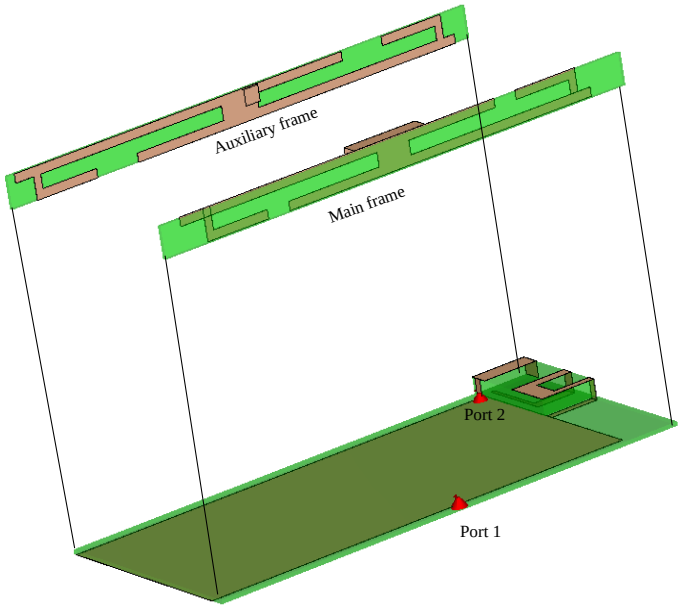

Fig. 7.12: Dual-element multiband antenna design

The initial simulated S-parameter result for the dual element antenna is shown in Fig. 7.13. It can be observed that the design covers six frequency bands in a MIMO operation. But the problem in this design is that the transmission coefficient S12 is high at the GSM850 band (about -7 dB). This is expected since the PILA antenna and the second

frame segment (auxiliary frame) are very close to each other. This can be understood from the calculated surface current distribution at 0.85 GHz as shown in Fig. 7.14. It can be observed that a part of the excited current from the metal frame antenna is coupled to the Antenna 2. To manage this, there are two possible solutions:

1) The first one which is not acceptable is to move the Antenna 2 away from the auxiliary frame (make the feeding point in the middle of the shorted top edge of the system PCB); this is because it will affect the antenna impedance matching and operational bandwidth at GSM850 and DCS1800 frequency bands, and this requires a modification of the Antenna 2 structure likes the antenna height.
2) As most of the recent Smartphone devices have asymmetrical metal frame, the design can be modified to have asymmetrical frame segments. This can be done modifying the auxiliary frame through removing the two inverted-L stubs and shortening the frame from the top by *13 mm*. The final design configuration is shown in Fig. 7.15. Fig. 7.16 shows that the isolation level between the two antennas is enhanced by around 4 dB at 0.85 GHz frequency band.

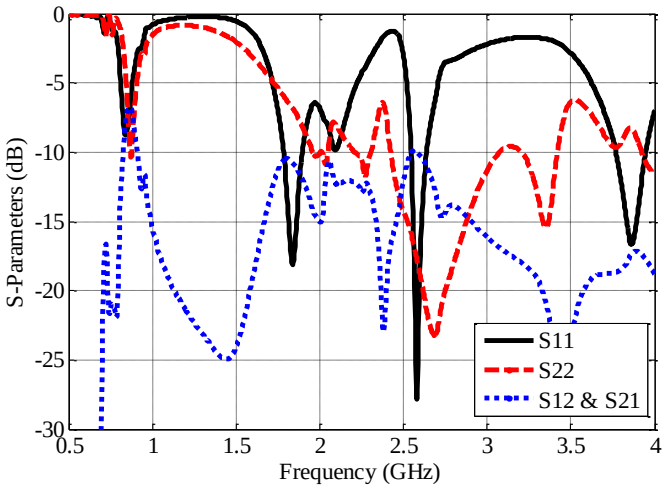

Fig. 7.13: Initial simulated S-parameters versus frequency in GHz

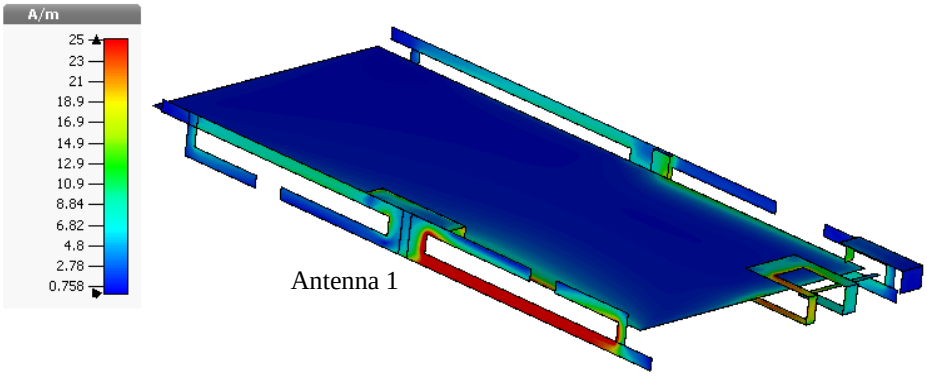

(a)

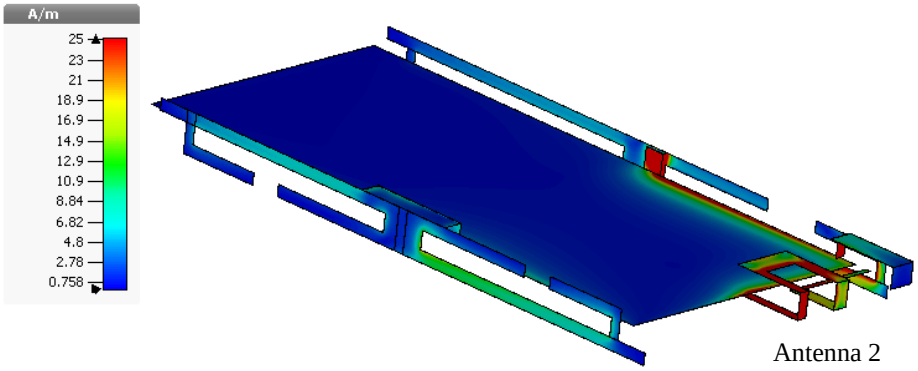

(b)

Fig. 7.14: Simulated surface current distribution at 0.85 GHz

(a) Antenna 1 and (b) Antenna 2

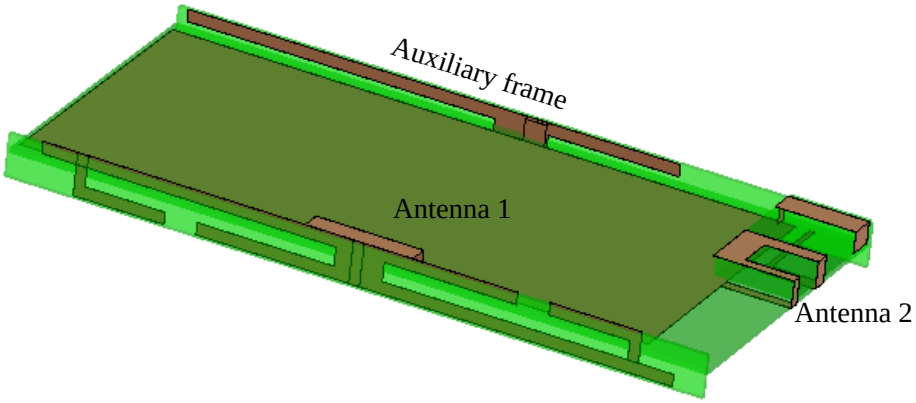

Fig. 7.15: Final configuration after modifying the auxiliary frame

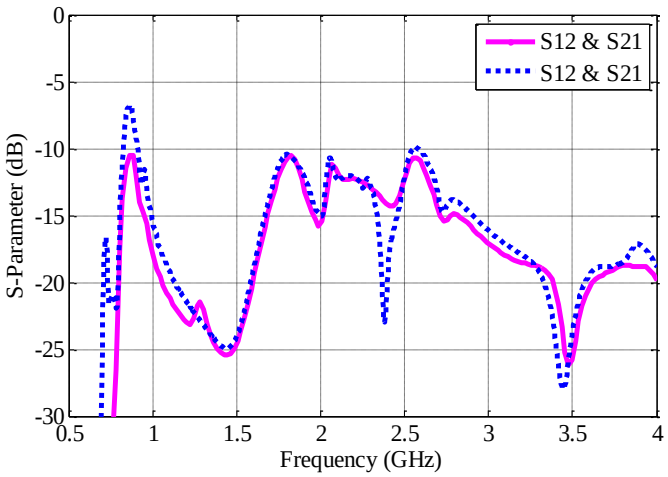

Fig. 7.16: Mutual coupling coefficient before and after modification

7.4.2 Prototype and S-Parameters

To validate the proposed design, a prototype was fabricated, tested and presented in Fig. 7.17. The simulated and measured S-parameter results are depicted in Fig. 7.18. Both results are in a good agreement and exhibit almost the same behaviour. Based on the -6 dB bandwidth criteria, the design has a MIMO operation over six frequency bands, which are: GSM850 (824-894 MHz), DCS1800 (1710-1880 MHz), PCS1900 (1850-1990 MHz), UMTS2100 (1920-2170 MHz), LTE2500 (2500-2700 MHz) and LTE3600 (3600-3800 MHz). Furthermore, the design covers the following band with no MIMO operation: WiFi/Bluetooth (2400-2485 MHz), S-DMB (satellite Digital Multimedia Broadcasting 2170-2200 MHz), LTE2300 (2300-2500 MHz) and LTE3400 (3400-3600 MHz).

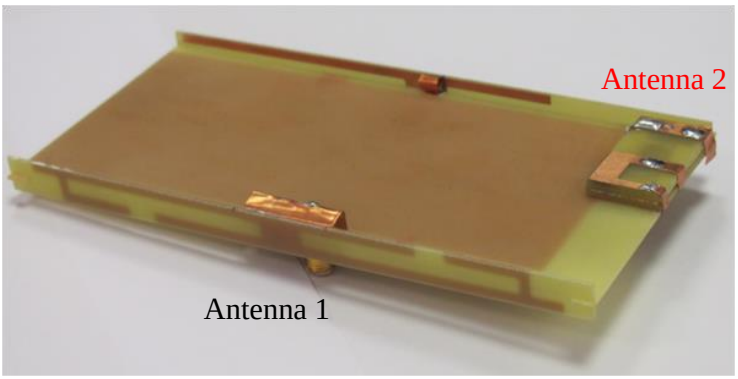

Fig. 7.17: Dual-element antenna prototype

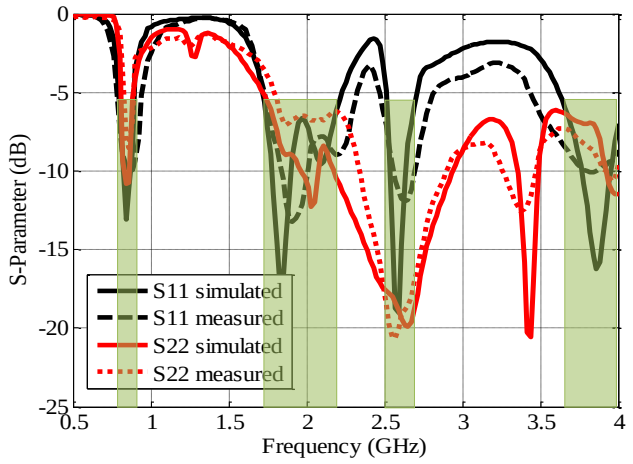

(a)

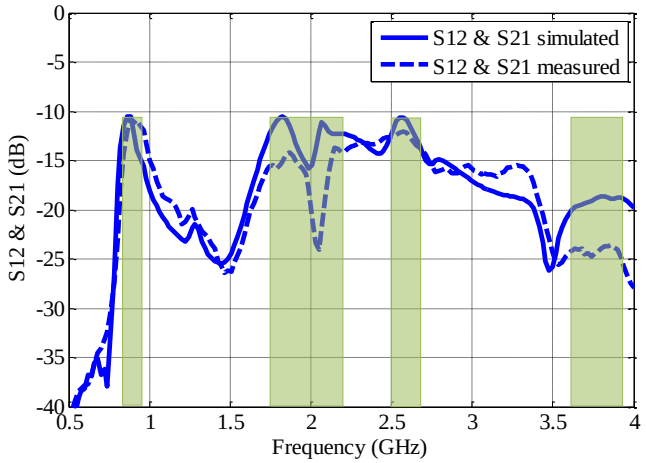

(b)

Fig. 7.18: Simulated and measured S-parameters

7.4.3 Far-Field Radiation Patterns

The measurement of the far-field radiation patterns was conducted inside an anechoic chamber at the University of Liverpool. Fig. 7.19 shows the 2D simulated and measured normalized radiation patterns at two frequencies 0.85 GHz and 2.0 GHz. In general, the measured patterns agree well with the simulated ones, especially, at the lower frequency as shown in Fig. 7.19(a). A slight difference occurs in higher frequency patterns (2.0 GHz), which corresponds to the effect of the SMA connectors, load terminal and the measurement cables. The big advantage of this design that can be observed is the both polarization and pattern diversities are achieved. Thus, the design can achieve a good

diversity gain over the covered frequency bands. Also, this can be observed from the simulated 3D radiation patterns as shown in Fig. 7.20.

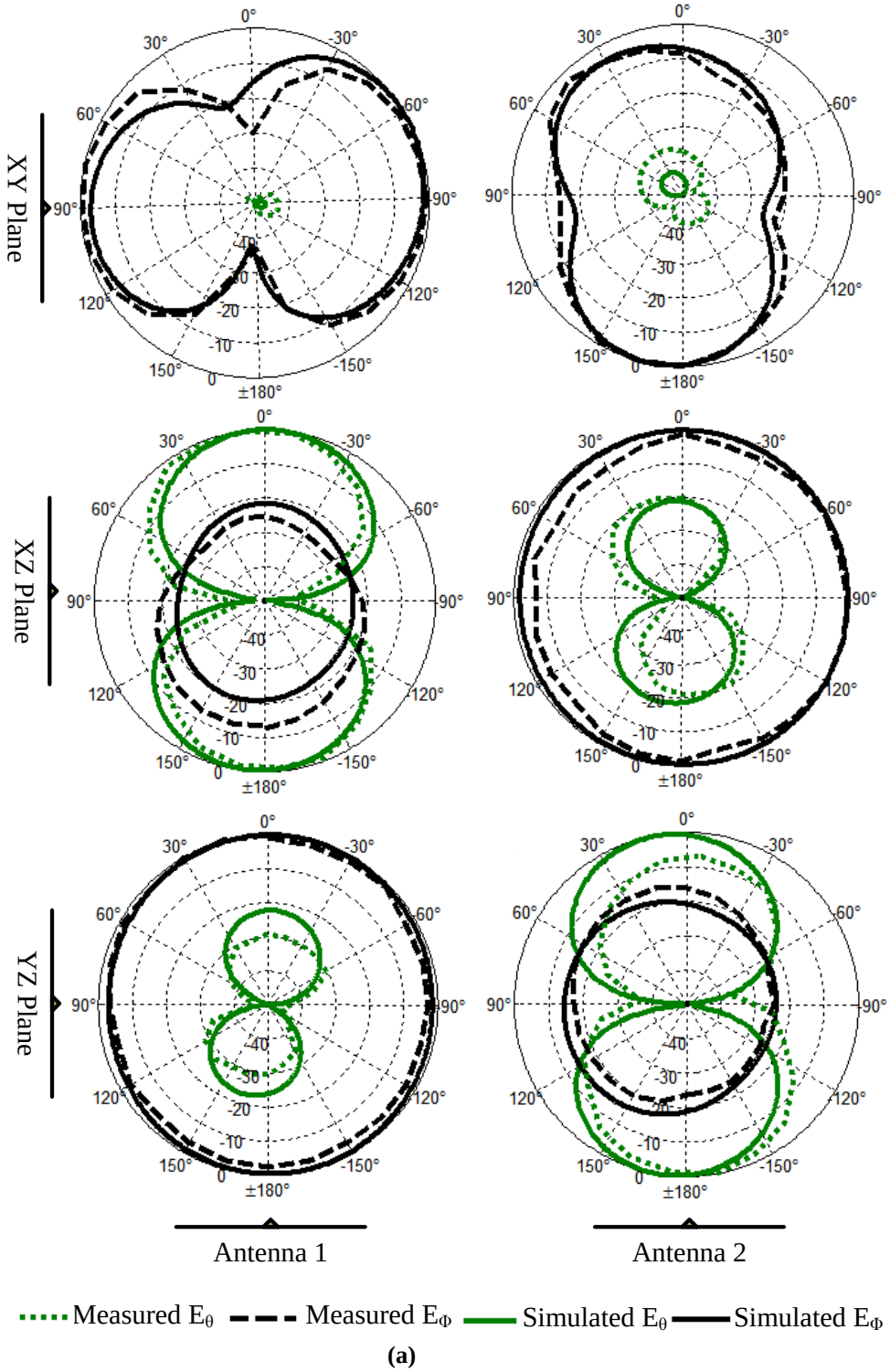

(a)

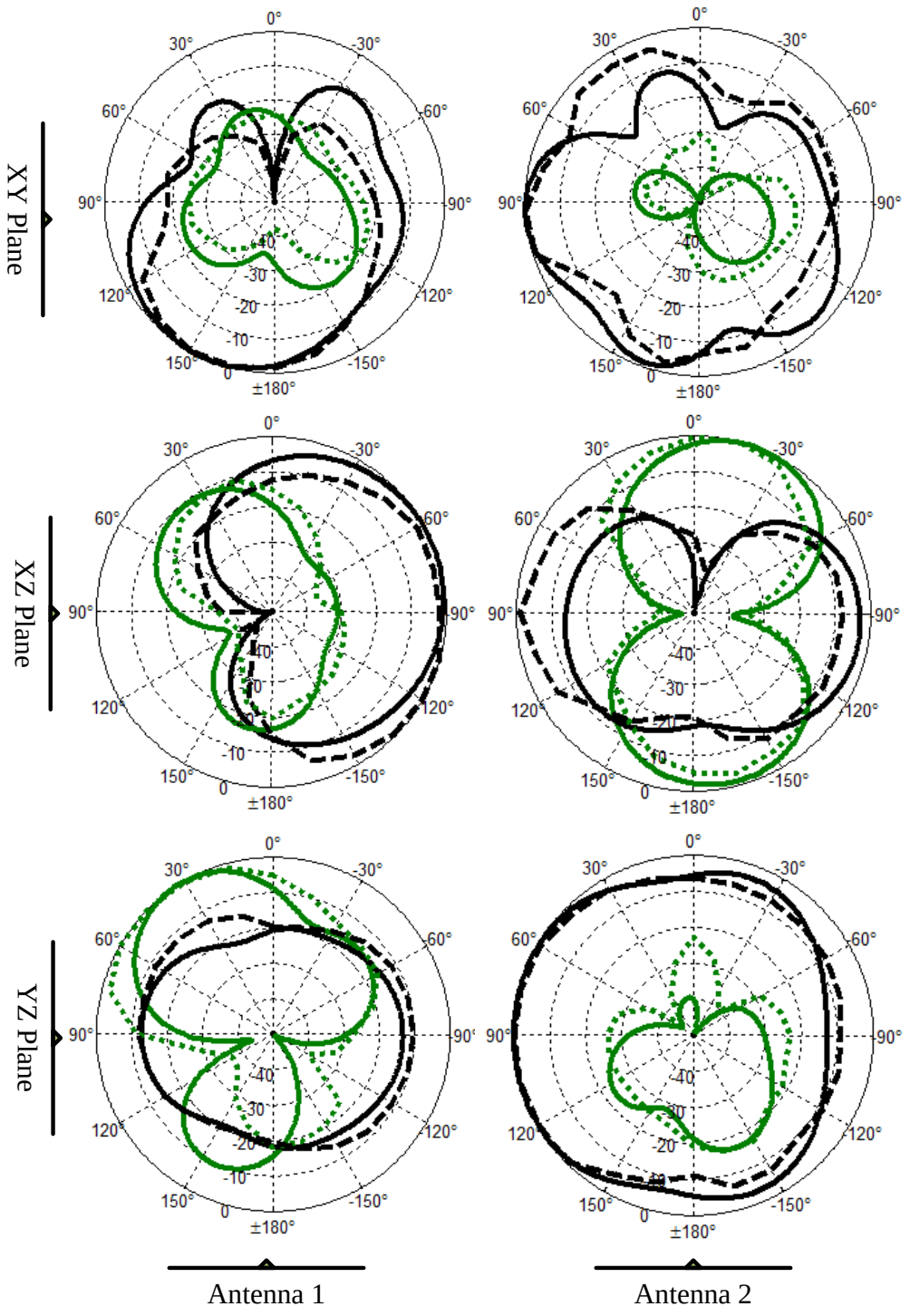

(b)

Fig. 7.19: Normalized far-field radiation patterns (a) at 0.85 GHz and (b) at 2.0 GHz

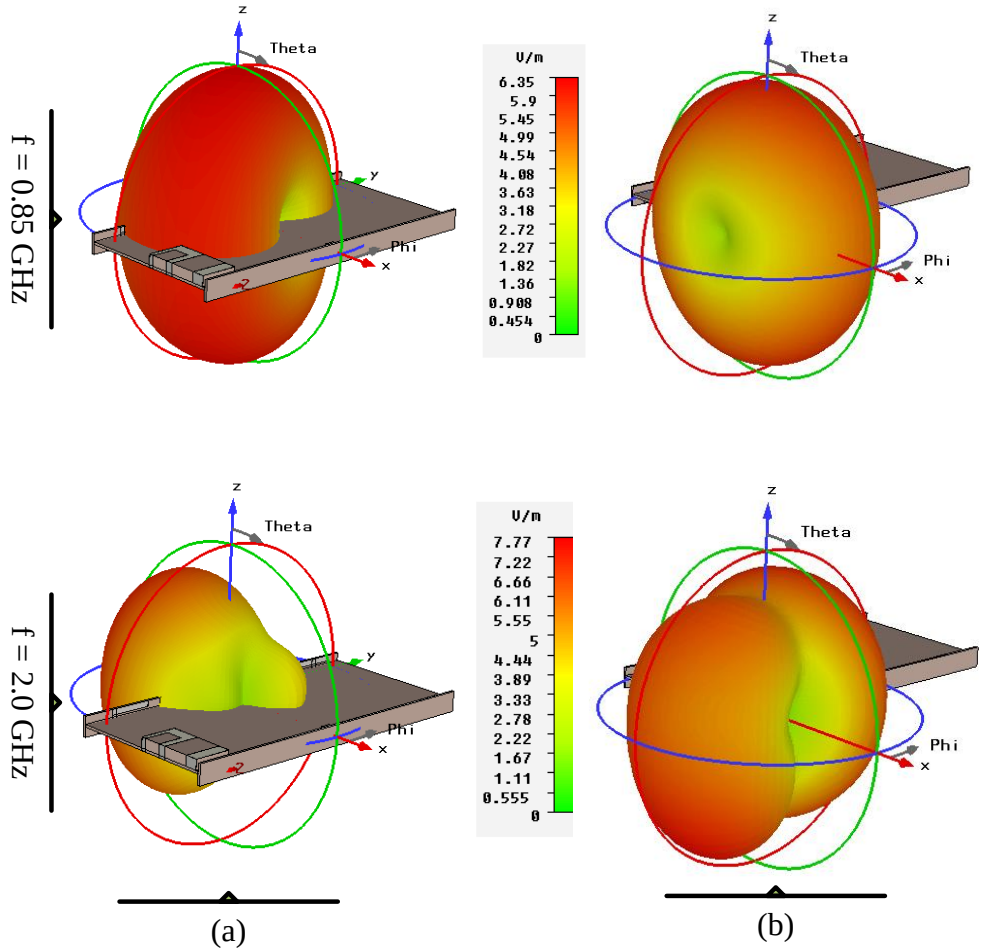

Fig. 7.20: Simulated 3D radiation patterns (a) at 0.85 GHz and (b) at 2.0 GHz

7.4.4 Diversity Performance Parameters

In order to achieve a good diversity gain, the proposed antenna must satisfy the MIMO and diversity conditions (ECC and MEG ratio described in Chapter 2).

The envelope correlation coefficient is measured inside a reverberation chamber. Both simulated and measured results are calculated using Eq. (2.21) and are depicted in Fig. 7.21. Both results are in a good agreement, especially, over frequency bands of interest. The results show that the maximum value of the envelope correlation stays below 0.15 which already satisfies the ECC coefficient condition (below 0.5).

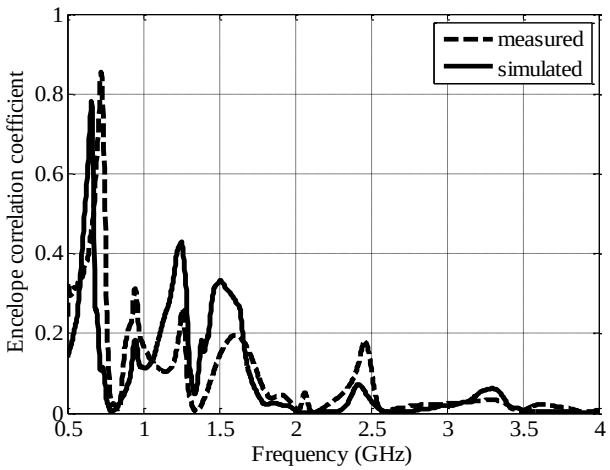

Fig. 7.21: Envelope correlation coefficient

The MEG ratio for the proposed antenna is evaluated from the 3D gain patterns using Eq. (2.18) and Eq. (2.19) and the results are summarized in Table 7.2. It can be observed from the table that the MEG for different antennas has a difference of less than 0.6 dB in the indoor environment and 1.35 dB in the outdoor environment.

Table 7.2: MEG in different environments

Environment	Frequency (GHz)	Mean Effective Gain (dB)		K
		Ant1	Ant2	
Indoor	0.85	-3.85	-3.85	0.00
	1.85	-3.78	-3.18	0.60
	2.1	-3.02	-3.53	0.51
	2.55	-2.35	-3.95	0.60
	3.75	-3.38	-3.28	0,10
Outdoor	0.85	-7.2	-6.9	0.30
	1.85	-6.65	-5.44	1.21
	2.1	-5.3	-6.1	0,80
	2.55	-5.0	-6.35	1.35
	3.75	-4.72	-5.2	0.48

After assessing the correlation and MEG results, the diversity gain of the proposed antenna is evaluated as a function of frequency using Eq. (2.25). Fig. 7.22 shows both the simulated and the measured apparent diversity gains calculated with a selection combining techniques at 0.99 reliability. The diversity gain results vary from 9.4 dB to 10.45 dB over the frequency band of interest.

The total antenna efficiency measurement was conducted inside a reverberation chamber using the two antenna approach. Table 7.3 summarizes both the simulated and the measured total efficiencies obtained at selected frequency points 0.85, 1.85, 2.1, 2.55 and 3.75 GHz. Both results are in a good agreement and the total efficiency is above 70 % on average. The slight difference between the simulated and measured results might be due to the fabrication errors, curve smoothing and the use of a glue material (not included in the simulation) in forming the thick FR4 substrate for Antenna 2.

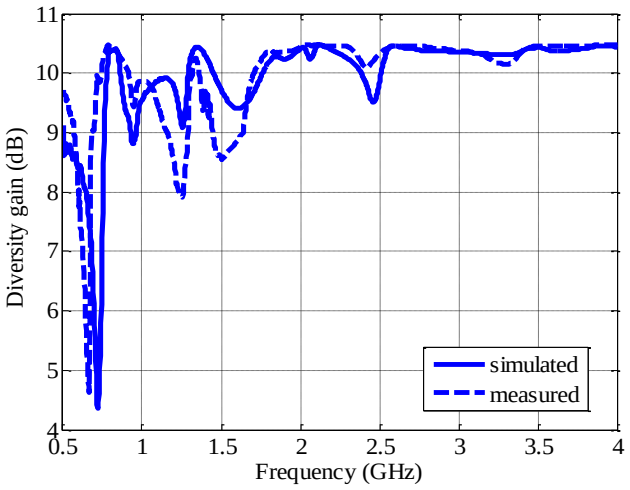

Fig. 7.22: Apparent diversity gain versus frequency

Table 7.3: Simulated and measured total efficiency

Frequency (GHz)	Antenna 1		Antenna2	
	Simulated	Measured	Simulated	Measured
0.85	83%	78%	85%	77%
1.85	79%	75%	72%	69%
2.1	72%	70%	70%	68%
2.55	77%	72%	83%	80%
3.75	85%	80%	71%	72%

7.4.5 Effect of Handset Components

In this section, we use a simulation model to investigate the effect of other handset mobile components like battery, and display on the antenna performance. Both battery and LCD touch screen are modelled as metallic boxes of sizes *70 mm × 40 mm × 4 mm* and *115 mm × 53 mm × 2 mm* (5.0 inches screen), respectively. As the handset components need to be DC-grounded, both components are grounded by small strips which are not considered. Using these assumptions, the proposed simulation is conducted using CST Microwave Studio. As can be seen from Fig. 7.23, even after including the battery and the LCD in the design, the total handset thickness is around 8 mm.

Fig. 7.24 shows the effect of including both the LCD display and battery models on the S-parameters. As can be seen from the three sub-figures, the presence of handset components affects only the deepness of the S-parameter curves. In particular, these components affect the impedance matching level of Antenna 1 at some frequency bands like 2.1 GHz and 2.55 GHz bands. This is also reflected on the total efficiency of Antenna 1 as shown in Fig. 7.25(a), in which the simulated efficiency is dropped by 14 % and 10 % (worst cases) at 2.05 GHz and 2.65 GHz, respectively.

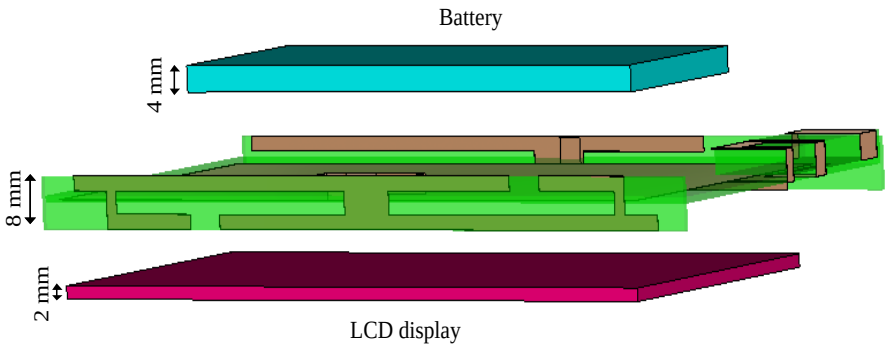

Fig. 7.23: Antenna Configuration with a display and battery

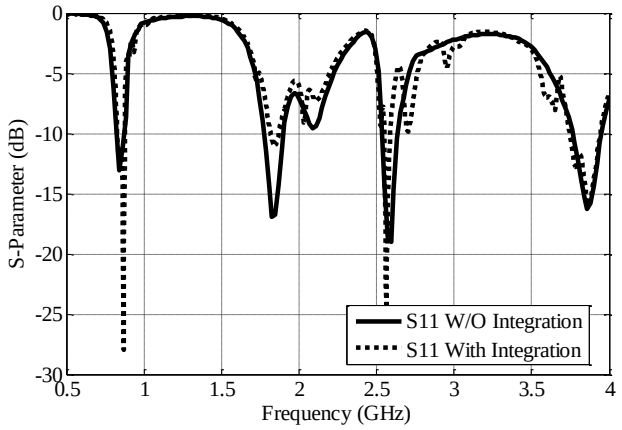

(a)

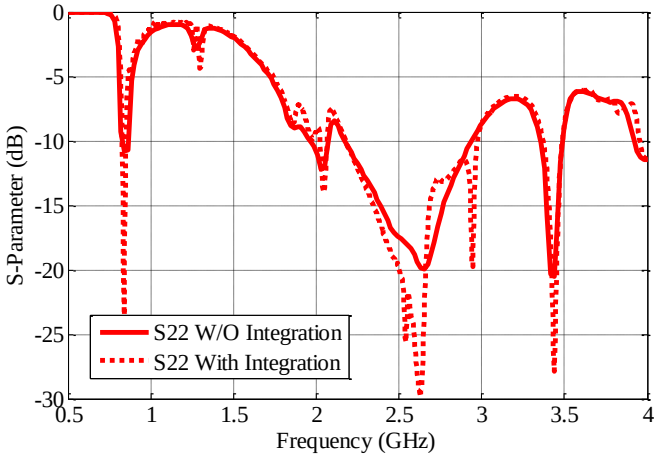

(b)

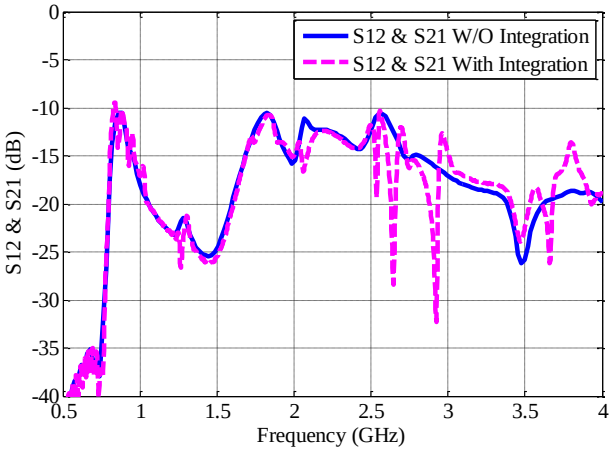

(c)

Fig. 7.24: Variation of the S-parameters of the antenna when including the LCD display and battery models (a) S_{11}, (b) S_{22} and (c) S_{12} and S_{21}

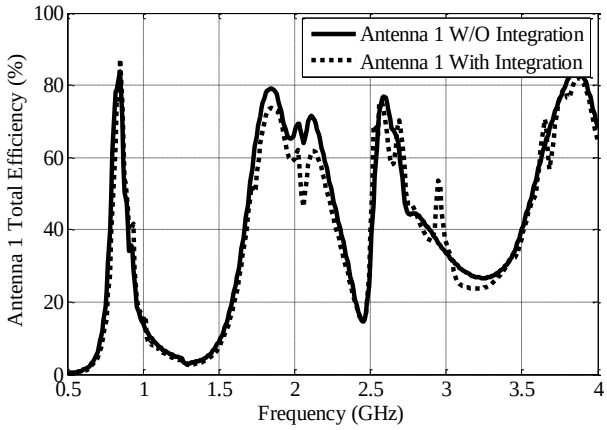

(a)

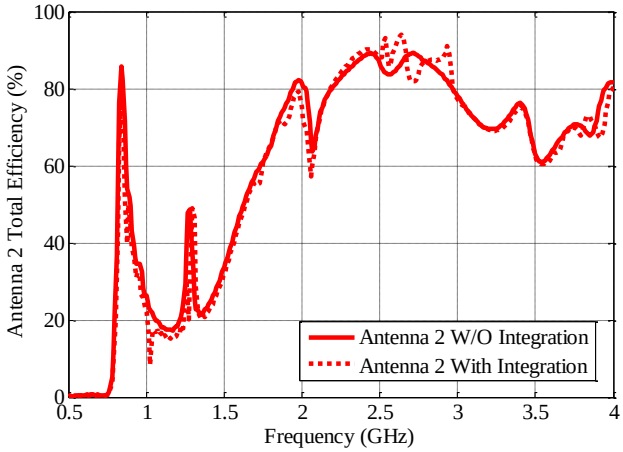

(b)

Fig. 7.25: Effect of the LCD display and battery models on the total efficiencies (a) Antenna 1 (metal frame) and (b) Antenna 2 (PILA with meandered strip monopole)

7.5 Summary

This chapter has dealt with the most challenging part in the design of MIMO antennas for handheld devices (multiband and MIMO antenna design). It has presented three antenna designs: the first two designs were single element designs while the final one was a combination of both single element antennas. In summary:

1) **Hexa-band metal frame antenna:** A new, simple and low-profile (height = 8 mm) hexa-band metal-frame antenna has been proposed for multiband smartphone applications. The multiband operation has been achieved using a modified metal frame that is loaded with two kinds of stubs. The working

mechanism and the design principle of the antenna have been presented in a simplified way. A prototype has been designed, fabricated and measured. The results have shown that the design can cover six frequency bands with S_{11}< -6 dB such bands like: GSM850, DCS1800, PCS1900, UMTS2100, LTE2500 and LTE3600. Other radiation characteristics (radiation patterns and radiation efficiency) are also obtained and evaluated. The interesting finding is that the design has a radiation pattern at 0.85 GHz orthogonal to the conventional chassis dipole mode, which in turns simplifies the implementation of MIMO antennas for such applications.

2) **Hepta-band PILA Antenna:** A new, low profile (height = 4 mm), small footprint hepta-band antenna has been proposed as an internal antenna for multiband handset applications. For better impedance bandwidth and to excite the conventional chassis dipole mode for applications below 1 GHz, it is located on the top edge of the system board over a cleared ground plane area. It composed of PILA as a main coupling element, which is coupled with a shorted parasitic meandered strip. A thick FR4 substrate has been used to work as a carrier and as a loading material for both the PILA and the parasitic strip. Based on the -6 dB bandwidth criteria, the design covers seven frequency bands which are: GSM850, DCS1800, PCS1900, UMTS2100, LTE2500, WiFi 2.4 GHz and LTE3600.
3) **Dual-element antenna for multiband smartphone applications:** As a combination of both the hexa-band metal frame antenna and the hepta-band PILA antenna, a dual element multiband MIMO antenna has been proposed. A slight modification of the metal frame antenna (segment 2) has been done to decrease its effect on the internal antenna (PILA). The prototype has been fabricated and tested, the results have shown that the design can cover six frequency bands in MIMO operation (S_{11}< -6 dB and S_{12}< -10 dB), while it covers LTE2300, 2.4 GHz WiFi and Bluetooth frequency bands as a single element. The diversity parameters have also been obtained and evaluated; the measured diversity gain from the calculated envelope correlation coefficient is better that 10 dB on average. The effect of handset components like LCD display and battery has been investigated, and the results showed that it can be a good candidate for real time applications. Finally, compared to other work in the literature, this design can offer a small thickness Smartphone (less than 9 mm) with a multiband use.

Reference

[1] M. A. Moharram and A. A. Kishk,"General decoupling network design between two coupled antennas for MIMO applications," *Progress in Electromagnetics Research Letters,* vol. 37, pp. 133-142, 2013.

[2] C. C-Yuk, C. C. Ho *et al.*,"Reduction of mutual coupling between closely-packed antenna elements," *IEEE Trans. Antennas Propag,* vol. 55, no. 6, pp. 1732-1738, June. 2007.

[3] M. T. Islam, M. S. Alam, "Compact EBG strucutre for allievating mutual coupling between antenna araay elements," *Progress In Electromagnetic Research,* vol. 137, pp. 425-438, 2013.

[4] A. C. K. Mak, C. R. Rowell and R. D. T. Murch.,"Isolation enhancement between two closely packed antennas," *IEEE Trans. Antennas Propag,* vol. 56, no. 11, pp. 3411-3419, Nov. 2008.

[5] Y. Wang and Z. Du.,"A wideband printed dual-antenna system with a novel neutralization line for mobile terminals," *IEEE Antennas and Propagation Letters,* vol. 12, pp. 1428-1431, 2013.

[6] H. Li, Z. Miers and B. K. Lau., "Design of orthogonal MIMO handset antennas based on characteristic mode manipulation at frequency bands below 1 GHz," *IEEE Trans. Antennas Propag.,* vol. 62, no. 5, pp. 2756-2766, 2014.

[7] R. A. Bhatti, S. Yi and S-O. Park.,"Closely mounted mobile handset MIMO antenna for the LTE 13 band application," *IEEE Antennas and Propagation Letters,* vol. 13, pp. 411-414, 2014.

[8] H. Bae. F. J. Harackiewicz *et al.*,"Compact mobile handset MIMO antenna for LTE700 applications," *Microwave and Optical Technology Letters,* vol. 52, no. 11, pp. 2419-2422, November. 2010.

[9] R. A. Bhatti, S. Yi and S-O. Park.,"Compact antenna array with port decoupling for LTE-standardized mobile phones," *IEEE Antennas and Propagation Letters,* vol. 8, pp. 1430-1433, 2009.

[10] J. Anguera, A. Andújar *et al*, "Advances in antenna technology for wireless handheld devices," *International Journal on Antennas and Propagation*., vol. 2013, Article ID: 838364, 2013.

[11] Y. L. Ban, Y. F. Qiang, Z. Chen, K. Kang and J. L. Wei-Li, "Low-profile narrow-frame antenna for seven-band WWAN/LTE smartphone applications ," *IEEE Antenna Wireless Propag. Lett.*, vol. 13, pp. 463-466, 2014.

[12] L. W. Zhang and Y. L. Ban, "Novel hepta-band coupled-fed antenna for WWAN/LTE metal-ring-frame smartphone applications ," *PIERS Proceeding.*, pp. 2190–2193. 2014.

[13] J. Zhong, K. K. Chen and X. Sun, "A novel multi-band antenna for mobile phone with metal frame," *in Proc. 8th International Conference on Wireless Communications, Networking and Mobile Computing (WiCOM)*, Sept. 2012, China.

[14] S. Eom, M. Ali, S. O. Park and H. Kim, "Embedded antenna for metallic handheld communication devices," *Progress in Electromagnetics Research B.*, vol. 57, pp. 127-138, 2014.

[15] Y. L. Ban, Y.F. Qiang, Z. Chen *et al*, "A dual-loop antenna design for hepta-band WWAN/LTE metal-rimmed smartphone applications," *IEEE Trans. Antennas Propag.*, vol. 63, no. 1, pp. 48-58, 2015.

[16] Z. Miers, H. Li and B. K. Kiong., "Design of bandwidth-enhanced and multiban MIMO antennas using charaterisitcs modes," *IEEE Antenna Wireless Propag. Lett.*, vol. 12, pp. 1696-1699, 2013.

Chapter 8: Conclusions and Future Work

8.1 Summary

Recently, the MIMO system became one of the key enabling wireless technologies, which is deployed to meet the increasing demand for higher data rates and better reliability in 3G and 4G mobile systems. Multi-antenna systems or antenna diversity schemes play an important role in achieving the MIMO functions (a high data rate and better system reliability). However, the design of MIMO antennas for small handset devices is very challenging due to the following:

1) The closely spaced antennas tend to be more coupled (correlated); the high correlation level destroys the performance parameters of the MIMO system.
2) To decrease the correlation between MIMO antennas, a suitable and reliable isolation (decoupling) technique should be employed.
3) The current wireless systems like: 2G, 3G and 4G are scattered over a wide frequency range in the type of discrete bands between 700 MHz up to 4.0 GHz. This adds another design difficulty in which MIMO antennas with a multiband operation are needed.
4) Antennas with small footprint and low profile are highly demanded to meet the recent handset design fashions in the mobile market.

Therefore, the overarching question that this thesis tries to answer is: how to find an antenna structure to tackle these design obstacles? An overview on the current state of the art of the handset antenna design has been introduced in the beginning. Followed by a brief familiarization on MIMO systems from the antenna diversity point of view, in which the performance parameters of a MIMO or diversity antenna such as the envelope correlation coefficient, power balance, diversity gain and total radiation efficiency were also addressed.

In this thesis, several antenna structures have been proposed as MIMO and diversity antennas. These designs can be divided into two main phases or themes:

In the first phase, two MIMO antennas were proposed based on the IMAT technology in which a single antenna with multi feeds or ports can be used to achieve diversity gain by exciting different modes. Both designs, the dual-feed water-based antenna

($h = 10\ mm$) and the dual-feed PIFA antenna ($h = 3\ mm$) were used for the wireless applications above 2.4 GHz.

The design of MEA system represents the second phase in this work. This phase is divided into two sub-phases:

The first sub-phase concerned with finding compact, low profile ($h = 5\ mm$) and wideband antennas for MIMO and diversity applications over the frequency range of 1.7-2.7 GHz. The chosen antenna structure was planar inverted-L antenna (PILA) due to its compactness, low profile and ease of fabrication. Before using this PILA antenna for MIMO and diversity applications, the single element design was presented first. Then, a dual-element PILA was proposed by employing both spatial and diversity diversities. Despite the design occupied a small footprint area over the system PCB, a new and more compact dual-element PILA system has been created by placing both antenna elements on the PCB top edge (collocated antennas). The isolation between antenna elements was achieved using a parasitic decoupling element inserted between antenna elements. The step impedance resonator (SIR) circuit theory has been employed as a novel design approach for the PDE. This gave a great advantage for the design in which the final design was compact, wideband, low profile and with a small footprint area over the PCB. According to these features, the investigation was continued to develop a four-element diversity antenna array for handset applications. Another copy of the compact dual-element PILA antenna was attached to the lower edge of the system PCB.

The second sub-phase dealt with finding a multiband MIMO antenna for recent Smarphones with a metal case. A new hexa-band metal frame antenna was integrated with a new hepta-band PILA antenna coupled with a shorted parasitic meandered monopole to form a low profile dual-element antenna. The design covers six frequency bands ranging from GSM850 toward LTE3600.

Finally, it is worth mentioning that the diversity performance parameters of all the proposed antenna solutions were obtained and evaluated based on both simulated and measured results. Most of them are in very good agreement. Although some of the designs are still not practical to be implemented in practice, the idea and the knowledge gained should be useful for practical design guidance.

8.2 Key Contribution

In this thesis, four different areas related to the MIMO and diversity antenna design are investigated. The major contributions in this thesis are detailed in the following four sections.

8.2.1 RDRA Water Antenna as a Diversity and MIMO Antenna

In chapter three, a novel dual-feed water-based antenna (height = 10 mm) was introduced for wireless applications between 2.4 GHz to 2.7 GHz. The novelty in this design was in the use of a low cost, transparent and friendly liquid dielectric material, which is the pure water ($\varepsilon_r = 81$). The proposed antenna has a rectangular tile shape. Two feeding probes were used to excite $TE^{y}_{1\delta 1}$ fundamental mode. A parasitic decoupling technique has been used for two purposed; 1) To reduce the mutual coupling between the antenna ports; 2) To act as a parasitic radiator that compensated the water dielectric loss and hence enhanced the total radiation efficiency. The diversity performance parameters were calculated and obtained based on both measured and simulated results, the design satisfied the diversity conditions and achieved an average diversity gain around 8.5 dB. The interesting finding from this work is that the; if the water loss is neglected, the proposed antenna can also cover 200 MHz bandwidth from 2.5 GHz to 2.7 GHz with an isolation level greater than 11 dB. Thus, this new antenna can be a good candidate for the recent transparent technology trend.

8.2.2 A New, Low Profile Dual-Feed PIFA as a Diversity and MIMO Antenna

Chapter four presented a new, novel, low profile (height = 3 mm) and wideband dual-feed planar inverted-F antenna (PIFA) for wireless applications over the frequency range of 2.35-2.25 GHz. Instead of using either parallel or orthogonal feed, A new feed arrangement (coplanar feed) was used, it exhibits a lower mutual coupling level. The polarization diversity was achieved by exciting two orthogonal radiation modes. The isolation between the feeds was achieved by an L-shaped ground plane slot. Thus, this single PIFA antenna can act as two separate antennas for diversity and MIMO applications with reduced space and cost.

8.2.3 New, Low Profile and Wideband PILA Antenna systems for MIMO and Diversity Applications

The third investigation of this work was concentrated on finding several small footprint, low profile and wideband multi-element planar inverted-L (PILA) antenna system for handset application in the frequency range of 1.7 GHz to 2.7 GHz. Three MIMO antenna designs were presented in addition to a novel approach for the design of a parasitic decoupling element between the antenna elements in MIMO antenna systems.

- The first antenna design was introduced in Chapter 5. A low profile (height = 5 mm) and wideband planar inverted-L antenna (PILA) has been proposed for handset diversity and MIMO applications. The single element was designed first; The radiator consists of modified PILA coupled with a ground plane notch that works as a parasitic radiator; a small ground plane strip was added to shift the lower edge frequency down to 1.7 GHz. Then, a dual-element PILA antenna was proposed, the two elements were arranged utilizing both pattern and spatial diversities to provide a reasonable isolation level. A good diversity performance has been achieved in terms of envelope correlation coefficient, mean effective gain ratio and diversity gain.
- Despite the proposed design in Chapter 5 has a small footprint, a thorough investigation was conducted in Chapter 6 to find more compact designs of multi-element PILA antenna. A compact dual-element PILA antenna (placed on the top edge of the system PCB) has been presented for handset applications between 1.7 GHz to 2.7 GHz. To obtain antennas isolation, a parasitic decoupling element was inserted between antenna elements, symmetrically. A novel design approach has been proposed for designing the optimal parasitic decoupling element that can help both the operational bandwidth and the isolation level. The compact dual-element was simulated, fabricated and tested; the measurement results demonstrated that this design is good for wireless hand portable applications.
- The third design was a four-element PILA antenna system operating between 1.7 GHz and 2.7 GHz. The antennas were arranged in a way that two elements were placed on the top shorted edge of the PCB, while the other two elements were located on the lower shorted edge of the PCB. The isolation was achieved by the following: 1) Employing parasitic decoupling elements

between antenna pairs on shorted edges of the PCB. 2) Exploiting both the space and pattern diversities between the top antennas and the lower antennas. The prototype was made and the resulted diversity gain was about 15.5 dB.

8.2.4 A New, Low Profile and Multiband Dual-Element Antenna for Metal ID Smartphones

In order to deal with the most challenging part in the design of MIMO antennas for handset applications, the final investigation of this work was focused on finding a multiband antenna solution for Smartphones with a metal frame case. Therefore, a low profile (height = 8 mm) dual-element hexa-band MIMO antenna has been proposed in Chapter 7. It compromises of a hexa-band metal frame antenna and a hepta-band PILA coupled with a shorted monopole strip. The isolation at the high frequency bands (above 1.7 GHz) was better than 11 dB, it was achieved from both the space diversity and orthogonal arrangement of the antenna elements. On the other hand, the isolation at GSM850 (better than 10 dB) was achieved from excitation different and orthogonal chassis modes around 850 MHz. The effect of handset components like LCD display and battery has been investigated, and the results showed that this design can be a good candidate for real time applications.

8.3 Future Work

Based on the conclusion drawn and the limitations of the work presented, future work can be carried out in the following areas;

- For dual-feed water-based, both the antenna size and the antenna profile are quite large. It would be better to reduce both of them. Thus, a suitable DRA miniaturization technique is needed.
- The number of PIFA feed can be further increased; this can be done by combining other feed arrangements in the structure. As an example, a combination of parallel-coplanar, coplanar-orthogonal feeding strips can be used to form a multiport (more than 2) PIFA MIMO antenna.
- As the neutralization line decoupling technique is still lack for a design approach, the same design theory employed in the design of the parasitic decoupling element can be employed to find an optimal neutralization line structure in terms of the footprint, decoupling level and decoupling bandwidth.

- It would be interesting to find an antenna structure that can cover the lower LTE frequency band in a wideband operation from 700 MHz up to 960 MHz.
- To cover more than one wireless application for frequencies below 1 GHz with a MIMO operation. It is difficult to achieve wideband isolation. Thus a frequency reconfigurable isolation circuit or structure can be a good candidate to achieve MIMO and diversity operation in the mobile handset below 1GHz.
- For MIMO operation below 1GHz, it would be better to use antenna structures that exhibit a very small amount of surface current on the mobile chassis. Loop antennas can be a good candidate as they excite a very small current on the system ground plane compared to other antenna structures.
- The concept of using one antenna element with multiple ports can be extended to other antennas such as planar monopole antennas, loop antennas etc.
- It would be interesting to calculate and investigate both the specific absorption rate (SAR) and antenna detuning (effects of the human head and hand on antenna performance) of the proposed antenna.

Appendix A1

The purpose of this appendix section is to detail the complete calculation for the measurement parameters of the two antenna efficiency method (Eq. (2.28)) in the RC chamber.

$\left\langle \left|S_{22,s}\right|^2 \right\rangle_{cor}$ is the mismatch correction for the reflection coefficient of AUT and it is given by

$$\left\langle \left|S_{22,s}\right|^2 \right\rangle_{cor} = \frac{\left\langle \left|S_{22,s}\right|^2 \right\rangle}{\left(1-\left|\langle S_{22}\rangle\right|^2\right)\left(1-\left|\langle S_{11}\rangle\right|^2\right)} \tag{A1.1}$$

where $\left|\langle S_{11}\rangle\right|^2$ and $\left|\langle S_{22}\rangle\right|^2$ are the free space reflection coefficients of the Tx and AUT antennas.

e_b is the enhanced backscatter constant and is given by:

$$e_b = \frac{\sqrt{\left\langle \left|S_{11,s}\right|^2 \right\rangle \left\langle \left|S_{22,s}\right|^2 \right\rangle}}{\left\langle \left|S_{21,s}\right|^2 \right\rangle} \tag{A1.2}$$

The chamber constant C_{RC} is given by:

$$C_{RC} = \frac{16\pi^2 V}{\lambda^2} \tag{A1.3}$$

where V is the volume of the chamber *3. 6 m* x *4.0 m* x *5.8 m* (width x height x length), λ is the free space wavelength

The chamber time constant τ_{RC} is given by:

$$\tau_{RC} = \frac{1}{Ln\left[PDP(t)\right]} = \frac{1}{Ln\left[\left\langle \left|h(t,n)\right|^2 \right\rangle\right]} = \frac{1}{Ln\left[IFT\left(S_{11n}(f)\right)\right]} \tag{A1.4}$$

Where *PDP(t)* is the power delay profile, *h(t,n)* is the impulse response of the chamber, *IFT* is the inverse Fourier transform, f is the frequency value.